Lib

Indian J. pure appl. Phys., Vol. 18 No. 10 pp 733-824
October 1980
CODEN : IJOPAU ISSN: 0019-5596
18 (10) 733-824 (1980)

107 x1

TCI
10.11 80

INDIAN JOURNAL OF PURE & APPLIED PHYSICS

Published by
PUBLICATIONS & INFORMATION DIRECTORATE, CSIR, NEW DELHI
in association with
THE INDIAN NATIONAL SCIENCE ACADEMY, NEW DELHI

a quantum leap in recorder technology now available to the discriminating research scientist a range of reliable 'state of the art' recording instruments

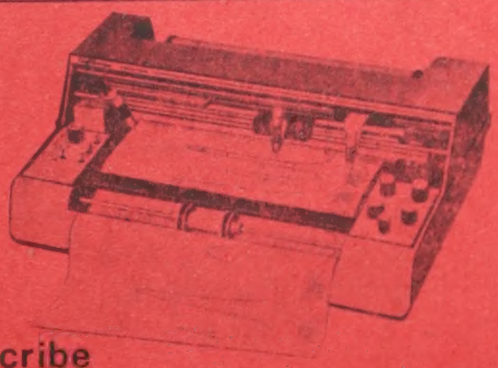

DigiScribe
Strip Chart Recorders One to Four Pens, 0.5 mV full scale and up, 0.5 sec response

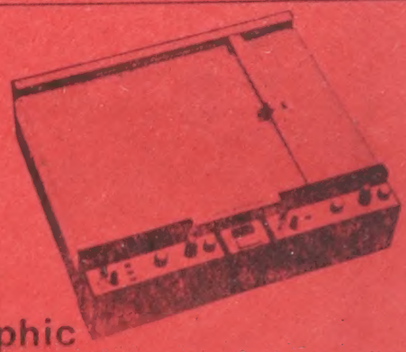

DigiGraphic
XY/t Recorders with plug-in modules to give wide ranges of sensitivity, time base facility and log recording.

HiScribe Oscillographic
Oscillographic Recorders DC to 80 Hz, One to eight channels. Heat or ink writing. Plug in modules to give wide range of sensitivities

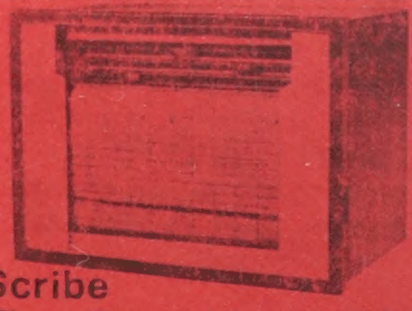

MultiScribe
One to Three Pen and 6, 12 and 24 point Recorders. Rack mounting with alarm contacts, cold junction compensation, and other features.

APPLICATIONS IN THE FIELDS OF

- METEOROLOGY • MATERIAL SCIENCES
- LIFE SCIENCES • PHYSICAL SCIENCES
- CHEMICAL AND ELECTROCHEMICAL SCIENCES
- BIOLOGICAL SCIENCES • PHYSIOLOGICAL AND BEHAVIOURAL SCIENCES • COMPUTER SCIENCES
- ENVIRONMENTAL AND POLLUTION STUDIES
- ENERGY STUDIES • PHARMACOLOGY
- MECHNICAL/ELECTRICAL ENEGINEERING
- METALLURY/METALLURGICAL ENGINEERING
- AERODYANAMICS/AERONAUTICAL ENGINEERING
- BIO-MEDICAL ENGINEERING
- QUALITY CONTROL APPLICATIONS

MANUFACTURED BY:

DIGITAL ELECTRONICS LIMITED

A Company in collaboration with

houston instrument | DIVN OF BAUSCH & LOMB

Office & Factory:

Digilog House, 74/II, C. Cross Road, Marol Industrial Area, MIDC, Andheri (East), Bombay-400 093, Phone: 577676, Gram: 'DIGILOG

chonkar associates

Indian Journal of Pure & Applied Physics

VOLUME 18 No. 10 OCTOBER 1980

EDITORIAL BOARD

Dr B A Dasannacharya
Bhabha Atomic Research Centre
Bombay

Prof. B M Deb
Indian Institute of Technology
Bombay

Prof. P Krishna
Banaras Hindu University
Varanasi

Prof. Krishnaji
Allahabad University
Allahabad

Prof. K V Ramanathan
Tata Institute of Fundamental Research
Bombay

Dr S Chandrasekhar
Indian National Science Academy
New Delhi/Raman Research
Institute Bangalore

Prof. A K Saha
Saha Institute of Nuclear Physics
Calcutta

Prof. N C Sil
Indian Association for
Cultivation of Science
Calcutta

Prof. R Srinivasan
Indian Institute of Science
Bangalore

Prof. K Venkata Ramiah
Osmania University
Hyderabad

Dr K L Chopra
Indian National Science Academy
New Delhi/Indian Institute of
Technology New Delhi

Shri Y R Chadha, *Ex-officio* Secretary & Chief Editor

EDITORIAL STAFF

Editors
D S Sastry & K S Rangarajan

Assistant Editors
G N Sarma, J B Dhawan & Tarun Banerjee

Published by the Publications & Information Directorate, CSIR, Hillside Road, New Delhi 110 012

Chief Editor : Y R Chadha

The Indian Journal of Pure & Applied Physics is issued monthly. The Directorate assumes no responsibility for the statements and opinions advanced by contributors. The editorial staff in its work of examining papers received for publication is assisted, in an honorary capacity, by a large number of distinguished scientists, working in various parts of India.

Communications regarding contributions for publication in the journal should be addressed to the Editor, Indian Journal of Pure & Applied Physics, Publications & Information Directorate, Hillside Road, New Delhi 110 012.

Correspondence regarding subscriptions and advertisements should be addressed to the Sales & Distribution Officer, Publications & Information Directorate, New Delhi 110 012.

Annual Subscription	**Single Copy**
Rs. 100.00 £ 16.50 $ 42.00	Rs. 10.00 £ 1.80 $ 4.50

50% Discount is admissible to research workers and students and 25 % discount to non-research individuals, on annual subscription. Payments in respect of subscriptions and advertisements may be sent by cheque, bank draft, money order or postal order marked payable *only* to **Publications & Information Directorate, New Delhi 110 012.** Claims for missing numbers of the journal will be allowed only if received within 3 months of the date of issue of the journal plus the time normally required for postal delivery of the journal and the claim.

© 1980 The Council of Scientific & Industrial Research, New Delhi.

CSIR SCIENTIFIC PERIODICALS

JOURNAL OF SCIENTIFIC & INDUSTRIAL RESEARCH (monthly)

With a fine record of over 35 years' service to the scientific community, this Journal has grown into India's leading general science periodical. Intended to fulfil the responsibility of helping the research workers to keep themselves abreast of current developments in various fields of science and technology, the Journal carries editorial features highlighting important scientific events in India and abroad; articles on science policy and management of science; review articles on topics of current research interest; technical reports on international and national conferences; reviews of scientific and technical publications; and notes on major advances in various fields.

Annual subscription	**Rs 60.00**	**£ 10.00**	**$ 25.00**
Single copy	**6.00**	**1.00**	**2.50**

INDIAN JOURNAL OF CHEMISTRY (monthly)

This Journal which is running the 18th year of its publication, Consists of the following two sections.

Section A : This section is devoted to papers in Inorganic, Physical, Theoretical and Analytical Chemistry.

Annual subscription	**Rs 70.00**	**£ 12.00**	**$ 30.00**
Single copy	**7.00**	**1.20**	**3.00**

Section B : This section is devoted to papers in Organic Chemistry including Medicinal Chemistry.

Annual subscription	**Rs 70.00**	**£ 12.00**	**$ 30.00**
Single copy	**7.00**	**1.20**	**3.00**

INDIAN JOURNAL OF PURE & APPLIED PHYSICS (monthly)

This Journal, which is running the 18th year of its publication, is devoted to original research communications (full papers and short communications) in all conventional branches of physics (except radio and space physics).

Annual subscription	**Rs 100.00**	**£ 16.50**	**$ 42.00**
Single copy	**10.00**	**1.80**	**4.50**

INDIAN JOURNAL OF RADIO & SPACE PHYSICS (bimonthly)

This Journal serves as a medium for the publication of original rearch work (full papers and communications) in various areas of radio and space physics.

Annual subscription	**Rs 60.00**	**£ 10.00**	**$ 25.00**
Single copy	**12.00**	**2.00**	**5.00**

INDIAN JOURNAL OF TECHNOLOGY (INCLUDING ENGINEERING) (monthly)

This Journal publishes papers reporting results of original research of applied nature pertaining to unit operations, heat and mass transfer, products, processes, instruments, and appliances, etc. The Journal is of special interest to research workers in the departments of applied sciences in universities, institutes of higher technology, commodity research laboratories, industrial cooperative research institutes, and industrial research laboratories.

Annual subscription	**Rs 60.00**	**£ 10.00**	**$ 25.00**
Single copy	**6.00**	**1.00**	**2.50**

INDIAN JOURNAL OF EXPERIMENTAL BIOLOGY (monthly)

This Journal, devoted to the publication of research communications in the fields of experimental botany, zoology, microbiology, pharmacology, endocrinology, nutrition, etc. is the only one in India with such a wide coverage and scope.

Annual subscription	**Rs 120.00**	**£ 20.00**	**$ 50.00**
Single copy	**12.00**	**2.00**	**5.00**

INDIAN JOURNAL OF BIOCHEMISTRY & BIOPHYSICS (bimonthly)

This Journal, published in association with the Society of Biological Chemists (India), Bangalore, is the only research Journal in India devoted exclusively to original research communications in biochemistry and biophysics.

Annual subscription	**Rs 40.00**	**£ 7.00**	**$ 17.00**
Single copy	**8.00**	**1.40**	**3.50**

INDIAN JOURNAL OF MARINE SCIENCES (quarterly)

Commencing publication from June 1972, this Journal is devoted to research communications (full papers and short communications) pertaining to various facets of marine research, viz. biological, physical, geological and chemical oceanography.

Annual subscription	**Rs 40.00**	**£ 7.00**	**$ 17.00**
Single copy	**12.00**	**2.00**	**5.00**

RESEARCH & INDUSTRY (quarterly)

Intended to serve as a link between science and industry, this Journal is addressed primarily to technologists, engineers, executives and others in industry and trade. It publishes informative original articles containing practical details of processes and products developed in India, which show promise of ready utilization, and technical digests on new processes, products, instruments and testing methods which are of interest to industry. Developments in Indian industry are regularly reported.

Annual subscription	**Rs 24.00**	**£ 4.00**	**$ 10.00**
Single copy	**7.25**	**1.30**	**3.50**

INDIAN JOURNAL OF TEXTILE RESEARCH (quarterly)

Commencing publication from March 1976, this Journal is devoted to the publication of papers reporting results of fundamental and applied researches in the field of textiles.

Annual subscription	**Rs 36.00**	**£ 6.00**	**$ 15.00**
Single copy	**12.00**	**2.00**	**5.00**

Please contact

THE SALES & DISTRIBUTION OFFICER
PUBLICATIONS & INFORMATION DIRECTORATE, CSIR
HILLSIDE ROAD, NEW DELHI 110 012

Indian Journal of Pure & Applied Physics

VOLUME 18 No. 10 OCTOBER 1980

CONTENTS

Solid State Physics

Phonon Mode Behaviour in Mixed Cuprous Halides 733
D N TALWAR & B K GHOSH

Lattice Vibration Modes in KHF_2 738
HITOSHI KANAMORI, KEI URABE & TETSURO NISHIMURA

Piezo-Induced Mechanoluminescence & Photoluminescence of Triphenylamine Crystals 743
B P CHANDRA

Cation Distribution of Mn_2FeO_4 — A Mössbauer Spectral Study 747
S BHARATI, M P GUPTA, A P B SINHA & S K DATE

Microtopographical Studies of *n*-Faces of Natural Analcite Crystals ... 751
M S JOSHI, P MOHAN RAO & A V ANTONY

Chemical Physics

Phonon Dispersion in Liquid Carbondisulphide 754
NILIMA LODHA, N S SAXENA & R C BHANDARI

Study of Molecular Reorientation in Phenothiazine by PMR 757
(Miss) RATNA SIRCAR, S C MISHRA & R C GUPTA

Theoretical & Mathematical Physics

Calculation of Thermodynamic Functions & Fluctuations in the Ground-State Particle Number for Interacting Bosons 760
K M KHANNA & S N MEHROTRA

Hydrodynamics of Persistent Mass Currents 767
K M KHANNA, A M PHUKAN & N C SARMAH

Effective Potential for the $O(N)$ Symmetric ϕ^6 Model 771
S MURUGESU & C H OH

Nuclear Physics

Mean Charged Multiplicities in High Energy Hadron-Nucleus Collisions ... 778
T AZIZ, A AHMAD, M ZAFAR, M IRFAN & M SHAFI

CONTENTS

Dielectrics & Microwaves

Dielectric Relaxation Study of Intermolecular Association through Hydrogen Bonding of *p*-Halophenols in Non-Polar Solvents 784
C K MISRA, M C SAXENA & A K SAXENA

Electronics

Axial Cylindrical Surface Wave Transmission across a Bend 788
G P SINHA & K P SHARMA

Spectroscopy

Electronic Absorption Spectra & Hydrogen Bonding Behaviour of Aniline & Phenetidines 793
T GANGULY & S B BANERJEE

Instrumentation

A Count Rate Integrator for Use with X-ray Spectroscopy Work 798
M BANERJEE & K G BHATNAGAR

COMMUNICATIONS

Leptonic & Hadronic Decay Widths of Next Quarkonium ($t\bar{t}$) 801
G Q SOFI

New Spectrum of NiCl Molecule in the Near Ultraviolet Region 802
A B DARJI & N R SHAH

Quark Model & Off-Shell Form-Factors of Nucleons 805
J THAKUR

NOTES

Neutron Irradiation Effects on Magnetocurrent in Semiconductor Diodes ... 807
SHANKER LAL AGRAWAL & RAMA SWAMI

Thermal Expansion of the Ceramic System Pb_{2-x} Ba_x $Li_{0.5}$ $Nb_{1.5}$ O_6 ... 809
R RAJAN & R K KHARE

Calculation of Ionic Radii of Alkali Halide Crystals through Screened Coulomb Potential 810
USHA PURI

Evaluation of Critical Currents & Voltages in the Single Injection Current in an Insulator 812
Y K SHARMA

CONTENTS

NOTES (contd)

Thermal Conductivities of Binary Gas Mixtures 815
J D PANDEY & S R PRAJAPATI

Estimation of Thermal Diffusion Factor of N_2-CO_2 Gas Mixture from Thermal Diffusion Column Data 816
S K DATTA & S ACHARYYA

RKRV Potential Energy Curve & Dissociation Energy of CaO 818
N SREEDHARA MURTHY & U D PRAHLLAD,
T V RAMAKRISHNA RAO & G THIMMA NAIDU

Energy Calculation of Anharmonic Oscillator by Dalgarno Sum Rule ... 821
ADARSH GHOSH & P G KHUBCHANDANI

Letters to the Editor

Errors in Line Width Analysis due to Unresolved Hyperfine Structures ... 823
D S PRABHANANDA

Indian Journal of Pure & Applied Physics
Vol. 18, October 1980, pp. 733-737

Phonon Mode Behaviour in Mixed Cuprous Halides

D N TALWAR* & B K GHOSH

Department of Physics, University of Allahabad, Allahabad 211 002

Received 11 *June* 1979

The two-mode behaviour of the Raman scattering vibrations of $CuCl_{1-x}Br_x$ and $CuCl_{1-x}I_x$ mixed crystals reported by T Murahashi and T Koda [*J. phys. Soc. Japan*, **40** (1976), 747] has been studied using a modified random-element-isodisplacement model with an effective electric field. The calculated long-wavelength transverse and longitudinal optical frequencies and their dependence on the composition x are calculated and compared with the existing experimental data. The force variations due to Br and I impurities producing gap modes in CuCl lattices are calculated and are found to be qualitatively in accordance with the results obtained from a more sophisticated lattice dynamical approach.

1. Introduction

Vibrational spectra of a large number of substitutional solid solutions of the type $A^{8-N}B^N_{1-x}C^N_x$ have been investigated intensively in the last few years by infrared absorption, neutron scattering and Raman scattering methods.[1-8] The experimentally observed spectra are generally in the form of fairly narrow lines with frequencies corresponding to the long-wavelength having optical vibrations. So far as the behaviour of optical phonons is concerned, the traditional division of solid solutions with composition x distinguishes essentially three types of crystal systems: one-mode (amalgamation) type, two-mode (persistent) type and one-two-mode type. A summary of the spectral and mode behaviour in various mixed crystals has been given by Chang and Mitra[1] and more recently by Barker and Sievers.[2] To explain the optical vibrations and to derive the criteria for one- and two-mode behaviour, the random-element-isodisplacement (REI) model[3] and its various ramifications[4-8] have been used. Although the REI model provides some basic understanding of the long-wavelength phonons, it fails to explain the true localized modes and specially the band modes. Using modified REI (MREI) model of Chang and Mitra,[1] Lucovsky *et al.*[7] have studied the long-wavelength optical phonons in $Al_{1-x}Ga_xP$ system and reported only the TO vibrations. Sobatta and Riede,[3] while calculating both the TO and LO mode frequencies for the same $Al_{1-x}Ga_xP$ system, noticed physically unreasonable results by MREI : e.g. for very weak oscillator strength, TO was found to be greater than LO mode frequency. Further, the criterion governing the mode behaviour of a solid solution on the basis of MREI model is sometimes disobeyed.[9]

Raman scattering spectra of mixed cuprous halides ($CuX_{1-x}Y_x$ with X, Y = Cl, Br and I) have been reported recently by Murahashi and Koda[9] for the composition x range (0-1). Apart from the calculation of the optical phonon modes by the MREI model, they analyzed the occurrence of impurity modes in the low concentration ($x \ll 1$) limit using linear-diatomic-chain model.[10] Murahashi and Koda,[9] however, realized that the linear-diatomic-chain model is insufficient for explaining precisely the occurrence of impurity modes (specially the gap modes) and the MREI model does not predict the observed mode behaviour in $CuCl_{1-x}Br_x$ system. The impurity modes in cuprous halides were studied earlier[11] by means of a more reliable lattice dynamical approach using the Green's function technique. When compared with the behaviour of isoelectronic impurities in ionic crystals (alkali halides)[12] and partially ionic (II-VI and III-V compound semiconductors) solids,[13,14] an interesting trend of force variation was noticed.

In the present paper we have studied the phonon mode behaviour in $CuCl_{1-x}Br_x$ and $CuCl_{1-x}I_x$ systems using MREI model including the influence of effective electric field on the motion of the ions. The calculated results have been compared with and discussed in relation to the existing experimental data. It has been noticed that the force variations obtained for Br and I impurities in CuCl lattice are qualitatively in accordance with the results obtained

* Present Address : Department of Physics, University of Houston, Central Campus, Houston, TX 77004 USA

from a more sophisticated lattice dynamical approach.

2. REI Model—A New Representation

The REI model for mixed ($AB_{1-x}C_x$) crystals is based on the assumption that the distribution of impurities between the sites in one sub-lattice is random and that the displacements of ions of each kind are homogeneous throughout the crystal. A successful variant of this model by including effective electric field acting on the atoms are proposed by Gorska and Nazarewicz.[4] The three equations of motion for the virtual crystal unit cell (Fig. 1) in the REI model can be written as:

$$\left.\begin{aligned} M_A \ddot{u}_A &= -(1-x)\,\phi_{AB}\,(u_A-u_B)-x\,\phi_{AC}\\ &\quad (u_A-u_C)+e_A E_{eff}\\ M_B \ddot{u}_B &= -\phi_{AB}\,(u_B-u_A)-x\,\phi_{BC}\,(u_B-u_C)\\ &\quad -e_B E_{eff}\\ M_C \ddot{u}_C &= -\phi_{AC}\,(u_C-u_A)-(1-x)\,\phi_{BC}\\ &\quad (u_C-u_B)-e_C E_{eff} \end{aligned}\right\} \quad ...(1)$$

where M_A, M_B and M_C are the masses of the atoms; u_A, u_B and u_C are their respective displacements from equilibrium; and e_A, $-e_B$ and $-e_C$ are the effective charges on A, B and C atoms respectively. The three coupling constants connected with A-B, A-C and B-C atoms are denoted by the terms ϕ_{AB}, ϕ_{AC} and ϕ_{BC} and they are assumed to be linear functions of the composition x, i.e.

$$\phi_{AB}(x)/\phi_{AB}(0) = \phi_{AC}(x)/\phi_{AC}(0) = \phi_{BC}(x)/\phi_{BC}(0) = (1-\theta x) \quad ...(2)$$

From charge neutrality, it follows that

$$e_A = (1-x)\,e_B + x e_C \quad ...(3)$$

In the case of cubic crystals, the local field E_{eff} can be represented by a sum of the macroscopic and Lorentz fields:

$$E_{eff} = E + \frac{4\pi}{3} P \quad ...(4)$$

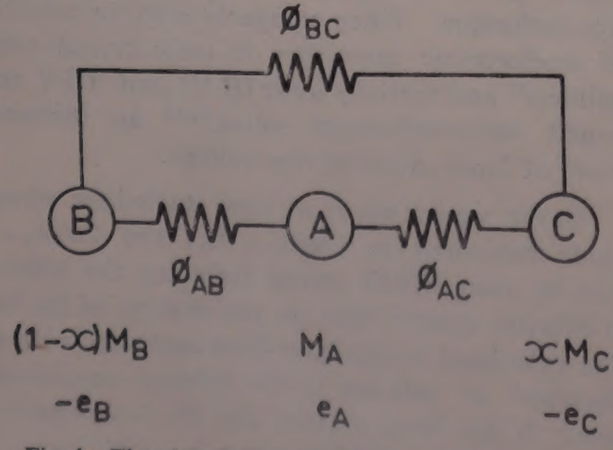

Fig. 1—The virtual crystal unit for the mixed crystals $AB_{1-x}C_x$

where P is the macroscopic polarization given by

$$P = N[e_A u_A - (1-x)\,e_B u_B - x e_C u_C] + N\alpha E_{eff}. \quad ...(5)$$

The term N in Eq. (5) is the atom pair density and α the electronic polarizability related to the high frequency dielectric constant ϵ_∞ by the well known Clausius-Mossotti formula:

$$\frac{4\pi}{3} N\alpha = \frac{\epsilon_\infty - 1}{\epsilon_\infty + 2} \quad ...(6)$$

Further, N and ϵ_∞ depending on x, are usually linearly interpolated between the values of the pure compounds AB and AC:

$$N = (1-x)\,N_{AB} + N_{AC}\,x \quad ...(7)$$

and $$\epsilon_\infty = (1-x)\,\epsilon_{\infty AB} + x\,\epsilon_{\infty AC} \quad ...(8)$$

The optical phonon modes of the system $AB_{1-x}C_x$ can be determined from the secular equation [Eq. (1)]. For TO phonons $E \approx 0$. Using Eqs. (1), (4) and (5), the TO mode frequencies ω_{TO_1} and ω_{TO_2} in the harmonic approximation yields:

$$\omega^2_{TO_{1,2}} = \frac{1}{2}(K_1+K_2) \pm \left[\frac{1}{4}(K_1-K_2)^2 + K_{12}K_{21}\right]^{1/2} \quad ...(9)$$

with

$$K_1 = \left[(1-x)\,\phi'_{AB}/M_A\right] + \left(\phi'_{AB}/M_B\right) + \left(\phi'_{BC}/M_B\right)$$

$$K_2 = \left(x\,\phi'_{AC}/M_A\right) + \left(\phi'_{AC}/M_C\right) + \left[(1-x)\,\phi'_{BC}/M_C\right]$$

$$K_{12} = x\left(\phi'_{AC}/M_A - \phi'_{BC}/M_B\right)$$

$$K_{21} = (1-x)\left(\phi'_{AB}/M_A - \phi'_{BC}/M_C\right)$$

and

$$\phi'_{AB} = \phi_{AB} - \frac{4\pi}{3} N e_A e_B \left(\frac{\epsilon_\infty+2}{3}\right)$$

$$\phi'_{AC} = \phi_{AC} - \frac{4\pi}{3} N e_A e_B \left(\frac{\epsilon_\infty+2}{3}\right)$$

$$\phi'_{BC} = \phi_{BC} - \frac{4\pi}{3} N e_B e_C \left(\frac{\epsilon_\infty+2}{3}\right)$$

The LO phonons, on the other hand, are characterized by vanishing electric displacement, $D = 4\pi E + P = 0$. Using this condition along with Eqs. (1),

(4) and (5), one may get ω_{LO1} and ω_{LO2} by an equation similar to Eq. (9), but ϕ'_{AB}, ϕ'_{AC} and ϕ'_{BC} are now replaced by ϕ''_{AB}, ϕ''_{AC} and ϕ''_{BC} where

$$\phi''_{AB} = \phi_{AB} + \frac{8\pi}{3} N e_A e_B \left(\frac{\epsilon_\infty + 2}{3\epsilon_\infty} \right)$$

$$\phi''_{AC} = \phi_{AC} + \frac{8\pi}{3} N e_A e_C \left(\frac{\epsilon_\infty + 2}{3\epsilon_\infty} \right)$$

$$\phi''_{BC} = \phi_{BC} - \frac{8\pi}{3} N e_B e_C \left(\frac{\epsilon_\infty + 2}{3\epsilon_\infty} \right)$$

3. Determination of Parameters and Results

To obtain the optic phonon energies for the mixed crystals $CuCl_{1-x}Br_x$ and $CuCl_{1-x}I_x$ as a function of concentration, we start from the macroscopic data of CuCl-CuBr and CuCl-CuI (Table 1). The physical constants can be derived in the following way. The atom pair density N_{AB} is related to the lattice constant a_{AB} in the zinc blende-type crystals by

$$N_{AB} = 4/a_{AB}^3 \qquad ...(10)$$

Using the well known LST relation one may obtain the LO frequency as

$$\frac{\omega_{LO\ AB}}{\omega_{TO\ AB}} = \left(\frac{\epsilon_{0\ AB}}{\epsilon_{\infty\ AB}} \right)^{1/2} \qquad ...(11)$$

and the Szigettis effective charge e^*_{AB} (= e_B in the present model) can be found by

$$e_{AB} = \left(\frac{\epsilon_{0AB} - \epsilon_{\infty\ AB}}{4\pi} \right) \frac{3\,\omega^2_{TO\ AB}}{(\epsilon_{\infty\ AB}+2)} \frac{\mu_{AB}}{N_{AB}} \qquad ...(12)$$

Table 1—Macroscopic Data for the Mixed Cuprous Halides

Parameter	CuCl	CuBr	CuI
a, Å	5·41	5·69	6·043
ϵ_∞	3·61*	3·71*	4·84*
ϵ_0	7·9*	6·6*	6·5*
ω_{LO}, cm^{-1}	207†, 210‡	170§, 166‡	160@, 148‡
ω_{TO}, cm^{-1}	168†, 170‡	136§, 135‡	124@, 130‡
ω_{imp}, cm^{-1}	150 (CuCl:Br) 148 (CuCl:I)	196 (CuBr:Cl)	186 (CuI:Cl)
μ	22·8	35·4	42·3

* Potts *et al.*, *Phys. Rev.*, **B9** (1974), 2711; *Solid St. Commun.*, **13** (1973), 389.

† Prevot B *et al.*, *J. Phys. C*, **10** (1977), 3999.

‡ Murahashi T & Koda T, *J. Phys. Soc. Japan*, **40** (1976), 747.

§ Hoshino *et al.*, *J. phys. Soc. Japan*, **41** (1976), 965.

@ Carabatos *et al.*, *Phys. Rev. Lett.*, **26** (1971), 770.

where

$$\mu_{AB} = \frac{M_A \cdot M_B}{M_A + M_B}$$

The parameters $\phi_{AB}(0)$, $\phi_{AC}(0)$, $\phi_{BC}(0)$ and θ can be obtained by solving Eq. (9) for the limiting values of x. For transverse optical vibrations this yields: For $x = 0$

$$\omega^2_{TO\ AB} = \frac{\phi_{AB}(0)}{\mu_{AB}} - \frac{4\pi}{9} \frac{N_{AB}}{\mu_{AB}} e^{*2}_{AB} (\epsilon_{\infty\,AB}+2)$$

and

$$\omega^2_{imp\,AB} = \frac{\phi_{AB}(0)+\phi_{BC}(0)}{M_C}$$

...(13)

For $x = 1$

$$\omega^2_{TO\,AC} = \frac{\phi_{AC}(0)(1-\theta)}{\mu_{AC}} - \frac{4\pi}{9} \frac{N_{AC}}{\mu_{AC}} (e_{\infty\,AC} + 2)$$

and

$$\omega^2_{imp\ AC} = \frac{[\phi_{AB}(0)+\phi_{BC}(0)]}{M_B}(1-\theta)$$

...(14)

where $\omega_{imp\ AB}$ and $\omega_{imp\ AC}$ are the impurity mode (gap or local) frequencies of C in AB and B in AC crystal respectively. Similar equations can be formulated for LO mode frequencies. The composition dependence of the optical phonons in the mixed crystals has thus been found taking θ as an adjustable parameter that provides a good fit to the experimental data.

4. Discussion

The results of our calculations together with the experimental data of Murahashi and Koda[9] are shown in Figs. 2 and 3 for the values of the parameters given in Table 2 for $CuCl_{1-x}Br_x$ and $CuCl_{1-x}I_x$ systems respectively. It can be noted that the REI model including the concept of effective electric field provides two-mode behaviour in concurrence with the Raman scattering measurements. The dependence of the LO and TO phonon modes with the composition x is generally good and is well within the expectations of the simplified model. We find that the mode-behaviour in $CuCl_{1-x}Br_x$ system is relatively better understood than in $CuCl_{1-x}I_x$ system. It is believed that the discrepancy in the calculated and the observed values in $CuCl_{1-x}I_x$ system is partly due to the non-availability of the experimental data for a major composition range and partly because of large difference in the LO (Γ) and TO (Γ) values observed from equally reliable two different (Raman scattering and

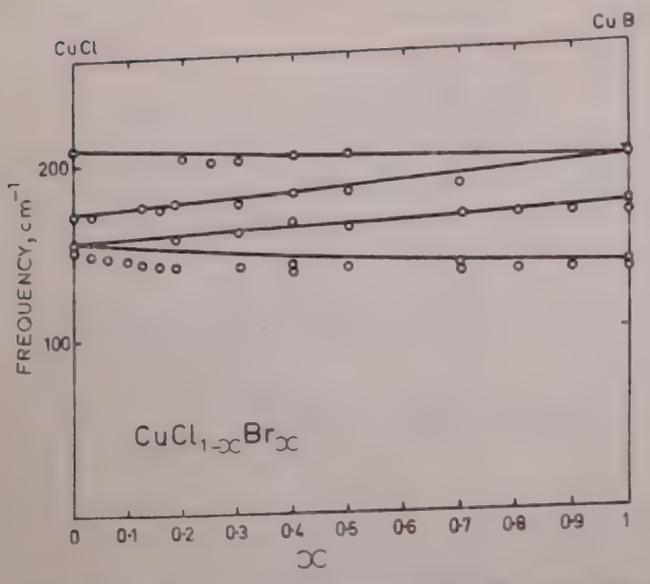

Fig. 2—LO and TO mode frequencies of $CuCl_{1-x}$ Br_x system [The solid lines correspond to the calculated values obtained by the present model for the values of the parameters given in Table 2. The experimental data of Murahashi and Koda[9] are represented by open circles]

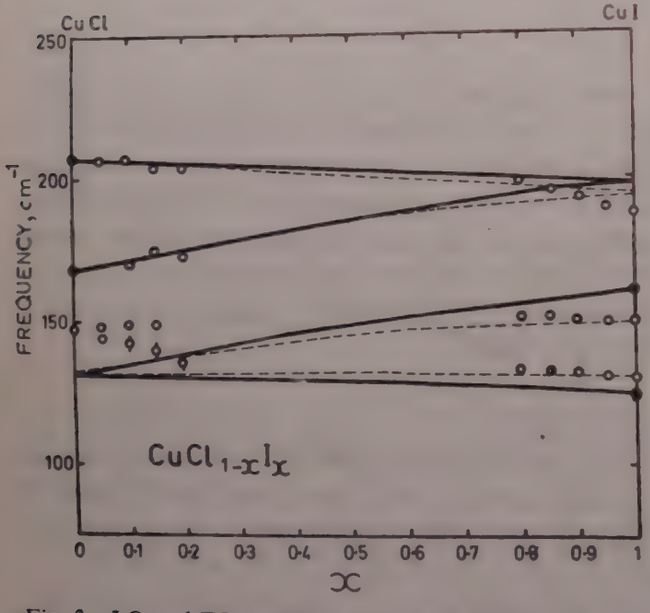

Fig. 3 – LO and TO mode frequencies of $CuCl_{1-x}$ I_x system [The dotted lines correspond to the values of the parameters fitted by the Raman data of Murahashi and Koda[9] (II set of parameters of Table 2). The solid lines correspond to the inelastic data of long-wavelength phonons. Full circles represent the neutron data.]

Table 2—Values of the Parameters Used in the Calculation of Long-Wavelength Optical Phonons by the REI Model with Effective Electric Field for $CuCl_{1-x}$ Br_x and $CuCl_{1-x}$ I_x Systems

	$CuCl_{1-x}$ Br_x	$CuCl_{1-x}$ I_x†	
		I	II
e^*_{AB}	0·525*e*	0·525*e*	0·525*e*
e^*_{AC}	0·590*e*	0·665*e*	0·505*e*
θ	0·204	0·216	0·264
ϕ_{AB} (0) ‡	0·505	0·505	0·505
ϕ_{AC} (0) ‡	0·660	0·718	0·710
ϕ_{BC} (0) ‡	0·480	0·540	0·570

† Two sets of parameters (I and II) calculated for $CuCl_{1-x}$ I_x systems are due to two different values available for long-wavelength phonons due to inelastic neutron scattering and Raman scattering experiments respectively. *e* stands for the electronic charge.

‡ The coupling constants are in 10^5 dyne/cm.

inelastic neutron scattering) sources of experiments. Again as the vibration of an impurity in the present model is governed by Eq. (13) in the extreme case of $x \approx 0$, this suggests a particular solution of the equation of motion of the impurity vibrating in an otherwise 'frozen' lattice — this is hardly a realistic situation for the vibration of heavy impurities producing gap modes. In actual case of a gap mode produced by Br (I) impurity atom in CuCl lattice, the Br (I) and Cu atoms vibrate in opposite phase; the mobile mass, should therefore, be taken as the reduced mass of CuBr (I) rather than that of the impurity mass alone. We feel that in the present model, the mobile mass is overestimated with respect to that involved in actual movements which is compensated for by choosing inconsistent values of the next nearest neighbours.

Since the coupling constant ϕ_{AC} (0) represents the interaction between Cu and isolated Br (I) impurity atoms in the low concentration limit ($x \approx 0$) and ϕ_{AB} (0) is the Cu-Cl binding in the host CuCl lattice, the force vibration due to Br (I) impurities in CuCl can be qualitatively calculated from the relation: ϕ_{AC} (0) $-$ ϕ_{AB} (0)]/ϕ_{AB} (0). It may be noted that the present simplified version of the REI model suggests stiffening in nearest-neighbour interaction ($\approx$ 30% due to Br and $\approx$ 42% due to I impurities in CuCl) which increases with the increase of the impurity size. Though the absolute values of force variation are different, the trend accords with that observed from a more sophisticated lattice dynamical approach using Green's function technique[11] and is consistent with the behaviour of isoelectronic impurities in ionic solids.[12] but is different from other zinc blende-type crystals.[13,14]

Acknowledgement

The authors are thankful to Dr Bal K Agrawal for his kind supervision and encouragement throughout the course of the work. One of us (DNT) is grateful to Drs M Vandevyver and K Kunc for many

helpful discussions. Thanks are also due to the authorities of CEA, Saclay for providing an opportunity to (DNT) as a collaborator in their services d'Electronique de Saclay.

References

1. Chang I F & Mitra S S, *Adv. Phys.*, 20 (1971), 359.
2. Barker A S & Sievers A J, *Rev. mod. Phys.*, 47 (1975), Suppl. 2.
3. Chen Y S, Shockley W & Pearson G L, *Phys. Rev.*, 151 (1966), 648.
4. Gorska M & Nazarewicz W, *Phys. Status Solidi B*, 65 (1974), 193.
5. Genzel L, Martin T P & Perry C H, *Phys. Status Solidi B*, I62 (1974), 83.
6. Jahney E, *Phys. Status Solidi B*, 74 (1976), 275; 75 (1976), 221.
7. Locovsky G, Burnham R D & Alimonda A S, *Phys. Rev.*, B14 (1976), 2503.
8. Sobotta H & Riede V, *Phys. Status Solidi*, 63 (1974), K143.
9. Murahashi T & Koda T, *J. phys. Soc. Japan*, 40 (1976), 747.
10. Lucovsky G, Brodsky M H & Burstein E, *Phys. Rev.*, B2 (1970), 3295.
11. Plumelle P, Talwar D N, Vandevyver M, Kunc K & Zigone M, *Phys. Rev. B* (1980), in Press.
12. Klein M V, cited in *Physics of color centres*, edited by W G Fowler (Academic Press, New York), 1968, 429.
13. Talwar D N & Agrawal Bal K, *Phys. Rev.*, B12 (1975), 1432; Vandevyver M & Plumelle P, *Phys. Rev.*, B17 (1978), 675.

Indian Journal of Pure & Applied Physics
Vol. 18, October 1980, pp. 738-742

Lattice Vibration Modes in KHF_2

HITOSHI KANAMORI, KEI URABE* & TETSURO NISHIMURA
Department of Electrical Engineering, Kyoto Technical University
Matsugasaki, Sakyo-ku, Kyoto 606, Japan

Received 4 *July* 1979

For long-wavelength lattice vibration in KHF_2, the symmetry coordinates and the normal coordinates of all the vibration modes have been derived using the GF-matrix method, and the latter briefly schematized. The force constants have also been derived. The frequencies of the optically inactive A_{2g} and B_{1u} modes have been predicted.

1. Introduction

Frequencies of long-wavelength lattice vibrations in KHF_2 crystal have been observed by means of Raman[1,2] and infrared[3,4] spectroscopy.

The material crystallizes in the space group D_{4h}^{18} ($I4/mcm$). The factor group analysis of the unit cell containing two formula units yields $A_{1g} + 2A_{2g} + B_{1g} + B_{2g} + 3A_{2u} + 2B_{1u} + 2E_g + 5E_u$ vibrations, where $A_{2u} + E_u$ species correspond to the acoustic vibration mode, $A_{1g} + B_{1g} + B_{2g} + 2E_g$ species to Raman active modes, and $2A_{2u} + 4E_u$ species to infrared active modes. The A_{2g} and B_{1u} modes are optically inactive.

In this paper, we have determined the force constants and normal coordinates of vibration modes by the use of the GF-matrix method, and predicted the frequencies of inactive modes.

2. Symmetry Coordinates

Fig. 1 shows the unit cell equivalent to the primitive cell, containing two formula units. The Cartesian coordinates (x_n, y_n, z_n) $(n = 1$ to $8)$ are set to denote the displacements of nth atom, parallel to the crystallographic (X, Y, Z)-axes.

The symmetry coordinates are given as follows:

$$(A_{1g})\quad S_1=(x_5+y_5-x_6+y_6+x_7-y_7-x_8-y_8)/\sqrt{8} \qquad \ldots(1)$$

$$(2A_{2g})\quad \left.\begin{aligned} S_2&=(z_1-z_2)/\sqrt{2}\\ S_3&=(x_5-y_5+x_6+y_6-x_7-y_7-x_8+y_8)/\sqrt{8}\end{aligned}\right\} \qquad \ldots(2)$$

$$(B_{1g})\quad S_4=(x_5-y_5-x_6-y_6+x_7+y_7-x_8+y_8)/\sqrt{8} \qquad \ldots(3)$$

$$(B_{2g})\quad S_5=(x_5+y_5+x_6-y_6-x_7+y_7-x_8-y_8)/\sqrt{8} \qquad \ldots(4)$$

$$(3A_{2u})\quad \left.\begin{aligned} S_6&=(z_1+z_2)/\sqrt{2}\\ S_7&=(z_3+z_4)/\sqrt{2}\\ S_8&=(z_5+z_6+z_7+z_8)/2\end{aligned}\right\} \qquad \ldots(5)$$

$$(2B_{1u})\quad \left.\begin{aligned} S_9&=(z_3-z_4)/\sqrt{2}\\ S_{10}&=(z_5-z_6-z_7+z_8)/2\end{aligned}\right\} \qquad \ldots(6)$$

$$(2E_g)\quad \left.\begin{aligned} S_{11a}&=(x_1-x_2)/\sqrt{2}\\ S_{11b}&=-(y_1+y_2)/\sqrt{2}\\ S_{12a}&=(z_5+z_6-z_7-z_8)/2\\ S_{12b}&=(z_5-z_6+z_7-z_8)/2\end{aligned}\right\} \qquad \ldots(7)$$

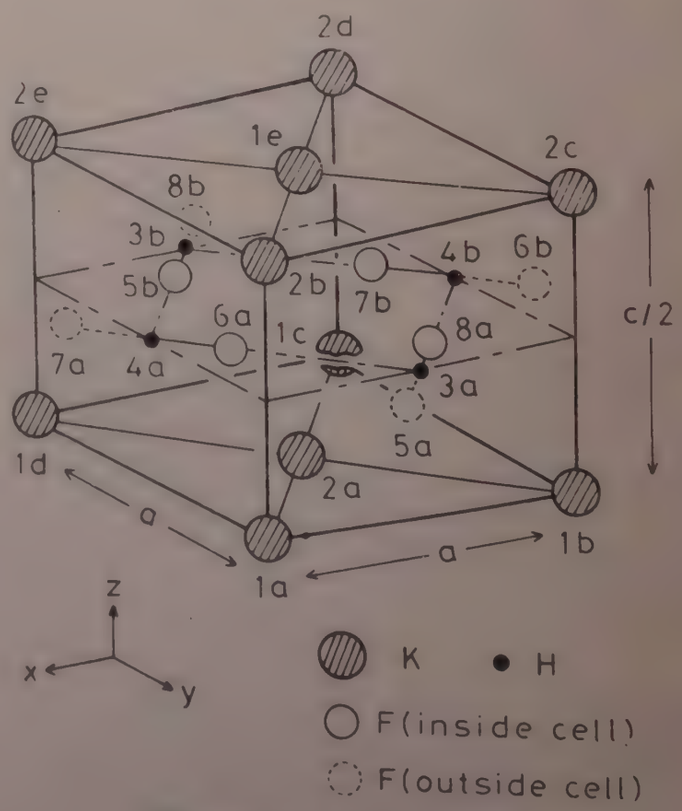

Fig. 1—Crystal structure of KHF_2

* Present Address: Industrial Products Research Institute Yatabe-machi, Ibaraki 305, Japan

$$
\left.
\begin{aligned}
(5E_u)\ s_{13a} &= (x_1 + x_2)/\sqrt{2}, \\
s_{13b} &= -(y_1 + y_2)/\sqrt{2} \\
s_{14a} &= (x_3 + x_4)/\sqrt{2}, \\
s_{14b} &= -(y_3 + y_4)/\sqrt{2} \\
s_{15a} &= (y_3 - y_4)/\sqrt{2}, \\
s_{15b} &= (-x_3 + x_4)/\sqrt{2} \\
s_{16a} &= (x_5 + x_6 + x_7 + x_8)/2 \\
s_{16b} &= -(y_5 + y_6 + y_7 + y_8)/2 \\
s_{17a} &= (y_5 - y_6 - y_7 + y_8)/2 \\
s_{17b} &= (-x_5 + x_6 + x_7 - x_8)/2
\end{aligned}
\right\} \quad \ldots(8)
$$

where s_{ia} and s_{ib} respectively transform according to the first and second rows of the doubly degenerate E representatives. From the symmetry coordinates, we can construct a U-matrix [Eq. (9) of Ref. 5].

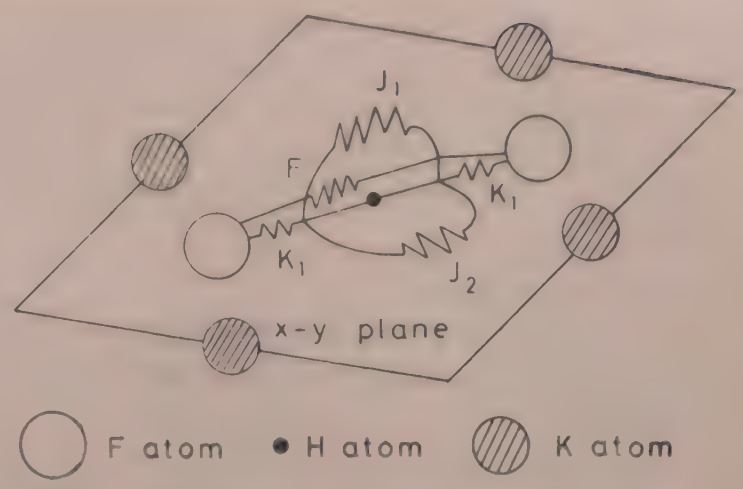

Fig. 2—Linear bending force constants J_1 and J_2, and a repulsive force constants F, put in F—H—F linear chain

3. Force Constants and Frequencies of Inactive Modes

For the calculation of force constants and frequencies of inactive modes by the GF-matrix method, we use five kinds of bond stretching coordinates and two kinds of linear bending coordinates and their relevant force constants shown in Tables 1 and 2. In Tables 1 and 2, the lables of atoms in Fig. 1 are used to specify the bonds and linear bendings. As shown in Fig. 2, we put linear bending force constants J_1 and J_2 along F—H—F linear chains in the XY plane; J_1 corresponds to the bending perpendicular to the XY plane, and J_2 to the bending in the XY plane (perpendicular to the c-axis). The repulsive force constant F expresses the repulsive force directly acting between the two F atoms in the F—H—F chain.

By inserting the eleven observed frequencies of the Raman and infrared active modes into the eigen values of the secular determinant [Eqs. (10)-(12) of Ref. 5], we have determined the eight force constants by means of the least square method. From the force constants we have predicted the frequencies of the inactive $2A_{2g}+2B_{1u}$ modes.

The observed frequencies and the calculated frequencies are given in Table 3. In Table 3, i.a.

Table 1—Bond Stretching Coordinates (Δr) and Their Relevant Force Constants (K)

End atoms of bonds	Force constant	No. of coordinates
$3a-8a$, $3b-5b$, $4a-6a$, $4b-7b$	K_1	4
$3a-6a$, $4b-8a$, $3b-7b$, $4a-5b$	K_2	4
$1e-3a$, $1e-4b$, $1e-3b$, $1e-4a$, $1d-4a$, $1a-3a$, $1a-4a$, $1b-3a$, $2a-3a$, $2a-4b$, $2a-3b$, $2a-4a$, $2e-4a$, $2b-3a$, $2b-4a$, $2c-3a$	K_3	16
$7b-8a$, $6b-8a$, $7b-8b$, $7b-5b$, $5b-7a$, $5b-6a$, $6a-5a$, $6a-8a$	K_4	8
$1e-8a$, $1e-7b$, $1e-5b$, $1e-6a$, $1c-7b$, $1d-5b$, $1a-6a$, $1b-8a$, $2a-8a$, $2a-7b$, $2a-5b$, $2a-6a$, $2d-7b$, $2e-5b$, $2b-6a$, $2c-8a$	K_5	16

Table 2—Linear Bending Coordinates ($\Delta\theta$) and Their Relevant Linear Bending Force Constants (J) and Repulsive Force Constant (F) [See Fig. 2]

Angle-forming atoms	Force constants	No. of coordinates
$5a-3a-8a$, $6a-4a-7a$	J_1, J_2, F	2

J_1 is perpendicular to the XY plane
J_2 is in the XY plane

Table 3—Observed and Calculated Frequencies of Lattice Vibration Modes

Mode	Obs.	Calc.
ν_1 (A_{1g})	602 (Ref. 4)	601
ν_2 (A_{2g})	i.a.*	182
ν_3 (A_{2g})	i.a.	79
ν_4 (B_{1g})	141 (Ref. 4)	127
ν_5 (B_{2g})	610 (Ref. 4)	611
ν_6 (A_{2u})	1234 (Ref. 2)	1234
ν_7 (A_{2u})	146 (Ref. 2)	156
ν_8 (A_{2u})	[acous.]	0
ν_9 (B_{1u})	i.a.	1234
ν_{10} (B_{1u})	i.a.	110
ν_{11} (E_g)	141 (Ref. 4)	137
ν_{12} (E_g)	102 (Ref. 4)	52
ν_{13} (E_u)	1440 (Ref. 2)	1440
ν_{14} (E_u)	1227 (Ref. 2)	1227
ν_{15} (E_u)	174 (Ref. 2)	177
ν_{16} (E_u)	130 (Ref. 2)	126
ν_{17} (E_u)	[acous.]	0

* i.a. denotes that they are optically inactive.

denotes optically inactive; their corresponding calculated frequencies are the frequencies predicted. The agreement between the observed and the calculated frequencies is good except in the case of E_g (ν_{12}) mode. The values of force constants are listed in Table 4.

4. Normal Coordinates

We express the normal coordinates as the linear combination of the symmetry coordinates as :

$$Q_1 = \sqrt{8}a_1 S_1 \quad \text{for } A_{1g} \quad \ldots(9)$$

$$\left.\begin{aligned} Q_2 &= \sqrt{2}a_2 S_2 + \sqrt{8}a_3 S_3 \\ Q_3 &= \sqrt{2}a_4 S_2 + \sqrt{8}a_5 S_3 \end{aligned}\right\} \text{for } A_{2g} \quad \ldots(10)$$

$$Q_4 = \sqrt{8}a_1 S_4 \quad \text{for } B_{1g} \quad \ldots(11)$$

$$Q_5 = \sqrt{8}a_1 S_5 \quad \text{for } B_{2g} \quad \ldots(12)$$

Table 4—Force Constants K, J and F (in mdyne/Å)

K_1	0·557	J_1	0·205
K_2	−0·0182	J_2	0·205
K_3	0.0308		
K_4	0·0454	F	1·726
K_5	0·0725		

Table 5—Coefficients in Normal Coordinates [Eqs. (9)-(16)]

a_1	1·000	a_{24}	−0·352	a_{47}	−0·236
a_2	0·249	a_{25}	−0·354	a_{48}	0·152
a_3	0·331	a_{26}	0·009	a_{49}	−0·135
a_4	0·559	a_{27}	0·009	a_{50}	0·225
a_5	−0·217	a_{28}	−0·001	a_{51}	−0·153
a_6	−0·001	a_{29}	0·352	a_{52}	0·236
a_7	0·707	a_{30}	0·354	a_{53}	−0·143
a_8	−0·018	a_{31}	−0·009	a_{54}	0·114
a_9	−0·364	a_{32}	−0·009	a_{55}	0·182
a_{10}	0·317	a_{33}	−0·001	a_{56}	0·145
a_{11}	0·366	a_{34}	0·349	a_{57}	0·185
a_{12}	0·354	a_{35}	−0·346	a_{58}	−0·193
a_{13}	0·354	a_{36}	−0·008	a_{59}	0·154
a_{14}	0·354	a_{37}	0·009	a_{60}	0·247
a_{15}	0·707	a_{38}	−0·001	a_{61}	0·195
a_{16}	−0·018	a_{39}	0·360	a_{62}	0·252
a_{17}	0·390	a_{40}	−0·358	a_{63}	−0·250
a_{18}	0·417	a_{41}	−0·009	a_{64}	−0·250
a_{19}	0·438	a_{42}	0·010	a_{65}	−0·250
a_{20}	0·302	a_{43}	−0·152	a_{66}	0·250
a_{21}	−0·371	a_{44}	0·136	a_{67}	0·250
a_{22}	0·426	a_{45}	−0·225	a_{68}	0·250
a_{23}	0·001	a_{46}	0·153		

$$\left.\begin{aligned} Q_6 &= \sqrt{2}a_6 S_6 + \sqrt{2}a_7 S_7 + 2a_8 S_8 \\ Q_7 &= \sqrt{2}a_9 S_6 + \sqrt{2}a_{10} S_7 + 2a_{11} S_8 \\ Q_8 &= \sqrt{2}a_{12} S_6 + \sqrt{2}a_{13} S_7 + 2a_{14} S_8 \end{aligned}\right\} \text{for } A_{2u} \quad \ldots(13)$$

(acoustic)

$$\left.\begin{aligned} Q_9 &= \sqrt{2}a_{15} S_9 + 2a_{16} S_{10} \\ Q_{10} &= \sqrt{2}a_{17} S_9 + 2a_{18} S_{10} \end{aligned}\right\} \text{for } B_{1u} \quad \ldots(14)$$

$$\left.\begin{aligned} Q_{11a} &= \sqrt{2}a_{19} S_{11a} + 2a_{20} S_{12a} \\ Q_{11b} &= \sqrt{2}a_{19} S_{11b} + 2a_{20} S_{12b} \\ Q_{12a} &= \sqrt{2}a_{21} S_{11a} + 2a_{22} S_{12a} \\ Q_{12b} &= \sqrt{2}a_{21} S_{11b} + 2a_{22} S_{12b} \end{aligned}\right\} \text{for } E_g \quad \ldots(15)$$

$$\left.\begin{aligned}
Q_{13a} &= \sqrt{2}a_{23} S_{13a} + \sqrt{2}a_{24} S_{14a} + \sqrt{2}a_{25} S_{15a} \\
&\quad + 2a_{26} S_{16a} + 2a_{27} S_{17a} + \sqrt{2}a_{28} S_{13b} \\
&\quad + \sqrt{2}a_{29} S_{14b} + \sqrt{2}a_{30} S_{15b} + 2a_{31} S_{16b} \\
&\quad + 2a_{32} S_{17b} \\
Q_{13b} &= -\sqrt{2}a_{23} S_{13b} - \sqrt{2}a_{24} S_{14b} - \sqrt{2}a_{25} S_{15b} \\
&\quad - 2a_{26} S_{16b} - 2a_{27} S_{17b} + \sqrt{2}a_{28} S_{13a} \\
&\quad + \sqrt{2}a_{29} S_{14a} + \sqrt{2}a_{30} S_{15a} + 2a_{31} S_{16a} \\
&\quad + 2a_{32} S_{17a} \\
Q_{14a} &= \sqrt{2}a_{33} S_{13a} + \sqrt{2}a_{34} S_{14a} + \sqrt{2}a_{35} S_{15a} \\
&\quad + 2a_{36} S_{16a} + 2a_{37} S_{17a} + \sqrt{2}a_{38} S_{13b} \\
&\quad + \sqrt{2}a_{39} S_{14b} + \sqrt{2}a_{40} S_{15b} + 2a_{41} S_{16b} \\
&\quad + 2a_{42} S_{17b} \\
Q_{14b} &= -\sqrt{2}a_{33} S_{13b} - \sqrt{2}a_{34} S_{14b} - \sqrt{2}a_{35} S_{15b} \\
&\quad - 2a_{36} S_{16b} - 2a_{37} S_{17b} + \sqrt{2}a_{38} S_{13a} \\
&\quad + \sqrt{2}a_{39} S_{14a} + \sqrt{2}a_{40} S_{15a} + 2a_{41} S_{16a} \\
&\quad + 2e_{42} S_{17a} \\
Q_{15a} &= \sqrt{2}a_{43} S_{13a} + \sqrt{2}a_{44} S_{14a} + \sqrt{2}a_{45} S_{15a} \\
&\quad + 2a_{46} S_{16a} + 2a_{47} S_{17a} + \sqrt{2}a_{48} S_{13b} \\
&\quad + \sqrt{2}a_{49} S_{14b} + \sqrt{2}a_{50} S_{15b} + 2a_{51} S_{16b} \\
&\quad + 2a_{52} S_{17b} \\
Q_{15b} &= -\sqrt{2}a_{43} S_{13b} - \sqrt{2}a_{44} S_{14b} - \sqrt{2}a_{45} S_{15b} \\
&\quad - 2a_{46} S_{16b} - 2a_{47} S_{17b} + \sqrt{2}a_{48} S_{13a} \\
&\quad + \sqrt{2}a_{49} S_{14a} + \sqrt{2}a_{50} S_{15a} + 2a_{51} S_{16a} \\
&\quad + 2a_{52} S_{17a} \\
Q_{16a} &= \sqrt{2}a_{53} S_{13a} + \sqrt{2}a_{54} S_{14a} + \sqrt{2}a_{55} S_{15a} \\
&\quad + 2a_{56} S_{16a} + 2a_{57} S_{17a} + \sqrt{2}a_{58} S_{13b} \\
&\quad + \sqrt{2}a_{59} S_{14b} + \sqrt{2}a_{60} S_{15b} + 2a_{61} S_{16b} \\
&\quad + 2a_{62} S_{17b} \\
Q_{16b} &= -\sqrt{2}a_{53} S_{13b} - \sqrt{2}a_{54} S_{14b} - \sqrt{2}a_{55} S_{15b} \\
&\quad - 2a_{56} S_{16b} - 2a_{57} S_{17b} + \sqrt{2}a_{58} S_{13a} \\
&\quad + \sqrt{2}a_{59} S_{14a} + \sqrt{2}a_{60} S_{15a} + 2a_{61} S_{16a} \\
&\quad + 2a_{62} S_{17a} \\
Q_{17a} &= \sqrt{2}a_{63} S_{13a} + \sqrt{2}a_{64} S_{14a} + 2a_{65} S_{16a} \\
&\quad + \sqrt{2}a_{66} S_{13b} + \sqrt{2}a_{67} S_{14b} + 2a_{68} S_{16b} \\
&\quad \text{(acoustic)} \\
Q_{17b} &= -\sqrt{2}a_{63} S_{13b} - \sqrt{2}a_{64} S_{14b} - 2a_{65} S_{16b} \\
&\quad + \sqrt{2}a_{66} S_{13a} + \sqrt{2}a_{67} S_{14a} + 2a_{68} S_{16a} \\
&\quad \text{(acoustic)}
\end{aligned}\right\} \text{for } E_u \quad \ldots(16)$$

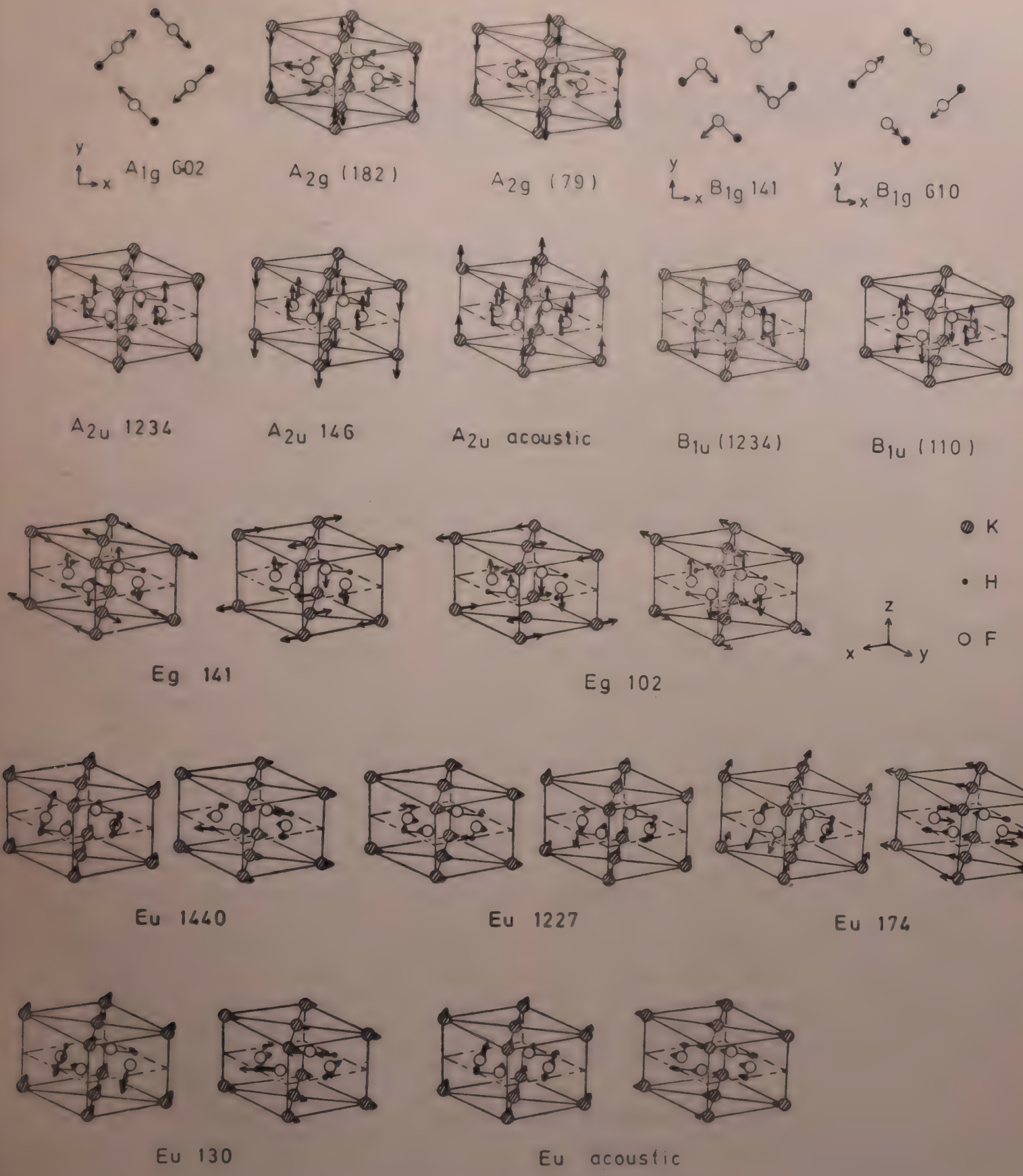

Fig. 3—Brief schemes of the normal modes in KHF_2

The coefficients a, which indicate the relative amplitudes of atomic motion in each mode, can be derived from the eigen vectors of the secular determinants [Eq. (13) of Ref. 5]. The values of a are listed in Table 5.

For example, the normal coordinate of ν_2 (A_{2g}) mode is

$$Q_{1a}=0{\cdot}249\,(z_1-z_2)\ +0{\cdot}331\,(x_5-y_5+x_6+y_6-x_7 - -y_7-x_8+y_8)$$

The brief schemes of all the normal coordinates are depicted in Fig. 3. In Fig. 3, the predicted frequencies of A_{2g} and B_{1u} modes are parenthesized.

In the A_{1g} and two B_{1g} modes, only F ions vibrate in XY plane. We can see rotatory internal vibration of F—H—F chains in the B_{1g} and two A_{2g} modes, and internal stretching in B_{2g} modes. In the three A_{2u} and two B_{1u} modes, we can see the vibration only in z-direction.

References

1. Mathieu J P & Couture-Mathieu L, *C. r. hebd, Séane. Acad. Sci., Pairs*, 228 (1950), 1054.
2. A Iqbal Z, *J. chem. Phys.*, 59 (1973), 6183.
3. Wilkinson G R, *Natn. Bur. Stand. (US) Spec. Publ.*, 301 (1969), 107.
4. Rush J J & Schroeder L W, *J. chem. Phys.*, 56 (1972), 2793.
5. Matsumoto M, Urabe K & Kanamori H, *Indian J. pure appl. Phys.*, 16 (1978), 263.

Indian Journal of Pure & Applied Physics
Vol. 18, October 1980, pp. 743-746

Piezo-Induced Mechanoluminescence & Photoluminescence of Triphenylamine Crystals

B P CHANDRA*
Department of Physics, Government College of Science, Raipur 492 002

Received 7 *July* 1979

The origin of mechanoluminescence (ML) in triphenylamine crystals has been investigated. The ML spectra resemble their photoluminescence spectra. The ML appears concurrently with the steps in the fracture region of the force versus compression curve of the crystals. Because an intense electric field may be produced as a result of the piezoelectrification of the newly-created surfaces, the molecular luminescence in tryphenylamine crystals may be excited either due to the excitation of the luminescence centres by the collision of accelerated electrons or due to the recombination of positive and negative carriers near the tip of the mobile cracks. Since the electric field between the newly-created surfaces may be neutralized internally before the filling up of the intervening space by the atmospheric nitrogen, the gas discharge may not accompany the molecular ML of triphenylamine crystals. The gas discharge may also be absent due to the quenching of the nitrogen emission by the molecules of the crystals.

1. Introduction

The emission of light during mechanical action on solids is known for hundreds of years. In earlier times, it was thought to be due to the heat produced during rubbing of the crystals[1] and given the name triboluminescence.[2] The recent investigations on a number of crystals have suggested that the emission of light during mechanical action on solids is not attributable to heat production or only to friction. However, it is caused by either one or the combined effect of the three mechanisms: first, by the piezoelectrification of the newly-created surfaces; second, by the cleavage-electrification of the newly-created surfaces; and third, by the movement of dislocations in crystals. In fact, the phenomenon of light emission during mechanical action on solids has been given the general name mechanoluminescence.[3,4] On the basis of mechanism of excitation, the machanoluminescence (ML) may be classified into three types: piezo-induced, cleavage-induced and dislocation-induced ML. The ML in sugar, tartaric acid, uranyl intrate, etc. is typical of piezo-induced ML.[5] The ML in copper sulphate, barium chlorate, sodium chloride, etc which are non-piezoelectric and show ML only during their fracture,[6,7] is typical of cleavage-induced ML, and the ML in coloured alkali halide crystals is an example of dislocation-induced ML.[8-10] The ML of zinc sulphide phosphors is still doubtful whether it is caused by the piezo-electrification[9,11] or by the movement of dislocations.[10,12]

On the basis of the ML spectra, the mechanoluminescent substances can be grouped into three classes,[13] (1) substances, the ML spectra of which resemble the discharge spectra of surrounding gases; (2) substances, the ML spectra of which resemble their molecular luminescence spectra; and (3) substances, the ML spectra of which consist of both the gas discharge and molecular spectra. The origin of gas discharge ML can be explained in terms of the creation of charged surfaces during the crystal fracture in which the excitation of gas molecules takes place by the electrons accelerated between the surfaces.[5,14,15] However, the complexity of ML resembling the molecular luminescence, has not yet been solved.[16] The present paper reports on the origin of ML in triphenylamine crystals. The ML and photoluminescence (PL) spectra are similar.

2. Experimental Details

Single crystals of triphenylamine were grown by the slow evaporation of their solution in acetone. The ML spectra were taken by following the method employed in the earlier investigation.[17] In this method, the crystals were broken in a glass vial with a stainless steel rod. The light emitted as a result of the application of this mechanical stress is split by a beam splitter which sends about 12% directly to an EMI 9558 Q photomultiplier tube, while the other 88% travels through a Bausch and Lomb 1-m excitation monochromator set at a particular wavelength and reaches to the second EMI 9558 Q photomultiplier tube. The photomultipliers were cooled to − 20°C

* Present Address: Department of Chemistry, University of California, Los Angeles, California 90024, USA

to avoid the noise during the measurements. The two readings (labelled I_λ and I_T for wavelength and total readings) were amplified and integrated over a large number of individual flashes. The ratio of I_λ/I_T removes variations in intensity caused by any variations in the applied mechanical energy, crystal size, etc. At least, four readings were taken at each wavelength. The results were averaged and plotted as a function of wavelength with error bars of one standard deviation. The PL spectra of crystals were obtained on a Spex Fluorolog spectrofluorometer. No corrections for the response characteristics of the instruments were made. The ML and PL spectra were taken at room temperature.

The simultaneous measurements of the ML versus compression curve and the force versus compression curve of single crystals were carried out using the method described previously.[18] In this method, the crystals were compressed by a table model Instron testing machine and the ML intensity was monitored by an IP 28 photomultiplier tube. The ML versus compression curve of the crystal was determined at the compression rate of $1{\cdot}69\times10^{-3}$ mm/sec. The crystals used for this purpose were made to the required size by grinding and polishing.

3. Results and Discussion

Fig. 1 shows the ML and PL spectra of triphenylamine crystals. It is seen that the ML spectra resemble their PL spectra. The PL of triphenylamine crystals which has lifetime 2·68 msec may be assigned to ($S_0 \rightarrow T_1$) excitation.[19] Thus, from the resemblance of PL and ML spectra, the latter may also be assigned to the ($S_0 \rightarrow T_1$) excitation. Fig. 1 shows the increased ML intensity towards higher wavelength side with respect to the PL Spectra. No gas discharge is found in the ML of triphenylamine crystals.

The force versus compression and the ML versus compression curve of an $6\times5\times4$ mm³ single crystal of triphenylamine is shown in Fig. 2. The ML appears only during the steps which occur in the fracture region of force versus compression curve of the crystal. The steps in the fracture region of the force versus compression curve are caused by the movement of cracks in the crystal.[20] Hence, the appearance of ML only when the steps occur in the force versus compression curve of a crystal suggests that the ML in these crystals requires the motion of cracks.

Because the ML does not appear in the elastic and plastic regions of the crystals, the dislocation-induced ML can be ruled out. Since triphenylamine is a molecular crystal, the possibility of cleavage-induced ML can also be eliminated.

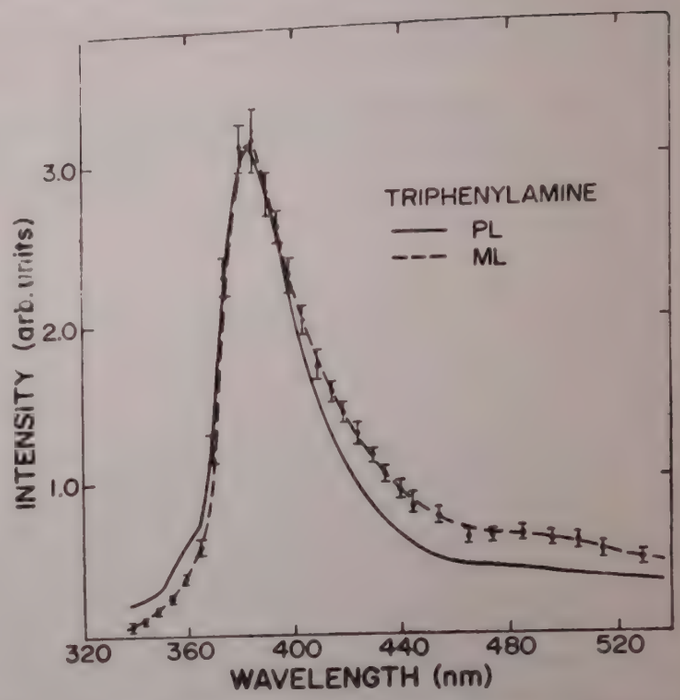

Fig. 1—Mechanoluminescence and photoluminescence spectra of triphenylamine crystals

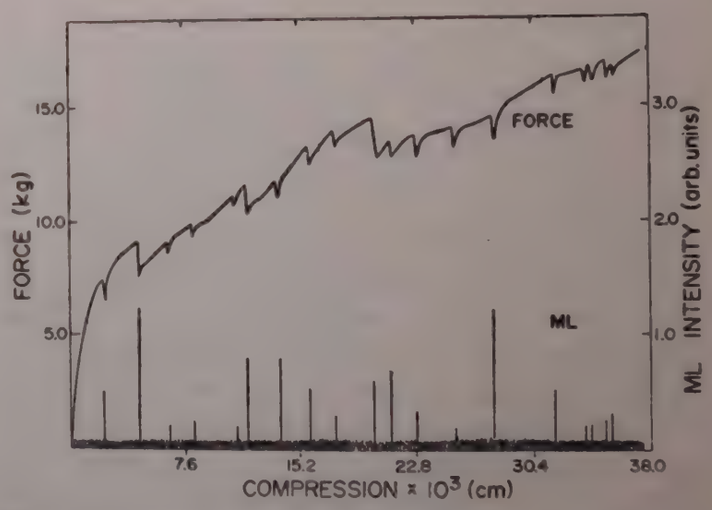

Fig. 2—ML versus compression curve of a $6\times5\times4$ mm³ triphenylamine crystal and its simultaneous force versus compression curve

As the triphenylamine crystals belong to the A_a space group[21] which is piezoelectric under compression, torsion and hydrostatic deformation, the origin of ML may be understood with the help of Langevin's model[22] of creation of charged surfaces during breaking of a crystal. Fig. 3 shows the piezoelectrification of newly-created surfaces during propagation of a crack in a crystal. When a stress is applied to a piezoelectric crystal, its one surface is positively charged and the opposite surface is negatively charged. Due to the movement of a crack in the crystal, new surfaces are created. The newly-created surface nearer to the positively charged surface of the crystal, is negatively charged, and the newly-created surface nearer to the negatively charged surface of the

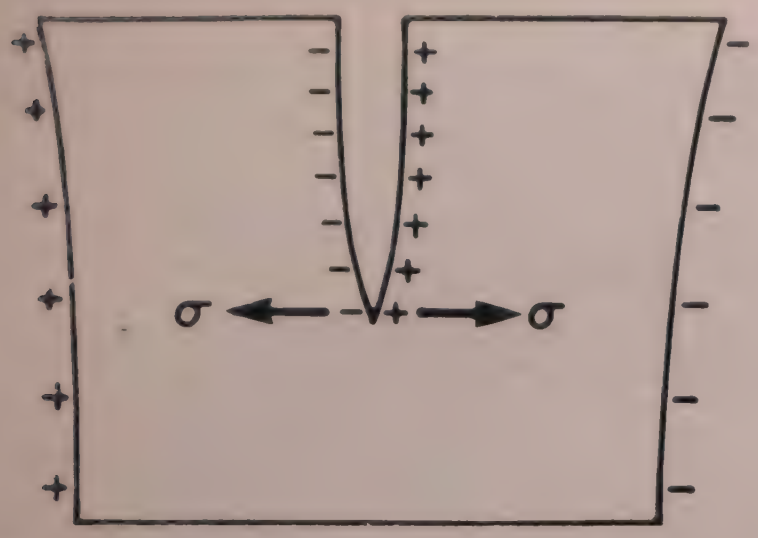

Fig. 3—Creation of charged surfaces during propagation of a crack in a piezoelectric crystal

crystal, is positively charged. Thus, an intense electric field may be produced between the newly-created surfaces of the crystal. For the simplification of the estimation of the electric field, let us make certain assumptions: (i) that the piezoelectric constants remain unchanged up to the fracture stress of the crystal, (ii) that the stress near the tip of the mobile crack acts along a polar direction of the crystal and, (iii) that the stress near the tip of the crack is not relaxed before the ML excitation. The piezoelectric and elastic constants of triphenylamine crystals have not been determined. However, it is known that the piezoelectric constants and the stress needed to separate the surfaces of the crystals are generally of the order of 10^{-12} coul N^{-1} and $10^{8}Nm^{-2}$ respectively.[23,24] Thus, the charge-density (ρ) near the tip of the mobile crack will be of the order of 10^{-4} cm^{-2}[22]. The electric field between the oppositely charged surfaces will be ρ/ϵ_0, that is, nearly 10^{7} Vm^{-1}, where ϵ_0 is the permittivity constant. This field is sufficient to break down the nitrogen molecules between the newly-created surfaces.[25] Further, the field needed for the dielectric breakdown of the crystal is more compared to that of the nitrogen molecules. As such, the appearance of gas discharge is expected during fracture of triphenylamine crystals. However, no gas discharge is found in the ML of triphenylamine crystals. This suggests that there is some process which provides a fast leakage of charge on the newly-created surfaces. It seems that the luminescence centres near the tip of the mobile cracks are ionized due to the intense electric field and the conduction of the electrons so obtained neutralizes the charge on the newly-created surfaces. If the charge leakage occurs very fast, the electric field between the newly-created surfaces may decrease to a less value before the filling up of the space between the newly-created surfaces by the atmospheric nitrogen. As such, the gas discharge ML cannot be observed. However, the molecular luminescence may be observed either due to the excitation of the luminescence centres by the collision of the accelerated electrons or due to the recombination of positive and negative carriers near the tip of the mobile cracks. The gas discharge may also be absent due to the quenching of the nitrogen emission by the molecules of the crystals.

Because most of the organic crystals exhibiting molecular ML are not cathodoluminescent, they are likely to prefer the ML excitation by the recombination of positive and negative carriers rather than the ML excitation by the collision of accelerated electrons to the luminescence centres. In this connection, it will be worth describing briefly the ionic states of organic molecular crystals. On the basis of the electronic states, the solids can generally be characterized as insulators, semiconductors, or metals.[26] However, in some respects organic molecular crystals differ from this scheme. As the electrons are highly localized, the concepts of a valence band and a conduction band are not very useful for the description of the lower energy states of the organic molecular solids. These states are described better by the Frenkel tight-binding model in which the molecular states are the progenitors of crystal states.[27] Generally, at higher energies, it is expected that crystal states are not present in the free molecules.[28] These states, known as the ionic states, consist of an electron and an ionized molecule. Such states may be similar to the exciton and conducting states of the other solids or may be somewhat unique to the molecular solid. As for example, ion pair states in which an electron and hole are localized on neighbouring lattice sites are unique to the molecular solid. In analogy with other solids,[29] recombination luminescence in molecular crystals is considered to be initiated by the long-range capture of one carrier by the Coulomb field of another trapped or free carrier. After the capture, energy is lost by phonon emission and the electron-hole pair cascades through the manifold of ionic exciton states. Finally, a bound neutral molecular state is formed which relaxes to the fluorescent or phosphorescent level.[30] The recombination luminescence is reported to be similar to the normal fluorescence[31,32] with increased intensity at the longer wavelengths,[33] presumably due to the emission from traps acting as recombination centres.[34] The ML spectra of triphenylamine crystals (Fig. 1) also have the increased intensity towards the higher wavelength side with respect to the PL spectra, which is in accord with the explanation of ML by the recombination of opposite carriers. The spectra of

pulsed infrared laser-induced visible luminescence are similar to the ML spectra.[35] This fact also supports the possibility of ML excitation as a result of the recombination mechanism.

On the basis of the mechanism described for the ML excitation of triphenylamine crystals, the ML excitation of other crystals can also be understood. If the electric field between the newly-created surfaces is neutralized both by the conduction of electrons through the crystal as well as through the breakdown of the gases between the newly-created surfaces, then the ML spectra may consist of molecular luminescence and the gas discharge spectra. However, if there is no internal path for the leakage of the charge, then the field between the newly-created surfaces may be neutralized only by the breakdown of the intervening gases and the ML spectra may consist of only the gas discharge spectra.

Acknowledgement

The author thanks Prof. Jeffrey I Zink for providing the experimental facilities and Gordon E Hardy for his help. The author is also grateful to the Ministry of Education and Social Welfare, Government of India, for the award of a National Scholarship for Postdoctoral Research in USA.

References

1. Wedgood T, *Phil. Trans. R. Soc.*, 82 (1792), 28.
2. Weidemann E, *Ann. phys. Chem.*, 34 (1888), 446.
3. Chandra B P & Shrivastava K K, *J. Phys. Chem. Solids*, 39 (1978), 939.
4. Sodomka L, *Phys. Status Solidi* (a), 45 (1978), k171.
5. Walton A J, *Adv. Phys.*, 26 (1977), 887.
6. Imhof A, *Phys. Z.*, 18 (1917), 78.
7. Wolff G, Gross G & Stranski I N, *Z. Electrochem.*, 56 (1952), 420.
8. Chandra B P & Elyas M, *Kristall U. Tech.*, 11 (1978), 134.
9. Meyer K, Obrikat D & Rossberg M, *Kristall U. Tech.*, 5 (1970), 5, 181.
10. Alzetta G, Chudacek I & Scarmozzino R, *Phys. Status Solidi* (a), 1 (1970), 775.
11. Chudacek I, *Czech. J. Phys.*, 16 (1966), 520.
12. Scarmozzino R, *Solid St. Commun.*, 9 (1971), 1159.
13. Wick F G, *J. opt. Soc. Am.*, 27 (1937), 275.
14. Chandra B P, *Czech. J. Phys.*, B28 (1978), 84.
15. Longchambon H, *Bull. Soc. Franc. Miner.*, 48 (1925), 130.
16. Zink J I, *Accounts Chem. Res.*, 11 (1978), 289.
17. Hardy G E & Zink J I, *Inorg. Chem.*, 15 (1976), 3061.
18. Chandra B P & Zink J I, *Phys. Rev.*, B21 (1980), 816.
19. Mclure D S, *J. chem. Phys.*, 17 (1949), 905.
20. Wooster W A, *Textbook on crystal physics* (The University Press, Cambridge), 1938, 53.
21. Howells E R, Lovell F M, Rogers D & Wilson A J C, *Acta crystallogr.*, 7 (1954), 298.
22. Langevin M, *Reports et discursions du conseil de Physique tenu a Bruxelles en* 1913, Sous les auspices de L' Institut Solvay (Paris Grunthier-Villars), 1921, 251.
23. Mason W P, *Piezoelectric crystals and their application to ultrasonics* (Van Nostrand, New York), 1950, 230.
24. Cottrell A H, *Dislocations and plastic flow in crystals*, (Clarendon Press, Oxford), 1931, 11.
25. Thomson J J & Thomson G P, *Conduction of electricity through Gases* (Cambridge University Press, Cambridge), 1933, 487.
26. Ziman J M, *Principles of the theory of solids*, (Cambridge University Press, Cambridge), 1964, 4.
27. Robinson G W, *Ann. Rev. Phys. Chem.*, 21 (1970), 429.
28. Lyons L E, *Aust. J. Chem.*, 21 (1970), 429; *J. chem. Soc., Lond.*, (1957), 5001.
29. Lax M, *Phys. Rev.*, 119 (1960), 1502.
30. Hanson D M, *Crit. Rev. solid st. sci.*, 3 (1972), 243.
31. Helfrich W & Schneider W G, *Phys. Rev. Lett.*, 14 (1965), 229.
32. Lohman F & Mehl W, *J. chem. Phys.*, 50 (1969), 2920.
33. Ewald Mand Durvcher G, *Chem. Phys. Lett.*, 12 (1971), 385.
34. Williams D F & Schadt M, *J. chem. Phys.*, 53 (1970), 3480.
35. Hardy G E, Chandra B P, Zink J I, Adamson A W, Fukuda R & Walters R T, *J. Am. chem. Soc.*, 101 (1979), 2787.

Indian Journal of Pure & Applied Physics
Vol. 18, October 1980, pp. 747-750

Cation Distribution of Mn_2FeO_4—A Mössbauer Spectral Study*

S Bharati, M P Gupta, A P B Sinha & S K Date†
National Chemical Laboratory, Pune 411 008

Received 22 *August* 1979

The Mössbauer effect spectra of Mn_2FeO_4 have been studied in the temperature ragne 77-650 K. The spectra were computer analyzed to give two resolved subspectra, one arising from the trivalent iron ion at the tetrahedral site (A-site) and the other from that at the octahedral site (B-site) of the cubic spinel. Mössbauer parameters, viz. isomer shift, quadrupole splitting and the hyperfine magnetic field have been computed. The cation distribution for this spinel has been proposed.

1. Introduction

The spinel system $Mn_xFe_{3-x}O_4$ ($O < x < 3$) has been studied for various electrical and magnetic properties.[1-4] The semiconducting property is attributed to the electron hopping between the divalent and trivalent iron ions,[1] similar to electron hopping process in the case of magnetites,[5] although this formalism is severely questioned in the recent ME studies on pure magnetite[6] and Zn substituted magnetite.[7] For the Mn-rich compositions, a canted spin structure is suggested from the studies of magnetic properties.[4] The suggested cation valence and its distribution for the entire somposition is also quite diverse. Wickham[8] suggested the distribution as $Mn^{2+}_{0.6}\ Fe^{3+}_{2.4}\left[\ Fe^{3+}_{0.4}\ Fe^{3+}_{1.6}\ \right]\ O^{2-}_4$ for the system $Mn_{0.6}Fe_{2.4}O_4$ while Finch *et al.*[9] had another suggestion for the valence distribution given by the formula:

$$Mn^{2+}_{0.54}\ Fe^{3+}_{0.46}\left[\ Fe^{2+}_{0.06}\ Fe^{3+}_{1.88}\ Mn^{3+}_{0.06}\ \right]\ O^{2-}_4.$$

It is generally agreed that the A-site is occupied exclusively by the divalent manganese and trivalent iron ions.[10] NMR studies[11,12] confirm this and in addition show that Mn^{3+} ions occupy the B-site. If cation distribution is according to this model, pairwise electron hopping between Fe^{2+}/Fe^{3+} is expected. Such an observation has so far escaped the notice of many investigators,[4,10,13] and a complete understanding regarding the occupancy of cations at B-site is still lacking. The distribution of cations at B-site will be controlled by the reaction $Mn^{2+} + Fe^{3+} \rightleftharpoons Mn^{3+} + Fe^{2+}$ that may lie to the left hand side or the right hand side of the equation, depending on the thermodynamic conditions. The cation distribution will in general be given by

$$Mn^{2+}_{1-\epsilon}\ Fe^{3+}_{\epsilon}\left[\ Mn^{3+}_{x-1}\ Fe^{3+}_{3-\epsilon-x}\ Mn^{2+}_{\epsilon}\right]\ O^{2-}_4 \quad \ldots \text{Model-I}$$

if the equation is stable on the left hand side or by

$$Mn^{2+}_{1-\epsilon}\ Fe^{3+}_{\epsilon}\left[\ Mn^{3+}_{x+\epsilon-1}\ Fe^{3+}_{3-2\epsilon-x}\ Fe^{2+}_{\epsilon}\right]\ O^{2-}_4 \quad \ldots \text{Model-II}$$

when the equation is stable on the right hand side.

Tanaka *et al.*[14] suggested the cation distribution to be in accordance with Model-II and proposed distribution as

$$Mn^{2+}_{0.91}\ Fe^{3+}_{0.09}\left[\ Mn^{3+}_{1.09}\ Fe^{3+}_{0.82}\ Fe^{2+}_{0.09}\right]\ O^{2-}_4$$

through a Mössbauer study. However, a detailed study by the investigators is not available and hence such conclusions cannot be drawn without ambiguity. Electrical conductivity measurements[15] in this system led Lotgering to conclude that the Verwey pairwise electron hopping between the Fe^{2+} and Fe^{3+} ions is not present at B-site, as Fe^{2+} is not stable in the presence of Mn^{3+}. Recent investigations of Lotgering and van Diepen[16] in their study of paramagnetic Mössbauer spectra of $Mn_{1.8}Fe_{1.2}O_4$ confirm their earlier results and support Model-I for cation distribution. These results are in disagreement with the NMR results[11,12] where Mn^{2+} at B-site is not detected, and therefore, they support Model-II. It is well known[15] that the Jahn-Teller ion Mn^{3+} deforms the cubic spinel lattice for the Mn-rich compositions. The divalent iron ions are trapped in these local

*NCL Communication No. 2488

†Present Address : Tata Institute of Fundamental Research Bombay 400 005

distortions, which delocalize at higher temperatures,[16] giving rise to the semiconducting property at these temperatures.

We have, therefore, undertaken to investigate the system once again by Mössbauer spectroscopy over a wide range of temperatures in order to resolve the controversy and to establish the cation distribution for this system.

2. Experimental Technique

Manganese ferrite Mn_2FeO_4 was prepared by the usual ceramic technique. High purity AR grade oxides of Fe_2O_3, Mn_2O_3 and Johnson-Mathey spec-pure iron powder were mixed stoichiometrically, pressed into pellets and sealed in vacuum. Initial heating was done slowly, heating for 4 hr each at 600 and 800°C. The temperature was then raised to 1000°C and heating was continued for 50 hr. The sample was removed from the furnace, at least once during the 1000°C heating, crushed, repelleted and sealed in vacuum once again before the heating was resumed. Absorbers for the Mössbauer measurements were made with the samples enriched to at least 30% ^{57}Fe. The X-ray diffractograph of the sample using Cu$K\alpha$ radiation was taken, which confirmed a single-phase spinel structure with a lattice constant $a = 8{\cdot}50 \pm 0{\cdot}02$ Å. This result is different from the earlier result of Sinha *et al.*[17] and Buhl[18] according to whom the spinel is tetragonally distorted by the Mn^{3+} Jahn-Teller ion. This arises obviously from the fact that their samples were synthesized in air and consequently had a higher Mn^{3+} concentration. The results of Finch *et al.*[9] and Ishii *et al.*[19] from the infrared absorption spectral studies show that such a distortion of the lattice becomes prominent only for compositions $x \geqslant 2{\cdot}25$. It is possible that lower concentrations of Mn only distort the lattice locally and the random distortions thus created do not destroy the cubicity of the lattice as a whole till $x \geqslant 2{\cdot}25$. Our X-ray results are in agreement with these observations.

Mössbauer spectra were taken with a conventional constant acceleration spectrometer operating in conjunction with a 1024-channel analyzer. The calibration of the spectrometer was done with an α-Fe foil, using a 5 mCi ^{57}Co:Pd source. The absorber with enriched Mn_2FeO_4 was made with 13 mg sample which was uniformly spread over a 2·54 cm diameter disk. Spectra were recorded in the temperature range 77-650 K. All the spectra were analyzed by means of a standard MOSFIT programme.

3. Results and Discussion

The spectra were recorded both on samples which were slowly cooled and those which were quickly quenched from 1000°C to room temperature by dropping the ampule in water. At low temperatures (77-300 K), magnetic hyperfine split lines were recorded. A collapse of the hyperfine split spectra into a sharp asymmetric doublet was observed at temperatures above 485 K. A complex spectrum was observed near the transition temperature.

In the magnetic region, the spectra were not a simple 6-line pattern, but broad and asymmetric lines were observed. Spectral analysis for random polycrystalline samples were used. From the systematics of the Mössbauer spectra of spinel in general, the two resolved subspectra were assigned to the trivalent iron ions at A- and B-sites. The systematics of internal magnetic field, quadrupole interaction and isomer shift in ferrite spinel systems,[20] are as follows:

(i) Isomer shifts increase in the sequence:

IS (tetrahedral Fe^{3+}) < IS (octahedral Fe^{3+}) < IS (tetrahedral Fe^{2+}) < IS (octahedral Fe^{2+})

(ii) Quadrupole splitting for both Fe^{2+} and Fe^{3+} in sites of cubic symmetry is zero, and for non-cubic symmetry $\Delta_Q (Fe^{3+}) \ll \Delta_Q (Fe^{2+})$

(iii) The magnetic hyperfine field H_n $(Fe^{2+}) < H_n (Fe^{3+})$

(iv) Correlation between the differential isomer shift IS (B)-IS (A) and the difference in H_n (B)-H_n (A) are observed.

Fig. 1 shows the experimental curve, resolved subspectra and the resultant synthetic curve at 77 K and 528 K. The magnetic order is lost at higher temperature. The Mössbauer parameters, viz. isomer shift (IS), quadrupole splitting (Δ_Q) and the hyperfine magnetic field (H_n) have been calculated and reported in Table 1. The degree of inversion x, given by the fraction of trivalent iron ion at B-site has been calculated from the total area of the resolved subspectra and the values are also given in Table 1.

Quadrupole splitting at lower temperatures is nearly zero, within the experimental error. The present system is an inverse spinel, and hence must have non-cubic charge distribution from the two sublattices A and B. Such a charge distribution should result in a non-zero EFG at the Fe site. Mössbauer result shows a zero quadrupole splitting. It is possible that the effect of strong magnetic interactions at lower temperatures mask the weak quadrupole interactions partly. As the quadrupole interactions only broaden the lines, without shifting them sufficiently, the experimental observation is made impossible with instruments presently available to us. The other reason could be the $\langle \cos^2\theta \rangle$ effect. Several other spinels like $NiFe_2O_4$ (Ref. 21),

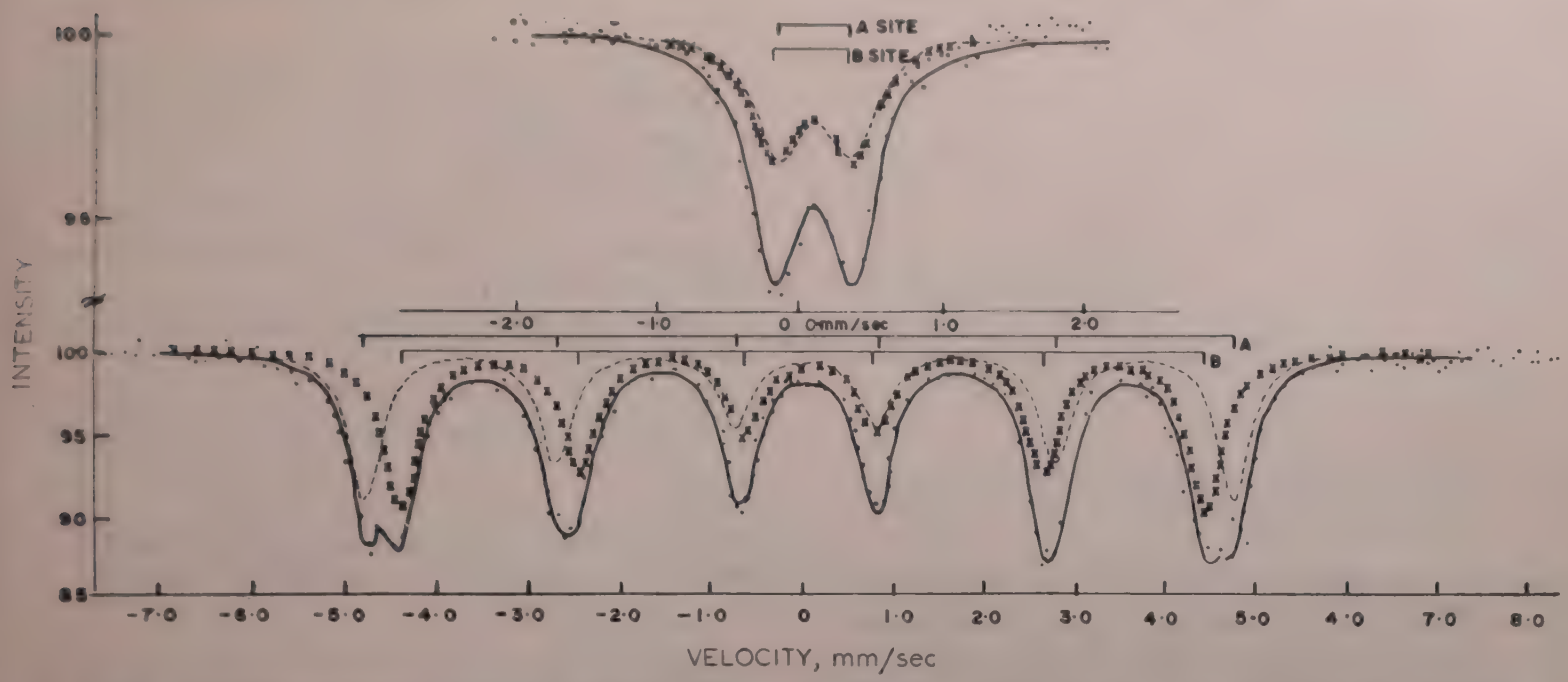

Fig. 1—Mössbauer spectra Mn_2FeO_4 showing experimental curve, resolved subspectra and the resultant synthetic curve at 77 and 528 K

Table 1—Calculated Values of Mössbauer Parameters

Temp. K	Site	IS (wrt iron metal) ±0·04 mm/sec	ΔQ ±0·8 mm/sec	H_n ±10 kOe	Degree of inversion (x) ±0·05
		Quenched sample			
77	A	0·24	0·06	497	—
	B	0·27	0·09	474	
300	A	0·27	−0·14	415	—
	B	0·30	−0·10	382	
528	A	0·29	0·52	—	—
	B	0·27	0·57	—	
643	A	0·21	0·52	—	0·53
	B	0·23	0·57	—	
758	A	0·25	0·52	—	0·56
	B	0·27	0·48	—	
		Annealed sample			
77	A	0·39	0·09	496	0·54
	B	0·39	0·09	485	
300	A	0·24	0·03	395	0·50
	B	0·29	0·04	366	
483	A	0·31	0·57	—	0·56
	B	0·33	0·44	—	
558	A	0 27	0·57	—	0 54
	B	0·18	0·57	—	
648	A	0·23	0 57	—	0·52
	B	0·25	0·61	—	

Fe Co Cr O_4 (Ref. 22, 23) also show a similar behaviour. At higher temperatures, when the magnetic order is lost, one observes the quadrupole split spectra. Table 1 shows that the quadrupole splitting is independent of temperature. It is not yet possible to explain this unusual observation in terms of any reasonable magnetic structure, although tentative suggestions have been put forward.[23]

A correlation between the isomer shift and H_n at A- and B-sites in spinels is usually observed.[29] Our observations do not show such correlations and experimental results show that H_n (A) is larger than H_n (B), similar to Fe_3O_4,[6] where $\langle S_z \rangle$ is 2 instead of 5/2. Iron ions which are situated at chemically equivalent sites, but have different $\langle S_z \rangle$ values have different H_n values. The magnetic field at A-site is normally lowered by the covalency effects. Superexchange interactions also influence H_n at these sites. These two effects compete with each other and it appears that in $MnFe_2O_4$-Mn_2FeO_4 system, the effects of superexchange have stronger influence over H_n than the covalency effects. Houston and Heeger[24] observed by NMR studies that the exchange coupling between the Fe-Fe atoms is stronger than those between Fe-Mn atoms. The ratio J_{Fe-Mn}/J_{Fe-Fe} was found to be $\cong 0{\cdot}7$. A similar observation, that is $H_n(A) > H_n(B)$ has also been made by Weiser *et al.*[25] and by Sawatzky *et al.*[4] in $MnFe_2O_4$. Neutron diffraction results[26] in $MnFe_2O_4$ also show that $\mu_A > \mu_B$.

From the value of the degree of inversion, it has been concluded that ϵ in Model-I takes the value 0·5, therefore, the cation distribution is proposed as

$$Mn^{2+}_{0.5}\ Fe^{3+}_{0.5}\ \left[\ Mn^{3+}_{1.0}\ Fe^{3+}_{0.5}\ Mn^{2+}_{0.5}\ \right]\ O^{2-}_4 .$$

NMR studies in $Mn_xFe_{3-x}O_4$ (Ref. 11, 12) clearly point out that Mn^{3+} should be present only on

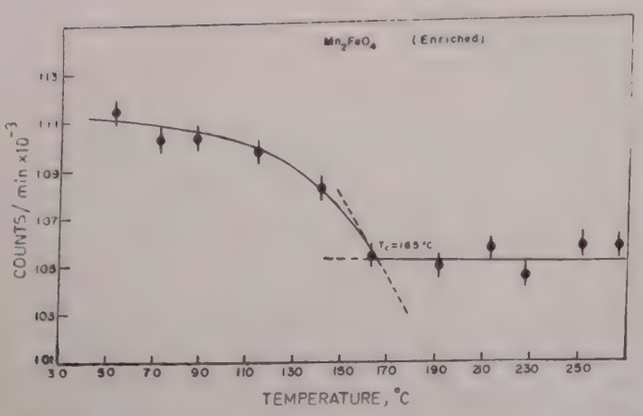

Fig. 2—Plot of γ-ray intensity against temperature observed in thermal scanning of Mn_2FeO_4

B-site and that Fe^{3+} will be at both A- and B-sites. This conforms to our proposal of cation distribution. These workers[11,12] suggest a pairwise electron hopping between Fe^{2+}-Fe^{3+} ions at B-site, but they fail to detect Mn^{2+} at the B-site. We have not observed Fe^{2+} at B-site from our Mössbauer studies. Lotgering and van Diepen[10] also failed to observe either the electron hopping or the Fe^{2+} ion at B-site.

Thermal scanning method has been used to determine the transition temperature in Mn_2FeO_4. The source and the absorber were kept stationary at zero velocity and the transmitted X-ray intensity was measured as a function of temperature. Fig. 2 shows a plot of γ-ray intensity against temperature. The transition temperature measured in this way was found to be 438 K, which is in fair agreement with the Mössbauer spectral collapse from a sextet to a doublet.

4. Conclusion

From the Mössbauer study of Mn_2FeO_4, the cation distribution has been determined and is given by the formula

$$Mn^{2+}_{0.5}\ Fe^{3+}_{0.5}\ \left[\ Mn^{3+}_{1.0}\ \ Fe^{3+}_{0.5}\ \ Mn^{2+}_{0.5}\ \right]\ O^{2-}_{4}.$$

The presence of Fe^{2+} could not be detected. Quadrupole splitting was found to be independent of temperature. The hyperfine field at A-site was found to be larger than that at the B-site.

References

1. Funatogawa Z, Miyata N & Usami S, *J. phys. Soc. Japan*, 14 (1959), 854.
2. Zaveta K, Svirna E & Malikova O, *Soviet Phys. Solid St.*, 4 (1963), 2628.
3. Lotgering F K, *Philips Res. Rep.*, 20 (1965), 320.
4. Sawatzky G A, van der Woude F & Morrish A H, *Phys. Rev.*, 187 (1969), 747.
5. Parker R & Tinsley C J, *Phys. Status Solidi* (a), 33 (1976), 189.
6. Haggström L, Annersten H, Ericsson T, Wappling R, Karner W & Bjaraman S, *Hyperfine Int.*, 5 (1978), 201.
7. San Lu-Pan & Evans B J, *J. appl. Phys.*, 49 (1978), 1458.
8. Wickham D G, *J. Inorg. Nucl. Chem.*, 31 (1969), 313.
9. Finch G I, Sinha A P B & Sinha K P, *Proc. R. Soc. Lond.*, A242 (1957), 28.
10. Lotgering F K & van Diepen A M, *J. Phys. Chem. Solids*, 34 (1973), 1369.
11. Kubo T, *J. phys. Soc. Japan*, 26 (1969), 1094.
12. Rotter M, Sedlak R, Simsa Z & Brabers V A M, *Phys. Status Solidi* (a), 40 (1977), K169.
13. Lotgering F K, *J. Phys. Chem. Solids.*, 25 (1965), 95.
14. Tanaka M, Mizoguchi T & Aiyama Y, *J. phys. Soc. Japan*, 18 (1963), 1091.
15. Goodenough J B, *Magnetism and chemical bonding*, (Interscience, New York), 1963.
16. Simsa Z, *Czech. J. Phys.*, B15 (1965), 435.
17. Sinha A P B, Sanjana N R & Biswas A B, *Acta Crystallogr.*, 10 (1957), 439.
18. Buhl R, *J. Phys. Chem. Solids*, 30 (1969), 805.
19. Ishii M, Nakahira M & Yamanaka T, *Solid St. Commun.*, 11 (1972), 209.
20. Evans B J, *Mossbauer effect methodology*, (Plenum Press, New York), Vol. 4, 1968, 139.
21. Daniels J M & Rosencwaig A, *Can. J. Phys.*, 48 (1970), 381.
22. Gupta M P, Sinha A P B & Date S K, *J. Phys. Chem. Solids*, 39 (1978), 1321.
23. Gupta M P, Ph D thesis, University of Poona, Pune 1977.
24. Houston T W & Heeger A J, *J. appl. Phys.*, 38 (1967), 1285.
25. Weiser E, Povitskii V A, Makarov E F & Kleinstück K, *Phys. Status Solidi, a* 25 (1968), 607.
26. Ligenza S, *Phys. Status Solidi*, (b), 86 (1978), 635.

Indian Journal of Pure & Applied Physics
Vol. 18, October 1980, pp. 751-753

Microtopographical Studies of *n*-Faces of Natural Analcite Crystals

M S Joshi, P Mohan Rao & A V Antony
Department of Physics, Sardar Patel University, Vallabh Vidyanagar 388 120

Received 27 *December* 1979

Surface topography of *n*-faces of natural analcite crystals is reported. Triangular growth hillocks and triangular oriented pits are illustrated and explained. Eccentricity of pits is attributed to inclined dislocations. Natural etching is shown to be very pronounced and rapid.

1. Introduction

Microtopographical studies of crystal faces enable one to understand their growth history, since all the phenomena of growth and dissolution of crystals are perfectly pictured on their habit faces. Several investigators[1-4] have reported growth mechanisms of various crystals by studying the surface structures of their habit faces. Joshi and Vagh[5] have studied distinction between rhombohedral faces of natural and synthetic quartz crystals using microtopography. In the case of natural crystals, direct observations on growth rate and mechanism are difficult. Therefore, study of surface structure imprinted on their habit faces is quite helpful to understand growth mechanism of such crystals.

Zeolites find important applications, mainly due to their selective adsorption and ion-exchange properties. Analcite is one of the more abundant natural species of zeolites. It belongs to the cubic system with space group $Ia\,3d$. An extensive study of *a*-faces of natural analcite has been carried out by the present authors. Microtopographical studies of *n*-faces of natural analcite crystals are reported in the present paper. From the observed surface structures, growth mechanism of these faces is suggested.

2. Experimental Procedure

Crystals were thoroughly cleaned with usual reagents and coated with silver films in a vacuum coating unit to enhance the contrast. Then, they were examined under a metallurgical microscope.

3. Observations

n-Faces ({211}) of natural analcite crystals show presence of oriented, triangular growth pyramids, whose outline is almost parallel to the triangular outline of the face on which they occur. One such case is illustrated in Fig. 1. Natural etching was invariably found on practically all *n*-faces examined in the present investigation. Fig. 2 shows oriented

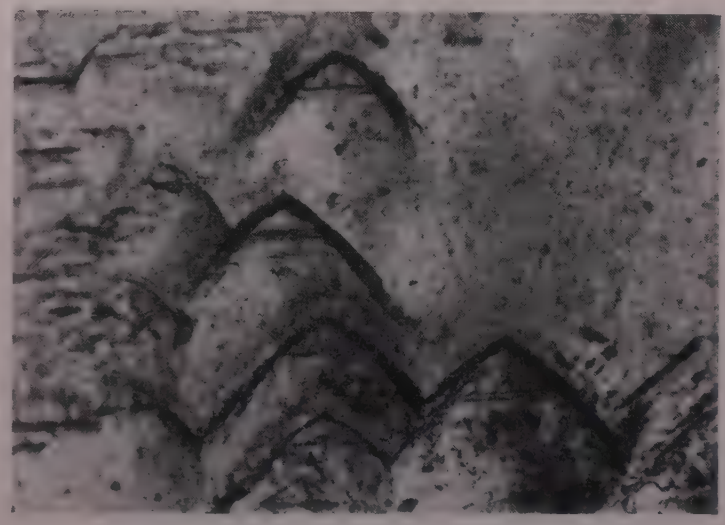

Fig. 1—Triangular growth pyramids (×260)

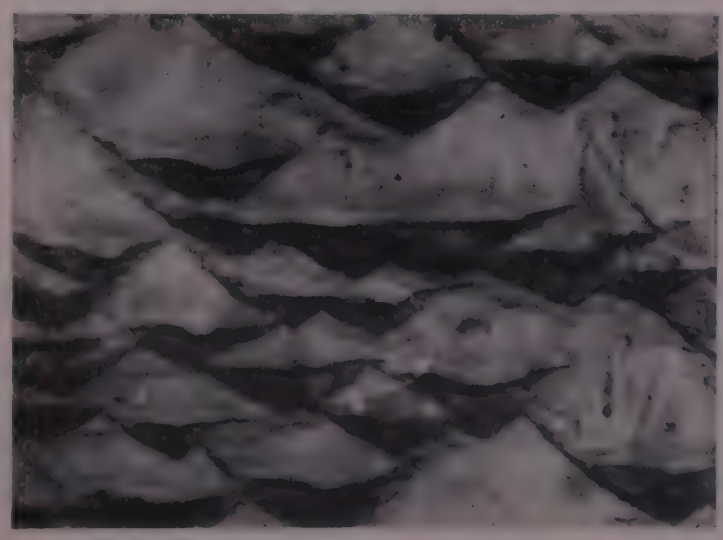

Fig. 2—Oriented triangular natural etch pits (×300)

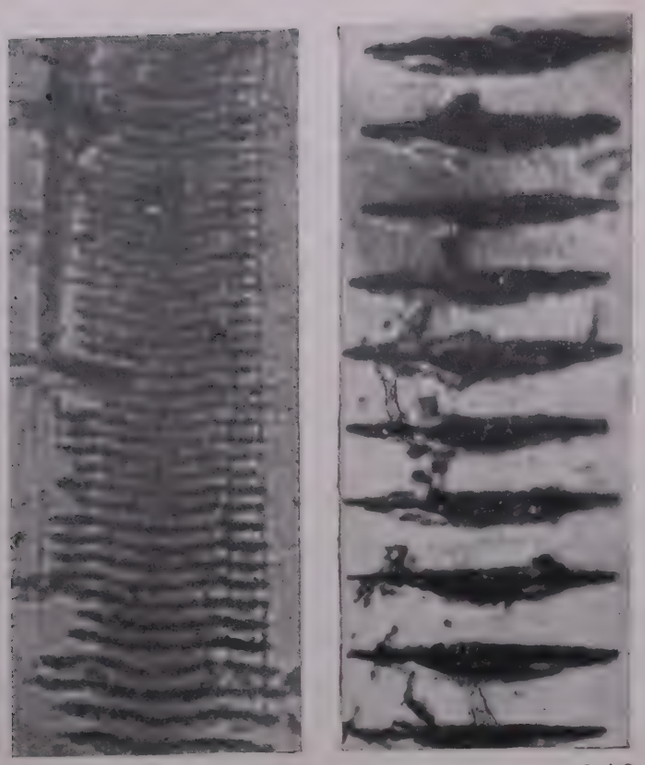

Fig. 3(a) and (b)—Rows of equidistant pits [3(a)×265; 3(b)×240]

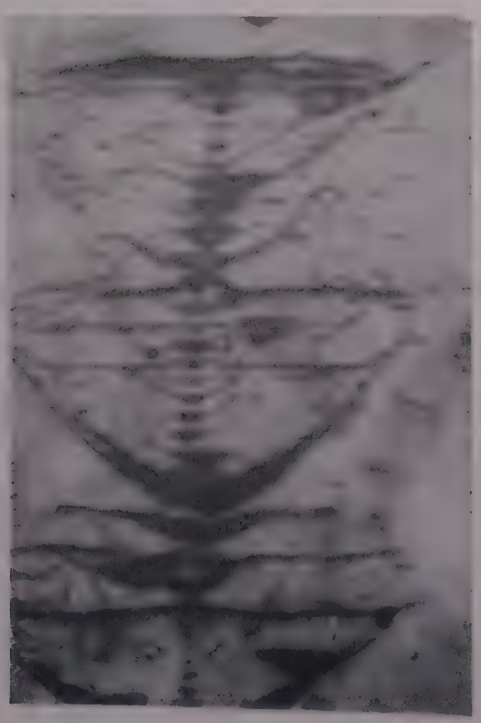

Fig. 4—Smaller pits within bigger pits aligned along a line (×380)

triangular natural etch pits. These etch pits are oriented oppositely with respect to triangular outline of the *n*-face on which they occur. Several cases were observed in which the etch pits are aligned to form rows of equidistant pits. Two such cases are shown in Figs. 3(a) and 3(b). We are inclined to suggest that they are at grain boundaries.

In some cases, oriented big triangular pits were observed and they were accompanied by densely populated extremely tiny oriented pits. The latter are formed very much later than the deep, big pits. Several cases were found in which smaller pits occur within bigger ones. One such case is shown in Fig. 4. Here, it is interesting to note that not only the deep pits, but also the smaller ones, all, are along a line. In some regions, etching is so pronounced that very deep pits result. One such case is shown in Fig. 5. On some faces, general dissolution has taken place leaving almost a flat surface. In such cases, some islands in the form of elevations are formed. This is shown in Fig. 6. These islands may be termed as etch islands.

4. Conclusions

From observations reported here we conclude that *n*-faces of natural analcite crystals grow and develop by two-dimensional nucleation and spreading

Fig. 5—Very deep etch pits (×380)

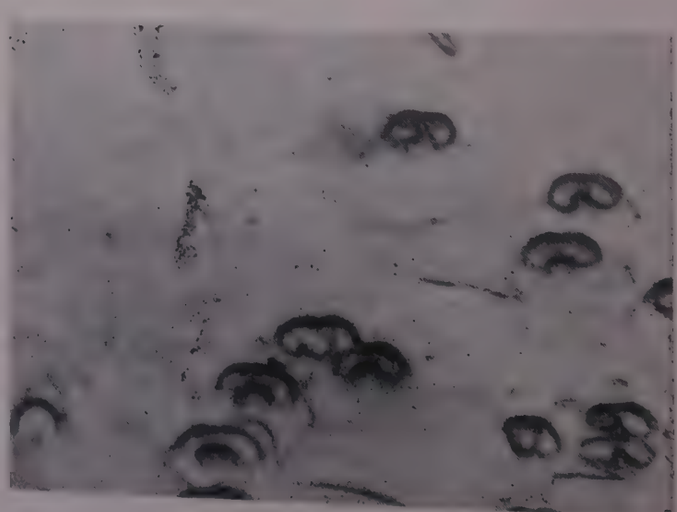

Fig. 6—Etch islands due to dissolution (×340)

of triangular growth layers. Pits are eccentric and hence we conclude that they are formed at points of emergence of dislocations inclined to the face concerned. Also grain boundaries exist in analcite crystals. We further conclude that these crystals have grown in environment in which *n*-faces are susceptible to etching. From the rounded nature of the apex of triangular pits and also from somewhat curved sides of triangular pits (Fig. 4) we conclude that etching rate was very fast, at least in such cases.

Acknowledgements

P M Rao is thankful to the University Grants Commission, New Delhi, and the management of SDM College, Ujire, for financial assistance and for grant of study leave respectively.

References

1. Joshi M S & Taku R K, *Indian J. pure appl. Phys.*, **10** (1972), 34.
2. Sunagawa I, *Fortschr. Miner.*, **52** (1975), 515.
3. Joshi M S & Paul B K, *Amer. Mineral.*, 62 (1977), 122.
4. Joshi M S & Antony A V, *Pramana*, 12 (1979), 251.
5. Joshi M S & Vagh A S, *Z. Krist.*, **121** (1965), 297.

Indian Journal of Pure & Applied Physics
Vol. 18, October 1980, pp. 754-756

Phonon Dispersion in Liquid Carbondisulphide

NILIMA LODHA, N S SAXENA & R C BHANDARI
Department of Physics, University of Rajasthan, Jaipur-4

Received 24 *March* 1979

The single relaxation method developed by R D Mountain [*J. Res. Natl. Bur. Stand. Wash.*, A70 (1966), 207] for the frequency spectrum of density fluctuations in liquids, where the internal degrees of freedom of the molecule is weakly coupled to the translational degrees of freedom of the liquid, has been used to calculate the frequency spectrum of liquid carbondisulphide. Employing this calculated frequency spectra for values of wavevector transfer (k) ranging from 1×10^5 to 3×10^5 cm^{-1}, phonon dispersion in carbondisulphide has been determined.

1. Introduction

Mountain[1] has developed a very elegant theory of the frequency spectrum of density fluctuations for molecular liquids, whose molecules possess an internal degree of freedom which is weakly coupled to the translational degree of freedom of the fluid. Recently, attemps[2,3] have also been made towards the calculations of frequency spectrum in case of liquid carbon tetrachloride and carbon disulphide. These authors[2,3] have shown that the theory of Mountain, which is based on the single relaxation approach is valid for these liquids and found that their calculation of frequency spectrum agrees with the corresponding Brillõuin spectra in these liquids at 20°C, which has been investigated using an He-Ne laser as an exciting source and a pressure-scanned Fabry-Perot spectrometer as an analyzer. We have extended this method to the study of phonon dispersion in liquid carbondisulphide.

2. Theory

The equation necessary for an analysis of intensity spectra scattered light is

$$I(\bar{r}, \omega) = I_0 \frac{Nk^4}{16\pi^4 r^2} \sin^2\phi \frac{\partial \epsilon}{\partial p} S(\mathbf{k}, \omega) \qquad ...(1)$$

Here I_0 is the incident intensity of a plane polarized wave with wave vector $\mathbf{k}_0$, which is scattered at the origin and is observed at $\bar{r}$, N is the number of molecules in the scattering volume, ϕ the scattering angle between the incident polarization and $\bar{r}$. The shift in the angular frequency of the scattered light is ω and the change in the wave vector in the medium of the scattered light is $\mathbf{k}$. The term $S(\mathbf{k}, \omega)$ is the space-time Fourier transform of the density-density correlation function $\langle \rho(0, 0)\, \rho(\bar{r}, t) \rangle$. This density-density correlation has been developed by Mountain[1] resulting in

$$\langle \rho(-k, 0)\, \rho(k, s) \rangle = \langle \rho(k, 0) \rangle \frac{F(s)}{G(s)} \qquad ...(2)$$

where $F(s)$ and $G(s)$ can be expressed as the third and fourth degree polynomials discussed in Ref. 1.

Then $S(\mathbf{k}, \omega)$ is obtained by replacing S by $i\omega$ and taking twice the real part from Eq. (2). The result being

$$S(\mathbf{k}, \omega) = \langle S(k)^2 \rangle 2\, Re \frac{F(i\omega)}{G(i\omega)} \qquad ...(3)$$

Rewriting the dynamic part as $\sigma(\mathbf{k}, \omega)$, we can write Eq. (3) as $S(\mathbf{k}, \omega) = \langle S(\mathbf{k})^2 \rangle \sigma(\mathbf{k}, \omega)$ ...(4)

where $\sigma(\mathbf{k}, \omega) = 2 \frac{N_1 D_1 + N_2 D_2}{D_1^2 + D_2^2}$ ...(5)

with N_1, D_1, N_2, D_2 defined as follows:

$$N_1 = -\omega^2 + a b_0 k^4 + C_0^2 k^2 \left(1 - \frac{1}{r}\right) + \frac{(a b_1 k^4 + b_1 k^2 \omega^2 \tau)}{(1 + \omega^2 \tau^2)^2}$$

$$N_2 = \omega \left[(a + b_0) k^2 + \frac{(b_1 k^2 - a b_1 k^4 \tau)}{(1 + \omega^2 \tau^2)} \right]$$

$$D_1 = -\omega^2 (a + b_0) k^2 + \frac{C_0^2 a k^4}{r} + \frac{(a b_1 k^4 \omega^2 \tau - \omega^2 b k^2)}{(1 + \omega^2 \tau^2)}$$

$$D_2 = \omega \left[-\omega^2 + C_0^2 k^2 + a b_0 k^4 + \frac{b_1 k^2 \omega^2 \tau + a b_1 k^4)}{(1 + \omega^2 \tau^2)} \right] \qquad ...(6$$

Eq. (3) is an exact expression for the frequency distribution of the scattered light. From the intensity spectrum, the Brillöuin width is obtained, which is given by the expression:[1]

$$2\,T_s = (a + b_0)\,k^2 - \left(\frac{C_0^2}{V^2}\right)\left(\frac{a\,k^2}{r}\right) + \frac{b_1\,k^2}{(1 + V^2\,k^2\,\tau^2)}(1 - a\,k^2\,\tau) \qquad \ldots(7)$$

where

$$\left[V(k)\cdot k\,\tau\right]^2 = \frac{1}{2}\left[(C_\infty k\,\tau)^2 - 1\right] + \frac{1}{2}\left[(1 - C_\infty^2 k^2\,\tau^2)^2 + 4\,C_0^2\,k^2\,\tau^2\right]^{1/2} \qquad \ldots(8)$$

3. Results and Discussion

Using Eq. (5) and (6), numerical calculations have been made in liquid carbondisulphide at 20°C for $\sigma(\mathbf{k}, \omega)$. We have evaluated these values of $\sigma(\mathbf{k}, \omega)$ for a representative set of physical parameters[4-6] and for different values of $\mathbf{k}$ (or scattering angles. The values of the parameters chosen for the calculation are as follows:

$a = 1{\cdot}95 \times 10^{-3}$ cm²/sec, $b_0 = 3{\cdot}84 \times 10^{-3}$ cm²/sec, $b_1 = 4{\cdot}76$ cm²/sec, $C_0 = 1{\cdot}142 \times 10^5$ cm/sec, $P_0 = 1{\cdot}262$ g/cm³, $\tau = 2{\cdot}04 \times 10^{-9}$ sec, $n = 1{\cdot}675$ and $r = 1{\cdot}55$

These values have been plotted against frequencies so as not to miss the Brillöuin peak in these intensity spectra in Fig. 1. The Brillöuin components, so obtained appear to be sharp and symmetrical because of low sound absorption. Precise values of full widths have been obtained directly from these spectra. Determination of these full widths (i.e. full width at half-intensity maxima) requires a great care, since the Brillöuin components are relatively narrow in this liquid. These widths are shown compared with the widths calculated using Eq. (7) in Table 1 and good agreement is observed.

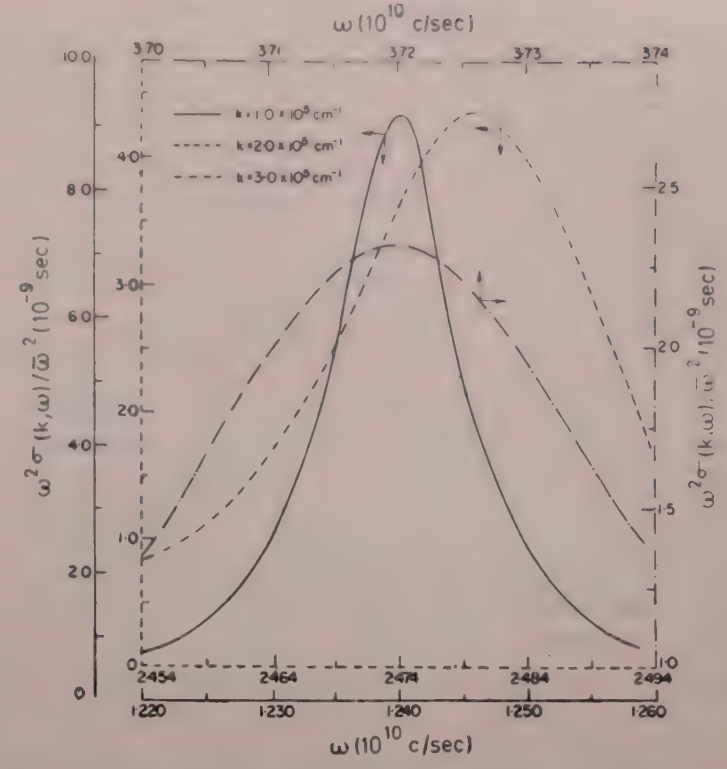

Fig. 2—Spectral function of longitudinal current-current correlation $\omega^2\,\sigma(\mathbf{k}, \omega)/\bar{\omega}^2$ as a function of frequency (ω) for different values of $\mathbf{k}$

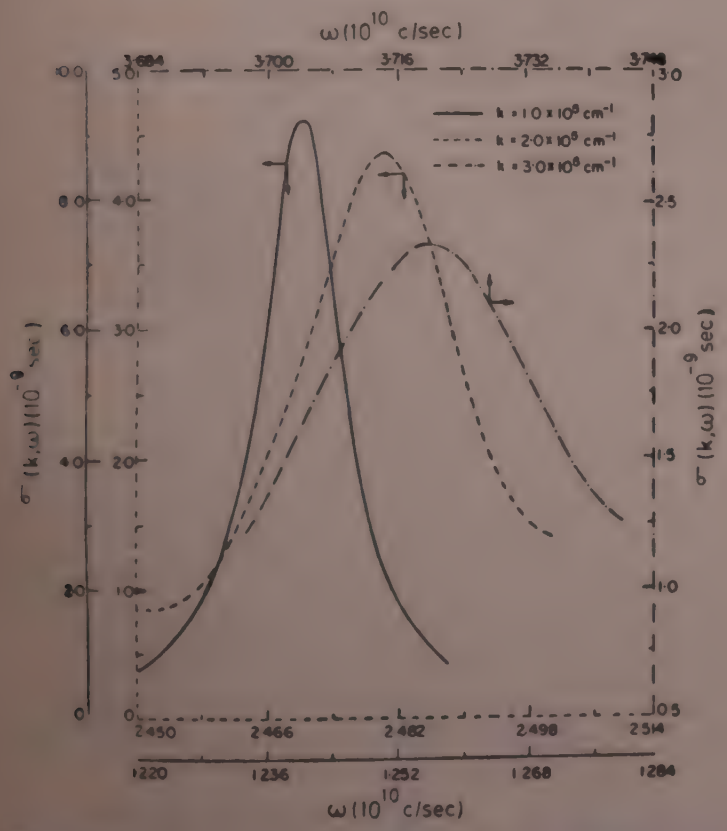

Fig. 1—Plot of $\sigma(\mathbf{k}, \omega)$ vs frequency (ω) for different values of wave-vector Transfer $\mathbf{k}$

Table 1—Comparison of Phonon Velocity and Brillöuin Widths

Wave vector k (10^5 cm^{-1})	Velocity, m/sec		Brillöuin, width MHz	
	calc.	Exptl.	from curves	from calc.
0·0	—	—	—	—
0·2	1254·89	—	—	—
0·4	1257·90	—	—	—
0·6	1257·50	—	—	—
0·8	1258·70	1257·50	—	—
1·7	1258·80	1258·50	116	113
1·4	1258·90	1258·50	160	159
2·0	1258 90	1258·50	250	250
2.4	1258·90	1259·00	320	329
3·0	1279·00	1259·50	490	474

From these calculated functions $\sigma(k, \omega)$, the spectral functions of longitudinal current-current correlations $\omega^2 \sigma(k, \omega)/\omega^{-2}$ are obtained corresponding to same fixed values of **k** for which $\sigma(k, \omega)$ were plotted. These spectral functions are plotted in Fig. 2 : and give well defined peaks at a certain fixed value of frequency (ω_{max}). Analysis of these curves is made by plotting the current-current correlation peak frequency (ω_{max}) against wave vector transfer **k**. It was seen that the frequency is a linear function of wave-vector with a constant phase velocity of 1240 m/sec for the wave vector region of $(1-3) \times 10^5$ cm^{-1}. This means that the phase velocity is independent of wave-vector transfer meaning thereby that no velocity dispersion is observed for high wave-vector transfer (i.e. $k > 1$ Å^{-1}) region whereas for lower **k**-values, there is a velocity dispersion as shown in Table 1 where the velocities are compared with experimentally[3] measured values.

Thus in view of the above situation, argument for the linear nature of the dispersion curve centre explained as due to the interaction between internal molecular vibrations and translational degrees of vibrations being weak.

References

1. Mountain R D, *J. Res. Natl. Bur. Stand. Wash.*, A70 (1966), 207.
2. Stegman G I A, Gornall W S, Voltlerra V & Stoicheff B P, *J. Acoust. Soc. Am.*, 49 (1971), 979.
3. Gewurtz S, Gornall W S & Stoicheff B P, *J. Acoust. Soc. Am.*, 49 (1975), 994.
4. Fabelinskii I L, *Usp. Fiz. Nauk.*, 63 (1957), 355, Translated in *Advance Phys. Sci.* 63 (1957), 474.
5. Herzfeld K F & Litovitz T A, *Absorption and dispersion of ultrasonic waves* (Academic Press, New York), 1959.
6. *Handbook of physics and chemistry* (Chemical Rubber Company, Cleveland, Ohio), 37th Edn, 1955.

Indian Journal of Pure & Applied Physics
Vol. 18, October 1980, pp. 757-759

Study of Molecular Reorientation in Phenothiazine by PMR

(Miss) Ratna Sircar, S C Mishra & R C Gupta

NMR & Microwave Research Laboratory
Department of Physics, University of Lucknow, Lucknow 226 007

Received 6 *September* 1979; *revised received* 16 *January* 1980

The wide line PMR investigation carried out on phenothiazine ($C_{12}H_8SNH$) in the temperature range 77-457 K (7·5 MHz) has shown that the second moment (S_2) of the spectra at 77 K is consistent with the theoretical value, thus suggesting the rigidity of the crystal lattice at 77 K. S_2 is practically constant upto 220 K. A phase transition is observed around 220 K. The lowering of the second moment is postulated to be due to the rotation of the molecule about the symmetry axis passing through S and N atoms. The possibilities of end-to-end turning are discussed and ruled out. The total reduction in the second moment in the transition region compares favourably with the theoretical computations. The activation energy for the reorientation of the molecule is estimated to be 8·1 kcal/mole.

1. Introduction

The wide line PMR spectroscopy of hydrocarbons furnishes valuable information about their crystal and molecular structure. The study of phenothiazine, a compound of great medical importance,[1] is directed towards correctly fixing its molecular and crystal structure[2] and also to check the possibilities of molecular reorientations as indicated by various studies.[3,4]

Preliminary information about the crystal structure of the compound has been given by several workers.[5-8] The detailed crystal structure was determined by Bell *et al.*[2] The crystals of phenothiazine are monoclinic with lattice dimensions, $a = 7·82$, $b = 5·92$, $c = 10·70$ Å, $\beta = 74·01°$, $D_m = 1·34$ g cm^{-3}, $Z = 2$, $D_c = 1·39$ g cm^{-3} with space group P_{21}.

The configurations of the bonds about the nitrogen are flattened tetrahedral and N—H bonds have a quasi-equatorial orientation with respect to heterocyclic chain. Aroney *et al.*[9] found that molecules have apparent configurations defined by dihedral angles of about 150°. Only H-intra configurations are permitted as regards the change of the carbon atoms and free valence indexes.[10] The bonding of the molecules along the S—N axis modifies the electronic properties, and the structure of the free radical N substitution affects the geometrical configurations of the molecules.[11] Lhoste *et al.*[12] showed that the excited aromatic residue interaction in the compound depends upon the macromolecular structure.

2. Experimental Procedure

The PMR derivative curves were recorded at the Tata Institute of Fundamental Research, Bombay using the wide line spectrometer[13] in the temperature range 77-457 K. The temperature variation was achieved using regulated flow of hot or cold nitrogen. The temperature measurements were made by sensitive thermocouples and maintaining the temperature at 77 K was achieved using dewars of liquid nitrogen. Modulation amplitude was kept small to minimize distortion. The accuracy in the measurements was about ± 1 gauss^2. The high purity sample of phenothiazine was obtained with the courtesy of the Central Drug Research Institute, Lucknow. The proton second moment (S_2) versus temperature curve is shown in Fig. 1.

3. Theoretical Computations

Rigid lattice proton second moment—Modified Van Vleck[14] powder relation was used to compute the intramolecular $S_2^{(1)}$ contribution to S_2. The hydrogen position coordinates were computed using bond lengths and bond angles given by Bell *et al.*[2] The result of two-dimensional analysis is shown in Table 1. $S_2^{(1)}$ was found to be 6·35 gauss.[2]

The intermolecular contribution $S_2^{(2)}$ was calculated using the method of Smith,[15] according to which

$$S_2^{(2)} = 358·1\,[4\pi N_p\,(3R^3V)^{-1}] \qquad ...(1)$$

with $V = 477·20$, $R^3 = 28·4$ and $N_p = 36$. The value of $S_2^{(2)}$ came out to be 15·93 gauss^2. The terms V, R and N_p in Eq. (1) represent the unit cell volume (in Å^3), proton radius and number of protons respectively.

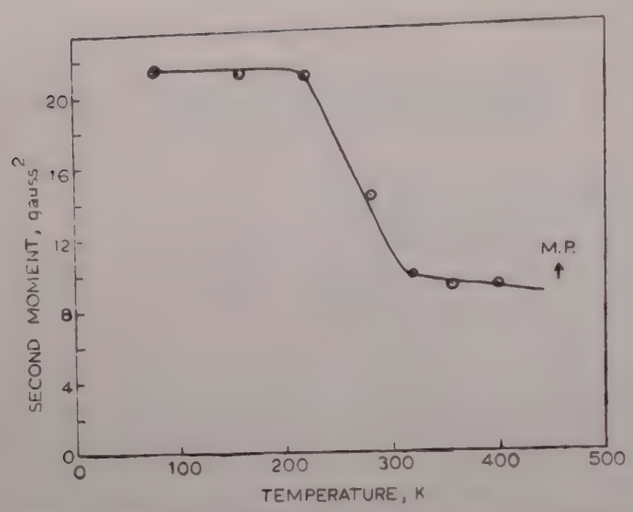

Fig. 1—Proton second moment versus temperature for Phenothiazine

The total theoretical rigid lattice proton second moment (S_2) is thus, $S_2 = S_2^{(1)} + S_2^{(2)} = 6{\cdot}35 + 15{\cdot}93 = 22{\cdot}28$ gauss.[2] This value compares favourably with the observed second moment at 77 K (21·39 gauss^2). *Rotational second moment*—The molecular reorientation and the group rotation bring about reduction in the second moment (S_2). The reduction in S_2 was computed using the method of Gutowsky and Pake.[16] For the hypothesis of molecular reorientation about the symmetry axis, the reduced intramolecular contribution $S_2^{(1)}$ came out to be 5·71 gauss.[2] Andrew and Eades[17] showed that the intermolecular contributions in such cases are reduced by a factor 0·24. Therefore, the presence of molecular reorientation must reduce $S_2^{(2)}$ to a value 3·82 gauss.[2] Thus, the value of the theoretical rotational second moment comes out to be $5{\cdot}71 + 3{\cdot}82 = 9{\cdot}53$ gauss^2.

Experimental second moment—The spectrum of the sample under investigation did not display any fine structure. The second moment calculations were made from the derivative curves using the trapezium rule expression which yields, $S = \Sigma\, h^2 f(h) / 3\, \Sigma\, h f(h)$. The values were corrected for the modulation amplitude.

4. Discussion

The theoretically computed value of S_2 (22·28 gauss^2) compares favourably with the experimental value at 77 K (21·39 gauss^2). This suggests that the crystal lattice is effectively rigid at liquid nitrogen temperature and all sorts of molecular motions are frozen. This also varifies the X-ray crystal structure.[3]

As seen from Fig. 1, the second moment remains practically constant upto 220 K. The total fall is negligible and is within the accuracy limit in the temperature region 77-220 K. An increase of temperature beyond 220 K results in an abrupt fall of the second moment up to temperature of 323 K and the value of experimental second moment at 323 K is $9{\cdot}80 \pm 1$ gauss.[2] This abrupt fall of the second moment is suggestive of some kind of molecular motion or group reorientation. In phenothiazine, with no substituent protonic group, the possibilities of molecular reorientation and of protonic oscillations seem to exist.

The theoretical calculations for rotational S_2 yield a value 9·53 gauss^2 which supports the postulate of molecular reorientation about the symmetry axis of the molecule which passes through S and N sites. If the possibility of molecular reorientation about an axis passing through the ends of the molecule be considered in such a case, the process must require an activation energy and space for the turning which will certainly affect the molecular associations in the intramolecular space. The calculated distance for such a case is 7·6 Å, which is evidently large.

The activation energy for the reorientation was roughly estimated using the formula of Waugh and Fedin.[18] According to them, the activation energy $E_r = 37\, T_c$ (cal/mole). Taking $T_c = 220$ K, the activation energy came out to be 8·1 kcal/mole. This amout of activation energy is easily available in the said temperature range, i.e. 220-323 K.

The dielectric studies carried out by Koga *et al.*[19] reveal the effect of butterfly flapping motion associated with the barrier height for the change in dipole orientation. At about 300 K, small dielectric relaxation time has been associated with the change in dipole orientation by the intramolecular change. Audier *et al.*[20] and Gilbert and Millard[21] presented evidence for competition among several centres in detecting the orientational fragmentations. The H-bond is strengthened and IR studies show that

Table 1—Two-dimensional Analysis of Position Coordinates of Hydrogen Atoms in Phenothiazine

Hydrogen	X Å	Y Å
H_1	2·553068	2·4870
H_2	4·706810	1·2435
H_3	4·5811972	−1·2435
H_4	2·427455	−2·4870
H_5	0·000000	−2·3075
H_6	−2·427455	−2·4870
H_7	−3·628597	−1·2435
H_8	−4·706810	1·24350
H_9	−2·553068	2·4870

the frequencies of the N—H vibrations are shifted to lower wavenumbers during the transition to crystalline state.[22] The electric studies showed that a transition in the vicinity of 305 K is associated with the presence of supercooled microregions in an apparently solid cast of materials.[23]

Acknowledgement

The authors express their deep sense of gratitude to Prof. R Vijayaraghavan, Tata Institute of Fundamental Research, Bombay, for making available the experimental facility. Thanks are also due to Prof. B G Gokhle, for encouragement and interest. One of the authors (RS) is thankful to CSIR, New Delhi, for providing financial assistance in the form of a junior research fellowship.

References

1. *Pharmacological agents*, Vol. 2, edited by M Gordon (Academic Press, New York).
2. Bell J D, Blount J F, Briscol O V & Freeman H C, *Chem. Commun.*, 24 (1968), 1655.
3. Camagni P & Lanzi G, paper presented at the Intern. Conf. mesons & recently discovered particles e[43°], *Congr. nazl. fis.*, Padua-Venice, 1957, XII, 4-5.
4. Nakamura M, Takahashi H & Higasi K, *Bull. chem. Soc. Japan*, 47 (1974), 1593.
5. Feil D, Linck M H & McDo J J H, *Nature, Lond.*, 207 (1965), 286.
6. Wood R G, McCale C H & Williance G, *Phil. Mag.*, 31 (1941), 71.
7. De Leenheen A & Heyndrikx, *J. Ass. Off. Analyt. Chem.*, 54 (3) (1971), 625-32.
8. D Leenheen A & Heyndrikx, *J. Ass. Off. Analyt. Chem.*, 54 (3) (1971), 633-9.
9. Aroney M J, Hoskins G M & Le Fevre Raynord J W, *J. chem. Soc.*, 10 (1968), 1206.
10. Tyutyulkov N, Simov D & Stoyanov S, *Dokl. Bolg. Acad. Nauk SSSR*, 23 (9) (1970), 1095.
11. Pallman B, *Agressologie*, 9 (1) (1968), 19-26.
12. Lhoste J M, Helene C & Plak M, *Rol. Biophys. Museum Natl. Hist Natl, Paris*, 69 (1968), 23566C.
13. Agarwal V D, *NMR study of some organic compounds*, Ph.D thesis, Lucknow University, Lucknow, 1970.
14. Van Vleck J H, *Phys. Rev.*, 74 (1948), 1168.
15. Smith G W, *J. chem. Phys.*, 42 (1965), 4299.
16. Gutowsky H S & Pake G E, *J. chem. Phys.*, 18 (1950), 162.
17. Andrew E R & Eades R G, *Proc. phys. Soc., A* 66 (1953), 415.
18. Waugh J S & Fedin E J, *Soviet Phys. Solid St.*, 4 (1963), 1633.
19. Koga Y, Takahashi H & Higasi K, *Bull. chem. Soc., Japan*, 46 (11), (1973), 3359-63.
20. Audier L, Azzaro M, Cambon A & Guldj R, *Bull. Soc. chim Fr.*, 3 (1968), 1013.
21. Gilbert J N T & Millard, *Org. Mass Spectrom.*, 21 (1969), 617-31.
22. Kdrya Vtesever N A, Push Kareva Z V & Gryazev V F, *Khim. Gelerolsiki. Soedin Akad. Nauk. Lat V. SSSR* (1968) (4) 523-4. Russ.
23. Gutmann F & Keyzer H, *Electrochim. Acta*, 13 (4) (1968), 693.

Indian Journal of Pure & Applied Physics
Vol. 18, October 1980, pp. 760-766

Calculation of Thermodynamic Functions & Fluctuations in the Ground-State Particle Number for Interacting Bosons

K M KHANNA

Materials Science Department, National Institute of Foundry & Forge Technology, Hatia, Ranchi 834 003

&

S N MEHROTRA

Department of Applied Physics, Birla Institute of Technology, Mesra, Ranchi 835 215

Received 17 *May* 1979; *revised received* 1 *February* 1980

Various thermodynamic properties such as internal energy, enthalpy, specific heats and entropy for interacting bosons are studied. The values of the transition temperature and the relative fluctuations in population of the levels in the condensed state of the system are calculated. Both the two-level and the three-level approximations are considered. The interatomic potential used is assumed to be composed of a hard core followed by either a square-well or a sum of both repulsive and attractive Gaussians.

1. Introduction

The theory of interacting bosons[1,2] provides the clue to a clear understanding and explanation of the anomalous behaviour of liquid ^{4}He-II. In this paper, we have studied various properties of interacting bosons, such as the thermodynamic functions, transition temperature and fluctuations in the ground-state particle number, using two different types of interaction potential[1,3,6,7] and both the two-level[3,4] and the three-level[5] systems. The radial distribution function, the second virial coefficient, the calculation of the velocities of the first and second sound and the structure factor, and the phenomenon of phonon dispersion[8] at long wavelengths and low temperatures for interacting bosons have already been discussed in our earlier papers.[7,9] Both the two-level[3,4] and the three-level[5] approximations for interacting bosons yield a T_c value very close to the λ-transition temperature in liquid ^{4}He. However, calculations of the transition temperature for interacting bosons, appearing in the literature,[3-4-5] can at best be regarded as only approximate, since many simplifying approximations were made in the equations on which they are based. We have, for the first time, been successful in obtaining a precise value of T_c, using very few approximations (calculated T_c value = 2·177 K, experimental T_λ = 2·176 K).

The physical significance and justification of the three-state assumption for interacting bosons has been discussed at length in our earlier communication.[5] It is found that, for such a system, the three-level approximation does give results, for the transition temperature, approximately equal to the experimental value of the λ-transition temperature of liquid ^{4}He. In order to present a better picture of the condensed state, it was very strongly felt that there must be at least two non-zero-momentum states in addition to the zero-momentum state in the condensed state. The condensed state is thus composed of three levels, and this is what we call the 'three-level approximation'. The zero-momentum state $\epsilon_0 = 0$ ($p=0$) is assumed to be macroscopically occupied, and the states ϵ_1 and ϵ_2 are non-zero-momentum states which are microscopically occupied. Our calculations[2,5] have shown that the addition of the third level gives far better results compared with the two-level approximation, and that the addition of the fourth level does not improve upon the values of T_c. These three levels (ϵ_0 and ϵ_1 below the cutoff momentum and ϵ_2 above the cutoff) sufficiently represent the excitation spectrum of the system in the lowest state of excitation.

The thermodynamic functions calculated by us at low temperatures are the specific heats C_p and C_v, internal energy, enthalpy and entropy. We find from our calculations that at very low temperatures ($T \ll 1$ K), the system shows a strange behaviour in so far as the behaviour of specific heat in the temperature range 0·05-0·3 K is concerned. We infer that there may well be another phase transition, somewhat similar to the λ-transition, in liquid ^{4}He in the neighbourhood of 0·15 K. In fact, Khanna

and Das[10] have already pointed out that the interacting bosons (and so also liquid ^{4}He) may have a transition temperature below 1K.

We have finally studied the fluctuations in the ground-state particle number and in the occupation numbers of the possible excited states (in the condensed phase) in the two-level[3,4] and the three-level[5] approximations for interacting bosons. A dilute Bose system[3] with strong repulsive core followed by a weak attractive square potential is studied for the purpose. Calculations show that, as we proceed from a non-interacting to an interacting system of bosons, the relative particle number fluctuations in the depletion of the ground-state under equilibrium conditions are considerably less than the reported values in literature (about 6·5% in the two-level[3,4] and about 11% in the three-level[5] approximations). In both these cases, the relative fluctuations in the equilibrium occupation numbers of the excited levels (in the condensed state) are more or less of the same order of magnitude. The relative fluctuations in population of the levels in the condensed state of the system of interacting bosons are thus not violent and the system considered is, therefore, a stable assembly. It is well known that fluctuations may occur about an equilibrium distribution and that it is possible to observe states other than the usual equilibrium states. Hence the calculation of the probability and extent of these deviations from equilibrium state—the phenomenon of fluctuations—is of fundamental importance in the study of statistical thermodynamics.

2. Theoretical Derivations

We consider a system of N interacting bosons enclosed in a box of volume Ω such that the density $\rho = N/\Omega$ is constant in the limit $N \to \infty$, $\Omega \to \infty$. We shall first calculate various thermodynamic functions for the system in equilibrium in the condensed state (near absolute zero) in both the two-level and the three-level approximations.

2.1 Two-level Approximation

In this approximation,[3,4] for interacting bosons, the condensed state is assumed to be composed of two non-degenerate energy levels $\epsilon_0 = 0$ and $\epsilon_1 = E_0 N$ (the energy per particle in the ground state).

2.1.1 Internal Energy (E)

The expression for E in terms of the partition function Q is

$$E = NkT^2 \left(\frac{\partial \ln Q}{\partial T} \right)_v$$

where

$$Q = \sum_i \omega_i \exp(\epsilon_i/kT) = 1 + \exp(-\epsilon_1/kT)$$

Thus,

$$E \text{ (per g)} = \frac{R\,\epsilon_1 \exp(-\epsilon_1/kT)}{Mk\,[1+\exp(-\epsilon_1/kT)]} \qquad \ldots(1)$$

where, R is the universal gas constant and M the atomic weight of ^{4}He.

2.1.2 Specific Heat (C_v)

C_v is obtained from Eq. (1) by the definition

$$C_v = \left(\frac{\partial E}{\partial T} \right)$$

Thus,

$$C_v \text{ (per g)} = \frac{R\,\epsilon_1^2}{Mk^2\,T^2} \frac{\exp(-\epsilon_1/kT)}{[1+\exp(-\epsilon_1/kT)]^2} \qquad \ldots(2)$$

2.1.3 Enthalpy, H

H is given by,

$$H = NkT^2 \left(\frac{\partial \ln Q}{\partial T} \right)_p$$

It is easily seen that $H = E$.

2.1.4 Specific heat, (C_p)

C_p is defined as

$$C_p = \left(\frac{\partial H}{\partial T} \right)_p$$

It is easily verified that $C_p = C_v$.

2.1.5 Entropy (S)

The expression for S in terms of Q is,

$$S = -Nk \ln(N/Q) + NkT \left(\frac{\partial \ln Q}{\partial T} \right)_p$$

or,

$$S \text{ (per g)} = -R/M \ln \left[\frac{R}{Mk\,[1+\exp(-\epsilon_1/kT)]} \right] + \frac{R\,\epsilon_1 \exp(-\epsilon_1/kT)}{MkT\,[1+\exp(-\epsilon_1/kT)]} \qquad \ldots(3)$$

2.2 Three-level Approximation

In the three-level approximation,[5] the condensed state is assumed to be composed of $\epsilon_0 = 0$, $\epsilon_1 = E_0/N$ and ϵ_2.

Thus the expressions for E, C_v and S are as follows

$$E \text{ (per g)} = \frac{R\,[\epsilon_1 \exp(-\epsilon_1/kT) + \epsilon_2 \exp(-\epsilon_2/kT)]}{Mk\,[1+\exp(-\epsilon_1/kT) + \exp(-\epsilon_2/kT)]} \qquad \ldots(4)$$

$$C_v \text{ (per g)} = \frac{R}{Mk^2\,T^2} [\epsilon_1^2 \exp(-\epsilon_1/kT) + \epsilon_2^2 \exp(-\epsilon_2/kT)] + (\epsilon_2-\epsilon_1)^2 \exp\{-(\epsilon_1+\epsilon_2)/kT\}/[1+\exp(-\epsilon_1/kT) + \exp(-\epsilon_2/kT)]^2 \qquad \ldots(5)$$

and

$$S\,(\text{per g}) = -\,R/M \ln\left\{\frac{R}{Mk\,\{1+\exp(-\epsilon_1/kT)+\exp(-\epsilon_2/kT)\}}\right\} + \frac{R}{MkT}\frac{[\epsilon_1\exp(-\epsilon_1/kT)+\epsilon_2\exp(-\epsilon_2/kT)]}{[1+\exp(-\epsilon_1/kT)+\exp(-\epsilon_2/kT)]} \quad ...(6)$$

Also $H = E$ and $C_p = C_v$.

2.3 Transition Temperature

For the two-level approximation[3,4] for interacting bosons,

$$N = \Omega\left(\frac{2\pi mkT_c}{h^2}\right)^{3/2}\left[I(0,1/2)+I\left(\frac{\epsilon_1}{kT_c},\frac{1}{2}\right)\right] = \Omega\left(\frac{2\pi mkT_c}{h^2}\right)^{3/2}\left[2{\cdot}612+I\left(\frac{\epsilon_1}{kT_c},\frac{1}{2}\right)\right], \quad ...(7)$$

where

$$I\left(\frac{\epsilon_1}{kT_c},\frac{1}{2}\right) = \sum_{n=1}^{\infty}\frac{\exp(-n\beta\epsilon_1)}{n^{3/2}}.$$

Now

$$\frac{N}{\Omega} = 2{\cdot}612\left(\frac{2\pi mkT_0}{h^2}\right)^{3/2}$$

Thus,

$$T_0^{3/2} = T_c^{3/2}\left[1+\frac{1}{2{\cdot}612}\,I\left(\frac{\epsilon_1}{kT_c},\frac{1}{2}\right)\right]$$

and

$$T_c = \frac{T_0}{\left[1+\frac{1}{2{\cdot}612}\,I\left(\frac{\epsilon_1}{kT_c},\frac{1}{2}\right)\right]^{2/3}} \quad ...(8)$$

Similarly, for the three-level approximation,[5] we get

$$T_c = \frac{T_0}{\left[1+\frac{1}{2{\cdot}612}\left\{I\left(\frac{\epsilon_1}{kT_c},\frac{1}{2}\right)+I\left(\frac{\epsilon_2}{kT_c},\frac{1}{2}\right)\right\}\right]^{2/3}} \quad ...(9)$$

Here [11,12]

$$I\left(\frac{\epsilon}{kT_c},\frac{1}{2}\right) = q, \text{ say,}$$

$$= -\,3{\cdot}545\alpha^{1/2}+2{\cdot}612+1{\cdot}460\alpha-0{\cdot}1041\alpha^2+0{\cdot}00425\alpha^3, \quad ...(10)$$

when $\alpha \leqslant 1$, where $\alpha = \epsilon/kT_c$. Since T_c appears on the R H S of Eqs. (8) and (9), we can use the iteration method for calculating T_c. No other approximations[3,5] in Eqs. (8) and (9) need be made. Substituting the full series expansion for $I(\epsilon/kT_c, 1/2)$ from Eq. (10) in Eqs. (8) and (9) and using the iteration method, we have obtained very precise values of T_c from Eqs. (8) and (9).

2.4 Fluctuations in the Ground-State Particle Number

We now derive expressions for the relative fluctuations in the population of the ground-state level and that of the excited levels of the condensed state for interacting bosons in both the two-level[3,4] and the three-level[5] approximations. The ground-state[3,5] $\epsilon_0 = 0$ is a macroscopically occupied single-particle state. The states[3,5] ϵ_1 and $\epsilon_2 = 3/2\ \epsilon_1$ are microscopically occupied non-zero-momentum states. Thus from Eq. (7), we get

$$dN = \left(\frac{\partial N}{\partial T_c}\right)dT_c+\left(\frac{\partial N}{\partial\epsilon_1}\right)d\epsilon_1,$$

$$\frac{dN}{dT_c} = \left(\frac{\partial N}{\partial T_c}\right)+\left(\frac{\partial N}{\partial\epsilon_1}\right)\left(\frac{d\epsilon_1}{dT_c}\right)$$

Now

$$\left(\frac{\partial N}{\partial T_c}\right) = \Omega\left(\frac{2\pi mk}{h^2}\right)^{3/2}\left[\frac{3}{2}\,T_c^{1/2}\left\{2{\cdot}612+\left(\sum_{n=1}^{\infty}\frac{\exp(-n\epsilon_1/kT_c)}{n^{3/2}}\right)\right\}+\frac{\epsilon_1}{kT_c^{1/2}}\left\{\sum_{n=1}^{\infty}\frac{\exp(-n\epsilon_1/kT_c)}{n^{1/2}}\right\}\right]$$

$$= \left(\frac{N}{2{\cdot}612}\right)\left(\frac{1}{T_0}\right)^{3/2}\left[\frac{3}{2}\,T_c^{1/2}\left\{2{\cdot}612+\left(\sum_{n=1}^{\infty}\frac{\exp(-n\,\epsilon_1/kT_c)}{n^{3/2}}\right)\right\}+\frac{\epsilon_1}{kT_c^{1/2}}\times\left\{\sum_{n=1}^{\infty}\frac{\exp(-n\,\epsilon_1/kT_c)}{n^{1/2}}\right\}\right];$$

$$\frac{\partial N}{\partial\epsilon_1} = -\,\Omega\left(\frac{2\pi mk}{h^2}\right)^{3/2}T_c^{3/2}\,\frac{1}{kT_c}\times\left[\sum_{n=1}^{\infty}\frac{\exp(-n\,\epsilon_1/kT_c)}{n^{1/2}}\right], = -\,\frac{1}{kT_c}\left(\frac{N}{2{\cdot}612}\right)\times\left(\frac{T_c}{T_0}\right)^{3/2}\left[\sum_{n=1}^{\infty}\frac{\exp(-n\,\epsilon_1/kT_c)}{n^{1/2}}\right].$$

Thus,

$$\left(\frac{dN}{dT_c}\right) = \left(\frac{N}{2{\cdot}612}\right)\left(\frac{1}{T_0}\right)^{3/2}\left[\frac{3}{2}\;T_c^{1/2}\right.$$

$$\times \left\{ 2{\cdot}612 + \left(\sum_{n=1}^{\infty} \frac{\exp(-n\epsilon_1/kT_c)}{n^{3/2}} \right) \right\}$$

$$+ \frac{\epsilon_1}{kT_c^{1/2}} \left(\sum_{n=1}^{\infty} \frac{\exp(-n\epsilon_1/kT_c)}{n^{1/2}} \right) \Bigg]$$

$$- \frac{1}{kT_c} \left(\frac{N}{2{\cdot}612} \right) \left(\frac{T_c}{T_0} \right)^{3/2}$$

$$\left[\sum_{n=1}^{\infty} \frac{\exp(-n\epsilon_1/kT_c)}{n^{1/2}} \right] \left(\frac{d\epsilon_1}{dT_c} \right);$$

$$\left(\frac{\Delta N}{N} \right) = \left(\frac{1}{2{\cdot}612} \right) \left(\frac{1}{T_0} \right)^{3/2}$$

$$\left[\frac{3}{2} \; T_c^{1/2} \left\{ 2{\cdot}612 \left(\sum_{n=1}^{\infty} \frac{\exp(-n\epsilon_1/kT_c)}{n^{3/2}} \right) \right\} \right.$$

$$\left. + \frac{\epsilon_1}{kT_c^{1/2}} \left(\sum_{n=1}^{\infty} \frac{\exp(-n\epsilon_1/kT_c)}{n^{1/2}} \right) \right] \Delta T_c$$

$$- \frac{1}{2{\cdot}612\, kT_c} \left(\frac{T_c}{T_0} \right)^{3/2}$$

$$\times \left(\sum_{n=1}^{\infty} \frac{\exp(-n\epsilon_1/kT_c)}{n^{1/2}} \right) \Delta\epsilon_1 \qquad \ldots(11)$$

It immediately follows from Eq. (11) that

$$\left(\frac{\Delta N_0}{N} \right) = \frac{3}{2} \left(\frac{1}{T_0} \right)^{3/2} T_c^{1/2} \, \Delta T_c \qquad \ldots(12)$$

$$\left(\frac{\Delta N_1}{N} \right) = \left(\frac{1}{2{\cdot}612} \right) \left(\frac{1}{T_0} \right)^{3/2}$$

$$\left[\frac{3}{2} \; T_c^{1/2} \left(\sum_{n=1}^{\infty} \frac{\exp(-n\epsilon_1/kT_c)}{n^{3/2}} \right) \right.$$

$$\left. + \frac{\epsilon_1}{kT_c^{1/2}} \left(\sum_{n=1}^{\infty} \frac{\exp(-n\epsilon_1/kT_c)}{n^{1/2}} \right) \right]$$

$$\times \Delta T_c - \frac{1}{2{\cdot}612\, kT_c} \left(\frac{T_c}{T_0} \right)^{3/2}$$

$$\times \left(\sum_{n=1}^{\infty} \frac{\exp(-n\epsilon_1/kT_c)}{n^{1/2}} \right) \Delta\epsilon_1 \qquad \ldots(13)$$

Since

$$N_0 = N \left(\frac{T_c}{T_0} \right)^{3/2}$$

and $\quad N_1 = \left(\frac{N}{2{\cdot}612} \right) \left(\frac{T_c}{T_0} \right)^{3/2} q_1,$

where

$$q_1 = \sum_{n=1}^{\infty} \frac{\exp(-n\epsilon_1/kT_c)}{n^{3/2}}$$

, we can easily see that

$$\left(\frac{\Delta N_0}{N_0} \right) = \left(\frac{\Delta N_0}{N} \right) \left(\frac{T_0}{T_c} \right)^{3/2} \qquad \ldots(14)$$

and

$$\left(\frac{\Delta N_1}{N_1} \right) = \left(\frac{\Delta N_1}{N} \right) \left(\frac{2{\cdot}612}{q_1} \right) \left(\frac{T_0}{T_c} \right)^{3/2} \qquad \ldots(15)$$

By a similar analysis, we get the following results for the three-level approximation[5]:

$$\left(\frac{\Delta N}{N} \right) = \left(\frac{1}{2{\cdot}612} \right) \left(\frac{1}{T_0} \right)^{3/2} \left[\frac{3}{2} \; T_c^{1/2} \right.$$

$$\left\{ 2{\cdot}612 + \left(\sum_{n=1}^{\infty} \frac{\exp(-n\epsilon_1/kT_c)}{n^{3/2}} \right) \right.$$

$$\left. \left. + \left[\sum_{n=1}^{\infty} \frac{\exp(-n\epsilon_2/kT_c)}{n^{3/2}} \right] \right\} \right.$$

$$+ \frac{1}{kT_c^{1/2}} \left\{ \epsilon_1 \left(\sum_{n=1}^{\infty} \frac{\exp(-n\epsilon_1/kT_c)}{n^{1/2}} \right) \right.$$

$$\left. + \epsilon_2 \left(\sum_{n=1}^{\infty} \frac{\exp(-n\epsilon_2/kT_c)}{n^{1/2}} \right) \right\} \Bigg] \Delta T_c$$

$$- \frac{1}{2{\cdot}612\, kT_c} \left(\frac{T_c}{T_0} \right)^{3/2} \left[\left(\sum_{n=1}^{\infty} \frac{\exp(-n\epsilon_1/kT_c)}{n^{1/2}} \right) \right.$$

$$\left. + \frac{3}{2} \left(\sum_{n=1}^{\infty} \frac{\exp(-n\epsilon_2/kT_c)}{n^{1/2}} \right) \right] \Delta\epsilon_1 \qquad \ldots(16)$$

$$\left(\frac{\Delta N_0}{N} \right) = \frac{3}{2} \left(\frac{1}{T_0} \right)^{3/2} T_c^{1/2} \, \Delta T_c \qquad \ldots(17)$$

$$\left(\frac{\Delta N_1}{N} \right) = \left(\frac{1}{2{\cdot}612} \right) \left(\frac{1}{T_0} \right)^{3/2}$$

$$\left[\frac{3}{2} \; T_c^{1/2} \left(\sum_{n=1}^{\infty} \frac{\exp(-n\epsilon_1/kT_c)}{n^{3/2}} \right) \right.$$

$$\left. + \frac{\epsilon_1}{kT_c^{1/2}} \left(\sum_{n=1}^{\infty} \frac{\exp(-n\epsilon_1/kT_c)}{n^{1/2}} \right) \right] \Delta T_c$$

$$- \frac{1}{2{\cdot}612\, kT_c} \left(\frac{T_c}{T_0} \right)^{3/2} \left(\sum_{n=1}^{\infty} \frac{\exp(-n\epsilon_1/kT_c)}{n^{1/2}} \right) \Delta\epsilon_1 \qquad \ldots(18)$$

and

$$\left(\frac{\Delta N_2}{N} \right) = \left(\frac{1}{2{\cdot}612} \right) \left(\frac{1}{T_0} \right)^{3/2}$$

$$\times \left[\frac{3}{2} \quad T_c^{1/2} \left(\sum_{n=1}^{\infty} \frac{\exp(-n\epsilon_2/kT_c)}{n^{3/2}} \right) \right.$$

$$\left. + \frac{\epsilon_2}{kT_c^{1/2}} \left(\sum_{n=1}^{\infty} \frac{\exp(-n\epsilon_2/kT_c)}{n^{1/2}} \right) \right] \Delta T_c$$

$$- \frac{1}{2{\cdot}612\, kT_c} \left(\frac{T_c}{T_0} \right)^{3/2} \left(\frac{3}{2} \sum_{n=1}^{\infty} \frac{\exp(-n\epsilon_2/kT_c)}{n^{1/2}} \right) \Delta\epsilon_1 \quad \ldots(19)$$

Also, since

$$N_0 = N \left(\frac{T_c}{T_0} \right)^{3/2}, \; N_1 = \left(\frac{N}{2{\cdot}612} \right) \left(\frac{T_c}{T_0} \right)^{3/2} q_1$$

and

$$N_2 = \left(\frac{N}{2{\cdot}612} \right) \left(\frac{T_c}{T_0} \right)^{3/2} q_2$$

where

$$q_1 = \sum_{n=1}^{\infty} \frac{\exp(-n\epsilon_1/kT_c)}{n^{3/2}}$$

and

$$q_2 = \sum_{n=1}^{\infty} \frac{\exp(-n\epsilon_2/kT_c)}{n^{3/2}},$$

we get

$$\left(\frac{\Delta N_0}{N_0} \right) = \left(\frac{\Delta N_0}{N} \right) \left(\frac{T_0}{T_c} \right)^{3/2} \quad \ldots(20)$$

$$\left(\frac{\Delta N_1}{N_1} \right) = \left(\frac{\Delta N_1}{N} \right) \left(\frac{2{\cdot}612}{q_1} \right) \left(\frac{T_0}{T_c} \right)^{3/2} \quad \ldots(21)$$

and

$$\left(\frac{\Delta N_2}{N_2} \right) = \left(\frac{\Delta N_2}{N} \right) \left(\frac{2{\cdot}612}{q_2} \right) \left(\frac{T_0}{T_c} \right)^{3/2} \quad \ldots(22)$$

Here[11,12]

$$\sum_{n=1}^{\infty} \frac{\exp(-n\epsilon/kT_c)}{n^{1/2}} = p, \text{ say,}$$

$$= 1{\cdot}772\, \alpha^{1/2} - 1{\cdot}460 + 0{\cdot}2082\alpha - 0{\cdot}01275\alpha^2, \quad \ldots(23)$$

when $\alpha \leqslant 1$, where $\alpha = \frac{\epsilon}{kT_c}$.

3. Numerical Calculations

Tables 1 and 2 give the results, in the two-level approximation,[3,4] for the various thermodynamic functions at temperatures near absolute zero. The values of ϵ_1, for the bosons interacting via a two-body potential composed of a hard core followed by a square well, are taken from an earlier paper[3] of Khanna and Phukan. The entropy values at different temperatures are exclusive of the chemical constants of the system.

Table 3 gives the values of the thermodynamic functions at low temperatures in the three-level approximation[5] for interacting bosons, assuming a Gaussian interaction potential.[1,6,7] The value of ϵ_1 is taken from the earlier calculations of Khanna *et al.*[1]

Table 1—Calculation of Thermodynamic Functions for Interacting Bosons at Low Temperatures (two-level approximation; $\epsilon_1 = 0{\cdot}1292 \times 10^{-16}$ erg; $T_c = 2{\cdot}171$ K)

Temp. T, K	$C_v\,(=C_p)$ (J/g K)	$E\,(=H)$ (J/g)	S (J/g K)
0·001	0	0	0
0·01	0·01563	$166{\cdot}9 \times 10^{-7}$	$166{\cdot}9 \times 10^{-6}$
0·05	0·8405	0·02588	0·8150
0·1	0·3684	0·05474	1·234
0·6	0·01255	0·08958	1·432
1·0	0·004539	0·09258	1·437

Table 2—Calculation of Thermodynamic Functions for Interacting Bosons at low Temperatures (two-level approximation; $\epsilon_1 = 0{\cdot}7010 \times 10^{-16}$ erg; $T_c = 2{\cdot}410$ K)

Temp. T, K	$C_v\,(=C_p)$ (J/g, K)	$E\,(=H)$ (J/g)	S (J/g, K)
0·01	0	0	0
0·05	0·008294	$408{\cdot}3 \times 10^{-7}$	$816{\cdot}4 \times 10^{-6}$
0·1	0·3316	0·006564	0·07759
0·2	0·9051	0·07688	0·5426
0·3	0·7809	0·1637	0·8970
0·4	0·5731	0·2313	1·092
0·5	0·4182	0·2803	1·2015
0·6	0·3124	0·3163	1·2680
1·0	0·1256	0·3960	1·3739

Table 3—Calculation of Thermodynamic Functions for Interacting Bosons at Low Temperatures (three-level approximation; $\epsilon_1 = 0{\cdot}8843 \times 10^{-16}$ erg; $\epsilon_2 = 1{\cdot}3264 \times 10^{-16}$ erg; $T_c = 2{\cdot}177$ K)

Temp. T, K	$C_v\,(=C_p)$ (J/g, K)	$E\,(=H)$ (J/g)	S (J/g, K)
0·01	0	0	0
0·05	$0{\cdot}9315 \times 10^{-3}$	$0{\cdot}3629 \times 10^{-5}$	$0{\cdot}07258 \times 10^{-3}$
0·1	0·1520	0·002402	0·0278
0·2	1·145	0·06701	0·4342
0·3	1·486	0·2054	0·9911
0·4	1·307	0·3470	1·399
0·5	1·037	0·4643	1·662
0·6	0·8067	0·5558	1·831
1·0	0·3361	0·7665	2·109

Table 4—Calculation of Relative Fluctuations in the Occupation Numbers of the States ϵ_0, ϵ_1 and ϵ_2 (three-level approximation)

ϵ_1 (10^{-16} erg)	$\epsilon_2 = \frac{3}{2}\epsilon_1$ (10^{-16} erg)	T_c, K	$\left(\frac{\Delta N_0}{N_0}\right)$	$\left(\frac{\Delta N_1}{N_1}\right)$	$\left(\frac{\Delta N_2}{N_2}\right)$	$\left(\frac{\Delta N}{N}\right)$
0·7010	1·052	2·108	−0·007117	0·007389	0·01179	+0·000451
0·6743	1·012	2·098	−0·02075	0·01322	0·02340	−0·002946
0·6112	0·9168	2·069	−0·04350	0·02924	0·05084	−0·00454
0·4834	0·7251	2·009	−0·07766	0·03856	0·07236	−0·01263
0·3003	0·4505	1·905	−0·1078	0·02921	0·06728	−0·02567
0·1292	0·1938	1·768	−0·08822	0·01470	0·04139	−0·02124

Table 5—Calculation of Relative Fluctuations in the Occupation Numbers of the States ϵ_0 and ϵ_1 (two-level approximation)

ϵ_1 (10^{-16} erg)	T_c, K	$\left(\frac{\Delta N_0}{N_0}\right)$	$\left(\frac{\Delta N_1}{N_1}\right)$	$\left(\frac{\Delta N}{N}\right)$
0·7010	2·410	−0·004978	0·008932	−0·000388
0·6743	2·402	−0·01124	0·02246	−0·000012
0·6112	2·384	−0·02642	0·04437	−0·002300
0·4834	2·342	−0·04676	0·06572	−0·006490
0·3003	2·269	−0·06480	0·06591	−0·014140
0·1292	2·171	−0·05249	0·04286	−0·011870

Tables 4 and 5 show the values of T_c and the relative fluctuations in the ground-state particle number and in the occupation numbers of the levels ϵ_1 and ϵ_2 in the two-level[3,4] and the three-level[5] approximations respectively. A dilute Bose system[3] with strong repulsive core and a weak attractive tail (square potential) is considered in these calculations. The values of ϵ_1 are based on Ref. 3.

4. Conclusions

Eq. (9), based on the three-level approximation,[5] gives a value of $T_c = 2{\cdot}177$ K, when we put $\epsilon_1 = 0{\cdot}8843 \times 10^{-16}$ erg and $\epsilon_2 = 3/2\,\epsilon_1 = 1{\cdot}3264 \times 10^{-16}$ erg. This value[1] of $\epsilon_1 = E_0/N$ corresponds to a high-density system of bosons interacting through a Gaussian potential.[1,6,7] Since this value of T_c is very close to the λ-transition temperature in liquid ^{4}He (2·176 K), our belief in the three-level approximation[5] and the Gaussian form[1,6,7] of the interparticle potential for interacting bosons becomes stronger.

We find from Tables 1-3 that the behaviour of specific heat for interacting bosons in the temperature range 0-1 K is quite anomalous and is like the familiar λ-transition in liquid ^{4}He. Our calculations predict the possibility of a phase transition occurring in liquid ^{4}He below 1 K, probably in the neighbourhood of 0·15 K, and this conclusion is in conformity with the earlier work of Khanna *et al.*[10] relating to the properties of interacting bosons at very low temperatures.

In Tables 4 and 5, we have listed the values of T_c as calculated from Eqs. (8) and (9), and these values of T_c have then been used in the calculation of relative fluctuations in the occupation numbers of the ground state and the possible excited levels of the condensed state for the two-level[3,4] and the three-level[5] approximations, respectively. As discussed in Ref. 5, the excitation spectrum for interacting bosons at very low temperatures may be represented by atleast three single-particle states (the ground state and two excited states). Of these three states, the state $\epsilon_0 = 0$ is macroscopically occupied and ϵ_1 and ϵ_2 are microscopically occupied. The occupation numbers of the levels decrease as we go to higher excited levels. The presence of attractive forces results in a depletion of particles from the zero-momentum state. Also, the lowering of the critical temperature means the existence of stronger interactions and stronger interactions result in larger depletion of the zero-momentum state. This is the significance of the the negative values, in our calculations, of the relative fluctuations in the ground-state particle number.

Our calculations clearly show that the fluctuations are not violent and the system of interacting bosons studied is thus a stable assembly. As is well known, these fluctuations are an essential characteristic of the statistical equilibrium state rather than departures from that state. The concept of fluctuations at thermodynamic equilibrium and the technique of calculating these deviations from the equilibrium state variables of an ensemble have great physical importance in equilibrium and non-equilibrium statistical mechanics.

References

1. Khanna K M, Das B K & Sinha O P, *Physica*, 76 (1974), 137.
2. Mehrotra S N, *Many-body techniques and their applications to interacting bosons*, Ph D thesis, Ranchi University, Ranchi, 1976.
3. Khanna K M & Phukan A N, *Physica*, 58 (1972), 263.
4. Khanna K M & Phukan A N, *Physica*, 60 (1972), 488.
5. Khanna K M & Mehrotra S N, *Physica*, **81A** (1975), 311.
6. Khanna K M & Das B K, *Physica*, 69 (1973), 611.
7. Khanna K M & Mehrotra S N, *Physica*, **85A** (1976), 616.
8. Aldrich III C H, Pethick C J & Pines D, *J. Low Temp. Phys.*, **25** (1976), 691.
9. Khanna K M & Mehrotra S N, *Physica*, **89A** (1977), 626.
10. Khanna K M & Das B K, *Czech. J. Phys.*, **B23** (1973), 1159.
11. Robinson J E, *Phys. Rev.*, **83** (1951), 678.
12. London F, *Superfluids*, Vol. II Appendix (John Wiley, New York), 1954.

Indian Journal of Pure & Applied Physics
Vol. 18, October 1980, pp. 767-770

Hydrodynamics of Persistent Mass Curernts

K M KHANNA
Materials Science Department, National Institute of Foundry & Forge Technology, Hatia, Ranchi 834 003
and
A N PHUKAN & N C SARMAH
Theoretical Physics Laboratory, Dibrugarh University, Dibrugarh 786 004

Received 9 *July* 1979; *revised received* 3 *September* 1979

Hydrodynamics of superfluid liquid ^{4}He is studied by considering the interaction between the normal and superfluid components. As a result of this interaction the pressure is reduced which, in turn, asserts the existence of attractive interaction between the normal and the superfluid components. It is further observed that the existence of attractive interaction is necessary for the maintenance of persistent mass currents.

1. Introduction

One of the peculiar properties of liquid helium is the persistent mass currents. The first theoretical study on the existence of persistent mass currents is due to Grobman and Luban,[1] where they have tried to explain this phenomenon in a single particle or quasi-particle model by assuming, after London, that one of the single particle states, a current carrying state, is macroscopically occupied. They have shown that persistent currents must be interpreted as a metastable phenomenon. A system of interacting bosons confined to a cylindrical container is selected as a model. Considering Bose-condensation, metastability of these currents at $T = 0$ K is formulated using the single particle model and the quasi-particle model. It is found that metastable circulating currents are possible at $T = 0$ K when the interactions between particles are sufficiently strong and angular momentum of the macroscopically occupied state does not exceed a critical value. The theoretical findings of Grobman and Luban[1] and experimental findings of Reppy and Depatie[2] are analogous in the total angular momentum of a persistent current. At a temperature T, $J_\rho(T)$ is proportional to the superfluid density $\rho_s(T)$ of stationary ^{4}He.

In another attempt, Bergmann[3] explained the existence of persistent mass currents by considering the interaction between helium particles and rigidly tied scatterers to the walls of the cylindrical container. Khanna,[4] argued that this assumption should make the walls of the container a rough surface which means that the angular momentum of the fluid rotating in the cylinder will not be a constant of motion. The Hamiltonian will not be rotationally invariant which implies that $[J, H] \neq 0$. The total angular momentum will become time dependent and rather a decreasing function of time. Hence as time passes, the angular momentum will decay and we could no longer call the currents set up as persistent currents. To avoid the difficulty Khanna in his work[4] assumed that the scatterers instead of being tied rigidly to the walls of the container, as considered by Bergmann,[3] are randomly distributed in the rotating liquid itself. This assumption seems to be a realistic one since when there are random scattering centres within the liquid, under certain conditions the Hamiltonian is rotationally invariant in the random phase approximation, i.e. $[J, H] = 0$; and hence in this approximation the total angular momentum J is a constant of motion and, therefore, the persistent currents will not decay with time. We, therefore, try to explain the existence of persistent mass currents in liquid He-II as a result of interaction between the normal and superfluid which comes into play when the superfluid is rotated above certain critical velocity.[2]

Following the same argument as given by Khanna,[4] we derive the hydrodynamic equations of a superfluid rotating in a cylinder such that it can sustain persistent mass currents. Khalatnikov[5] has derived the equations of hydrodynamics from conservation law and Galilean principle of relativity. We consider that as a result of the interaction between the normal and superfluid, a mutual force of friction will result. Hence, we introduce an additional force in the expression for energy of the form $B(\mathbf{V}_s - \mathbf{V}_n)^m$ which represents the interaction between the components of the superfluid and the normal fluid. The extra

term is introduced in view of the fact that the mutual force of friction is proportional to $(\mathbf{V}_s - \mathbf{V}_n)^m$, where m lies between 3 (at low temperatures) and 4 (at $T\lambda$) (Ref. 6). The constant B is the constant of proportionality whose value will have to be determined. By introducing this additional term we aim to have the hydrodynamical equations for superfluid which will support persistent mass currents in superfluid He-II which has already been observed experimentally.[2]

2. Basic Equations

Conservation laws for physical quantities are described by differential equations which state that the time derivative of the conserved quantity is equal to the divergence of some vectors. The law of conservation of mass is given by

$$\dot{\rho} + \text{div } \mathbf{j} = 0 \qquad \ldots(1)$$

where ρ is the total density and $\mathbf{j}$ the current (the momentum per unit volume). The momentum conservation law is

$$\frac{\partial j_i}{\partial_t} + \frac{\partial \Pi_{ik}}{\partial_{rk}} = 0 \qquad \ldots(2)$$

where Π_{ik} is the momentum flux density tensor. If we consider a non-dissipative process, then the flow will be reversible and the entropy S will be conserved. Let F be the entropy flux vector. Then we have

$$\dot{S} + \text{div } \mathbf{F} = 0 \qquad \ldots(3)$$

Since entropy is only connected to the excitation, it should be carried along the normal motion. Thus,

$$\mathbf{F} = S\,\mathbf{V}_n$$

We know that a superfluid has two types of motions; consequently it will have two hydrodynamic equations. The first hydrodynamical equation for superfluid is given by Eq. (1). The second is the equation which gives the time derivative of $\mathbf{V}_s$. Since curl $\mathbf{V}_s = 0$, we can write the second hydrodynamical equation for superfluid as

$$\dot{\mathbf{V}}_s + \nabla \left(\phi + \frac{\mathbf{V}_s^2}{2} \right) = 0 \qquad \ldots(4)$$

where ϕ is some scalar function. Eqs. (1 - 4) give the complete set of hydrodynamic equations for the superfluid.

In the above equations we have introduced the unknown terms Π_{ik}, $\mathbf{F}$ and ϕ. Now we proceed to determine their form. For this purpose we consider the energy conservation law which is given by

$$\frac{\partial E}{\partial_t} + \text{div } \mathbf{Q} = 0 \qquad \ldots(5)$$

In Eq. (5), E is the energy per unit volume of the liquid and $\mathbf{Q}$ is the energy flux. The unknown quantities are so assumed that Eq. (5) is satisfied automatically. Galilean relativity principle allows us to determine the dependence of all quantities on the velocity $\mathbf{V}_s$ for a given value of the difference $\mathbf{V}_n - \mathbf{V}_s$.

Let us consider a new reference frame K_0. Let, in this frame, the velocity of superfluid be zero, i.e. the frame K_0 moves with a velocity $\mathbf{V}_s$ with respect to the original frame K. The values of the required quantities are related by the following formulae in different frames.

$$\mathbf{j} = \rho\,\mathbf{V}_s + \mathbf{j}_0 \qquad \ldots(6)$$

$$\Pi_{ik} = \rho V_{si}\,V_{sk} + V_{si}\,j_{0k} + V_{sk}\,j_{0i} + \pi_{ik} \qquad \ldots(7)$$

$$E = \frac{\rho \mathbf{V}_s^2}{2} + \mathbf{V}_s.\mathbf{j}_0 + E_0 \qquad \ldots(8)$$

$$\mathbf{Q} = (\rho \mathbf{V}_s^2/2 + \mathbf{V}_s.\mathbf{j}_0 + E_0)\,\mathbf{V}_s + \mathbf{V}_s^2/2\,\mathbf{j}_0 + \pi.\mathbf{V}_s + \mathbf{q} \qquad \ldots(9)$$

$$\mathbf{F} = S\,\mathbf{V}_s + \mathbf{f} \qquad \ldots(10)$$

In Eqs. (6)-(10), $\mathbf{j}_0$ is the momentum, Π_{ik} the momentum flux tensor, E_0 the energy, $\mathbf{q}$ the energy flux vector, $\mathbf{f}$ the entropy flux in the frame K_0 where the liquid moves with velocity $\mathbf{V}_n - \mathbf{V}_s$. The energy E_0 satisfies the thermodynamic identity

$$dE_0 = Tds + \mu\,d\rho + (\mathbf{V}_n - \mathbf{V}_s).\,d\mathbf{j}_0 \qquad \ldots(11)$$

where μ is the chemical potential and T the temperature. The term $(\mathbf{V}_n - \mathbf{V}_s).d\mathbf{j}_0$ expresses the fact that the velocity is the derivative of the energy with respect to the momentum. Thus we have from symmetry that the vector $\mathbf{j}_0$ is directed along $\mathbf{V}_n - \mathbf{V}_s$, so that we have

$$\mathbf{j}_0 = \rho_n\,(\mathbf{V}_n - \mathbf{V}_s) \qquad \ldots(12)$$

From Eqs. (6) and (12) we have

$$\mathbf{j} = \rho\,\mathbf{V}_s + \mathbf{j}_0 = \mathbf{j}_s\,\mathbf{V}_s + \rho_n\,\mathbf{V}_n \qquad \ldots(13)$$

We now differentiate E with respect to time. Then time derivatives are expressed by means of Eqs. (1)-(4). Using Eq. (9) we calculate div $\mathbf{Q}$. Inserting E and div $\mathbf{Q}$ in Eq. (5) and rearranging we get

$$\text{div } \mathbf{q} = -(m.\nabla).\mathbf{V}_s + (\mathbf{V}_n - \mathbf{V}_s).(\nabla.m) + \mathbf{j}_0.\{(\mathbf{V}_n - \mathbf{V}_s).\nabla\}\,\mathbf{V}_n + \{\mathbf{j}_0 - \rho\,(\mathbf{V}_n - \mathbf{V}_s)\}.\nabla(\phi - \mu) - \nabla T.\{\mathbf{f} - S\,(\mathbf{V}_n - \mathbf{V}_s)\} - \text{div } (\mathbf{f}T + \mathbf{j}_0\mu) \qquad \ldots(14)$$

We introduce the tensor

$$m_{ik} = \Pi_{ik} + [E_0 - TS - \mu\rho - \{(\mathbf{V}_n - \mathbf{V}_s).\mathbf{j}_0\}]\,\delta_{ik} \qquad \ldots(15)$$

As we have assumed the non-dissipative system, m_{ik}, $\mathbf{q}$, $\mathbf{f}$ and ϕ are functions of the thermodynamic variables and velocities and they do not depend on their space or time derivative. Let

$$m_{ik} = j_{0i}\,(V_{nk} - V_{sk})$$

$$\mathbf{f}=S(\mathbf{V}_n-\mathbf{V}_s)$$

$$\phi=\mu$$

Therefore,

$$\mathbf{q}=T\mathbf{f}+\mu\mathbf{j}_0-\{(\mathbf{V}_n-\mathbf{V}_s).\mathbf{V}_s\}\,\mathbf{j}_0+(\mathbf{V}_n-\mathbf{V}_s)\,(\mathbf{V}_n.\mathbf{j}_0) \quad ...(16)$$

Finally we may write

$$\mathbf{F}=\mathbf{f}+S\mathbf{V}_s=S\mathbf{V}_n \quad ...(17)$$

$$\Pi_{ik}=\rho V_{si}\,V_{sk}\,V_{si}\,j_{0k}+V_{nk}\,j_{0i} -[E_0-TS-\mu\rho-\{(\mathbf{V}_n-\mathbf{V}_s).\mathbf{j}_0\}]\,\delta_{ik} \quad ...(18)$$

$$\mathbf{Q}=(\mu+V_s^2/2)\,(\mathbf{j}_0+\rho\mathbf{V}_s)+ST\mathbf{V}_n+\mathbf{V}_n(\mathbf{V}_n.\mathbf{j}_0) \quad ...(19)$$

Inserting the expressions for $\mathbf{F}$, ϕ and Π_{ik} into Eqs. (2)-(4) we obtain the complete set of hydrodynamic equations for the superfluid.

Now, the expression within square brackets in Eq. (18) is for the pressure. From definition, it will be equal to the derivative of the total energy with respect to the volume, when the total mass, entropy and momentum of relative motion are kept constant. Therefore,

$$p=\frac{\partial\,(E_0\,V)}{\partial V}$$

$$=-E_0-TS+\mu\rho+\{(\mathbf{V}_n-\mathbf{V}_s).\mathbf{j}_0\} \quad ...(20)$$

3. Effect of the Interaction Term $B(\mathbf{V}_s-\mathbf{V}_n)^m$ on Pressure

We now examine the effect of the interaction term $B(\mathbf{V}_s-\mathbf{V}_n)^m$, where m lies between 3 and 4. First, we make the calculations with $m=4$, i.e. with the interaction term $B(\mathbf{V}_s-\mathbf{V}_n)^4$.

On introducing the additional energy term in the energy E, the energy is given by

$$E=\rho V_s^2/2+\mathbf{V}_s.\mathbf{j}_0+E_0+B(\mathbf{V}_s-\mathbf{V}_n)^4$$

Let

$$E_1=B(\mathbf{V}_s-\mathbf{V}_n)^4$$

Therefore,

$$\dot{E}_1=\dot{B}(\mathbf{V}_s-\mathbf{V}_n)^4+4B(\mathbf{V}_s-\mathbf{V}_n)^3\,(\dot{\mathbf{V}}_s-\dot{\mathbf{V}}_n)$$

Since $\dot{\mathbf{V}}_n=0$, $\nabla\phi=0$ and $\nabla(V_s^2/2)=0$ we have

$$\dot{E}_1=\dot{B}(\mathbf{V}_s-\mathbf{V}_n)^4 \quad ...(21)$$

Then introducing the additional energy term, the energy flux $\mathbf{Q}$ becomes

$$\mathbf{Q}=\left[\frac{\rho V_s^2}{2}+\mathbf{V}_s.\mathbf{j}_0+E_0+B(\mathbf{V}_s-\mathbf{V}_n)^4\right]\mathbf{V}_s + \frac{V_s^2}{2}\mathbf{j}_0+\pi.\mathbf{V}_s+\mathbf{q}$$

Let

$$\mathbf{Q}_1=B(\mathbf{V}_s-\mathbf{V}_n)^4\,\mathbf{V}_s$$

Therefore,

$$\text{div}\,\mathbf{Q}_1=B(\mathbf{V}_s-\mathbf{V}_n)^4\,\nabla.\mathbf{V}_s \quad ...(22)$$

and

$$\text{div}\,\mathbf{q}_1=-\dot{E}_1-\text{div}\,\mathbf{Q}_1$$

$$=-\dot{B}(\mathbf{V}_s-\mathbf{V}_n)^4-B(\mathbf{V}_s-\mathbf{V}_n)^4\,\nabla.\mathbf{V}_s$$

Thus,

$$\mathbf{q}_1=-B\mathbf{V}_s\,(\mathbf{V}_s-\mathbf{V}_n)^4 \quad ...(23)$$

Therefore, the new energy flux vector will become

$$\mathbf{q}=T\mathbf{f}+\mu\mathbf{j}_0-[(\mathbf{V}_n-\mathbf{V}_s).\mathbf{V}_s]\mathbf{j}_0+(\mathbf{V}_n-\mathbf{V}_s)\,(\mathbf{V}_n.\mathbf{j}_0)+\mathbf{q}_1$$

$$=T\mathbf{f}+\mu\mathbf{j}_0-[(\mathbf{V}_n-\mathbf{V}_s).\mathbf{V}_s]\mathbf{j}_0+(\mathbf{V}_n-\mathbf{V}_s)\,(\mathbf{V}_n.\mathbf{j}_0) -B\mathbf{V}_s\,(\mathbf{V}_s-\mathbf{V}_n)^4 \quad ...(24)$$

and the new momentum flux density tensor is given by

$$\Pi_{ik}=\rho V_{si}\,V_{sk}+V_{si}\,j_{0k}+V_{nk}\,j_{0i} -[E_0-TS-\mu\rho-\{(\mathbf{V}_n-\mathbf{V}_s).\mathbf{j}_0\} +B\mid\mathbf{V}_s\mid(\mathbf{V}_s-\mathbf{V}_n)^4] \quad ...(25)$$

and finally the resultant pressure is given by

$$p=\partial\,(E_0\,\mathbf{V})/\partial\,\mathbf{V}$$

$$=-E_0+TS+\mu\rho+(\mathbf{V}_n-\mathbf{V}_s).\mathbf{j}_0-B\mid\mathbf{V}_s\mid(\mathbf{V}_s-\mathbf{V}_n)^4 \quad ...(26)$$

When the interaction term is $B(\mathbf{V}_s-\mathbf{V}_n)^3$ the resultant pressure expression becomes

$$p=-E_0+TS+\mu\rho+(\mathbf{V}_n-\mathbf{V}_s).\mathbf{j}_0 -2B\mathbf{V}_s\,(\mathbf{V}_s-\mathbf{V}_n)^3 \quad ...(27)$$

4. Discussion

It is clear from Eqs. (26) and (27) that due to the interaction of the normal and superfluid components the pressure in the system is reduced by an amount $B\mid\mathbf{V}_s\mid(\mathbf{V}_s-\mathbf{V}_n)^4$ when $m=4$ and $2B\mathbf{V}_s(\mathbf{V}_s-\mathbf{V}_n)^3$ when $m=3$, where B is the constant of proportionality which has the dimension MT^2/L^3 when $m=4$ and MT/L^2 when $m=3$. Now, if we put these dimensional values of B along with the corresponding dimensional values of $\mid\mathbf{V}_s\mid(\mathbf{V}_s-\mathbf{V}_n)^4$ when $m=4$ and $2\mathbf{V}_s(\mathbf{V}_s-\mathbf{V}_n)^3$ when $m=3$ in the additional term in the pressure expressions given by Eqs. (26) and (27) we find that both the terms $B\mid\mathbf{V}_s\mid(\mathbf{V}_s-\mathbf{V}_n)^4$ and $2B\mathbf{V}_s(\mathbf{V}_s-\mathbf{V}_n)^3$ have the same dimensions, i.e. ML^2/T^3. So, it is seen that whatever be the power ($m=3$ or 4) on the interaction term the dimensions of the consequent contribution to the pressure p are the same. The said contribution has the dimensions of energy per unit time. This indirectly establishes the consistency of the result, i.e. the contribution to the pressure term has the same magnitude.

The reduction of pressure is a consequence of the net attractive interaction that comes into play between the normal and superfluid components after the liquid is rotated above the critical velocity. Experimentally, we know that there exist mass currents which rotate the cylindrical vessel on heating

above the critical temperature. Our result, manifested in the net decrease of pressure, will support the existence of mass current.

If the superfluid component has a velocity very large compared to the normal component which may be the case when $T<0{\cdot}7$ K or so, $-B \mid V_s \mid (V_s-V_n)^4$ [say $= \chi$] becomes $-B \mid V_s \mid V_s^4$ when $m = 4$ and $-2BV_s\,(V_s-V_n)^3$ [say$=\chi'$] becomes $-2BV_s^4$ when $m=3$. The negative signs show that the pressure is reduced. In the region of temperature when V_s and V_n are comparable, the expression for χ or χ' remains the same as in Eq. (26) or Eq. (27). For temperatures higher than T_λ, the normal component may predominate and $V_n \gg V_s$, when $\chi=B \mid V_s \mid V_n^4$ and $\chi'=2BV_s.V_n^3$. Since this value of χ or χ' contains both V_s and V_n, the mutual friction between the superfluid and the normal component will be large for temperatures more than T_λ.

It is not quite clear why the existence of persistent mass currents should be supported by the interaction between He-particles tied rigidly to the walls of the container (Borgmann[3]) and why it should not be considered as an internal affair of the liquid, i.e. as a consequence of the interaction between the normal and superfluid components. It was this consideration which led us to make the calculations presented in this paper. The reduction of pressure indicated that to support the existence of persistent mass currents the net interaction between the normal and the superfluid components should be attractive.

References

1. Grobman W D & Luban M, *Phys. Rev.*, **147** (1966), 166.
2. Reppy J D & Depatie D, *Phys. Rev. Lett.*, **12** (1964), 187.
3. Bergmann D, *Phys. Rev.*, **157** (1967), 169.
4. Khanna K M, *Indian J. pure appl. Phys.*, 7 (1969), 384.
5. Khalatnikov I M, *Theory of superfluidity*, (W A Benjamin, New York), 1965.
6. Gorter C J & Mellink J H, *Physica*, **15** (1949), 285.

Indian Journal of Pure & Applied Physics
Vol. 18, October 1980, pp. 771-777

Effective Potential for the $O(N)$ Symmetric ϕ^6 Model

S MURUGESU & C H OH
School of Physics, Science University of Malaysia, Penang, Malaysia

Received 6 *November* 1978; *revised received* 13 *June* 1979

The effective potential for the ϕ^6 model is evaluated and renormalized up to the two-loop level. We find that there is no spontaneous symmetry breaking in one- and two-(space-time) dimensions whereas in three-dimensions, spontaneous symmetry breaking does occur.

1. Introduction

In the pursuit of understanding dynamical symmetry breaking due to higher order radiative corrections, the $\lambda\phi^4$ model has been extensively studied. It was found[1,2] that in one-, two- and four[3]-dimensions,* spontaneous symmetry breaking is impossible in the large-N limit, where N is the number of components of the spinless field $\phi_a(x)$, whereas in the three-dimensions there is a spontaneous symmetry breaking. But in three-dimensions, the $\lambda\phi^4$ model is not the most general renormalizable theory of its type. Hence it is interesting to add a ϕ^6 coupling term and the resulting model is the most general renormalizable scalar field theory in three-dimensions. Needless to say the ϕ^6 model exhibits a much richer critical behaviour; one finds the presence of a first-order and a second-order phase transition and a tricritical point.

The purpose of this study is to compute the effective potential,[4] $V(\phi)$, exactly to the two-loop level by using the formalism of Refs. 5-7 and to the leading order in the $1/N$ expansion. We find that spontaneous symmetry breaking does not occur in one- and two-dimensions whilst in three-dimensions it is possible. Our conclusion agrees with the recent work of Townsend[8] who, following the technique of Refs. 1 and 9, has also computed the effective potential for the ϕ^6 model to the leading order of $1/N$ expansion but has not calculated the one-loop and two-loop effective potentials.

In Section 2, we show how the first derivative of the effective potential† for the ϕ^6 model is derived from the Dyson-Schwinger functional differential equation for the effective action $\Gamma[\phi]$ (the generating functional for one-particle-irreducible Green's functions). Section 3 gives the result for the effective potential to the two-loop level and the propagator in the one-loop approximation. Renormalization of the one- and two-loop effective potentials is performed in Section 4, which leads to the same qualitative conclusion on symmetry breaking as in the large-N limit case. In Section 5, the leading order of $1/N$ expansion for the effective potential is evaluated by considering only the dominant terms in the expression for $\partial V/\partial\phi_a$ found in Section 2. As expected, the result agrees with that of Ref. 8 although techniques employed are different.

2. The Effective Potential

Consider N self-interacting spinless bosons in the presence of an external source, with $O(N)$-symmetric interaction, described by the Lagrangian

$$\mathcal{L}\{\tilde{\phi}_a(x), j\} = \frac{1}{2}\left[(\partial_\mu \tilde{\phi}_a)^2 - \mu^2 \tilde{\phi}^2\right] - \frac{1}{4!}\lambda\tilde{\phi}^4 - \frac{1}{6!}\eta\tilde{\phi}^6 + j_a(x)\tilde{\phi}_a(x) \quad ...(1)$$

where μ^2, λ and η are respectively the bare squared mass and bare coupling constants, $\tilde{\phi}^2 = \tilde{\phi}_a(x)\tilde{\phi}_a(x)$ and the sum over repeated internal indices is implied. The generating functional $Z[j]$, of the connected Green's functions, is

$$\exp(i Z[j]/\hbar) = \int [d\tilde{\phi}_a] \exp\left[\frac{i}{\hbar}\int d^n x\, \mathcal{L}\{\tilde{\phi}_a(x), j\}\right] \quad ...(2)$$

where n indicates the space-time dimensions. By a functional Legendre transformation, the effective action, $\Gamma[\phi(x)]$, is defined by

$$\Gamma[\phi(x)] = Z[j] - \int d^n x\, j_a(x)\phi_a(x) \quad ...(3)$$

* A different approach to the two-dimensional ϕ^4 model leads to the existence of second-order phase transition.[10]

† In the investigation of dynamical symmetry breaking, the expression for the first derivative of the effective potential is more useful than that of the effective potential itself.

with

$$\frac{\delta Z[j]}{\delta j_a(x)} = \phi_a(x), \quad \frac{\delta\Gamma[\phi(x)]}{\delta\phi_a(x)} = -j_a(x) \quad \ldots(4)$$

where $\phi_a(x)$ is the classical field. It is then straightforward to write down the Dyson-Schwinger functional differential equation for the effective action. To the order of approximation we are working, the result is

$$\begin{aligned}
&\frac{\delta\Gamma[\phi(x)]}{\delta\phi_a(x)} + \partial^2\phi_a(x) + \mu^2\phi_a(x) \\
&\quad + \frac{1}{3!}\lambda\phi^2(x)\phi_a(x) \\
&+ \frac{1}{5!}\eta\phi^4(x)\phi_a(x) - i\hbar\left[\frac{1}{6}\lambda\{2\phi_b(x)G_{ba}(x,x) \right. \\
&+ \phi_a(x)G_{bb}(x,x)\} + \frac{2}{5!}\eta\{2\phi^2(x)\phi_e(x)G_{ea}(x,x) \\
&+ \phi^2(x)\phi_a(x)G_{ee}(x,x) \\
&\left. + 2\phi_b(x)\phi_e(x)\phi_a(x)G_{eb}(x)\}\right] \\
&-\hbar^2\left[\frac{1}{6}\lambda\frac{\delta G_a(\ ,x)}{\delta j_a(x)}\right. \\
&+ \frac{1}{5!}\eta\left\{2\phi^2(x)\frac{\delta G_{ee}(x,x)}{\delta j_a(x)}\right. \\
&+ 8\phi_b(x)G_{eb}(x,x)G_{ea}(x,x) \\
&+ 4\phi_b(x)\phi_e(x)\frac{\delta G_{ea}(x,x)}{\delta j_b(x)} \\
&+ 4\phi_a(x)\phi_b(x)\frac{\delta G_{ee}(x,x)}{\delta j_b(x)} \\
&+ 4\phi_b(x)G_{ee}(x,x)G_{ab}(x,x) \\
&+ \phi_a(x)G_{bb}(x,x)G_{ee}(x,x) \\
&\left.\left. + 2\phi_a(x)G_{eb}(x,x)G_{eb}(x,x)\right\}\right] = 0 \qquad \ldots(5)
\end{aligned}$$

where we have defined

$$G_{ab}(x,y) = \frac{\delta^2 Z[j]}{\delta j_a(x)\,\partial j_b(x)} \qquad \ldots(6)$$

as the exact two-point Green's function.

One can now start a systematic approximation of solving Eq. (5) by loop-expanding $\Gamma[\phi(x)]$ and $G_{ab}(x,y)$,[7]

$$\left.\begin{aligned}
\Gamma[\phi(x)] &= \sum_{k=0}^{\infty}\hbar^k\Gamma^k[\phi(x)] \\
G_{ab}(x,y) &= \sum_{k=0}^{\infty}\hbar^k G^k_{ab}(x,y)
\end{aligned}\right\} \ldots(7)$$

Eq. (5) is then equivalent to a system of equations for $\Gamma_k[\phi(x)]$, $k = 0, 1, 2, \ldots$ By setting $\phi_a(x)$ equal to a *constant* field ϕ_a, the functional differential equations for $\Gamma_k[\phi(x)]$ are converted to ordinary differential equations for (unrenormalized) $V_k(\phi)$, where $V(\phi)$ is the effective potential and

$$V(\phi) = \sum_{k=0}^{\infty}\hbar^k V_k(\phi)$$

3. The Two-Loop Approximation

It is not difficult to see[7] that the computation of $\partial V(\phi)/\partial\phi_a$ to the two-loop level reduces to the evaluation of the particle propagator $\bar{G}$ to the one-loop approximation, where $\bar{G}$ means G calculated with the constant field ϕ_a. We proceed to evaluate $\bar{G}^{(0)}$ and $\bar{G}^{(1)}$.

The inverse of Green's function G, i.e. the proper vertex, is given by

$$\Delta_{ab}(x,y) = -\frac{\delta^2\Gamma[\phi(x)]}{\delta\phi_a(x)\,\delta\phi_b(y)} \qquad \ldots(8)$$

The tree-approximation of $\Delta_{ab}(x,y)$ for the constant field can be derived from Eq. (5) and we have

$$\bar{\Delta}^{(0)}_{ab}(x,y) = \left(\frac{1}{2\pi}\right)^n\int d^n k\, e^{ik(x-y)}\,\bar{\Delta}^{(0)}_{ab}(k) \qquad \ldots(9)$$

Here

$$\begin{aligned}
\bar{\Delta}^{(0)}_{ab}(k) &= (m_2^2-k^2)\left(\delta_{ab} - \frac{\phi_a\phi_b}{\phi^2}\right) \\
&\quad + (m_1^2-k^2)\frac{\phi_a\phi_b}{\phi^2}
\end{aligned}$$

and

$$m_1^2 = \mu^2 + \frac{\lambda}{2}\phi^2 + \frac{\eta}{4!}\phi^4 \qquad \ldots(10a)$$

$$m_2^2 = \mu^2 + \frac{\lambda}{6}\phi^2 + \frac{\eta}{5!}\phi^4 \qquad \ldots(10b)$$

Expression (9) is readily inverted to give the free-particle propagator,

$$\bar{G}^{(0)}_{ab}(x,y) = \left[\frac{1}{2\pi}\right]^n\int d^n k\, e^{ik(x-y)}\,\bar{G}^{(0)}_{ab}(k) \qquad \ldots(11)$$

with

$$\begin{aligned}
\bar{G}^{(0)}_{ab}(k) &= \frac{1}{m_2^2-k^2}\left(\delta_{ab} - \frac{\phi_a\phi_b}{\phi^2}\right) \\
&\quad + \frac{1}{m_1^2-k^2}\frac{\phi_a\phi_b}{\phi^2}
\end{aligned} \qquad \ldots(12)$$

Now $\bar{G}^{(1)}$ can be written in terms of $\bar{G}^{(0)}$ and its derivative. Making use of Eq. (11) and after a somewhat lengthy calculation, we find

$$\bar{G}^{(1)}_{ab}(x,x) = \frac{i}{6}\left\{\frac{1}{5}\eta\phi_a\phi_b[3E + (N-1)F]J\right.$$

$$+\left(\lambda+\frac{\eta}{10}\phi^2\right)\left[\left(\delta_{ab}-\frac{\phi_a\phi_b}{\phi^2}\right)[E+(N+1)F]K+\frac{\phi_a\phi_b}{\phi^2}[3E+(N-1)F]J\right]$$

$$+\frac{1}{5}\eta\phi^2 E\left[\left(\delta_{ab}-\frac{\phi_a\phi_b}{\phi^2}\right)K+\frac{3\phi_a\phi_b}{\phi^2}J\right]-3\phi_a\phi_b\left[\left(\lambda+\frac{\eta}{6}\phi^2\right)^2 Q+\frac{N-1}{9}\left(\lambda+\frac{\eta}{10}\phi^2\right)^2 L\right]$$

$$-\frac{2}{3}\left(\lambda+\frac{\eta}{10}\phi^2\right)^2\phi^2\left(\delta_{ab}-\frac{\phi_a\phi_b}{\phi^2}\right)M\Big\} \qquad ...(13)$$

where

$$E=\int\frac{d^nk}{(2\pi)^n}\frac{1}{m_1^2-k^2},\quad F=\int\frac{d^nk}{(2\pi)^n}\frac{1}{m_2^2-k^2} \qquad ...(14a)$$

$$J=\int\frac{d^nk}{(2\pi)^n}\left(\frac{1}{m_1^2-k^2}\right)^2,\quad K=\int\frac{d^nk}{(2\pi)^n}\left(\frac{1}{m_2^2-k^2}\right)^2 \qquad ...(14b)$$

$$L=\int\frac{d^nk}{(2\pi^n)}\frac{d^nk'}{(2\pi)^n}\times\frac{1}{(m_2^2-k^2)(m_2^2-k'^2)[m_1^2-(k-k')^2]^2} \qquad ...(14c)$$

$$M=\int\frac{d^nk}{(2\pi)^n}\frac{d^nk'}{(2\pi)^n}\times\frac{1}{(m_1^2-k^2)(m_2^2-k'^2)[m_2^2-(k-k')^2]^2} \qquad ...(14d)$$

$$Q=\int\frac{d^nk}{(2\pi)^n}\frac{d^nk'}{(2\pi)^n}\times\frac{1}{(m_1^2-k^2)(m_1^2-k'^2)[m_1^2-(k-k')^2]^2} \qquad ...(14e)$$

Substituting expressions (11) and (13) into the differential equations for $V(\phi)$ as derived from Eq. (5), we obtain after some tedious computation the effective potential up to the two-loop level:

$$\frac{\partial V_0(\phi)}{\partial\phi_a}=\mu^2\phi_a+\frac{1}{6}\lambda\phi^2\phi_a+\frac{1}{5!}\eta\phi^4\phi_a \qquad ...(15)$$

$$\frac{\partial V_1(\phi)}{\partial\phi_a}=-\frac{i\lambda}{6}\left[2\phi_b\bar{G}^{(0)}_{ba}(x,x)+\phi_a G^{(0)}_{bb}(x,x)\right]-\frac{2i\eta}{5!}\left[2\phi^2\phi_e\bar{G}^{(0)}_{ea}(x,x)+\phi^2\phi_a\bar{G}^{(0)}_{ee}(x,x)+2\phi_b\phi_e\phi_a\bar{G}^{(0)}_{eb}(x,x)\right]$$

$$=-\frac{i}{6}\phi_a\left[\lambda[3E+(N-1)F]+\frac{\eta\phi^2}{10}[5E+(N-1)F]\right] \qquad ...(16)$$

and

$$\frac{\partial V_2}{\partial\phi_a}=\frac{1}{12}\phi_a\Big\{\frac{1}{3}\Big[9JE+(N-1)(3JF+KE+2C)+(N^2-1)KF+6D\Big]\lambda^2-\frac{1}{10}\Big[15E^2+6(N-1)EF+(N^2-1)F^2\Big]\eta$$

$$-\frac{1}{9}\Big[27Q+(N-1)(2M+3L)\Big]\lambda^3\phi^2+\frac{1}{15}\Big[30EJ+(N^2-1)KF+(N-1)(7FJ+2KE+4C)+20D\Big]\lambda\eta\phi^2$$

$$+\frac{1}{300}\Big[75EJ+(N^2-1)FK+(N-1)(15FJ+3EK+6C)+50D\Big]\eta^2\phi^4-\frac{1}{90}\Big[135Q+(N-1)(6M+11L)\Big]\lambda^2\eta\phi^4$$

$$-\frac{1}{900}\Big[225Q+(N-1)(6M+13L)\Big]\lambda\eta^2\phi^6-\frac{1}{9000}\Big[125Q+(N-1)(2M+5L)\Big]\eta^3\phi^8\Big\} \qquad ...(17)$$

where

$$C=-\int\frac{d^nk}{(2\pi)^n}\frac{d^nk'}{(2\pi)^n}\left(\frac{1}{k^2-m_2^2}\cdot\frac{1}{k'^2-m_2^2}\cdot\frac{1}{(k-k')^2-m_1^2}\right) \qquad ...(18)$$

and

$$D = -\int \frac{d^n k}{(2\pi)^n} \frac{d^n k'}{(2\pi)^n} \left(\frac{1}{k^2 - m_1^2} \cdot \frac{1}{k'^2 - m_1^2} \cdot \frac{1}{(k-k')^2 - m_1^2} \right) \quad ...(19)$$

4. Renormalization

The tree approximation does not require any renormalization and from expression (15), we see that there exist three regions for parameters λ and μ^2 for which ϕ^2 can have non-vanishing value, η being positive. This is fully discussed in Ref. 8. To renormalize the one-loop effective potential, one needs to evaluate E and F in Eqs. (14 a, b). There are three cases according to different space-time dimensions, namely $n = 3, 2, 1$.

(a) $n = 3$

Using the following prescription for the renormalized parameters $\bar{\mu}^2$ and $\bar{\lambda}$,

$$\bar{\mu}^2 = \mu^2 + \frac{1}{12\pi^2} \lambda \hbar \Lambda (N+2) \quad ...(20a)$$

$$\bar{\lambda} = \lambda + \frac{1}{20\pi^2} \eta \hbar \Lambda (N+4) \quad ...(20b)$$

where Λ is the cut-off parameter, we obtain the renormalized effective potential to the one-loop approximation

$$\frac{\partial}{\partial \phi_a}(V_0 + \hbar V_1) = \left(\bar{\mu}^2 + \frac{1}{6}\bar{\lambda}\phi^2 + \frac{1}{5!}\eta\phi^4\right)\phi_a - \frac{1}{24\pi}\bar{\lambda}\hbar[3\bar{m}_1 + (N-1)\bar{m}_2]\phi_a - \frac{1}{240\pi}\eta\hbar\phi^4 \cdot [5\bar{m}_1 + (N-1)\bar{m}_2]\phi_a \quad ...(21)$$

where

$$\bar{m}_1^2 = \bar{\mu}^2 + \frac{1}{2}\bar{\lambda}\phi^2 + \frac{1}{4!}\eta\phi^4 \quad ...(22a)$$

and

$$\bar{m}_2^2 = \bar{\mu}^2 + \frac{1}{6}\bar{\lambda}\phi^2 + \frac{1}{5!}\eta\phi^4 \quad ...(22b)$$

Notice that to the order we are working there are no renormalizations for the coupling constant η and the wavefunction.

From expression (21), one has no difficulty to see that spontaneous symmetry breaking can occur. In the many-field limit, the condition for spontaneous symmetry breaking is

$$\bar{\mu}^2 + \frac{1}{6}\bar{\lambda}\phi^2 + \frac{1}{5!}\eta\phi^4 = 0$$

which is the same as in the tree approximation case but with renormalized parameters. Hence there are three regions of parameters $\bar{\mu}^2$ and $\bar{\lambda}$ for which spontaneous symmetry breakdown is possible. Actually, $\bar{\mu}^2$ and $\bar{\lambda}$ obtained by the renormalization prescription (20) differ from the physical mass and coupling constant by finite quantities.

(b) $n = 2$

The prescription for renormalized parameters is now

$$\bar{\mu}^2 = \mu^2 + \frac{1}{24\pi}\lambda\hbar(N+4)\ln\Lambda^2 \quad ...(23a)$$

and

$$\bar{\lambda} = \lambda + \frac{1}{40\pi}\eta\hbar(N+4)\ln\Lambda^2 \quad ...(23b)$$

We find

$$\frac{\partial}{\partial\phi_a}(V_0 + \hbar V_1) = (\bar{\mu}^2 + \frac{1}{6}\bar{\lambda}\phi^2 + \frac{1}{5!}\eta\phi^4)\phi_a - \frac{1}{8\pi}\hbar\phi_a\left[(\bar{\lambda} + \frac{\eta}{6}\phi^2)\ln\bar{m}_1^2 + \frac{1}{3}(N-1)(\bar{\lambda} + \frac{\eta}{10}\phi^2)\ln\bar{m}_2^2\right] \quad ...(24)$$

One observes that there does not exist a non-vanishing value of ϕ^2 for which the first derivative of $(V_0 + \hbar V_1)$ becomes zero; thus no spontaneous symmetry breaking is possible in the one-loop approximation.

(c) $n = 1$

No renormalization is necessary and we obtain

$$\frac{\partial}{\partial\phi_a}(V_0 + \hbar V_1) = \left(\mu^2 + \frac{\lambda}{6}\phi^2 + \frac{\eta}{5!}\phi^4\right)\phi_a - \frac{1}{24}\hbar\phi_a\left[(3\lambda + 1/2\,\eta\phi^2)/m_1 + (\lambda + \frac{1}{10}\eta\phi^2)(N-1)/m_2\right] \quad ...(25)$$

Again no spontaneous symmetry breaking is possible.

We now proceed to renormalize the two-loop effective potential and consider only the case $n = 3$. The renormalization conditions used are as follows:

$$\left.\frac{\partial^2 V}{\partial\phi_a^2}\right|_{\phi=0} = \mu_R^2 \quad ...(26a)$$

$$\left.\frac{\partial^4 V}{\partial\phi_a^4}\right|_{\phi=0} = \lambda_R \quad ...(26b)$$

$$\left.\frac{\partial^6 V}{\partial\phi_a^6}\right|_{\phi=0} = \eta_R \quad ...(26c)$$

In comparison to the one-loop case, we note that the dimensionless coupling constant η needs to be renormalized. The computation is tedious and lengthy and the result is

$$\frac{\partial V}{\partial \phi_a} = \left(\mu_R^2 + \frac{1}{6}\lambda_R \phi^2 + \frac{1}{120}\eta_R \phi^4 \right) \phi_a$$

$$- \frac{1}{192\pi}\hbar\lambda_R \left[5(N-1)\mu_R \right.$$

$$\left. + \frac{1}{2} D_1 \phi^4 \left(\frac{1}{M_1} + \frac{N-1}{15 M_2} \right) \right] \phi_a$$

$$+ \frac{1}{32\pi^2}\hbar^2\lambda_R^2 \left[1 + \frac{1}{222732}(N-1) \times \right.$$

$$(6809N - 55229)$$

$$- \frac{(N+8)M_1}{12\mu_R} - \frac{1}{36}(N-1)(4N+5)M_2$$

$$- \frac{1}{4M_1}\left(\frac{1}{23}(N+22)\mu_R - \frac{1}{3}(N-1)M_2 \right)$$

$$- \frac{1}{3M_2}(N-1)\left(\frac{1}{4}\mu_R - \frac{1}{27}M_1 \right)$$

$$\left. - \frac{1}{9}(N-1)(R-R_0) - \frac{1}{9}(S-S_0) \right] \phi_a$$

$$+ \frac{1}{64\pi^2}\hbar^2\eta_R \left[\frac{1}{30}\mu_R^2 (N+2)(N+4) \right.$$

$$- \frac{1}{5}(N+4)\mu_R M_1$$

$$- \frac{1}{15}(N-1)(N+4)\mu_R M_2$$

$$- \frac{1}{36} D_1 \phi^6 \left(\frac{\pi^2}{M_1} - \frac{N-1}{25 M_2} \right)$$

$$+ \frac{1}{30}(N-1)M_2[6M_1 + (N+1)M_2]$$

$$\left. + \frac{1}{2}M_1^2 \right] \phi_a$$

$$- \frac{1}{128\pi^2}\hbar^2\lambda_R^3\phi^2 \left[\frac{1}{12 M_1 \mu_R}(N+8) \right.$$

$$+ \frac{(N-1)^2}{9M_2}$$

$$\left. - \frac{(N-1)}{108 M_2 \mu_R}(N+8) + \frac{32}{85} V T^2 \right] \phi_a$$

$$- \frac{1}{192\pi^2}\hbar^2\lambda_R\eta_R\phi^2 \left[\frac{7N+23}{30}\frac{\mu_R}{M_1} \right.$$

$$+ \frac{1}{30}(N-1)(N+3)\frac{\mu_R}{M_2}$$

$$\left. - \frac{(N-1)}{30}\left(\frac{7M_2}{M_1} + \frac{2M_1}{M_2} \right) \right.$$

$$- \frac{1}{30}(N^2+29) - \frac{45}{2}(N-1)(R-R_0)$$

$$\left. - \frac{1}{4}(S-S_0) \right] \phi_a$$

$$- \frac{1}{1024\pi^2}\hbar^2\lambda_R^2\eta_R \left[\frac{1}{9M_1\mu_R}(N+8) \right.$$

$$+ \frac{1}{135 M_2 \mu_R}(N-1)(N+8)$$

$$\left. + \frac{128}{675}\pi^2 U \right] \phi_a$$

$$- \frac{1}{384\pi^2}\hbar^2\eta_R^2\phi^4 \left[\frac{1}{20 M_1}(N+4)\mu_R \right.$$

$$+ \frac{(N-1)}{300 M_2}(N+4)\mu_R$$

$$- \frac{(N-1)}{100}\left(\frac{M_1}{M_2} + \frac{5M_2}{M_1} \right)$$

$$+ \frac{(N-1)}{300}(R-R_0) - \frac{1}{46}(S-S_0)$$

$$\left. - \frac{1}{60}(2N^2+13) \right] \phi_a$$

$$- (10800)^{-1}\hbar^2\lambda_R\eta_R^2 T\phi^6\phi_a$$

$$- (108000)^{-1}\hbar^2\eta_R^3 X\phi^8\phi_a$$

$$+ \frac{1}{6}\hbar^2\phi \left[C_1 + \frac{1}{20}D_2\phi^2 \right.$$

$$\left. + \frac{1}{40}(N+2)D_1\mu_R \right] \phi_a \qquad \ldots(27)$$

where

$$M_1^2 = \mu_R^2 + \frac{1}{2}\lambda_R\phi^2 + \frac{1}{4!}\eta_R\phi^4 \qquad \ldots(28a)$$

$$M_2^2 = \mu_R^2 + \frac{1}{6}\lambda_R\phi^2 + \frac{1}{5!}\eta_R\phi^4 \qquad \ldots(28b)$$

$$D_1 = -\frac{1}{16\pi\mu_R}(N+14)\lambda_R\eta_R$$

$$- \frac{5}{288\pi\mu_R^2}\lambda_R^3(N+26) \qquad \ldots(28c)$$

$$T = 225 Q_R + 13(N-1)L_R + 6(N-1)M_R \qquad \ldots(28d)$$

$$U = 675 Q_R + 55(N-1)L_R + 30(N-1)M_R \qquad \ldots(28e)$$

$$V = 135 Q_R + 15(N-1)L_R + 10(N-1)M_R \qquad \ldots(28f)$$

$$X = 125 Q_R + 5(N-1)L_R + 2(N-1)M_R \qquad \ldots(28g)$$

$$C_1 = \frac{\lambda}{24\pi\mu_R} C_2 (N+8) + \frac{1}{40\pi}(N+2) D_1 \mu_R - \frac{1}{32\pi} \lambda_R^2 \left[-\frac{1}{3\mu_R^2} (N+8) B - \frac{1}{\pi} \frac{\partial^2 S}{\partial \phi_a^2}\bigg|_{\phi=0} - \frac{N-1}{3\pi} \frac{\partial^2 R}{\partial \phi_a^2}\bigg|_{\phi=0} \right] + \frac{1}{80\pi\mu_R}(N+4) B \eta_R - \frac{1}{32\pi\mu_R^2} \lambda_R^3 \left[\frac{(N-1)}{216} (3N+133) - \frac{16}{45} \pi V_0 \mu_R^2 \right] + \frac{1}{32\pi} \lambda_R \eta_R \left[\frac{1}{20\pi} (1-N^2) \mu_R + 2N + 5 \right] \quad ...(28h)$$

$$D_2 = \frac{1}{16\pi\mu_R} \eta_R C_2 (N+14) + \frac{(N+10)}{16\pi\mu_R} D_1 \lambda_R + \frac{1}{192\pi\mu_R^3} \lambda_R^3 \left[5(N+26) B + \frac{512}{15} \frac{\partial^2 U}{\partial \phi_a^2}\bigg|_{\phi=0} \right] + \frac{1}{2304\pi^2\mu_R^2} \lambda_R^4 \left[\frac{1}{6\mu_R^2} (25N^2+17N - 177) - \frac{1}{35} 7N^2 + 473) \right] - \frac{1}{96\pi} \lambda_R \eta_R \left[3(N+14) B \mu_R^{-3} - 8(N-1) \frac{\partial^2 R}{\partial \phi_a^2}\bigg|_{\phi=0} - 40 \frac{\partial^2 S}{\partial \phi_a^2}\bigg|_{\phi=0} \right] - \frac{1}{48\pi\mu_R^2} \lambda^2{}_R \eta_R \times \left[11 + \frac{(N-1)}{360}(55N+361) + \frac{(N-1)\pi}{12\mu_R} - \frac{16}{15}\pi^2 V_0 \mu_R^2 - \frac{1}{576\pi}(65N^2+1836N+4579) \right] - \frac{5}{288\pi^2\mu_R^3} \lambda_R^2 \left[(3N+24)\pi C_2 - (N-1)\mu_R^3 \frac{\partial^4 R}{\partial \phi_a^4}\bigg|_{\phi=0} - \mu_R^3 \frac{\partial^4 S}{\partial \phi_a^4}\bigg|_{\phi=0} \right] - \frac{1}{640\pi^2} \eta_R^2 (N^2+2N+72) \quad ...(28i)$$

with R and S being the finite parts of C and D as given by expressions (18) and (19) (i.e. the infinite part ln Λ being removed away), and

$$B = \frac{1}{24\pi}(N+2) \lambda_R \mu_R \quad ...(29a)$$

$$C_2 = \frac{1}{48\pi\mu_R}(N+8) \lambda_R^2 + \frac{1}{40\pi}(N+4) \mu_R \eta_R \quad ...(29b)$$

Here Q_R, L_R and M_R are respectively the finite integrals Q, L and M with $n = 3$ and $m_1 \to M_1$, $m_2 \to M_2$ and the quantities R_0, S_0, etc. mean R, S, etc. evaluated at $\phi = 0$.

The two-loop renormalized effective potential is clearly very involved and we are unable to see whether expression (27) indicates a spontaneous symmetry breaking. Since in the 3-dimension space-time, the one-loop and the leading $1/N$ approximations both indicate there is a spontaneous symmetry breaking, it is reasonable to conjecture that there exists a non-vanishing ϕ which renders expression (27) to vanish. The use of renormalization group equation* will be of little help here since the renormalization group equation will only improve the results by extending the range of ϕ^2 for which the calculation remains valid. Looking at the one-loop case (for $n = 3$) we note that, provided $\bar{\lambda}$ is small, the value of ϕ for which the spontaneous symmetry breaking occurs is inside the domain of validity of the approximation.

5. The Many-Field Limit

Expression (5) readily allows us to evaluate $\partial V(\phi)/\partial \phi_a$ in the many-field limit. In the bubble approximation,[6] Eq. (5) becomes considerably simpler as terms containing $\delta G_{ab}(x, x)/\delta j_a(x)$ contribute non-bubble diagrams and can be neglected. Since G_{ee} is proportional to N, further simplification

* The renormalization group equation for the massless ϕ^6 model is the same as the ϕ^4 model except the coupling constant λ in the latter is replaced by η. The usual γ factor in the differential equation of the renormalization group vanishes.

is achieved in the large-N limit and expression (5) reduces to the form

$$\frac{\delta \Gamma}{\delta \phi_a} - \frac{\delta \Gamma_0}{\delta \phi_a} = \frac{1}{6} i \hbar \phi_a (x) G_{bb} (x, x) \left(\lambda + \frac{1}{10} \eta \phi^2 (x) \right) + \frac{1}{5!} \eta \hbar^2 \phi_a (x) [G_{bb} (x, x)]^2 \quad ...(30)$$

The large-N limit of $G_{ab}^{-1} (x, y)$ is now derived from Eq. (30) by a functional differentiation and we get

$$G_{ab}^{-1} (x, y) = G_{ab}^{-1(0)} (x, y) - \frac{1}{6} \hbar G_{ee} (x, x) \delta_{ab} \delta^n (x-y) \cdot \left[i (\lambda + \frac{1}{10} \eta \phi^2) + \frac{1}{20} \eta \hbar G_{ff} (x, x) \right] \quad ...(31)$$

Now in the presence of a constant field, one can write the exact propagator as

$$\bar{G}_{ab} (x, y) = (\delta_{ab} - \phi_a \phi_b) g (x, y) + \phi_a \phi_b h (x, y) \quad ...(32)$$

If $g (k)$ is the Fourier transform of $g (x, y)$ and

$$B (\phi) = \int \frac{d^n k}{(2 \pi)^n} g (k) \quad ...(33)$$

then owing to the dominance of the term proportional to δ_{ab} in the propagator, we may replace Eq. (31) by

$$g^{-1} (k) = -k^2 + \mu^2 + \frac{1}{6} \lambda [\phi^2 - i N \hbar B (\phi)] + \frac{1}{5!} \eta [\phi^2 - i \hbar N B (\phi)]^2 \quad ...(34)$$

Setting $\phi_a (x)$ to be constant field ϕ_a and substituting Eqs. (32)-(34) into Eq. (30) we arrive at the result

$$\frac{\partial V}{\partial \phi_a} = \left[\mu^2 + \frac{1}{6} \lambda [\phi^2 - i \hbar N B (\phi)] + \frac{1}{5!} \eta [\phi^2 - i \hbar N B (\phi)]^2 \right] \phi_a \quad ...(35)$$

and

$$B (\phi) = \int \frac{d^n k}{(2 \pi)^n} \left[- k^2 + \mu^2 + \frac{1}{6} \lambda [\phi^2 - i N \hbar B (\phi)] + \frac{1}{5!} \eta [\phi^2 - i N \hbar B (\phi)]^2 \right]^{-1} \quad ...(36)$$

Thus our results* agree completely with those of Ref. 8 although methods used are different. To get the large-N limit of $V (\phi)$, it seems to us that our method is more straightforward. The renormalization program and the discussion of spontaneous symmetry breaking in the many-field limit are discussed in Ref. 8 and we need not repeat here.

* The $i G_{ab}$ of Ref. 8 is identical to G_{ab} here.

References

1. Coleman S, Jackiw R & Politzer H D, *Phys. Rev.*, **D10** (1974), 2491.
2. Root R G, *Phys. Rev.*, **D10** (1974), 3322.
3. Abbott L F, Kang J S & Schnitzer H J, *Brandeis university preprint* "Bound states, tachyons, and restoration of symmetry in the $1/N$ expansion", 1975.
4. For a discussion of the effective potential see, e.g. S Coleman, "*Secret symmetry*", in the Proceedings of the Ettore Majorana Summer School, 1973.
5. Abdus Salam & Strathdee J, *Phys. Rev.*, **D12** (1974), 1129.
6. Schnitzer H J, *Phys. Rev.*, **D10** (1974), 1800.
7. Oh C H, *Prog. theoret. Phys.*, 55 (1975), 1251.
8. Townsend P K, *Phys. Rev.*, **D12** (1975), 2269.
9. Cornwall J M, Jackiw R & Tomboulis E, *Phys. Rev.*, **D10** (1974), 2428.
10. Chang S J, *Phys. Rev.*, **D13** (1976), 2778.

Indian Journal of Pure & Applied Physics
Vol. 18, October 1980, pp. 787-783

Mean Charged Multiplicities in High Energy Hadron-Nucleus Collisions

T Aziz, A Ahmad, M Zafar, M Irfan & M Shafi
Department of Physics, Aligarh Muslim University, Aligarh 202 001

Received 5 *March* 1979; *accepted* 25 *February* 1980

The data on the mean charged multiplicities in proton-nucleus and pion-nucleus collisions in the energy range ~ 7 GeV and above have been compiled. An analysis regarding the energy and mass number dependence of the multiplicities is given in terms of the created charged particles. The mean normalized multiplicity R_A in both the cases may be more suitably expressed as $R_A = a + b\,A^c$. The values of a and b remain essentially same in both the cases whereas $c = 1/3$ in proton-nucleus collisions and $= 1/4$ in pion-nucleus collisions. The $A^{1/3}$ and $A^{1/4}$ behaviour in the two cases is discussed in terms of the inelastic cross-sections.

1. Introduction

In recent years, it has been realized that the observed multiparticle final states of hadron-nucleon collisions are insufficient to provide enough insight into the production processes involved in these interactions. For a deeper understanding, it is necessary to have knowledge of the intervening reactions in the production process leading to the final states. The nuclear targets in this respect are ideal, for they provide a unique possibility of interference through the space-time development of these processes. The idea has resulted in the revival of interests in the hadron-nucleus interaction studies. Two kinds of collision pictures have generally been envisaged to explain the experimental results—the single-step models and the double-step models.[1] In the single-step models, the multiparticle final state is reached instantaneously leading to an internuclear cascade in the hadron-nucleus collisions. In the double-step models, the multiparticle final state is delayed t hrough the formation of intermediate states or state of well defined life-times. The double-step models may be further classified as (i) the independent-contribution and (ii) the collective-contribution models. In the independent-contribution models the intermediate states are assumed to be formed through the successive collisions of the projectile with the target nucleus and these states contribute independently towards the total number of final-state particles. The diffractive excitation[1,2] and the energy flux cascade[3] models may be put under this category. The basic assumption of the collective-contribution models is that simultaneous collision of the projectile with a number of nucleons along the trajectory of the incident particle takes place. The projectile and the target intermingle together and form a single system (or conglomerate). The system so formed contributes towards the total number of final-state particles as a whole. The statistical,[4,5] hydrodynamical[6] and a number of recently developed tube models[7-11] fall under this category. In order to differentiate between different kinds of collision pictures, extensive experimental data are required for different target elements over a wide energy range.

In the present paper, an attempt has been made to compile the data regarding the multiplicities in hadron-nucleus collisions in the energy range ~ 7 to 3000 GeV and with the help of these results it has been tried to establish the energy and mass number dependence of multiplicities. An important parameter in this respect is the mean normalized multiplicity, R_A, which has been thought to be a good measure of development of multiparticle production. It may be defined as

$$R_A(\mathrm{h}, E) = \frac{\langle N_e \rangle (\mathrm{h}, E)}{\langle n_e \rangle (\mathrm{h}, E)} \qquad \ldots(1)$$

where $\langle N_e \rangle$ is the average number of particles created in collisions of hadron (h) with the nucleus of mass number A, at an energy E, and $\langle n_e \rangle$ is the same quantity for nucleon target. The energy and mass number dependences of this parameter are useful to distinguish the different kinds of models. In particular, an energy-independent value of R_A may be taken as ruling out the possibilities of instantaneous production and to favour the particle

production through intermediate stages. As we shall see, it may further distinguish between the independent contribution and collective contribution models. Before proceeding with the estimation of the created particles in the final state, it would be helpful to consider the following aspects

(a) A study of inclusive rapidity (Y) distribution shows that :

(i) Value of $\frac{d\sigma}{dY}$ is larger for $pp \rightarrow \pi^+$ than for $pp \rightarrow \pi^-$ in both the forward ($Y > Y_{cm}$) and backward ($Y < Y_{cm}$) hemispheres. The excess being dominant in the forward hemisphere, because energetic protons of forward hemisphere could not be identified and, therefore, could not be removed.[12]

(ii) Value of $\frac{d\sigma}{dY}$ is larger for $\pi^- A \rightarrow \pi^-$ than for $\pi^+ A \rightarrow \pi^-$ in the forward hemisphere. As the value of Y increases the difference increases, the backward hemisphere remaining essentially unchanged.[13,14]

(iii) Value of $\frac{d\sigma}{dY}$ for $\pi^\pm A \rightarrow \pi^\circ$ remains unchanged in both the forward and backward hemispheres.[13]

(b) A study of inclusive momentum (p) distribution[15] shows that

(i) Value of $\frac{d\sigma}{dp}$ is larger for $\pi^- A \rightarrow \pi^-$ than for $\pi^- A \rightarrow \pi^+$ and the difference increases with increasing momentum.

(ii) Value of $\frac{d\sigma}{dp}$ is larger for $\pi^- p \rightarrow \pi^-$ than for $\pi^- p \rightarrow \pi^+$ and the difference increases with increasing momentum in the same way as above.

(iii) Value of $\frac{d\sigma}{dp}$ remains essentially the same for $\pi^- A \rightarrow \pi^-$ and $\pi^- p \rightarrow \pi^-$, possibly slightly smaller for $\pi^- A$.

(iv) Value of $\frac{d\sigma}{dp}$ remains essentially the same for $\pi^- A \rightarrow \pi^+$ and $\pi^- p \rightarrow \pi^+$, possibly slightly larger for $\pi^- A$.

From the above mentioned results the following inferences may be drawn.

(i) The final channel retains the history of the initial channel and the leading particle effect is always present. It increases with increasing Y and/or p of the observed particles.

(ii) There is also some charge transfer of interacting particles. It is reported[16] that the charge transfer increases with increasing multiplicity of secondary particles. Further, the charge transfer for π^- meson is more than that for proton in a $\pi^- p$ collision.

For a proper knowledge of the development of multiparticle final state, it is, therefore, necessary that the contributions of initial channel particles be excluded. However, completely unambiguous separation is not possible. With these facts in mind we proceed to estimate the mean normalized multiplicity R_A.

2. Data and Analysis

The multiplicities in hadron-nucleus collisions, in general, have been designated by n_s. The values of $\langle n_s \rangle$ for collisions of protons with emulsion nuclei are given in Table 1, where $\langle n_s \rangle$ is the average multiplicity of charged shower particles with relative velocity $\beta \geqslant 0{\cdot}7$ (this excludes some very small number of slow pions and includes initial channel proton which often appears as charged). In Tables 2 and 3, values of $\langle n_s \rangle$ for collision of protons with different target nuclei and for π^--nucleus collisions are respectively given. The corresponding quantity observed in hadron-nucleon collisions is $\langle n_{eh} \rangle$, which is the total number of charged particles in the final state. The values of $\langle n_{eh} \rangle$ for proton-proton collisions at different energies have been taken from the compilation of Albini *et al.*[46] and the following fit has been used to extrapolate $\langle n_{eh} \rangle$ at energies where experimental value is not available.

$$\langle n_{eh} \rangle_{pp} = (1{\cdot}17 \pm 0{\cdot}10) + (0{\cdot}30 \pm 0{\cdot}05) \ln S + (0{\cdot}13 \pm 0{\cdot}01) (\ln S)^2 \quad \ldots (2)$$

where S is the square of centre of mass energy in pp collisions.

In the case of pp collisions, it is observed that nearly 1·27 to 1·4 protons are present in the final state[47-50] which are not created particles. Thus in order to find the actual number of charged mesons created, we should subtract this number from total $\langle n_{eh} \rangle$. A standard assumption is made so that in pp collisions, the average number of created charged particles is

$$\langle n_c \rangle (p) = \langle n_{eh} \rangle - 1{\cdot}33 \quad \ldots (3)$$

In case of p-nucleus collisions the targets are assumed to appear as grey ($\beta < 0{\cdot}7$) and the incident

Table 1—Values of Average Charged Shower Multiplicities $\langle n_s \rangle$ for Collisions of Protons with Emulsion Nuclei

Energy GeV	$\langle n_s \rangle_{em}$	Ref.	$\langle n_s \rangle_{CNO}$	Ref.	$\langle n_s \rangle_{AgBr}$	Ref.
7	3·2 ±0·1	17	2·9±0·1	•	3·5±0·1	•
21	5·8 ±0·2	18				
21·5	6·28±0·11	19				
22·5	6·5 ±0·3	17	5·3±0·3	•	7·2±0·3	•
24	6·6 ±0·1	20	5·2±0·1	20	7·1±0·1	20
28	6·6 ±0·1	22	5·6±0·4		7·1±0·4	
50	8·7 ±0·3	20	6·7±0·2	20	9·5±0·2	20
67	8·8 ±0·3	18				
	9·3 ±0·1	20	7·0±0·2	20	10·1±0·2	20
	9·57±0·23	23	7·4±0·3		11·0±0·3	
	11·08±0·18	19				
200	14·53±0·22	19				
	13·9 ±0·2	23				
	13·5 ±0·2	24				
	13·8 ±0·2	20	10·5±0·2	20	15·0±0·2	20
	13·08±0·3	23	10·5±0·6		15·2±0·6	
	13·04±0·4	25	10·7±0·2		14·7±0·5	
	13·2 ±0·2	26				
300	15·1 ±0·2	26	12·1±0·5	29	16·7±0·5	29
400	16·8 ±0·4	26				
	16·4 ±0·21	27				
1000	19·2 ±1·9	23	13·1±1·8		23·1±3·6	
3000	22·5 ±2 0	28	17·2±2·0		26·8±2·0	

Data without reference are from separation of reference 30;

• Corrected for corresponding corrected value of $\langle n_s \rangle_{em}$

Table 2—Values of Average Charged Shower Multiplicities $\langle n_s \rangle$ for Collisions of Protons with Different Target-Nuclei

Target	Energy GeV	$\langle n_s \rangle$	Ref.
^{12}C	85	7·89±0·43	31
	120	10·13±0·42	31
	173	11·44±0·64	31
	379	12·28±0·83	31
^{27}Al	160	11·25±0·76	31
	260	12·87±1·18	31
	400	15·5 ±0·7	32
	520	14·02±2·49	31
^{56}Fe	160	12·25±0·89	31
	260	13·21±1·16	31
	520	16·05±2·9	31
^{119}Sn	160	13·31±1·3	31
	260	15·41±1·4	31
	400	20·3 ±0·9	32
	520	17·05±3·6	31
^{207}Pb	160	14·75±1·41	31
	260	15·61±1·51	31
^{184}W	300	18·6 ±1·5	33
	400	21·7 ±0·9	32
^{52}Cr	300	13·8 ±1·2	33
^{64}Cu	160	8·0 ±0·6	34
	260	12·2 ±1·1	34
	400	18·4 ±0·6	32
	600	15·7 ±1·3	34
^{20}Ne	28	5·7 ±0·2	35

Table 3—Values of Average Charged Shower Multiplicities n_s for π^--Nucleus Collisions

Energy GeV	$\langle n_s \rangle_{em}$	Ref.	$\langle n_s \rangle_{CNO}$	Ref.	$\langle n_s \rangle_{AgBr}$	Ref.
17	5·3 ±0·3	18	4·1±0·4	18	5·7±0·3	18
17·5					6·7±0·2	36
20	5·8 ±0·3	36				
40					6·98±0·2	45
50	8·17±0·12	37				
60	9·23±0·07	38			9·9 ±0·2	38
	8·59±0·27	39				
200	11·94±0·34	39				
	12·0 ±0·1	40				

Energy GeV	Ref.	$\langle n_s \rangle_{^{12}C}$	$\langle n_s \rangle_{^{20}Ne}$	$\langle n_s \rangle_{^{27}Al}$	$\langle n_s \rangle_{^{64}Cu}$	$\langle n_s \rangle_{^{207}Pb}$	$\langle n_s \rangle_{^{238}U}$
10·5	43		3·74±0·06				
40	41	6·32±0·06					
100	44	7·83±0·13					
175	44	9·04±0·13		8·36±0·14	9·75±0·21	11·66±0·15	11·78±0·23
200	43		10·0±0·2		11·15±0·15	13·6 ±0·2	

proton also appears in the shower. This obviously is not a created particle. The incident proton appears as a proton in about 60 to 70% of the cases and in the rest of the cases as a neutron losing its charge. So this number should also be excluded. Thus we make a standard assumption that the average number of created charged particles in the final state of p-nucleus collisions is

$$\langle N_c \rangle (\mathrm{p}) = \langle n_s \rangle - 0{\cdot}67 \qquad \ldots(4)$$

From these values we have

$$R_A(\mathrm{p}) = \frac{\langle N_c \rangle (\mathrm{p})}{\langle n_c \rangle (\mathrm{p})} = \frac{\langle n_s \rangle - 0\,67}{\langle n_{ch} \rangle - 1{\cdot}33} \qquad \ldots(5)$$

The values of R_A have been estimated using this expression and plotted against energy in Fig. 1. It may be seen from Fig. 1 that R_A remains practically constant in the entire energy range from $\sim$ 20 GeV and above for average emulsion ($A \simeq 60$), CNO ($A = 14$) and AgBr ($A = 94$) nuclei. The average values of R_A for these nuclei in the energy range $\sim$ 20 GeV and above are

$R_{\mathrm{CNO}} = 1{\cdot}53 \pm 0{\cdot}11$, $R_{\mathrm{em}} = 2{\cdot}03 \pm 0{\cdot}08$ and

$R_{\mathrm{AgBr}} = 2{\cdot}24 \pm 0{\cdot}13$

The target size dependence of R_A on A may be expressed in two ways,

$$R_A = A^{\alpha} \qquad \ldots(6)$$

and

$$R_A = a + b\,A^{c} \qquad \ldots(7)$$

Eq. (6) gives $\alpha \simeq 0{\cdot}17$ and Eq. (7) gives $a \simeq 2/3$, $b \simeq 1/3$ and $c \simeq 1/3$.

The composite nature of emulsion, however, creates ambiguities in such an analysis and it is better if the pure targets are available. Unfortunately, the situation in this direction is not encouraging enough. Some results in a narrow band of energies are available, mostly corresponding to cosmic ray energies. The values of $\langle n_s \rangle$ for pure targets are given in Table 2. The values of R_A for

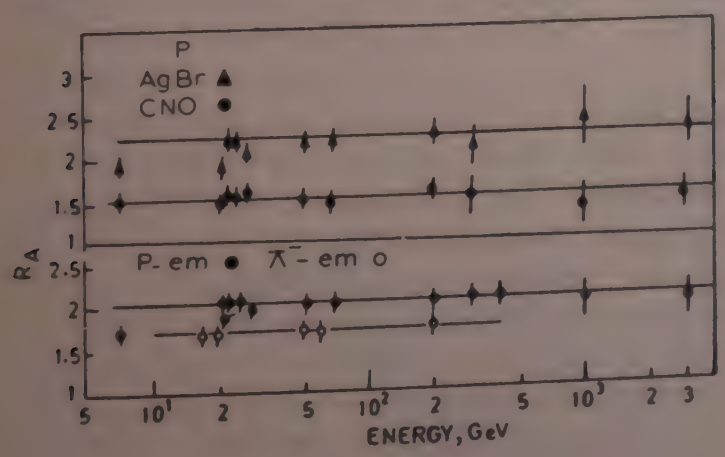

Fig. 1—Variation of R_A with energy

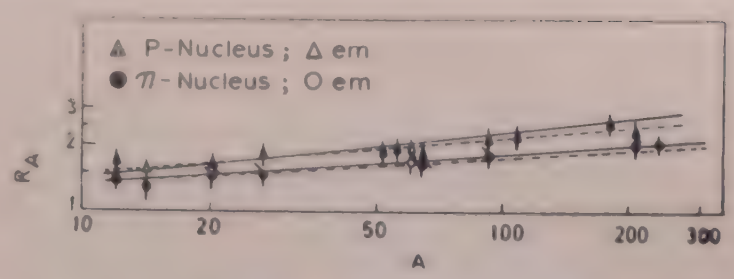

Fig. 2—Variation of R_A with target size A [Solid lines correspond to the fit of the form $R_A = a + bA^{\alpha}$ and broken lines correspond to the fit of the form $R_A = A^{\alpha}$. Triangles correspond to p-nucleus collisions and circles to π^--nucleus collisions. Open circles in both the cases correspond to emulsion.]

these targets have been estimated using Eq. (5) and the average values of R_A with respect to A have been plotted in Fig. 2. A fit of the form of Eq. (6) gives $\alpha = 0{\cdot}17 \pm 0{\cdot}02$, shown by the broken line (Fig. 2). The dependence of R_A on A given by Eq. (7) gives $\langle a \rangle = 0{\cdot}65$, $\langle b \rangle = 0{\cdot}35$ and $\langle c \rangle = 0{\cdot}34$. Since the value of $\langle c \rangle$ is very close to 1/3 we take $R_A = a + bA^{1/3}$ and then $\langle a \rangle = 0{\cdot}646 \pm 0{\cdot}046$ and $\langle b \rangle = 0{\cdot}354 \pm 0{\cdot}035$.

Thus, for proton-nucleus collisions we have,

$$R_A = A^{0{\cdot}17 \pm 0{\cdot}02}$$

or

$$R_A = (0{\cdot}646 \pm 0{\cdot}046) + (0{\cdot}354 \pm 0{\cdot}035)\ A^{1/3}$$

The prediction of the latter expression is shown by the solid line in Fig. 2.

The data regarding the pion-nucleus collisions are poor. In fact, very few experiments have been performed so far. The values of $\langle n_s \rangle$ for pion collisions with emulsion nuclei together with some other targets are given in Table 3. To estimate the value of R_A the following procedure has been adopted. Considering the results of π^- p-collisions[51] and assuming that the number of π^+, π^- and π° mesons created is equal, we find that at least 1·396 charged particles are not created. From the results of Kladnitskaya *et al.*[16] on charge transfer in π^- p-collision, it follows that $\simeq 0{\cdot}61$ charge is transferred and therefore, 1·39 charged particles of the final channel are the initial channel particles and they should be excluded. Thus we may take

$$\langle n_c \rangle (\pi^-) = \langle n_{ch} \rangle - 1{\cdot}4 \qquad \ldots(8)$$

for π^- p-collisions. The data on $\langle n_{ch} \rangle$ have been taken from Albini *et al.*[46] and for the values $\langle n_{ch} \rangle$ at energies where experimental results are not available, the following fit has been used.

$$\langle n_{ch} \rangle (\pi^-) = (0{\cdot}02 \pm 0{\cdot}27) + (1{\cdot}07 \pm 0{\cdot}13) \ln S + (0{\cdot}5 \pm 0{\cdot}02)(\ln S)^2 \qquad \ldots(9)$$

where S is the square of c.m. energy in π^- p-collisions.

In case of π^--nucleus collisions, the targets appear as grey, and the incident pion appears as a shower (charged or neutral) in the final state. From the experimental results it follows that leading pion loses its charge by ~0·4-0·6. Assuming the charge symmetry, i.e. equal numbers of π^+, π^- and π^0 are created we find from the π^--carbon collision results[15,41,42] that the average number of π^- mesons not created is $\simeq 0{\cdot}5$. Thus the average number of created particles in π^--nucleus collisions may be taken to be

$$\langle N_c \rangle (\pi^-) = \langle n_s \rangle - 0{\cdot}5 \quad \ldots (10)$$

Taking these values of $\langle N_c \rangle (\pi^-)$ and $\langle n_c \rangle (\pi^-)$ we have

$$R_A(\pi^-) = \frac{\langle N_c \rangle (\pi^-)}{\langle n_c \rangle (\pi^-)} = \frac{\langle n_s \rangle - 0{\cdot}5}{\langle n_{ch} \rangle - 1{\cdot}4} \quad \ldots (11)$$

The values of R_A have been estimated using this expression for emulsion and plotted in Fig. 1. It may be seen from Fig. 1 that the value of R_A remains practically constant in the entire energy range from ~ 17 GeV to 200 GeV. The average value of $R_{em} = 1{\cdot}71 \pm 0{\cdot}07$.

The values of R_A have also been estimated for CNO, AgBr and other target nuclei and the average values have been plotted with respect to A in Fig. 2. A dependence of the form of Eq. (6) gives $\langle \alpha \rangle = 0{\cdot}125 \pm 0{\cdot}028$ (shown by the broken line) and that of Eq. (7) gives $\langle a \rangle = 0{\cdot}64$, $\langle b \rangle = 0{\cdot}35$ and $\langle c \rangle = 0{\cdot}26$. Since value of $\langle c \rangle$ is very close to 1/4 it seems better to express $R_A = a + bA^{1/4}$ and this gives $\langle a \rangle = 0{\cdot}628 \pm 0{\cdot}072$ and $\langle b \rangle = 0{\cdot}372 \pm 0{\cdot}056$ and thus

$$R_A = (0{\cdot}628 \pm 0{\cdot}072) + (0{\cdot}372 \pm 0{\cdot}056)\, A^{1/4} \quad \ldots (12)$$

The prediction of this expression is shown by solid line in Fig. 2

3. Discussion

From the above analysis, we see that in both the proton-nucleus and pion-nucleus collisions, the value of the mean normalized multiplicity (R_A) turns out to be essentially energy independent. This indicates that the production of particles occurs through intermediate stages. The target size dependence of R_A as expressed by Eqs. (6) and (7) has got some deeper consequences. A dependence of the form $R_A = A^\alpha$ may be directly compared with the collision pictures where all the target nucleons act collectively and contribute as a whole, towards the total number of final-state particles. The second kind of dependence of the form $R_A = a + bA^c$ which is more general may be directly compared with the collision pictures where a number of intermediate states are formed through the successive collisions of incident hadron with the target nucleons and it is predicted that R_A varies as $R_A = \alpha + \beta \nu$, where ν is the number of collisions inside the nucleus. If we use the observation[46] that at a given energy of incident hadron, the final state multiplicity in elementary collisions is independent of the quantum number of the incident hadron, then it follows that for the same number of collisions inside the nucleus the multiplicity in hadron-nucleus collisions should also be independent of the quantum number of the incident hadron. That means at a given energy, R_A should be independent of the nature of the incident particle and should depend only on the effective (target thickness) number of collisions (ν) inside the nucleus since a and b remain essentially unchanged in the two cases. (In fact, this is nothing but a part of universality hypothesis used in coherent-tube pictures[8-11]). It seems, therefore, quite reasonable to take $\langle \nu \rangle_{pA} \simeq A^{1/3}$ and $\langle \nu \rangle_{\pi^- A} \simeq A^{1/4}$ and then $R_A = a + b\nu$ simply. These results are in agreement with the observed inelastic cross-sections of proton-nucleus[52,53] and pion-nucleus[44] collisions. Since σ_{pA} varies as $\sim A^{2/3}$ and $\sigma_{\pi^- A}$ varies as $\sim A^{3/4}$ it follows[44] from the expression $\nu_{hA} \sim \frac{\sigma_{hn} A}{\sigma_{hA}}$ that ν_{pA} should vary as $\sim A^{1/3}$ and that $\nu_{\pi^- A}$ as $\sim A^{1/4}$. Here σ_{hn} and σ_{hA} are inelastic cross-sections of hadrons on nucleons and nuclei respectively. Coming now to the dependence of the form $R_A = A^\alpha$ we have $\alpha = 0{\cdot}17$ in proton-nucleus collisions and $\alpha = 0{\cdot}125$ in pion-nucleus collisions we can say that $R_A \simeq A^{1/6}$ in p-nucleus collisions and $\simeq A^{1/8}$ in π^--nucleus collisions. Taking $\nu \sim A^{1/3}$ in p-nucleus collisions and $\sim A^{1/4}$ in π^--nucleus collisions we find that $R_A \simeq \nu^{1/2}$ for both p-nucleus and π^--nucleus collisions. This agrees with the fact that final state multiplicities are independent of the quantum number of the incident hadron and depend only upon the effective target thickness involved. The collective contribution pictures predict the value of R_A as $\sim \nu^\alpha$ where α is determined from the energy dependence of multiplicity in elementary collisions. The data[46] suggest that the multiplicities vary as S^α, where $\sqrt{S}$ is the c.m. energy in these collisions. The

value of $\alpha \simeq 1/4$ in the energy range $\sim$ 20 GeV and above.[46] Since the c.m. energy in hadron-nucleus collisions is $\sqrt{S_{h\nu}} \simeq \sqrt{S\nu}$ we have $R_A \simeq \nu^{1/4}$ in all the collective contribution pictures. The analysis, therefore, leads to a dependence of R_A on ν which in no way is compatible with the collective contribution pictures of multiparticle production. Taking the logarithmic dependence of multiplicity on energy it follows that R_A varies as $\simeq \left(1 + \frac{\ln \nu}{\ln S}\right)$ which is even weaker than $\nu^{1/4}$. We, therefore, can say that only those double step pictures are allowed in which several intermediate states are formed and all of them contribute independently to the final-state particles. Further, the values of a and b in the expression of $R_A = a + b\nu$ are in close agreement with the predictions of energy flux cascade model[3] ($a = 2/3$, $b = 1/3$) and disagree with the predictions of the diffractive excitation models[1,2] ($a = b = 1/2$).

References

1. Dar A & Vary J, *Phys. Rev.*, D6 (1972), 2412.
2. Fishbane P M & Trefil J S, *Phys. Rev.*, D8 (1973), 1467.
3. Gottfried K, Vth Int. Conf. on High Energy Physics and Nuclear Structure, Uppsala, Sweden, June 18-22, 1973, p. 79; *Phys. Rev. Lett.*, **32** (1974), 957.
4. Fermi E, *Prog. theor. Phys.*, 5 (1950), 570.
5. Fermi E, *Phys. Rev.*, **81** (1951), 683.
6. Blenkij S Z & Landau L D, *Nuovo Cim. Suppl.*, 3 (1956), 15.
7. Fredriksson S, Royal Inst. of Technology, Stockholm, Sweden preprint TRITA-IFY-75-13, 1975.
8. Berlad G, Dar A & Eilam G, *Phys. Rev.*, D13 (1976), 161.
9. Takagi F, *Lett. Nuovo Cim.*, 14 (1976), 559.
10. Takagi F, *Prog. theor. Phys.*, 57 (1977), 939.
11. Kohli J M, III High Energy Phys. Symp., Bhubaneswar Nov. 1-5, Vol. II (1976), p. 339.
12. Morse W M *et al.*, *Phys. Rev.*, D15 (1977), 66.
13. Yeager W M *et al.*, *Phys. Rev.*, D16 (1977), 1294.
14. AADLMT Collaboration, *Soviet J. nucl. Phys.*, 25 (1977), 533.
15. BBDKSTTUH Collaboration, *Soviet J. nucl. Phys.*, 25 (1977), 539.
16. Kladnitskaya E N *et al.*, *Soviet J. nucl. Phys.*, 26 (1977), 176.
17. Winzeler H, *Nucl. Phys.*, 69 (1965), 661.
18. Kozodaeva O M *et al.*, *Soviet J. nucl. Phys.*, 22 (1976), 377.
19. Friedlander E M, Marcu M & Nitu R, *Lett. Nuovo Cim.*, 9 (1974), 341.
20. Azimov S A *et al.*, *Soviet J. nucl. Phys.*, 26 (1977), 180.
21. Barbaro-Gallieri A *et al.*, *Nuovo Cim.*, 21 (1961), 469.
22. Babecki J *et al.*, *Phys. Lett.*, 47B (1973), 268.
23. Alma-Ata-Leningrad-Moscow Collaboration, *Soviet J. nucl. Phys.*, 19 (1974), 537.
24. Tretyakova M I, *Proc. Int. Symp. on many particle hydrodynamics*, Eisenach, Germany, June 4-10, (1974), pp 477.
25. Gurtu A, Malhotra P K *et al.*, *Pramana*, 3 (1974), 311.
26. Tsi-Chu, Kim C O *et al.*, *Lett. Nuovo Cim.*, 20 (1977), 257.
27. Agarwal M M *et al.*, *Nucl. Phys.*, B131 (1977), 61.
28. Lohrman E & Teucher M W, *Nuovo Cim.*, 25 (1962), 957.
29. Hebert J *et al.*, *Phys. Rev.*, D15 (1977), 1867.
30. Kohli J M, *Lett. Nuovo Cim.*, 13 (1975), 19.
31. Jones W *et al.*, 14th Int. Cosmic Ray Conf. Munich, Germany, Aug. 15-29, 1975, p. 2263.
32. Fumuro F. *et al.*, 15th Int. Cosmic Ray Conf. Plovdic, Bulgaria, Aug. 13-26, 1977, p. 59.
33. Florian J R *et al.*, *Phys. Rev.*, D13 (1976), 558.
34. Atanelishvili M I *et al.*, *Soviet Phys. JETP Lett.*, 18 (1973), 288; 19 (1974), 221.
35. Miller D J & Nowak R, *Lett. Nuovo Cim.*, 13 (1975), 39.
36. Gierula J, Proc. 11th Int. Cosmic Ray Conf., Budapest 1969, p 157.
37. Aziz T *et al.*, unpublished work.
38. Takiabaev Zh S, Morozova P V & Titova N S, *Soviet J. nucl. Phys.*, 20 (1975), 209.
39. Babecki J *et al.*, Kracow Report, 929/PH, (1976).
40. Anzon Z V *et al.*, *Nucl. Phys.*, B129 (1977), 205.
41. Angelov N S *et al.*, *Soviet J. nucl. Phys.*, 25 (1977), 537.
42. Azimov S A *et al.*, *Soviet J. nucl. Phys.*, 22 (1976), 608.
43. Elliott J R *et al.*, *Phys. Rev. Lett.*, 34 (1975), 607.
44. Busza W *et al.*, *Phys. Rev. Lett.*, 34 (1975), 836.
45. Ya Inogamova T *et al.*, Joint Institute of Nuclear Physics, Dubna Report No. R1.8464, 1974.
46. Albini E *et al.*, *Nuovo Cim.*, 32A (1976), 101.
47. Ammosov V V *et al.*, *Nuovo Cim.*, 40A, (1977), 237.
48. Daniel R R *et al.*, Tata Institute of Fundamental Research Report, TIFR-BC-73-4, 1973.
49. Boggild H *et al.*, *Nucl. Phys.*, B27 (1971), 285.
50. Chadha S *et al.*, *Phys. Rev.*, D10 (1974), 2817.
51. Berger E L *et al.*, Preprint CERN/D. PH-11/Phys., 1974, 74-9.
52. Denisov S P *et al.*, *Nucl. Phys.*, B61 (1973) 62.
53. Denisov S P *et al.*, *Soviet J. nucl. Phys.*, 18 (1974), 173.

Indian Journal of Pure & Applied Physics
Vol. 18, October 1980, pp. 784-787

Dielectric Relaxation Study of Intermolecular Association through Hydrogen Bonding of *p*-Halophenols in Non-polar Solvents

C K Misra,* M C Saxena & A K Saxena

EPR & Microwave Research Laboratory, Physics Department, Lucknow University, Lucknow

Received 2 *May* 1979

Measurements of dielectric constant (ϵ'), dielectric loss (ϵ'') in 3-cm microwave region, static dielectric constant (ϵ_0) and refractive index n_D of *p*-fluorophenol, *p*-chlorophenol and *p*-bromophenol in dilute solutions of benzene, *p*-dioxane, carbon tetrachloride and cyclohexane at 23 C have been carried out. With the help of these data, relaxation times (τ) and distribution parameters (α) have been evaluated. Free-energies of activation for dipole reorientation and viscous flow have also been calculated. It has been found that log τ versus log η plot for each solute is nonlinear. The results have been analyzed in terms of molecular motions of the system and it has been found that the dipole rotation process is appreciably influenced by self-association of the solute, besides solute-solute-solvent interaction.

1. Introduction

Phenols are strongly associated in the liquid state and undergo hydrogen bonding[1] with many solvents. In spite of numerous studies made in respect of self-association of phenol, there is still considerable disagreement regarding the extent of association[2] and the nature of molecular aggregates[3,4] of phenols in organic solvents. Association of phenol has been studied by many physical methods, notable among which are IR, NMR and polarization measurements. Woolley and Helper[5] found by the calorimetric method that phenol is considerably more self-associated in cyclohexane and carbon tetrachloride than in benzene. They also indicated that phenol interacts most strongly with π-electron of benzene resulting in OH—π bonding. Fischer[6] employed rf measurements to study association of phenol in CCl_4. The potentiality of dielectric relaxation measurements in microwave region as a method of studying weak molecular interactions has been amply demonstrated.[7,8] Magee and Walker[9] investigated phenol in a number of non-polar solvents and found that even at the lowest concentration the relaxation time, of phenol is substantially lengthened by intermolecular association due either to solute-solute interactions, or to hydrogen bonding of phenol to the π-electron cloud of the solvent (*p*-xylene) or to both factors. Magee and Walker[10] also investigated *p*-chlorophenol along with other substituted phenols for their dielectric behaviour, and for *p*-chlorophenol the value of relaxation time obtained was as high as 39 psec which they attributed to intermolecular association.

In the present paper, the dielectric behaviour of some *p*-halophenols, namely *p*-fluorophenol, *p*-chlorophenol and *p*-bromophenol in dilute solutions of non-polar solvents, namely, benzene, *p*-dioxane, carbon tetrachloride and cyclohexane has been studied to observe the presence of molecular interactions.

The most probable relaxation time τ and the distribution parameter α have been estimated from the knowledge of a' and a'' at a single microwave frequency, and a_0 and a_∞, utilizing the following equations by Higasi,[11]

$$\left.\begin{aligned} \tau &= \frac{1}{\omega}\left[\frac{A^2 + B^2}{C^2}\right]^{1/[2(1-\alpha)]} \\ 1 - \alpha &= \frac{2}{\pi}\tan^{-1}\left(\frac{A}{B}\right) \end{aligned}\right\} \quad ...(1)$$

where

$$\left.\begin{aligned} A &= a''(a_0 - a_\infty) \\ B &= (a_0 - a')(a' - a_\infty) - a''^2 \\ C &= (a' - a_\infty)^2 + a''^2 \end{aligned}\right\} \quad ...(2)$$

The quantities a_0, a_∞, a' and a'' are defined as

$$\left.\begin{aligned} \epsilon_0 &= \epsilon_{10} + a_0 C_2 \\ \epsilon_\infty &= \epsilon_{1\infty} + a_\infty C_2 \\ \epsilon' &= \epsilon_1' + a' C_2 \\ \epsilon'' &= a'' C_2 \end{aligned}\right\} \quad ...(3)$$

where ϵ_0 is the static dielectric constant and $\epsilon_\infty = n_D^2$ is the permittivity at high frequency. The subscript 1 refers to the pure solvent, C_2 is the molar concentration of polar solute and a_0, a_∞, a' and a'' are the

* Present address : Lecturer, Department of Physics, BSNVD College, Lucknow.

slopes of the straight lines obtained by plotting dielectric quantity against concentration. It is found that plots remain linear in the concentration range 0·0015-0·014 *M*. Free-energies of activation for dipolereorientation and viscous flow have been evaluated, using Eyring theory of rate process.[12]

2. Experimental Procedure

The dielectric constant (ϵ') and dielectric loss (ϵ'') were measured at *X*-band ($\lambda = 3{\cdot}1$ cm) (Ref. 13) using the technique of Roberts and Von Hippel[14] modified by Dakin and Works.[15] The static dielectric constant (ϵ_0) at 300 kHz was measured by a diploemeter based on the principle of heterodyne beat method. The refractive indices n_D of all the solutions were measured by Abbe's refractometer. The viscosity and density measurements were carried out by Ostwald viscometer and pyknometer respectively. The measurements for ϵ' and ϵ'' are accurate up to $\pm$ 1 and $\pm$ 5% respectively. The chemicals were obtained from the Aldrich Chemicals Co. Inc., USA. Physical properties of the chemicals were checked against the literature values. The solvents (AR grade) obtained from the British Drug House, England, were distilled twice before use.

3. Results and Discussion

The values of a_0, a', a'' and a_∞ for the three solutes in different non-polar solvents under investigation are reported in Table 1. The values of τ, α and activation energy of the solutes are given in Table 2. Table 2 shows that in each solvent τ increases from *p*-fluoro to *p*-bromo through *p*-chlorophenol. This is expected because the size of the solute molecule increases from *p*-fluoro to *p*-bromo through *p*-chlorophenol. Further, each solute has non-zero value of α. It is indicative of the fact that the dielectric absorption in the present system is contributed by the molecular as well as intramolecular-OH group rotation. Table 2 also shows that α values are appreciably higher in benzene, *p*-dioxane and CCl_4 than in cyclohexane. For some substituted phenols, Kraft *et al.*[16] obtained the value of α in *p*-dioxane as high as 0·29. Many others[17] obtained higher values of α in benzene and *p*-xylene solutions and attributed them to solute-solvent interaction. Therefore, it is suggested that higher values of α in benzene, *p*-dioxane and CCl_4 may be due to the presence of molecular interactions.

The presence of —OH group rotation is expected to lower the observed values of τ in each solute. But our results show high values of τ. It is, therefore, suggested that in each solvent —OH group rotation is hindered and the extent of hindrance varies with the nature of the solvent besides the viscosity influences.

For all the *p*-halophenols, the relaxation time lengthens in the solvent order: cyclohexane < benzene < *p*-dioxane < carbon tetrachloride. The order of

Table 1—Values of a_0, a', a^* and a_∞ of the Solutes in Non-polar Solvents at 23°C

Solvent	a_0	a'	a^*	a_∞
	p-Fluorophenol			
Benzene	8·00	2·89	2·67	0·454
Cyclohexane	3·34	2·35	1·33	0·307
p-Dioxane	11·25	3·62	3·39	0·285
Carbon tetrachloride	14·00	4·11	3·82	0·250
	p-Chlorophenol			
Benzene	5·45	2·00	1·79	0·500
Cyclohexane	4·45	2·75	1·77	0·375
p-Dioxane	6·67	2·01	1·85	0·411
Carbon tetrachloride	10·17	3·03	2·70	0·542
	p-Bromophenol			
Benzene	6·01	2·15	1·98	0·454
Cyclohexane	7·50	3·99	3·31	0·187
p-Dioxane	10·01	2·87	2·69	0·375
Carbon tetrachloride	9·21	2·50	2·37	0·275

Table 2—Values of τ, α, ΔF_ϵ and ΔF_η of solutes in Non-polar Solvents

Solvent	$\tau \times 10^{12}$ sec	α	ΔF_ϵ kcal/mole	ΔF_η kcal/mole
	p-Fluorophenol			
Benzene	28·6	0·16	3·04	2·89
Cyclohexane	11·0	0·04	2·48	3·29
p-Dioxane	34·1	0·23	3·15	3·30
Carbon tetrachloride	41·1	0·27	3·26	3·18
	p-Chlorophenol			
Benzene	29·7	0·14	3·06	2·89
Cyclohexane	13·4	0·01	2·60	3·29
p-Dioxane	40·8	0·21	3·25	3·30
Carbon tetrachloride	45·7	0·23	3·32	3·18
	p-Bromophenol			
Benzene	29·9	0·15	3·07	2·89
Cyclohexane	14·6	0·06	2·65	3·29
p-Dioxane	43·6	0·25	3·28	3·30
Carbon tetrachloride	47·4	0·26	3·34	3·18

solvent viscosity η is: benzene (0·6) < cyclohexane (0·91) < carbon tetrachloride (0·94) < *p*-dioxane (1·3 cP). Therefore, the effect of η alone does not account for the relaxation behaviour. Further, it is found that for each solute log τ vs log η plot is non-linear (Fig. 1). The deviation from linearity may be attributed to intermolecular association in solution. Singh and Viz[18] also obtained for some organic polar molecules nonlinear behaviour of log τ vs log η plot. They interpreted their results in the light of solute solvent interactions.

Fately *et al.*[19] confirmed through IR studies that cyclohexane does not interact with *p*-fluorophenol and *p*-chlorophenol and remains inactive[20] for most of the solutes. Therefore, in cyclohexane, τ of each solute lengthens probably due to solute-solute interactions resulting in self-association through OH—X (= F, Cl, Br) bonding. Whetsel and Lady[3] also found that hydroxyl compounds in cyclohexane exist as associated ones.

One of the most interesting features of the present study is the values of τ of *p*-halophenols in benzene which has the lowest viscosity amongst the solvents investigated. Woolley and Helper[5] investigated association of phenol in dilute solutions of benzene and cyclohexane and concluded that besides self-association of phenol in benzene, phenol interacts with π-electrons of benzene which is an electron donor[21] resulting in OH—π bonding. The interaction of the acidic proton of phenol is likely to be increased by *p*-halogen substitution.[23] Therefore, abnormal lengthening of τ in benzene may be attributed to the formation of OH—π bonding resulting due to the π-electron interaction with the solute besides its self-association. Magee and Walker[9] also observed that phenol in *p*-xylene exists in multimer forms and interacts with electrons of *p*-xylene.

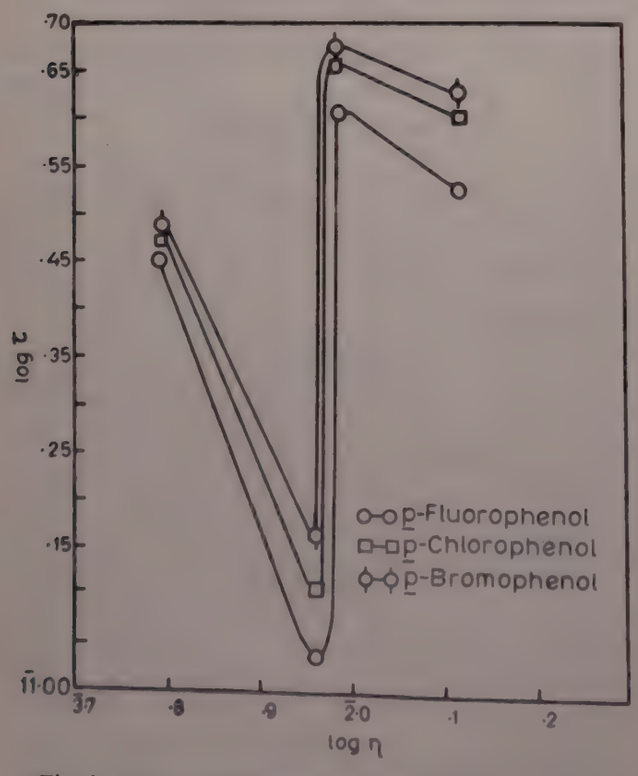

Fig. 1—Log τ versus log η plots of the halophenols

It is found that τ of each solute in *p*-dioxane is greater than that in benzene. Magee and Walker[9] pointed out a smaller percentage of association of phenol in more interacting solvents but it must still be considerable. Therefore, larger value of τ of each solute in *p*-dioxane than in benzene may be attributed to different molecular aggregates of the solute in *p*-dioxane besides its high viscosity. However, the interaction of *p*-dioxane with the solute through OH—O bonding may also be a factor for lengthening τ.

Also, τ for all solutes is highest in carbon tetrachloride (Table 2). IR data[23] on phenol + CCl_4 system show that 40% of phenol is polymerized even at the concentration of 0·02 mole fraction. Carbon tetrachloride is considered as a weak proton acceptor or electron donor[5] and *p*-halophenols are considered as proton donors. Therefore, in these systems donor-acceptor interactions may also occur. Therefore, the highest lengthening of τ in CCl_4 is perhaps due to self-association of the solute and solvent effect besides donor-acceptor interactions. The behaviour of CCl_4 observed in the present study follows a general trend and is exhibited by a number of polar molecules. Chitoku and Higasi[24] explained higher values of τ in CCl_4 due to its 'sticky' nature which arises possibly from the fairly large short-range forces between the molecules of the solute and carbon tetrachloride.

It is also observed that, for each solute, the value of τ in benzene, *p*-dioxane and carbon tetrachloride increases with the basicity of the solvent. Tamros[25] and Brown and Broody[26] also observed increase in τ with the basicity of the solvent and interpreted this behaviour on the basis of donor-acceptor interaction. The basicity of the solvent should, to some extent, be reflected in its ionization potential.[27] The ionization potential of the solvent follows the order: benzene (9·25 eV) < *p*-dioxane (9·52 eV) < carbon tetrachloride (11·1 eV) while in these solvents τ follows the order : benzene < *p*-dioxane < carbon tetrachloride. Crosseley and Smyth[28] also observed an increase in τ of some haloethanes with the ionization potential of the solvent which they attributed to solute-solvent interactions.

Free-energies of activation for dipole reorientation (ΔF_τ) and for viscous flow process (ΔF_η) are

also presented in Table 2. It has been found that for each solute in an inert solvent cyclohexane ΔF_e is smaller than ΔF_n. This may be due to the fact that in viscous flow process, translational motion is also present in addition to the rotational motion present in dipole-reorientation. Similar results have been reported by Krishnaji and Mansingh.[29] It has also been observed that in each solvent ΔF_e increases from *p*-fluorophenol to *p*-bromophenol through *p*-chlorophenol. In interacting solvents (benzene, *p*-dioxane and CCl_4) free-energies of activation are found to be larger probably due to the presence of larger species in the solution. This suggests that ΔF_e increases with the size of the molecule. Similar results have been reported by Dhar *et al.*[30]

The present study of *p*-halophenols shows non-zero distribution parameter which is indicative of the presence of molecular and intramolecular —OH group rotations in the system. Neither τ nor α shows any definite trend with the solvent viscosity; τ and α are found to be maximum in carbon tetrachloride and minimum in cyclohexane. As cyclohexane has been found to be inactive[20] for most of the solutes, comparatively high τ in cyclohexane suggests the possibility of solute-solute interaction resulting in self-association of the solute through hydrogen bonding. Whetsel and Lady[3] found that hydroxyl compounds in cyclohexane exists as associated ones. Abnormally high values of α and τ in benzene, *p*-dioxane and carbon tetrachloride are indicative of the presence of solute-solvent interaction besides self-association of the solute.

Acknowledgement

The authors are grateful to Prof. B G Gokhale, for providing facilities and encouragement throughout the work. Financial support to one of the authors (CKM) by the University Grants Commission, New Delhi, and to another (AKS) by CSIR, New Delhi, is gratefully acknowledged.

References

1. Vinogradov S N & Linnel R M, *Hydrogen bonding* (D Van Nostrand Reinhold Co., New York), 1970.
2. Parker A, *J. Chem. Rev.*, 69 (1969), 1.
3. Whetsel K B & Lady J H, *Spectrometry of fuels* (Plenum Press, New York) 1970, 259, 279.
4. Woolley E M, Travers T G, Erno B P & Helper L G, *J. phys. Chem.*, 75 (1971), 3591.
5. Woolley E M & Helper L G, *J. phys. Chem.*, 76 (1972), 3058.
6. Fischer E, *Z. Naturf.*, 8a (1953), 168.
7. Boule P, *J. chem. Phys.*, 57 (1972), 5285.
8. Chitoku K & Higasi K, *Bull. chem. Soc. Japan*, 40 (1967), 773.
9. Magee M D & Walker S, *Can. J. Chem.*, 49 (1971), 1107.
10. Magee M D & Walker S, *J. phys. Chem.*, 74 (1970), 2378.
11. Higasi K, *Bull. chem. Soc. Japan*, 39 (1966), 2157.
12. Glasstone S, Laidler K J & Eyring H, *The theory of rate process* (McGraw-Hill, New York), 1941.
13. Vyas A & Saxena M C, *J. scient. ind. Res.*, 16B (1957), 148.
14. Roberts S & Von Hippel A, *J. appl. Phys.*, 17 (1946), 610.
15. Dakin T W & Works C N, *J. appl. Phys.*, 18 (1947), 610.
16. Kraft J, Walker S & Magee M D, *J. phys. Chem.*, 79 (1975), 881.
17. Kartizky A, *Physical methods in heterocyclic chemistry*, Vol. 4 (Academic Press, London), 1971.
18. Singh B & Viz J K, *Bull. chem. Soc., Japan*, 48 (1975), 2551.
19. Fateley J W, Garison G L & Bentley F F, *J. phys. Chem.*, 77 (1975), 199.
20. Schneider W G, *J. phys. Chem.*, 48 (1968), 4742.
21. Slifkin M A, *Charge transfer interaction in biomolecules* (Academic Press, London), 1971.
22. Jain M K, *Principles of organic chemistry* (S Nagin & Co., New Delhi), 1975.
23. Mecke R, *Discuss Faraday Soc.*, 9 (1950), 161.
24. Chitoku K & Higasi K, *Bull. chem. Soc. Japan*, 39 (1966), 2160.
25. Tamros M, *Discuss. Faraday Soc.*, 74 (1952), 3375.
26. Brown H C & Broody J P, *Discuss. Faraday Soc.*, 74 (1952), 3570.
27. Vendeneyev V J, Gurich L V, Condratiyev V N, Medvedev V A & Frankevich Ye L, *Bond energies, ionization potentials and electron affinities* (Edward Ltd, London), 1966.
28. Crosseley J & Smyth C P, *J. Am. chem. Soc.*, 91 (1969), 2482.
29. Krishnaji & Mansingh A, *J. chem. Phys.*, 42 (1965), 2503.
30. Dhar R L, Shukla J P & Saxena M C, *Z. phys. Chem.*, 76 (1971), 232.

Indian Journal of Pure & Applied Physics
Vol. 18, October 1980, pp. 788-792

Axial Cylindrical Surface Wave Transmission across a Bend

G P Sinha & K P Sharma

P G Department of Physics, Bhagalpur University, Bhagalpur 812 007

Received 22 *September* 1979

An approximate expression for the power transmission coefficient (T) of a small bend in a metallic cylindrical corrugated rod (single wire transmission line) propagating axial cylindrical surface waves, has been developed. The behaviour of such surface waves in negotiating a small bend has been reported. T for different bend angles in cylindrical metallic rods of different surface reactances have been determined experimentally and the results obtained by calculation for bends up to 10 have been confirmed. An equivalent-T network has been suggested to represent a bend and with its help the behaviour of the bend has been discussed.

1. Introduction

The behaviour of a surface wave on a flat surface when the supporting surface has a slight curvature has already been reported by Barlow and coworkers.[1,2] It has been suggested that when the surface wave is supported on a cylindrical surface having a longitudinal curvature, energy is radiated outward from the bend, away from the centre of curvature, and on the inside of the bend the field is more strongly evanescent so that no radiation occurs in that direction. Chiba[3] reported an experimental study of such a radiation from a bend in a single wire transmission line. This study is primarily confined to the frequency range 100-700 MHz and to the variation of power losses in this frequency range with the radius of curvature of the bend and the bend angle. However, no theoretical calculation of the power transmission coefficient T of a bend in a single wire transmission line is available. In this paper, an approximate calculation of T across small angles has been done and the behaviour of surface wave transmission across bends studied. Experimental study of the problem has been made in the microwave region at a frequency of 9·6 GHz using corrugated cylindrical metallic rods of different surface reactances. The study is important from the point of view of signal transmission by a single wire line at microwave frequencies.

2. Theoretical Calculation of T

The points on the circumference of a circle of radius r with its centre at the bend point O when projected on the median plane of the bend will be an ellipse of semi-major axis $r \sec\alpha$ and semi-minor axis r (Fig. 1). A plane of transverse dimension r through the axis of the guide at any azimuth has an intercept η on the median plane at the bend given by

$$\frac{\eta^2 \cos^2\theta}{r^2 \sec^2\alpha} + \frac{\eta^2 \sin^2\theta}{r^2} = 1 \qquad \ldots (1)$$

Eq. (1) yields

$$\eta = r \sec\alpha \ (\cos^2\theta + \sec^2\alpha \sin^2\theta)^{-1/2}$$

$$\text{and } \frac{d\eta}{d\theta} = -\frac{1}{2} r \sec\alpha \ \tan^2\alpha \sin 2\theta \ (\cos^2\theta + \sec^2\alpha \sin^2\theta)^{-3/2}$$

For small α,

$$\sec\alpha \approx 1 \text{ and } \tan\alpha \approx \alpha$$

In such a condition

$$\frac{d\eta}{d\theta} = -\frac{1}{2} r \alpha^2 \sin 2\theta \qquad \ldots (2)$$

If ψ be the angle between η and r for any azimuth θ.

$$\eta = r \sec\psi$$

so that

$$\frac{d\eta}{d\psi} = r \tan\psi \sec\psi$$

$$\approx r\psi \text{ for small } \alpha$$

In such a condition

$$\frac{d\psi}{d\theta} = -\frac{1}{2} \frac{\alpha^2 \sin 2\theta}{\psi}$$

$$\text{Or} \quad -\int \psi \, d\psi = \frac{1}{2}\alpha^2 \int \sin 2\theta \, d\theta$$

$$\text{Or} \quad 2\psi^2 + C = \alpha^2 \cos 2\theta \qquad \ldots (3)$$

where C is the constant of integration.

$$\text{When } \theta = \frac{\pi}{2}, \ \psi = 0$$

so that

$$C = -\alpha^2$$

Hence $\psi = \alpha \cos\theta$

Electric field tangential to the median plane will be

$$\mathbf{E}_t = \mathbf{E}_r \cos\psi + \mathbf{E}_x \sin\psi \qquad ...(4)$$

Assuming that the fields in the transverse plane 1 in Fig. 1 at a small bend (at $x = 0$) are approximated by the axial cylindrical surface wave fields in the form

$$\mathbf{E}_r = -\frac{2\beta}{\pi u} k_1(ur),\ \mathbf{H}_\theta = -\frac{2}{\pi}\frac{\omega\epsilon_0}{u} k_1(ur)$$

and $\mathbf{E}_x = -j\frac{2}{\pi} k_0(ur)$

where u is the radial decay coefficient, β the axial phase coefficient of the wave $\omega\ (= 2\pi f)$ the angular frequency of the wave, ϵ_0 the permittivity of the free space, j the phasor operator, and $k_0(ur)$ and $k_1(ur)$ are respectively the modified Bessel's functions of zeroth and first order and of second kind. Substituting these values in Eq. (4), we get

$$\mathbf{E}_t = -\frac{2}{\pi}\left[\frac{\beta}{u} k_1(ur)\cos\psi + j\,k_0(ur)\sin\psi\right]$$

$$\exp[\ j\beta x]$$

at a point on the median plane at a longitudinal distance x from the bend ($x = 0$),

As $r = \eta\cos\psi$, $x = \eta\sin\psi$ and $\psi = \alpha\cos\theta$

$$E_t = -\frac{2}{\pi}\left[\frac{\beta}{u} k_1\{u\eta\cos(\alpha\cos\theta)\}\cos(\alpha\cos\theta) + j\,k_0\{u\eta\cos(\alpha\cos\theta)\}\sin(\alpha\cos\theta)\right]$$

$$\exp\left[-j\beta\eta\sin(\alpha\cos\theta)\right] \qquad ...(5)$$

Further, for any θ, let $\mathbf{H}_\theta$ make an angle ϕ with the median plane at the bend. We find that $\phi = 0$ when $\theta = 0°$. Had the median surface been conical at the bend, maintaining an angle α with the transverse plane (1), ϕ would have been zero for all values of θ. But as it is plane, it approaches a maximum value of α at $\theta = \pi/2$. Thus when ψ is zero, ϕ is maximum, and when ψ is maximum, ϕ is zero. This suggests that ϕ may be taken in the form

$$\phi = \alpha\sin\theta$$

Hence the magnetic field tangential to the median plane at a point on the median plane, at a longitudinal distance x from the bend ($x=0$), is

$$\mathbf{H}_t = \mathbf{H}_\theta\cos\phi = \frac{2}{\pi}\frac{\omega\epsilon_0}{u} k_1(ur)\exp[-j\beta x]\cos\phi$$

$$= -\frac{2}{\pi}\frac{\omega\epsilon_0}{u}\left[k_1\{u\eta\cos(\alpha\cos\theta)\}\cos(\alpha\sin\theta)\right]\exp\left[-j\beta\eta\sin(\alpha\cos\theta)\right] \qquad ...(6)$$

Taking small α approximations of $\cos(\alpha\cos\theta)$, $\sin(\alpha\cos\theta)$, $\cos(\alpha\sin\theta)$ and $\sin(\alpha\sin\theta)$ as $J_0(\alpha)$, $2J_1(\alpha)\cos\theta$, $J_0(\alpha)$ and $2J_1(\alpha)\sin\theta$ respectively, we have,

$$\mathbf{E}_t = -\frac{2}{\pi}\left[\frac{\beta}{u} J_0(\alpha)\,k_1\{u\eta J_0(\alpha)\} + j\,2J_1(\alpha)\cos\theta\,k_0\{u\eta J_0(\alpha)\}\right]\exp\left[-j2\beta\eta J_1(\alpha)\cos\theta\right] \qquad ...(7)$$

and

$$\mathbf{H}_t = -\frac{2}{\pi}\frac{\omega\epsilon_0}{u}\left[J_0(\alpha)\,k_1\{u\eta J_0(\alpha)\}\right]\exp\left[-J2\beta\eta J_1(\alpha)\cos\theta\right] \qquad ...(8)$$

With the tangential electric and magnetic fields in the median plane for a small bend thus approximated, application of Lorentz Reciprocity theorem as suggested by Barlow and Brown,[1] to the problem gives τ, the complex constant whose amplitude and phase define the transmission properties of the bend in the form

$$\tau = \frac{2J_0(\alpha)\,[J_0(\alpha)P + 2uJ_1(\alpha)Q]}{s^2\{k_1^2(us) - k_0(us)k_2(us)\}} \qquad ...(9)$$

where

$$P = \int_0^S \eta\,k_1^2[uJ_0(\alpha)\eta]\,J_0[4\beta J_1(\alpha)\eta]\,d\eta$$

$$Q = \int_0^S \eta\,k_0\{uJ_0(\alpha)\eta\}\,k_1\{uJ_0(\alpha)\eta\}\,J_1\{4\beta J_1(\alpha)\eta\}\,d\eta$$

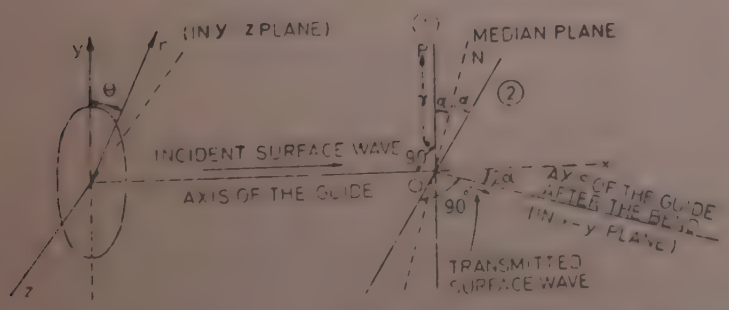

Fig. 1—Geometry of transmission of axial cylindrical surface wave across a bend

and s is the radius of the guide. The quantity being real, the phase of τ is zero or $\pm \pi$. P and Q are determined by numerical integration using Simpson's rule for small α. Q and hence the term $2 u J_1(\alpha)/\beta$ has been found to be insignificant compared to $J_0(\alpha)$ P. Hence,

$$\tau = |\tau| = \frac{2 J_0^2(\alpha) P}{s^2 \{k_1^2 (u s) - k_0 (u s) k_2 (u s)\}} \quad \ldots(10)$$

Therefore, for small bends

$$T = |\tau|^2 = \frac{4 J_0^4(\alpha) P}{s^4 [k_1^2 (u s) - k_0 (u s) k_2 (u s)]^2} \quad \ldots(11)$$

Variation of T with bend angle 2α for $u = 0{\cdot}1\ \text{cm}^{-1}$ (i.e. surface reactance $Xs = 1{\cdot}95$ ohm) and $s = 0{\cdot}3$ cm, as calculated by this expression, is shown in Fig. 2.

T is about 0·99 up to a bend angle of 10°. Calculation also shows that $4P^2$ differs from the denominator of the expression for T by about 1% only for $s = 0{\cdot}3$ cm. Hence, the expression for T may be further approximated to $J_0^4(\alpha)$ for a wide range of u, and hence for Xs for the single wire line, provided α is small; this further indicates that for small bend angles, T is almost independent of u or of Xs of the guide.

As discussed by Barlow and Brown,[1] the amplitude and phase of the wave transmitted past the bend in a flat surface is $-\tau$. As the phase of τ is zero or $\pm \pi$ for a small bend in a single wire line, such a bend attenuates the guided wave with a phase shift of zero or $\pm \pi$. Hence, while the surface wave would travel round a curved surface of large radius of curvature in a flat surface without attenuation,[1] the axial cylindrical surface wave on a cylindrical rod would travel with attenuation under a similar situation. Thus the problem of radiation from a bend in a single wire transmission line is serious even when the radius of curvature of the bend is large.

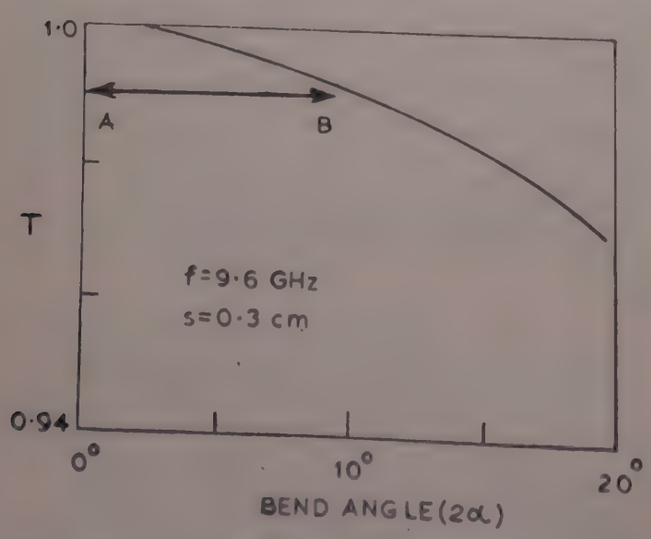

Fig. 2—Variation of T for small angle bends (by calculation)

3. Experimental Determination of T

The experimental scheme adopted was to launch radial cylindrical surface waves over a cylindrical metallic corrugated rod ($X_s = 1{\cdot}95$ ohm and $s = 0{\cdot}3$ cm, and length = about 75 cm) and then connecting it to cylindrical metallic corrugated rods (about 30 cm in length) of different surface reactances one by one. Bends of different angles and different curvatures were made in the smaller rods for investigation.

Sharma[4] utilized the method of Storer *et al.*[5] for investigating the behaviour of a discontinuity in the path of surface waves on a flat surface by making measurements through a junction. The same method could have been used in the present study. However, the authors[6] made a thorough study of the transmission of axial cylindrical surface waves across a discontinuity in surface reactance. It was concluded that the power reflection coefficients (PRC) of such a discontinuity is too small to be measured and the radius of the reflection coefficient circle (RCC) obtained from the reflection coefficient data near the discontinuity corresponding to different positions of a short circuit termination on the other side of the discontinuity, directly gives T of the discontinuity. With the bend of radius of curvature 7·75 cm in the smaller guide similar reflection coefficient data were obtained near the junction of the two guides. It was found that the centre of the RCC is not significantly displaced from the origin of the polar coordinate system for bends of not only small angles but also of large angles. It was, therefore, concluded that not only the discontinuity in surface reactance but also a bend has a negligible PRC. In such a situation, the radius of RCC gives T of the surface reactance discontinuity and the bend conjointly; from this, T of the bend follows from the previously determined value of T of the surface reactance discontinuity.

Bends of the smaller radii of curvature could not be made as the width of the corrugation of the single wire line would be adversely changed in bending the guide. A bend of radius of curvature 7·75 cm was found satisfactory from this point of view. The experimental results are shown in Fig. 3. It is seen that in conformity with the prediction by approximate calculation, T of bends up to 10° approximates to unity and in this range of bend T is almost independent of the surface reactance of the guide.

As the bend angle increases, T decreases. The decrease is very rapid for a guide of low surface reactance but it is slow for a guide of high surface reactance.

4. An approximate Circuit Equivalent for the Bend in the Single Wire Transmission Line

The bend may be replaced by a four-terminal network. The input and the output reference planes of this network may be selected on the straight portions on the two sides of the bend so that the incoming and outgoing guided waves are in phase. Further, a bend is a symmetrical discontinuity in a single wire transmission line and has PRC approaching to zero. Hence for the input and output reference planes as specified above, the scattering matrix of the bend will be

$$S = \begin{bmatrix} 0 & |S_{12}| \\ |S_{12}| & 0 \end{bmatrix} \begin{bmatrix} 0 & T^{1/2} \\ T^{1/2} & 0 \end{bmatrix}$$

where T is the power transmission coefficient of the bend.

The coefficients of the impedance matrix will then be

$$Z_{11} = Z_{22} = \frac{1+T}{1-T} = |Z_{11}|$$

and $$Z_{12} = Z_{21} = \frac{2T^{1/2}}{1-T} = |Z_{12}|$$

Hence the equivalent-T representing the bend between such input and output reference planes will

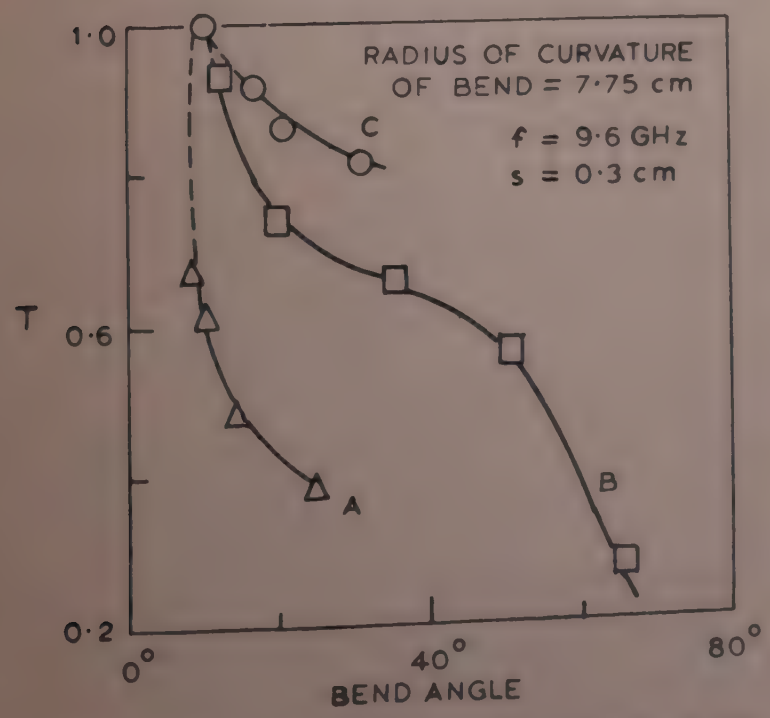

Fig. 3—Variation of T with bend angle (by experiments) [Xs values in ohm for different curves : ○—○, 75·4; □—□, 50; and △—△, 20·5]

Fig. 4—Variation of the resistive series element of the equivalent-T for the bend with bend angle [Xs values (in ohm) for different curves : ○—○, 75·4; □—□, 50; and △—△, 20·5]

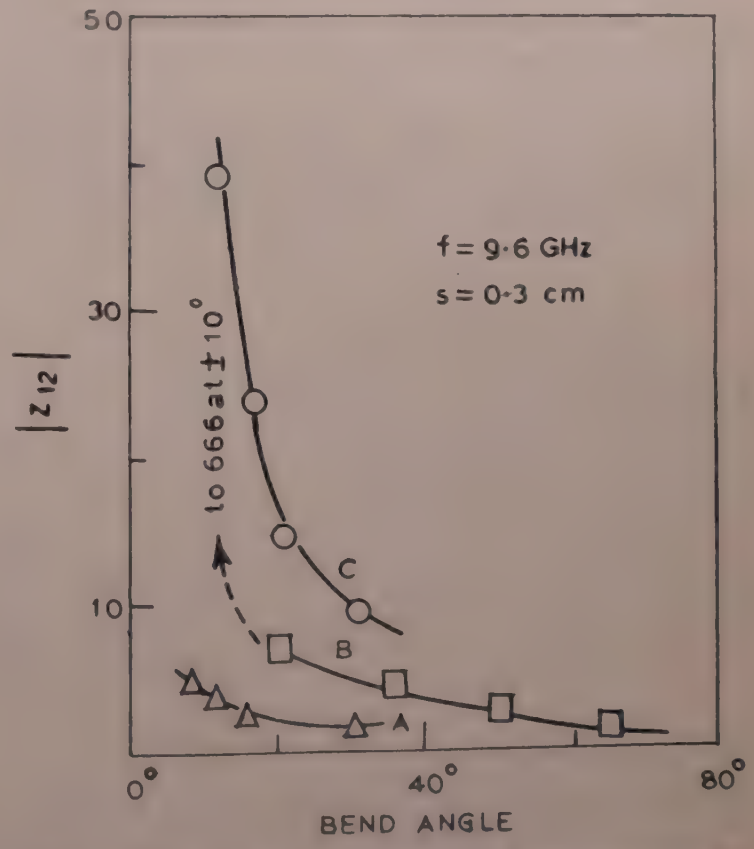

Fig. 5—Variation of the shunt element of the equivalent-T for the bend with bend angle [Xs values (in ohm) for different curves: ○—○, 75·4; □—□, 50; and △—△, 20·5]

have a resistive element $|Z_{11}| - |Z_{12}|$ in each of its series arms and a resistive element $|Z_{12}|$ in its shunt limb. Variation of the resistive series element of the equivalent-T for the bend with bend angle for guides of different surface reactances is shown in Fig. 4. Fig. 5 gives the variation of shunt resistive element of the equivalent-T with bend angle for guides of different surface reactances. The series resistive element is much lower compared to the shunt resistive element for bends in guides of low as well as high surface reactances over a long range of bend angles. Therefore, the effect of the bend is, to a first approximation, analogous to shunting a

transmission line by a resistance. The power absorbed in the resistance is equivalent to the power radiated from the bend. A lower value of this shunt-resistance is approached for higher bend angles and hence power reflection may be expected from a bend of large angle. From an experiment with a 90° bend of radius of curvature 7·75 cm in a guide of 20·5 ohm surface reactance, it was found that the reflection coefficient data do not vary significantly as the position of short circuit in the experimental arrangement is changed. From these data it was concluded that even this bend has PRC of about 0·02 and is too small to be measured accurately.

5. Discussion

From the investigation it is concluded that T for small bends approaches unity and even a bend of somewhat large angle of 15° in a guide of high surface reactance can have T of more than 0·94. Hence in such a guide a 90° turn, achieved in six steps of 15°, will have a net T of not less than 0·82. This is the only way of reducing power loss in a practical one wire transmission line which has to be turned at higher angles in practice.

Acknowledgement

This work was carried out in the PG Department of Physics, Bhagalpur University, Bhagalpur, under the Faculty Improvement Programme of the University Grants Commission (UGC), New Delhi. The financial assistance given by UGC is gratefully acknowledged.

References

1. Barlow H M & Brown J, *Radio surface waves*—International monographs on radio (Clarendon Press, Ltd, Oxford), 1962, 34-37; 142-50.
2. Barlow H M & Cullen A L, *Proc. Instn elect. Engrs*, 100 (Pt. III) (1953), 339-41.
3. Chiba J, *IEEE Trans. Microwave Theory Tech.*, 25 (2) (1977), 94-100.
4. Sharma K P, *Proc. Instn elect. Engrs*, 106 (Pt B) (1959), 116-22.
5. Storer J E, Sheingold L S & Stein S, *Proc. Inst. Radio Engrs*, 41 (1953), 1004.
6. Sinha G P & Sharma K P, *Indian J. pure appl. Phys.*, Communicated.

Indian Journal of Pure & Applied Physics
Vol. 18, October 1980, pp. 793-797

Electronic Absorption Spectra & Hydrogen Bonding Behaviour of Aniline & Phenetidines

T GANGULY & S B BANERJEE
Optics Department, Indian Association for Cultivation of Science, Jadavpur, Calcutta 700 032

Received 25 *July* 1979

The absorption spectra of aniline and phenetidines in binary and ternary solutions in cyclohexane and dioxane have been recorded. The spectral changes have been explained in terms of electronic charge density on the nitrogen atom. Predominance of 1:1 aniline-dioxane and phenetidine-dioxane complex has been discussed.

1. Introduction

Hydrogen bonding behaviour of primary aromatic amines acting as proton donors has been studied by methods of infrared[1-10] as well as ultraviolet spectroscopy.[11,12] The present paper deals with the electronic absorption spectra of aniline and isomeric phenetidines in binary and ternary solutions in 'proton acceptor' and 'neutral' solvents. The observed changes in the frequency and the intensity of the bands have been discussed and an attempt has been made to relate the hydrogen bonding properties of the amino group with electronic charge density on the nitrogen atom.

2. Experimental Details

The compounds were supplied by Messers British Drug House, London. Dioxane (ρ = 1·04 g/ml; b.p. 101·4°C), aniline (ρ = 1·022 g/ml; b.p. 184·4°C), *ortho*-phenetidine (ρ = 1·048 g/ml; b.p. 229·2°C), *meta*-phenetidine (ρ = 1·054 g/ml; b.p. 248°C) and *para*-phenetidine (ρ = 1·0613 g/ml; b.p. 254·2°C) were used after distillation under reduced pressure. Cyclohexane was of spectroscopic purity and was used without further purification. The absorption spectra were measured with a Hilger UV Spectrophotometer. Experimental details were the same as reported in a previous publication.[12]

In this investigation, the aromatic amines (aniline and isomeric phenetidines) were the proton donors, and dioxane and cyclohexane were the proton acceptor and the inert solvent respectively. The concentration of proton acceptor solvent dioxane was increased in steps and in every step the concentration of proton donor (aniline or a phenetidine) was kept fixed at a very low value ($\sim 10^{-4}$-10^{-5}mole/litre) compared to that of proton acceptor.

3. Theory

The association equilibrium constant (K) was calculated by the equation,[13]

$$\frac{1}{\epsilon-\epsilon_f} = \frac{1}{K}\cdot\frac{1}{\epsilon_b-\epsilon_f}\cdot\frac{1}{C}+\frac{1}{\epsilon_b-\epsilon_f} \quad ...(1)$$

where, ϵ_f = molar extinction coefficient of the non-hydrogen bonded molecule. ϵ = molar extinction coefficient for a solution in which dioxane concentration is C and ϵ_b = molar extinction coefficient for the hydrogen bonded molecule. All these extinction coefficients refer to a given frequency; ϵ_b for the hydrogen bonded species was calculated for every frequency from Eq. (2), which can be easily derived from Eq. (1).

$$\epsilon_b = \epsilon + \frac{\epsilon-\epsilon_f}{KC} \quad ...(2)$$

The hydrogen bonded curves were obtained by plotting ϵ_b against ν (in cm^{-1}) (Ref. 12-15).

On plotting $1/(\epsilon-\epsilon_f)$ against $1/C$, straight lines were obtained and extrapolating them to the point $1/(\epsilon-\epsilon_f) = 0$, the values of K were readily obtained, as $K = -1/C$ at this limit.

The free-energy change (ΔF), energy of hydrogen bond formation (ΔH) and the f-values were calculated from the well known relations.

$$\Delta F = -RT\ln K \quad ...(3)$$

$$\Delta H = -\frac{Rd(\ln K)}{d(1/T)} \quad ...(4)$$

$$\text{and } f = 4{\cdot}32\times 13^{-9}\int \epsilon\, d\nu \quad ...(5)$$

A plot of $R\ln K$ versus $1/T$ (Fig. 1) yielded a straight line whose slope gave ΔH. The method of least squares was adopted for calculating ΔH and K. Further details are to be found in earlier papers.[12,14]

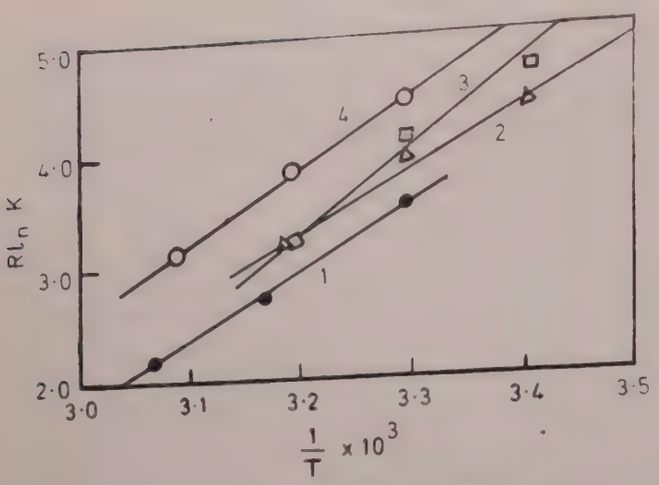

Fig. 1—Plot of $R \ln K$ versus $1/T$ for determination of hydrogen-bonding energy (ΔH)

4. Results and Discussion

In cyclohexane solution, aniline and isomeric phenetidines show two systems of π-electronic absorption bands, designated as transition I and transition II in this paper, in the regions from 2640 to 3260 Å and 2180 to 2520 Å respectively. When proton-acceptor solvent dioxane is added to aniline-cyclohexane or phenetidine-cyclohexane solution, it is found that the absorption maxima shift towards longer wavelengths. The integrated absorption $\int \epsilon \, d\nu$ increases with concentration gradually [Fig. 2 (a) and Fig. 2 (b)] and then tends to a constant value indicating that intermolecular hydrogen bond formation between aniline or phenetidine with dioxane is almost complete at concentration $> 0{\cdot}5$ M/l. The calculated values of association

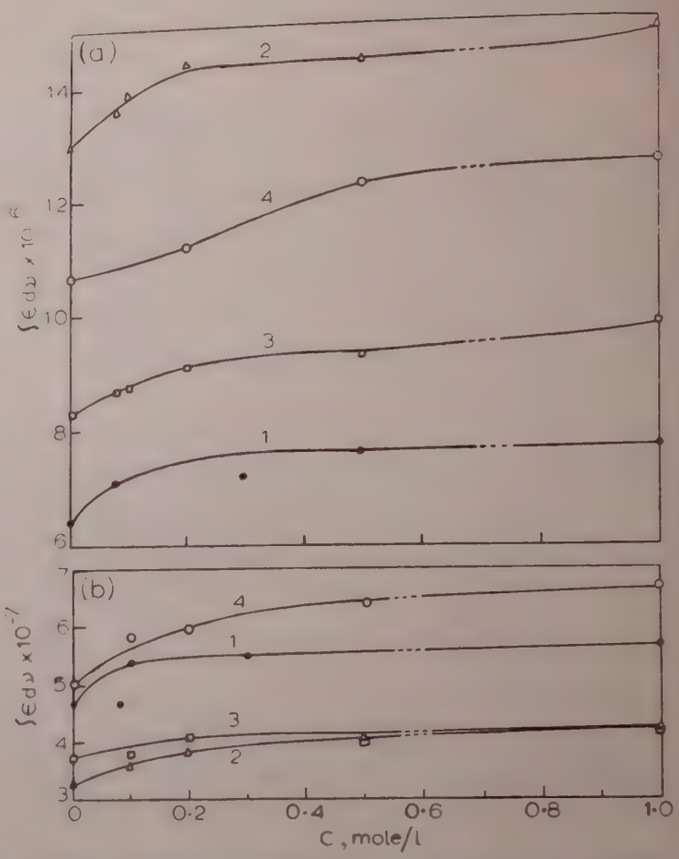

Fig. 2—Plot of integrated absorption versus dioxane concentration [(a), Transition I; and (b), transition II]

equilibrium constant K (in l/M) for various frequencies in the two π-electronic transitions (Table 1) agree fairly well with each other.

From the measured hydrogen bond enthalpies (Table 1) which are in the order: *m*-phenetidine > aniline > *p*-phenetidine > *o*-phenetidine, it is apparent that *m*-phenetidine is a stronger hydrogen-bonding agent than aniline. This may be understood by considering the electron density at the NH_2 site due to substitution of OC_2H_5 group in different positions of the benzene ring in terms of some suitable parameters and one convenient parameter that suggests itself as the Hammett σ-factor that has been widely used in understanding several features of infrared absorption spectra of hydrogen-bonded systems. On examining the σ-values[16] it is seen that electronic charge density on nitrogen atom of the NH_2 group in *m*-phenetidine ($\sigma = +0{\cdot}15$) should be smaller than that in the parent molecule aniline ($\sigma = 0$) and *p*-phenetidine ($\sigma = -0{\cdot}25$). This means that the NH_2 group in *m*-phenetidine should be a stronger proton donor than that in either aniline or *p*-phenetidine. The lowest value of ΔH for *o*-phenetidine may be attributed to partial shielding of NH_2 group by the *ortho* OC_2H_5 group.

It is observed that on formation of hydrogen bond, the band maxima shift towards longer wavelengths. In other words, the spectral shift $\delta\nu =$

Table 1—Data on Equilibrium Constants and Thermodynamic Parameters of the Systems of Aniline, *o*-, *m*- and *p*-Phenetidine with Dioxane and Cyclohexane

System (Hammett σ-factor)	Temp. K	K (l/m) transition I	K (l/m) transition II	Mean K	$-\Delta F$ (kCal/mole)	$-\Delta H$ (kCal/mole)
	303·00	6·00	6·00	6·00	1·074	
Aniline	315·00	4·00	3·98	3·99	0·863	5·97
(σ=0·00)	325·00	3·00	3·00	3·00	0·706	
ortho-	293·00	8·96	9·00	8·98	1·273	
Phenetidine	303·00	7·59	7·00	7·295	1·192	5·23
	313·00	5·02	5·01	5·015	0·999	
(σ= −0·35)						
meta-	293·00	10·43	10·90	10·665	1·373	
Phenetidine	303·00	8·014	8·020	8·017	1·248	6·82
	313·00	5·19	4·82	5·005	0·998	
(σ= +0·15)						
para-	303·00	9·340	9·344	9·342	1·340	
phenetidine	313·00	6·98	7·02	7·00	1·205	5·89
	323·00	5·00	5·00	5·00	1·029	
(σ= −0·25)						

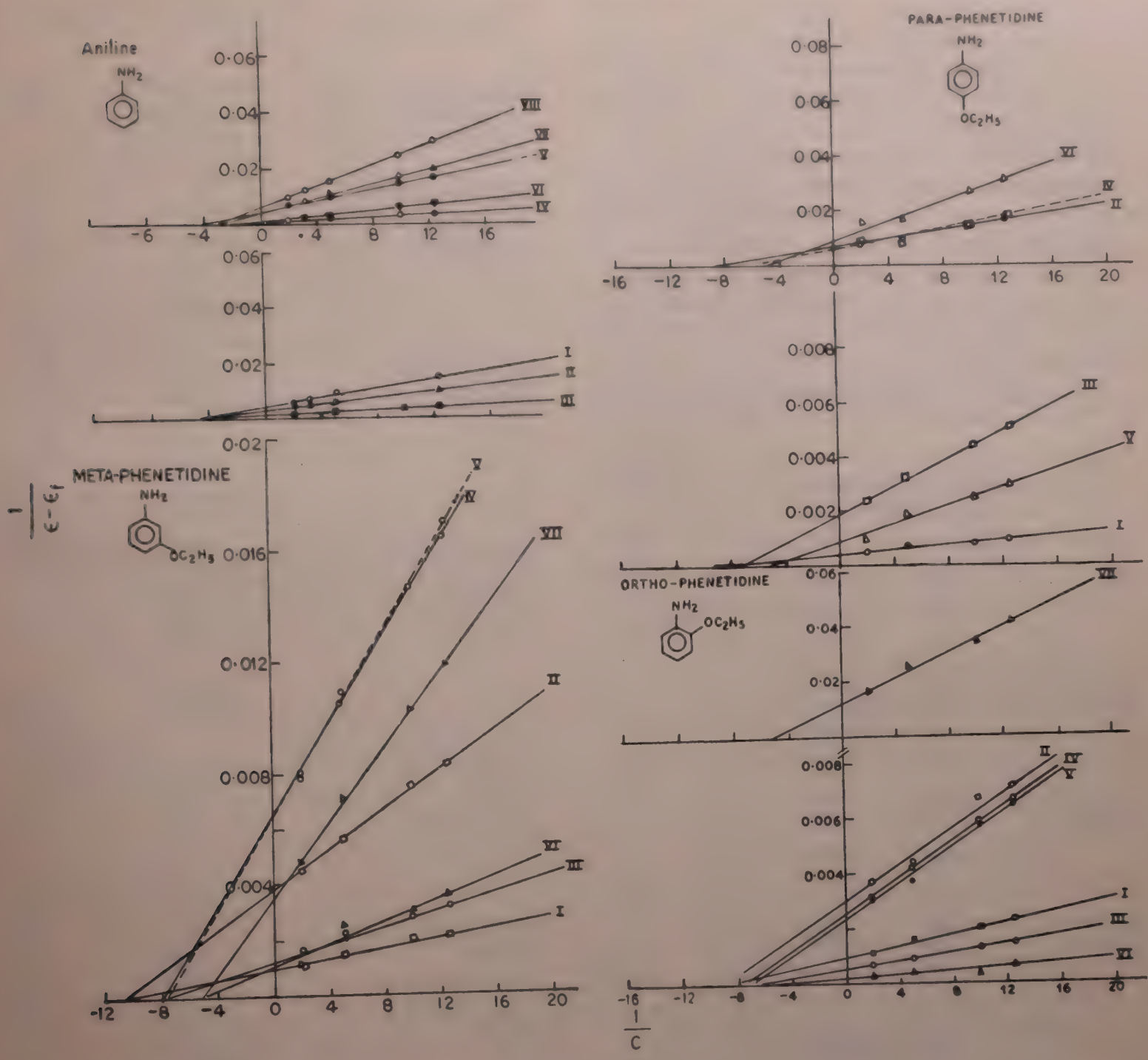

Fig 3—Plot of $1/(\epsilon - \epsilon_f)$ versus $1/C$ for determination of K for different systems.

Aniline-dioxane-cyclohexane system

[(I), λ = 2870 Å at 303 K; (II), λ = 2890 Å at 303 K; (III), λ = 2360 Å at 303 K; (IV), λ = 2350 Å at 315 K; (V), λ = 2890 Å at 315 K; (VI), λ = 2350 Å at 325 K; (VII), λ = 2890 Å at 325 K; (VIII), = 2880 Å at 325 K)

m-Phenetidine-dioxane-cyclohexane system

[(I), λ = 2350 Å at 293 K; (II), λ = 2875 Å at 293 K; (III), λ = 2400 Å at 303 K; (IV), λ = 2880 Å at 303 K; (V), λ = 2870 Å at 303 K; (VI), λ = 2330 Å at 313 K; and (VII), λ = 2880 Å at 313 K]

p-Phenetidine-dioxane-cyclohexane system

[(I), λ = 2390 Å at 303 K; (II), λ = 3050 Å at 303 K; (III), λ = 2400 Å at 313 K; (IV), λ = 3070 Å at 313 K; (V), λ = 2370 Å at 323 K; (VI), λ = 3070 Å at 323 K]

o-Phenetidine-dioxane-cyclohexane system

[(I) λ = 2390 Å at 293 K; (II), λ = 2900 Å at 293 K; (III), λ = 2370 Å at 303 K; (IV), λ = 2900 Å at 303 K; (V), λ = 2920 Å at 303 K; (VI), λ = 2390 Å at 313 K; and (VII), λ = 2910 Å at 313 K]

$\nu_b - \nu_f < 0$, the subscripts b and f referring to hydrogen bonded system and the free molecule respectively. For a particular electronic transition (Table 2) all the vibrational components show more or less uniform shift.

In the aniline compounds studied, two types of complexes, viz. 1:1 and 1:2 could be possibly formed. But interestingly enough, the linear plot of $1/(\epsilon - \epsilon_f)$ versus $1/C$ (Fig. 3) indicates presence mostly of 1:1 complex at the concentrations at which the spectra were measured. Presumably, in hydrogen-bond formation only one hydrogen atom of the NH_2 group is involved.

It is seen from an examination of the f-values for the two transitions I and II listed in Table 3

Table 2—Frequency Shift on Hydrogen Bond Formation (frequency in cm^{-1})

System	Transition	ν_f	ν_b	$\delta_\nu = \nu_b - \nu_f$	Mean δ_ν
Aniline	I	35,200	35,078	−122	−122·0
	II	42,905	42,721	−184	
		42,540	42.359	−181	−182·5
ortho-phenetidine	I	34,833	34,591	−242	
		34,354	34,119	−235	−238.5
	II	41,828	41,653	−175	
		42,359	42,181	−178	−176·5
meta-phenetidine	I	34,833	34,712	−121	
		35,078	34,954	−124	−122·5
	II	42,003	41,653	−350	
		43,090	42,721	−369	−359·5
para-phenetidine	I	32,885	32,563	−322	
		32,670	32,354	−316	−319·0
	II	42,181	41,828	−353	−353·0

Table 3—Intensity Change Due to Hydrogen Bond Formation

Svstem	Transition	f_f^*	$f_b^\dagger$	f_b/f_f	$\Delta f = f_b - f_f$
Aniline	I (2650-3010 Å)	0·0277	0·0339	1·2238	0·0062
	II (2180-2490 Å)	0·2017	0·2436	1·2077	0·0419
o-phenetidine	I (2640-3050 Å)	0·0562	0·0644	1·1459	0·0082
	II (2260-2500 Å)	0·1426	0·1827	1·2812	0·0401
m-phenetidine	I (2700-3040 Å)	0·0358	0·0424	1·1843	0·0066
	II (2280-2500 Å)	0·1616	0.1806	1·1176	0·0190
p-phenetidine	I (2740-3260 Å)	0·0460	0·0543	1·1804	0·0083
	II (2200-2520 Å)	0·2173	0·2881	1·3258	0·0708

* free species and

† bonded speeies.

Table 4—Change of Intensity with Proton-Acceptor (dioxane) Concentration

Proton-donor concentration moles/l	Temp. K	Proton-acceptor (dioxane) concentration in moles/l	$\int \epsilon\, d\nu \times 10^{-6}$
Aniline of conc.		0	6·41
$2·195 \times 10^{-4}$		0·08	7·07
(Transition I)	303	0·3	7·20
		0·5	7·60
		large conc.	7·84 (Calc.)
Aniline of conc.		0	46·7
$2·195 \times 10^{-5}$		0·08	46·5
(Transition II)	303	0·1	54·1
		0·3	54·9
		0·5	52·2
		large conc.	56·4 (Calc.)
o-Phenetidine		0	13·0
of conc.		0·08	13·6
$2·77 \times 10^{-4}$	303	0·1	13·9
(Transition I)		0·2	14·4
		0·5	14·4
		large conc.	14·9. (Calc.)
o-Phenetidine		0	33·0
of conc.		0·1	35·8
3×10^{-5}	303	0·2	38·4
(Transition II)		0·5	40·7
		large conc.	42·3 (Calc.)
m-Phenetidine		0	8·28
of conc.	303	0·08	8·72
$3·07 \times 10^{-4}$		0·1	8·74
(Transition I)		0·2	9·10
		0·5	9·27
		large conc.	9 81 (Calc.)
m-Phenetidine		0	37·4
of conc.	303	0·1	37·5
$3·07 \times 19^{-5}$		0·2	40·7
(Transition II)		0 5	40·0
		large conc.	41·8 (Calc.)
p-Phenetidine		0	10·66
of conc.		0·1	10·92
$3·09 \times 0^{-4}$	303	0·2	11·18
(Transition I)		0·5	12·28
		large conc.	12·58 (Calc.)
p-Phenetidine		0	50·3
of conc.		0·1	58·3
$3·09 \times 10^{-5}$	303	0·2	59·5
(Transition II)		large conc.	66·7 (Calc.)

that for each compound the oscillator strengths for the bonded molecules (f_b) are always greater than those for the free molecules (f_f). This indicates an enhanced interaction between the lone pair electrons on N-atom and the ring π-electrons and corroborates the view[12,13] that there is an increase in σ-electron density on N-atom of the NH_2 group on hydrogen bond formation. Due to this increase in the electronic charge density on the nitrogen atom resulting from formation of $-N\begin{matrix}H\\H\end{matrix}$ ..... O bond in which one hydrogen atom at one end of the NH_2 group is involved, the hydrogen atom at the free end of the group becomes less acidic so that its proton-donating capacity or its capacity for taking part in hydrogen bond formation decreases. The case of hydrogen bonding involving hydroxy groups discussed by Bellamy and Pace[17] may be noted in this connection. In such a situation, formation of 1:1 complex should be favoured rather than 1:2 complex. This would explain the predominance of 1:1 aniline-dioxane and phenetidine-dioxane complex mentioned earlier.

References

1. Krueger P J & Thompson W H, *Proc. R. Soc.*, 243A (1957), 143.
2. Medhi K C, Banerjee S B & Kastha G S, *Indian J. Phys.*, 36 (1962), 457.
3. Medhi K C & Kastha G S, *Indian J. Phys.*, 37 (1963), 139.
4. Medhi K C & Kastha G S, *Indian J. Phys.*, 37 (1963), 275.
5. Whetsel K B & Lady J H, *J. phys. Chem.*, 69 (1965), 1596.
6. Lauransan J, Pineau P & Lascombe J, *J. Chim. Phys.*, 63 (1966), 635.
7. Whetsel K B & Lady J H, *J. phys. Chem.*, 71 (1967), 1421.
8. Lauransan J & Pineau P, *J. Chim. Phys.*, 65 (1968), 1937.
9. Nishimura S & Li N C, *J. phys. Chem.*, 72 (1968), 2908.
10. Madec C, Lauransan J & Sau Magne P, *J. phys. Chem.*, 75 (1971), 1157.
11. Nagakura S & Baba H, *J. Am. chem. Soc.*, 74 (1952), 5693.
12. Ganguly T & Banerjee S B, *Indian J. Phys.*, 51B (1977), 392.
13. Baba H & Sujuki S, *J. chem. Phys.*, 35 (1961), 1118.
14. Ganguly T & Banerjee S B, *Spectrochim. Acta*, 34A (1978), 617.
15. Sujuki S & Baba H, *J. chem. Phys.*, 38 (1963), 349.
16. Hamett L P, *Physical organic chemistry* (McGraw-Hill, New York and London), 1940, 188.
17. Bellamy L J & Pace R J, *Spectrochim. Acta*, 22 (1966), 525.

Indian Journal of Pure & Applied Physics
Vol. 18, October 1980, pp. 798-800

A Count Rate Integrator for Use with X-ray Spectroscopy Work

M Banerjee & K G Bhatnagar
Department of Physics, Holkar Science College, Indore

Received 20 *November* 1979

In the counter method of recording X-ray spectra, apart from the amplifiers and channel analyzer, one very important unit is the count rate integrator. An integrator designed and fabricated for this purpose is described. Its output voltage is proportional to the frequency of the input pulses. It is linear, drift free and of 1% accuracy over the region 5 counts/sec to 10^4 counts/sec.

1. Introduction

X-ray absorption spectroscopy has established itself as a potent tool for studying the electronic structure of elements and chemical bonding in compounds and alloys. For obtaining absorption spectrum, white X-rays are passed through the sample and dispersed along a curve.[1] Dispersed X-ray beam intensity is either recorded on X-ray photographic film over long exposures or else an X-ray detector is uniformly moved over each wavelength position and count rate recorded through a count rate integrator on a moving paper chart. The latter method has many distinct advantages.[2]

In the counter method of recording absorption spectrum, the count rate integrator sets the, sensitivity and accuracy of recording. The voltage analogue of count rate from the integrator should be linear and drift free over the entire region of interest. A count rate integrator designed with these points in view is described in this paper.

2. Design and Operation of the Integrator

The principle of measurement and operation of the count rate integrator is outlined in Fig. 1. Pulses from preceding stage, i.e analyzer are reshaped with the help of diode D, capacitor C_1 and resistor R_1 so as to result into slowly rising pulses of time duration greater than about 20 μsec; in order to operate the Schmitt trigger. The Schmitt trigger (minimum acceptable height $\sim$ 0·5 V), converts positive going pulses

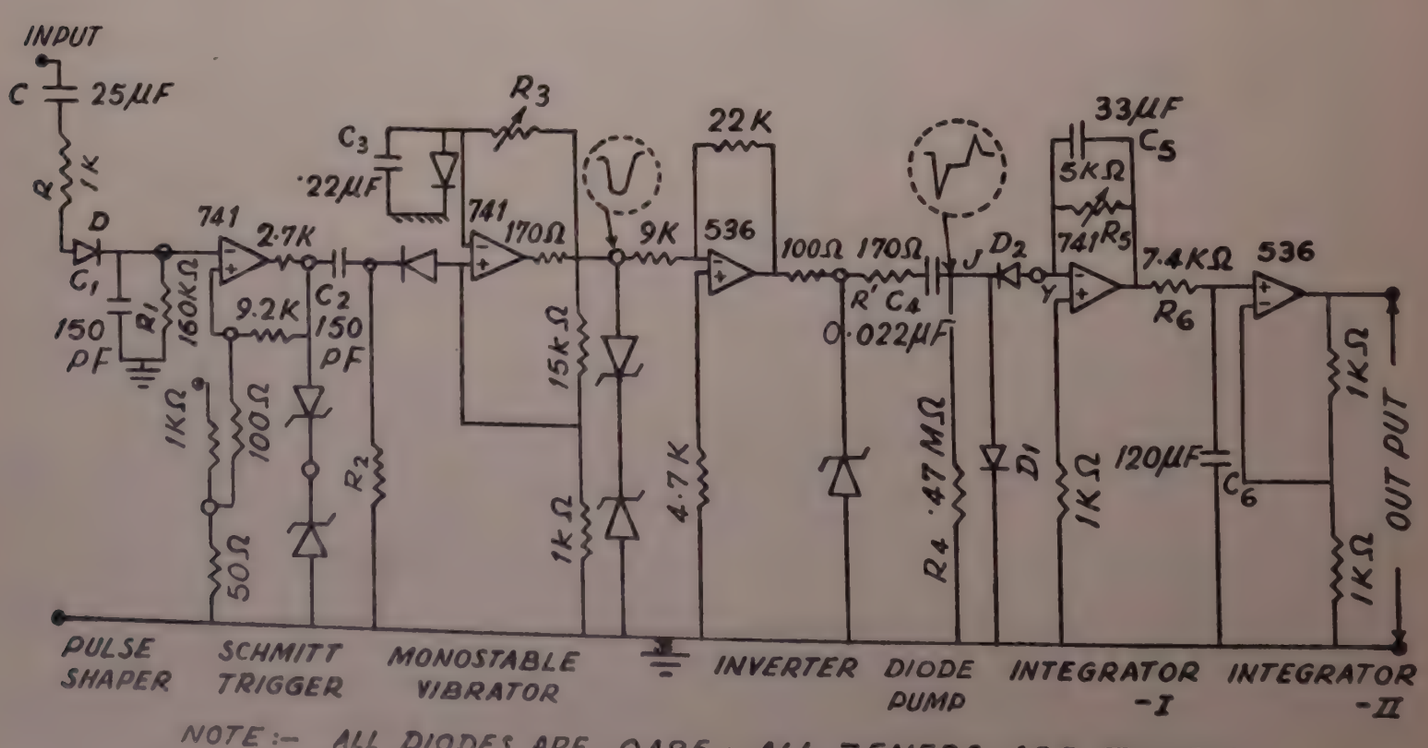

Fig. 1—Principle of operation and circuit of the count rate integrator

into zener stabilized negative pulses of 10 V height. These pulses are differentiated through capacitor C_3 and resistor R_2 to obtain negative going pulses which trigger the following monostable multivibrator which is designed to deliver zener stablized negative going pulses of duration (τ) $\approx$ 40 μsec determined by capacitor C_3 and potentiometer R_3. The output from the monostable multivibrator is fed to the inverter stage designed with low drift IC 536. The positive going pulses at the inverter output are zener stablized to a fixed height (V_z) of 5 V.

Pulses from the inverter which have constant height V_z and width τ are charge integrated by the fast and then a slow integrating stage respectively (in cascade through an intermediate stage termed as diode pump). The first charge integrating stage is set to operate with a low RC time R_5C_5 ($\approx$ few msec) and is thus made to follow with sufficient speed the count rate in the range of 1000 counts/sec. The second integrating stage is designed with large RC time R_6C_6 ($\approx$0·9 sec) in order to accommodate very low count rates ($\approx$ few counts/sec).

The diode pump which consists of the capacitor C_4 and diodes D_1 and D_2, helps in greatly improving the linearity[3] of the count rate integrator. For every pulse entering the diode pump section, a definite amount of charge ΔQ is delivered to the input of the I-integrator. The magnitude of ΔQ depends upon the magnitude of the input pulse and the diode pump capacitor. These two factors remaining constant, ΔQ is independent of running frequency. As the pulses delivered by the monostable multivibrator are of definite fixed height and width, the charge delivered by the diode pump to the input of I-integrator is the same for each pulse, irrespective of the running frequency. The total charge delivered per sec by the diode pump is $f.\Delta Q$ where f is the frequency of pulses. This charge is integrated by the I-integrator whose average output voltage is given by:

$$V = f.\Delta Q.R_5 \qquad \ldots(1)$$

so that the output voltage V is proportional to the frequency f of the input pulses. However, for very low frequencies ($\approx$ few counts/sec), the voltage V will be very small and hence we connect a second intergrator whose integration time R_6C_6 is adjusted according to need.

3. Linearity of the Integrator

The linearity of the integrator depends mainly upon the diode pump. To achieve linearty, i.e. exact proportionality between output voltage and frequency of the input pulses, it is necessary that the charge ΔQ delivered by the diode pump to the input of I-integrator should be independent of running frequency. This is assisted by the input Y being at virtual ground so that the diode pump discharges into constant potential level. As a pulse at the input triggers the monostable multivibrator, discharge of the pump condenser C_4 starts via diode D_1 and the series resistor R'. The discharge continues for a period τ of the monostable pulse (which through inverter stage is introduced into the diode pump). After discharge of the positive charge through D_1, the negative charge remaining on the pump condenser forward biases the diode D_2. An equal amount of charge ΔQ from C_5 recharges the pump condenser and brings it to original condition. The charge transfer to the integrator takes place during the period τ of the monostable pulse.

For achieving linearity both processes, i.e. the discharging and recharging of C_3 should be complete.

The duration of the monostable pulse is kept large enough to ensure complete discharge of the capacitor. Total recharging is ensured by low impedance diodes.

The charge transfer process which is complicated by the hole storage in the diode is minimized by the use of resistor R_4 which maintains a low impedance path for the stored charge. R_4 also helps to make charging and discharging more definite and less susceptible to thermal variation in diode parameters. Thermal variations are also checked by using resistances of 1% tolerance and good quality condensers. Tantalum capacitors are used at important places.

Integrator resistances and condensers are chosen carefully[4] for the linear working in the entire region of study.

4. Experimental Procedure

The block diagram of the entire experimental set-up is shown in Fig. 2. The proportional counter is moved along the circumference of the Rowland circle of Cauchois type of spectrometer. The pulses from the counter after due amplification are fed into the single channel analyzer. The output of the analyzer

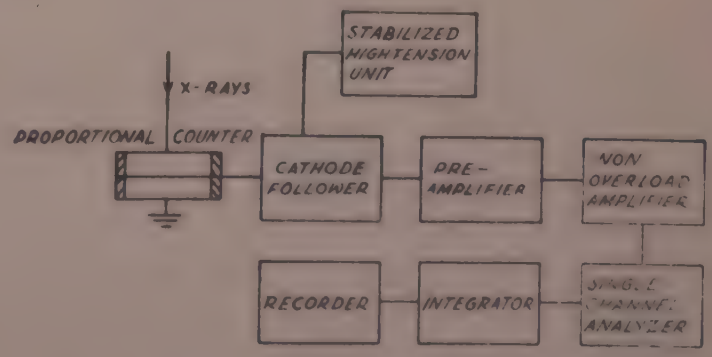

Fig. 2—Block diagram of experimental set-up

is introduced into the integrator. The output voltage of the integrator is proportional to the frequency of the input pulses, which in turn depends upon the intensity of X-rays, is recorded by the following chart-recorder as the counter moves along the circumference.

Before including the integrator in the assembly it was tested fully. Voltage levels at various important nodes were measured in the quiescent state. Pulse shapes were also studied oscilloscopically for 40V high pulses (rise-time 1 μsec and width 4 μsec) from a pulse height analyzer which is the stage preceding the integrator in the assembly. Both these features are indicated in Fig. 1.

A systematic count rate measurement was made with pulses obtained from a systronics pulse generator and correlated with the analogue voltages measured with a Philips multimeter. The observations showed that there is a linear relation between the frequency of input pulses and the output voltage. The count rate integrator was found to operate uniformly with 1% linearity over the range of 5 counts/sec to 10^4 counts/sec. Linearity could be achieved for still lower count rates by increasing the RC time (R_6C_6) of the second integrator. But as the integrator is designed to operate with a pen recorder of nominal pen response of one second, the present value of RC constant was chosen. As the count rate variation in a X-ray absorption spectrometer is generally spread at most to two orders of magnitude, the integrator is expected to yield very satisfactory results.

Acknowledgement

One of the authors (MB) is thankful to CSIR, New Delhi, for the award of a junior research fellowship.

References

1. Allison S K & Compton A H, *X-rays in theory and experiments*, (McGraw-Hill New York), 2nd Edn, 1968, 750.
2. Azaroff L V, *X-ray spectroscopy* (McGraw-Hill, New York), 1974, 288.
3. Unsworth P J, *J. Phys.*, E2 (1969), 407.
4. Clayton G B, *Operational amplifiers* (Newnes-Butterworths, London), 4th Edn, 1977, 126.

Communications

Leptonic & Hadronic Decay Widths of Next Quarkonium ($t\bar{t}$)

G Q Sofi

Department of Physics, S P College, Srinagar 190 001

Received 17 October 1979; *revised received* 15 *December* 1979

Predictions for the energy spectrum, leptonic and hadronic decay widths of a new heavy quarkonium family $\zeta (t\bar{t})$, of quark mass $M_Q \simeq 15$ GeV, have been made within the context of a plausible universal potential model.

As is well known, the explanation of the J/ψ and ψ' particles as states of a bound system of a charmed quark and its antiquark has been a great success, which seems to be duplicated by the Υ and Υ' states. Shortly after the first experimental discovery of ψ and ψ', a few groups[1,2] suggested a non-relativistic potential treatment, interpreted ψ and ψ' as ground state and first excited triplicate state with quantum numbers 1^{--} (J^{PC}), and predicted the existence of three P states between them and in addition a D state around 3·77 GeV.

In this communication, we would like to report the detailed predictions of potential model for the hypothetical $\zeta (t\bar{t})$ family of higher-lying vector meson system with a mass of about 30 GeV/c² [Ref. 3].

Model—We shall analyze the toponium spectroscopy using a potential of the type[4,5]

$$V(r) = -\frac{4}{3}\alpha_S \frac{(M_Q)}{r} + kr \qquad ...(1)$$

where $\alpha_S (M_Q)$ is the effective quark-gluon coupling constant evaluated at the heavy quark mass and k is the slope of the linear potential, which has been taken to be 0·20 GeV².

The radial part of the Schrödinger equation in the centre of mass system using the natural units $c = \hbar = 1$ is

$$\frac{d^2 u(r)}{dr^2}\left[m_t \left\{ E - V(r) \right\} - \frac{l(l+1)}{r^2} \right] u(r) = 0 \qquad (2)$$

where the radial wavefunction is $R(r) = u(r)/r$ and m_t is the top quark mass taken as 15 GeV. In the S state ($l = 0$) $u(r)$ must vanish at the origin. The results of masses are given in Table 1.

Leptonic decay widths—The leptonic decay widths are sensitive to the new quark charge. The leptonic decay width in the non-relativistic limit is given by[6]

$$\Gamma (V \to e^+e^-) = 16\pi\alpha^2 \frac{(e_Q^2)}{M_V^2} \left| \psi (0) \right|^2 \qquad ...(3)$$

where M_V is the mass of the vector meson, e_Q is the quark charge, and $\psi (0)$ is the $Q\bar{Q}$ wavefunction at the origin where the annihilation takes place.

The leptonic widths calculated for charmonium and upsilon families are somewhat large and this problem can be mitigated by applying radiative corrections.[7] A transcription from QED to QCD yields.[8]

$$\Gamma (V \to e^+e^-) = 16\pi\alpha^2 \frac{e_Q^2}{M_V^2} \left| \psi (0) \right|^2 \times \left\{ 1 - \frac{16\alpha_S (m_Q)}{3\pi} \right\} \qquad ...(4)$$

where α_S is the strong QCD coupling strength. The results are given in Table 2. For the states ζ, ζ' and ζ'' we find values of 0·76, 0·34 and 0·26 for the

Table 1—Mass Spectrum for Heavy Quark States with $m_Q = 15$ GeV (All masses are in GeV, N is the principal quantum number : l and J are the orbital and total angular momentum, respectively)

$N/$:	0	1 (J)	2 (J)	3 (J)
1	29·42			
2	30·07	29·83 (0)		
		29·88 (1)		
		29·92 (2)		
3	30·40	30·26 (0)	30·17 (1)	
		30·30 (1)	30·20 (2)	
		30·33 (2)	30·22 (3)	
4	30·72	30·58 (0)	30·50 (1)	30·41 (2)
		30·60 (1)	30·55 (2)	30·46 (3)
		30·65 (2)	30·59 (3)	3·049 (4)

Table 2—Leptonic and Hardonic Decay Widths (in keV) for ζ, ζ' and ζ'' States

State	Decay Width	
	Leptonic	Hadronic
ζ (29·42)	2·534	0·143
ζ' (30·07)	1·876	0·104
ζ'' (30·40)	1·587	0·087

wavefunction at the origin squared, yielding leptonic widths of 2·534, 1·876 and 1·587 keV respectively.

Hadronic decay widths—According to QCD, the direct hadronic decay of the vector meson V may be considered as the annihilation of Q and $\bar{Q}$ into three gluons, which combine together to become hadrons. The expression for hadronic decay width is written as[7]

$$\Gamma_{\text{direct}}(V \to \text{hadrons}) = \frac{160\,(\pi^2-9)}{81} \left| \frac{\alpha_S^3}{M_V^2} \right| \psi(0) \Big|^2 \quad \ldots(5)$$

and after applying the radiative correction, Eq. (5) takes the form[9]

$$\Gamma_{\text{direct}}(V \to \text{hadrons}) = \frac{160\,(\pi^2-9)}{81} \left| \frac{\alpha_S^3}{M_V^2} \right| \psi(0) \Big|^2 \times \left(1 - \frac{16\,\alpha_S(m_Q)}{3\,\pi} \right) \quad \ldots(6)$$

The results are given in Table 2.

Conclusion—We have anticipated the properties of the next quarkonium system $\zeta(t\bar{t})$. A new quark-antiquark potential is presented, radiative corrections are taken into account which tends to strongly suppress the widths. This first radiative corrections reduce the predicted leptonic and hadronic widths greatly. By applying the radiative correction to the charmonium and upsilon families, the decay widths are found to be in agreement with the experiment.[10-12] Hence it is expected that the decay widths we anticipate may be correct and await experimental confirmation.

I would like to thank Dr Mubarak Ahmad for helpful discussions and I am also thankful to Prof. Peerzada and Prof. Mam for their constant encouragement.

References

1. Appelquist T *et al.*, *Phys Rev. Lett.*, 34 (1975), 365.
2. Eichten E *et al.*, *Phys. Rev. Lett.*, 34 (1975), 369.
3. Harari H *et al.*, *Physics Lett.*, 78B (1978), 459.
4. Celmaster W *et al.*, *Physics Rev. D*, 17 (1978), 879.
5. Celmaster W, SLAC-PUB-2151 (1978), unpublished.
6. Van Royan R & Weisskopf V F, *Nuovo Cim.*, 50 (1967), 617.
7. Jackson J D, Quigg C & Rosner J L, LBL-7977 Preprint and *Proc. Int. Conf. on High energy Physics, Tokyo*, 1978, 391.
8. Quigg C, FERMI LAB. Conf. 79/89-THY (1979).
9. Quigg C, FERMI LAB. Conf. 78/82-THY (1978).
10. Darden C W *et al.*, *Physics Lett.*, 76B (1978), 246; 80B (1979), 419.
11. Bielein J K *et al.*, *Physics Lett.*, 78B (1978), 360.
12. Flugg G, DESY-79/26 (1979), 31-33.

New Spectrum of NiCl Molecule in the Near Ultraviolet Region

A B Darji & N R Shah
Physics Department, M S University of Baroda
Baroda 390 002

Received 15 *March* 1980

The spectrum of NiCl molecule in the near ultraviolet region 3440-3950 Å has been photographed on a 2-m plane grating spectrograph (Carl-Zeiss) at dispersions of 7·35 Å/mm in the first order and 2·30 Å/mm in the third order from a high frequency discharge. The bands have been analyzed to form five fragmentary new band systems. From the vibrational analysis, vibrational constants of the systems of NiCl molecule have been reported.

The spectrum of NiCl molecule is known to have several band systems designated as A_1, A_2, A_3, B_1, B_2, C, D, E_1 and E_2 starting from shorter wavelength side in the region 3900-8750 Å, which have been studied by various authors.[1-5] In addition to these, Rao *et al.*[6] observed a few more band systems in the region 6350-8750 Å. They have designated them as F, G, H, I and J systems. Further Rao *et al.*[7] have reported four systems designated as I, II. III and IV in the region 4860-5490 Å. The complex nature of the NiCl spectrum demands a detailed reinvestigation at a high dispersion and resolution. During a course of study of NiBr molecule we[8] have recently reported a band system in the region 3650-3900 Å. In view of this, study of the spectrum of NiCl molecule was undertaken and the results obtained are reported here.

Experimental procedure—The spectrum of NiCl molecule was excited in a high frequency discharge using an anhydrous sample of pure $NiCl_2$. The spectrum in the region 3440-3950 Å was recorded at a reciprocal dispersion of 7·35 Å/mm in the first order and 2·30 Å/mm in the third order of a 2-m plane grating spectrograph (Carl-Zeiss) using Ilford N-30 plates. A two-step filter was used just in front of the slit to record the bands with proper intensity. Measurements of band heads were made against standard lines of nickel on Abbe comparator.

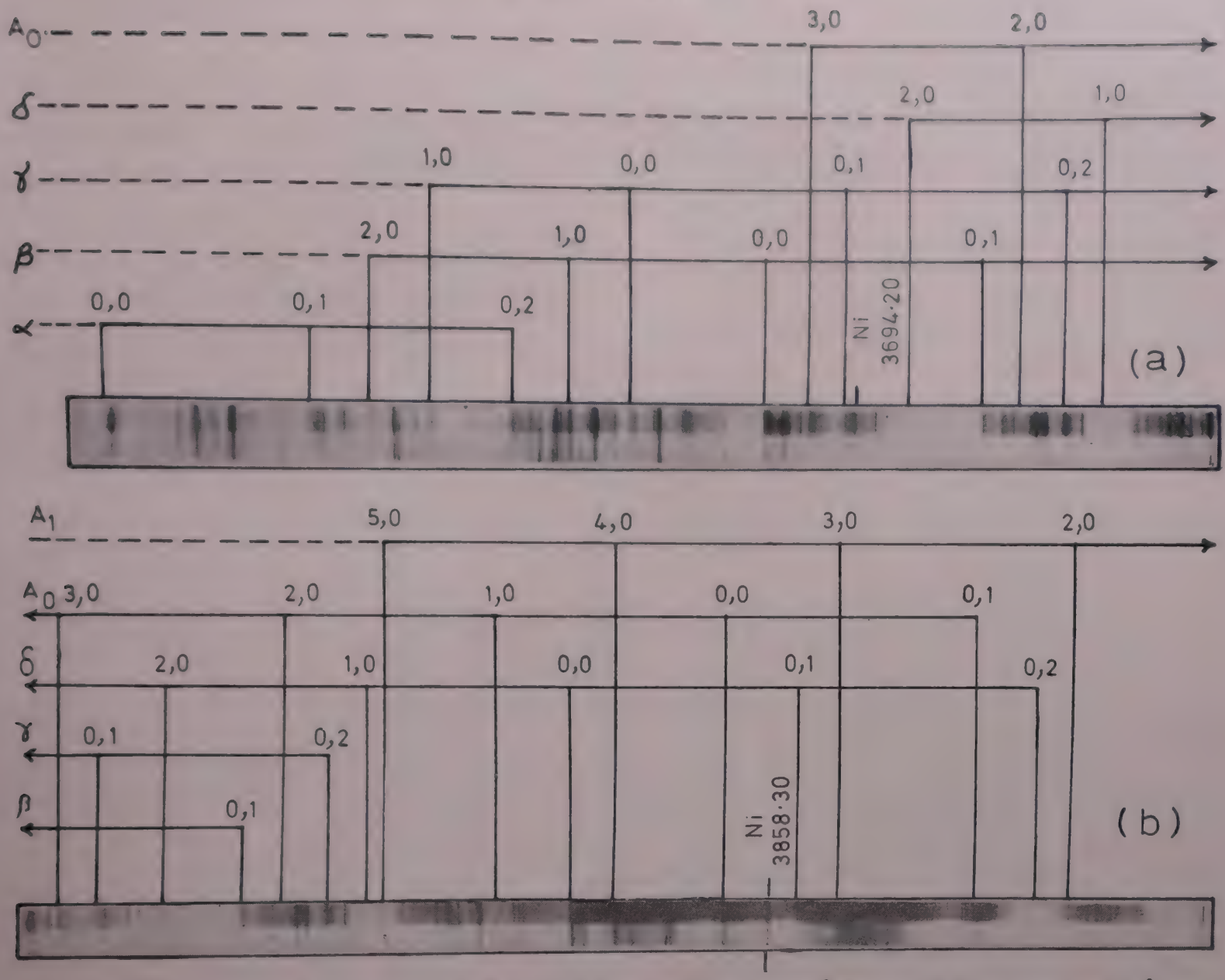

Fig. 1 (a) and (b)—Grating spectrogram of NiCl molecule in the region 3440-3950 Å recorded at a dispersion of 7·35 Å/mm

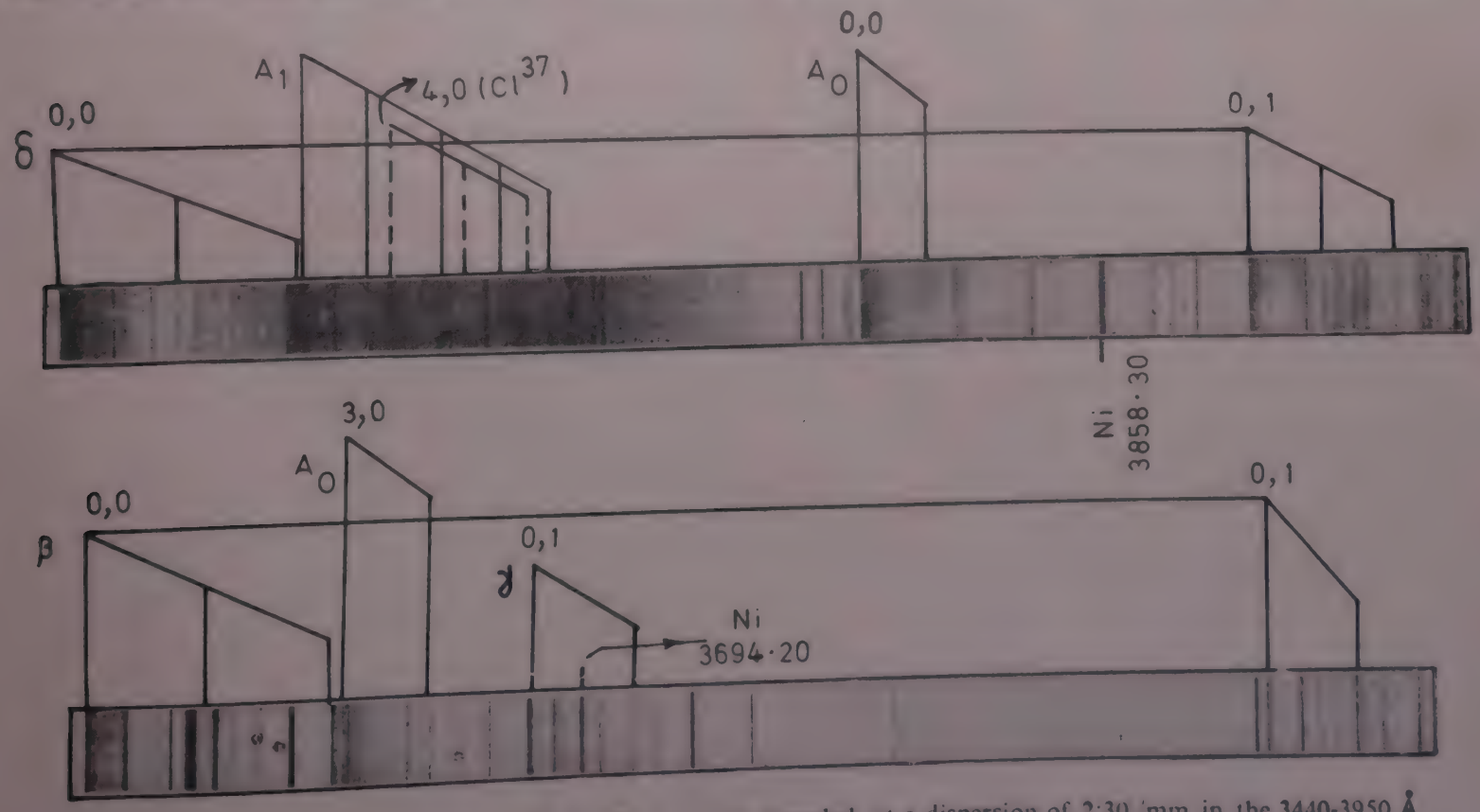

Fig. 2—Parts of the grating spectrogram of NiCl molecule recorded at a dispersion of 2·30 /mm in the 3440-3950 Å

Table 1—Band Head data of NiCl in the Region 3440-3950 Å

Intensity	Wavenumber in vacuum ν, cm^{-1}	Assignment ν' ν''	$\nu_{obs} - \nu_{calc}$ cm^{-1}	Difference of calculated and observed isotopic shifts $[\Delta\nu = \Delta\nu_{obs} - \Delta\nu_{calc}]$ Chlorine$^{35-37}$	Nickel$^{58-60}$
		α-system			
1	29053·8	1,0	0·0	0·7	
2	28641·8	0,0	0·0	—	—
1	28624·6	1,1	0·0	—	—
1	28607·9	2,2	−0·5	—	—
3	28212·6	0,1	0·0	0·4	—
1	28197·9	1,2	−0·5	0·2	—
2	27785·4	0,2	−0·4	−0·3	−0·6
		β-system			
2	28057·2	2,0	−0·2	0·8	0·4
1	28009·0	3,1	−0·6	0·6	—
2	27673·9	1,0	0·0	−0·2	−0·6
3	27630·8	2,1	−0·1	0·8	—
2	27583·3	3,2	0·3	−0·4	—
6	27287·1	0,0	0·0	—	—
4	27246·2	1,1	−0·1	—	—
5	27204·2	2,2	0·2	—	—
4	27157·0	3,3	0·1	—	—
4	26857·9	0,1	0·2	−0·8	0·7
3	26820·9	1,2	0·4	−0·6	−0·4
2	26779·6	2,3	0·5	0·5	−0·3
		γ-system			
3	27955·2	1,0	0·2	−0·2	—
5	27556·8	0,0	0·0	—	—
4	27529·2	1,1	0·0	—	—
4	27127·8	0,1	−0·1	0·4	—
6	26699·9	0,2	0·1	−0·3	−0·6
		δ-system			
1	26998·5	R 2,0	—	—	—
2	26995·5	Q 2,0	0·4	0·4	0·8
1	26632·2	R 1,0	—	—	—
3	26629·3	Q 1,0	0·1	−0·6	0·5
4	26594·7	Q 2,1	0·2	0·3	—
6	26264·0	R 0,0	—	—	—
10	26261·1	Q 0,0	0·0	—	—
6	26228·5	Q 1,1	0·0	—	—
3	26996·6	Q 2,2	0·2	—	—
2	26166·5	Q 3,3	−0·4	—	—
4	25863·6	R 0,1	—	—	—
7	25860·5	Q 0,1	0·1	0·5	−0·6
5	25832·1	Q 1,2	0·8	0·7	—
		δ-system			
6	25801·2	Q 2,3	−0·6	−0·1	—
4	25772·5	Q 3,4	0·2	−0·3	—
1	25465·7	R 0,2	—	—	—
3	25462·5	Q 0,2	−0·3	−0·2	0·5
		A_0-system			
2	27199·0	R 3,0	—	—	—
5	27196·0	Q 3,0	−1·0	−0·8	−0·6
3	27166·8	Q 4,1	0·7	−1·0	−0·7
1	26799·9	R 2,0	—	—	—
2	26797·3	Q 2,0	0·3	0·6	0·9
3	26770·6	Q 3,1	0·9	0·8	−0·4
2	26397·8	R 1,0	—	—	—
4	26394·5	Q 1,0	−0·5	−0·6	−0·9
2	26371·1	Q 2,1	−0·3	0·2	0·6
2	26346·8	Q 3,2	0·1	−0·1	−0·5
4	25995·3	R 0,0	—	—	—
8	25992·4	Q 0,0	0·0	—	—
3	25971·2	Q 1,1	−0·2	—	—
2	25948·6	Q 2,2	0·6	—	—
2	25564·0	R 0,1	—	—	—
6	25567·9	Q 0,1	0·6	−0·3	−0·8
4	25547·9	Q 1,2	0·5	−0·6	—
2	25527·0	Q 2,3	−0·3	0·4	—
		A_1-system			
1	26572·0	R 5,0	—	—	—
2	26575·3	Q 5,0	0·1	0·2	0·4
4	26125·3	Q 7,3	0·9	0·6	—
5	26143·3	Q 6,2	−0·2	0·4	—
6	26161·9	Q 5,1	−0·6	0·3	0·7
7	26181·3	R 4,0	—	—	—
9	26184·3	Q 4,0	0·4	0·3	−0·2
5	25752·6	Q 5,2	0·4	0·5	—
7	25771·1	Q 4,1	−0·4	−0·2	—
6	25789·9	R 3,0	—	—	—
10	25792·7	Q 3,1	0·0	0·3	0·8
3	25379·0	Q 3,1	−0·8	0·4	—
2	25397·1	R 2,0	—	—	—
4	25400·2	Q 2,0	−0·1	0·6	0·5

Table 2—Vibrational Constants (in cm^{-1}) of $^{58}Ni^{35}Cl$ Molecule

System	$\nu_{(0,0)}$	ν_e	ω'_e	ω''_e	$\omega'_e x'_e$	$\omega''_e x''_e$
α	28641·8	20650·8	414·0	432·1	1·00	1·50
β	27287·1	27305·8	393·2	429·8	2·40	0·795
γ	27556·8	27570·63	402·7	429·8	2·00	0·92
δ	26261·1	26277·5	370·2	403·2	1·05	1·30
A_0	25992·4	26000·3	405·5	427·2	1·16	1·04

Results and discussion—The spectrum of NiCl molecule in the region 3440-3950 Å as seen on the negative plate has been reproduced in Figs. 1 (a) and (b). All the bands are degraded to longer wavelength side and are heavily masked by atomic lines of nickel. Some bands are double headed whereas some are single headed. Most of the band heads are weak in intensity and are badly overlapped by atomic lines. They are seen to form a few progressions and short and close sequences. The spectrum recorded at a dispersion of 2·3 Å mm and reproduced in Fig. 2 resolves clearly most of the heads and thus helps to proceed with the analysis. By taking bands at 28641·8, 27287·1, 27556·8, 26261·1 and 25992·4 cm^{-1} as the (0,0) bands of five systems α, β, γ, δ and A_0 respectively, the vibrational analysis has been carried out. For some of the bands in higher progressions isotopic effect of nickel and bromine has been observed. In addition to this, the bands of A_1 and δ systems show double headed nature which can be ascribed to intense Q and weak R heads. A large number of additional bands have been observed for the A_1 system. Isotopic shifts for nickel and chlorine have been observed for some bands and the observed isotopic shifts are in good agreement with calculated shifts. Intensity, wavenumber in vacuum, assignments and difference between observed and calculated wavenumbers, and isotopic shifts of chlorine and nickel for the bands are given in Table 1. The vibrational constants obtained from the analysis of the bands are given in Table 2.

From the knowledge of the theoretically derived molecular states of NiCl the above systems may be ascribed to electronic transitions between multiplet excited states $^4\Pi$ and $^2\Pi$ and a multiplet lower state Π^2. However, for knowing the exact nature of the molecular states involved in the above band systems, rotational analysis is obviously necessary.

The authors are thankful to Prof. M M Patel for his keen interest and useful discussions during the course of this work.

References

1. More K R, *Phys. Rev.*, 54 (1938), 122-125.
2. Mesnage P, *Annls. Phys.*, 12 (1939), 5-87.
3. Krishnamurty V G, *Indian J. Phys.*, 26 (1952), 207-25.
4. Reddy S P & Rao P T, *Proc. phys. Soc. Lond.*, 75 (1960), 275-79.
5. Bulewicz E M & Phillips L F, *Trans. Faraday Soc.*, 57 (1961), 921-31.
6. Rao S V, Reddy S P & Rao P T, *Z. phys.*, 166 (1962), *Lond*, 261-64.
7. Rao N V K & Rao P T, *Curr. Sci.*, 38 (1969), 589.
8. Darji A B & Shah N R, *Curr. Sci.*, 48 (1979), 809-10.

Quark Model & Off-Shell Form-Factors of Nucleons*

J Thakur

Department of Physics, Science College, Patna University
Patna 800 005

Received 23 *July* 1979

The electromagnetic properties of nucleons in a nucleus can be described by two extra form-factors g_e, g_m in addition to the usual G_E, G_M for nucleons on mass shell. These form factors which measure off-shell variation are the derivatives with respect to external energy of the corresponding off-shell form factors. The quark model has been used in impulse approximation to relate the form-factors g_e and g_m to the derivative of the quark model nucleon wavefunction. These form-factors have been calculated for the MIT bag model and compared with the results obtained previously using isobar dominance of the dispersion integral.

It is customary in nuclear physics to assume that the electromagnetic current of nucleons in a nucleus consists of impulse terms (current of free nucleons) plus an exchange term which is necessary in the presence of exchange forces to ensure current conservation. The usual derivation of this exchange current[1] was found to be inadequate in that it could not ensure current conservation at all momentum transfers unless specific dynamical assumptions were made regarding the form-factors used.[2] Recently, we have pointed out that this situation arises because off-shell effects are not properly taken into account in constructing the current.[3,4] Careful inclusion of off-shell effects necessitates the inclusion of two additional form-factors $g_e(q^2)$, $g_m(q^2)$ which are really the derivatives of the half off-shell form-factors:

$$g_e(q^2) = \frac{d}{dW} G_B(q^2, W, M) \mid_{W=M} \quad . (1)$$

$$g_m(q^2) = \frac{d}{dW} G_M(q^2, W, M) \mid_{W=M} \quad . (2)$$

*Presented at the IV High Energy Conference, Jaipur December 1978

where $g_e(0) = 0$ to ensure current conservation. These off-shell effects are proportional to the interaction potential and vanish for free nucleons. They were estimated by deriving a dispersion integral[4] for the form-factors previously used by Bincer[5] and assuming that the integral is saturated by the lightest isobar with nucleonic quantum numbers. This gives

$$g_{ei}(q^2) = \frac{G_{Ei}(q^2) - e_i}{680} \text{ MeV}^{-1} \quad \ldots(3)$$

$$g_{mi}(q^2) = \frac{G_{Mi}(q^2) - e_i}{680} \text{ MeV}^{-1} \quad \ldots(4)$$

The effect of these form-factors is small for most low-momentum phenomena but it is there, in principle, to complicate things particularly at not too small momentum transfers when interaction current terms are known to dominate the simple impulse terms for processes such as electron scattering. In particular, the extraction of the small neutron form-factor from the scattering data on deuteron may need correction on this account.

We now apply quark model to calculate the same quantity. For the electric form-factor, in impulse approximation, we have the result

$$G_E(q^2) \equiv G_E(q^2, M_f, M_i) = \int d\tau \; \Psi_f^* \; O_E \; \Psi_i \quad \ldots(5)$$

where O_E are appropriate quark operators and Ψ_i are quark wavefunctions. Varying M_f in this model is equivalent to varying Ψ_f and taking the derivative. Thus we get

$$g_e(q^2) = \int d\tau \; \frac{\partial \Psi_f^*}{\partial E_0} \; O_E \; \Psi_i$$

$$= \frac{1}{2} \; \frac{\partial}{\partial E_0} \int d\tau \; \Psi_f^* \; O_E \; \Psi_i \quad \ldots(6)$$

where $E_0 = M$ is the nucleon rest energy in the quark model. The derivative may be evaluated by using the relation

$$\frac{\partial}{\partial E_0} = \left(\frac{\partial E_0}{\partial \lambda} \right)^{-1} \frac{\partial}{\partial \lambda}$$

where λ is some parameter. It is easy to see that this definition is consistent with charge conservation in the sense $g_e(0) = 0$. For small q, G_E^p is determined by its slope which is related to the rms radius of proton. Similarly, we let $g_e(q^2) = -1/6 \; q^2 \; R^2$ where R^2 (units $= fm^2$ MeV^{-1}) is a measure of the shift of rms radius due to off-shell effects. Then we have

$$R^2 = \frac{1}{2} \frac{\partial \langle r^2 \rangle}{\partial E_0} \quad \ldots(7)$$

In the MIT bag model in zero order, $E_0 \propto R_0^{-1}$, $\langle r^2 \rangle \propto R_0^2$ where R is the equilibrium bag radius. Thus we have

$$R^2 = -\frac{\langle r^2 \rangle}{M} \quad \ldots(8)$$

A result similar to this in sign but slightly different in magnitude is obtained on using the older forms of the quark model. Analogous results may be derived for the magnetic form factor also. These results do not take into account the SU (6) breaking effects and differ in sign from the estimate made earlier.[4] We note, however, that both these models are crude and more realistic calculations may be postponed till experimental results are in a position of clarifying the whole situation.

References

1. Lock J A & Foldy L L, *Anls. Phys.*, **93** (1975), 276.
2. Friar J L & Fallieros S, *Phys. Rev.*, **C13** (1976), 461.
3. Thakur J & Lock J A, *Physics Lett.*, **67B** (1977), 29.
4. Thakur J, *Physics Lett.*, **82B** (1979), 341.
5. Bincer A M, *Phys. Rev.*, **118** (1960), 855.

Notes

Neutron Irradiation Effects on Magnetocurrent in Semiconductor Diodes

SHANKER LAL AGRAWAL & RAMA SWAMI

Electronics & Radio Physics Laboratory, Department of Physics, Banaras Hindu University, Varanasi 221 005

Received 13 *July* 1979

Fast neutron irradiation effects on magnetically induced forward current change, usually referred to as magnetocurrent, in semiconductor diodes are reported. Commercially available diodes were irradiated by 14 MeV fast neutrons. In case of germanium diodes, magnetocurrent is found to decrease with irradiation whereas in case of silicon diodes it increases. This behaviour of diodes has been explained on the basis of changes in basic physical properties of charge carriers.

It is well established that semiconductor devices, when placed in nuclear radiation environment, are found to show significant changes in their physical and electrical properties. The most basic device effected by irradiation is a *p-n* junction diode. Though, the neutron radiation effects in diodes are well understood,[1-3] very little work has been devoted to radiation induced changes in their magneto-electrical properties. Keeping this in view, the effect of fast neutron irradiation on magnetically induced changes in forward current (usually referred as magnetocurrent) of semiconductor diodes are reported in this note.

For the present study, commercially available germanium (DR25 and OA79) diodes and silicon (BY125 and BY127) diodes manufactured by Bharat Electronics Ltd, India, were chosen. The magnetocurrent was measured using the circuit arrangement shown in Fig. 1.

For a fixed current in diode, the voltage across it was measured with the help of a digital voltmeter (DVM). Then keeping the voltage across the diode fixed, change in forward diode current (magnetocurrent) was measured on application of 17 kOe magnetic field. Orientation of the diode in magnetic field was adjusted to yield maximum magnetocurrent.

After carrying out a pre-irradiation measurement, the diodes were irradiated by 14 MeV neutrons (neutron flux $\sim 10^8$n/cm^2) at the Vande Graff Accelerator facilities of the Physics Department, Banaras Hindu University and the Indian Institute of Technology, Kanpur. Post-irradiation measurement of magnetocurrent was then carried out by the method described above (Fig. 1). The maximum possible observational error in the current measurement was within $\pm$ 0·1 mA ($\pm$ 0·3%). Ambient temperature was kept constant in all the measurements to avoid undesired effects introduced by its variation. In Table 1, pre- and post-irradiated magnetocurrents of the diodes under test, at various injection levels are reported. The data can be interpreted on the basis of radiation induced changes in the physical properties of diodes.

As analyzed by Karakushan *et al.*,[4-6] the magnetocurrent in diodes basically depends upon the resistivity of base material (ρ), d/L ratio (L, the diffusion length of minority carriers and d, the thickness of the base material) and magnetoresistance $\left(\frac{1}{\rho}\frac{d\rho}{dH}\right)$. It has been shown that the magnetocurrent in germanium diodes increases with d/L ratio upto a value of 3-4 and then decreases. Similarly, silicon diodes also show an increase of magnetocurrent with d/L ratio. But as the resistivity of silicon is larger than germanium, the d/L ratio for optimum magnetocurrent in silicon diodes[6] lies in between 10 and 12. Beyond this value of d/L ratio, magnetocurrent decreases in this case also. Thus upto the optimum magnetosensitivity of diodes, magnetocurrent decreases with increase in resistivity and increases with increase of d/L ratio.

Several workers,[2,7-9] have reported the increase of resistivity and decrease in mobility and life-

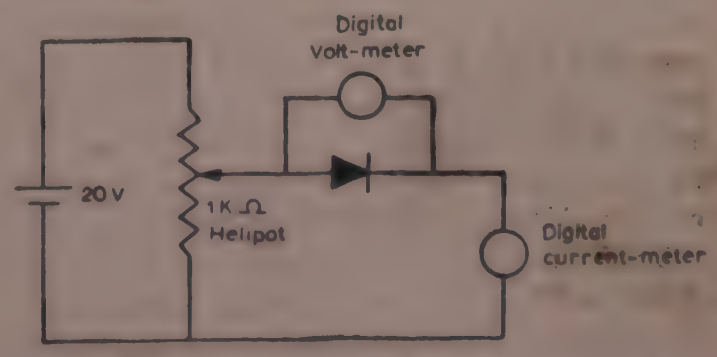

Fig. 1—Circuit arrangement for the measurement of magnetocurrent

Table 1—Magnetocurrent of Pre-irradiated and Post-irradiated Diodes at Different Current Levels

Diode type	Semiconductor material	Current I_1 in pre-irradiated diode (in mA) with H=0 kOe	Current I_2 in pre-irradiated diode (in mA) with H=17 kOe	Magneto-current in per-centage $\frac{\Delta I_1}{I_1} \times 100\% \simeq I_2\text{-}I_1$	Current I_3 in post-irradiated diode (in mA) with H=17 kOe	Magneto-current in per-centage $\frac{\Delta I_2}{I_2} \times 100\% \simeq I_3\text{-}I_1$	Place & time of irradiation
DR25	Germanium	50·00	37·90	24·20	39·70	20·60	IIT, Kanpur
		60·00	45·20	24·83	48·10	19·83	2·30 hr
OA79	Germanium	30·00	25·30	15·67	29·40	2·00	IIT, Kanpur
		40·00	34·10	14·75	39·70	0·75	2·30 hr
BY125	Silicon	30·00	28·00	6·67	27·70	7·67	Physics Depart-ment, BHU
		40·00	38·20	4·50	37·40	6·50	2·00 hr
BY127	Silicon	53·10	50·50	4·89	50·10	5·65	IIT, Kanpur
		61·70	59·00	4·37	58·10	5·83	2·30 hr

time of charge carriers in germanium and silicon under neutron irradiation. However, from their observations it is clear that lifetime of minority carriers in semiconductors is most sensitive to irradiation. Usually this lifetime is greatly changed by moderate radiation doses which only slightly affects other properties (for instance conductivity).[3] Due to this fact, in some of the studies of radiations induced changes in devices, other parameters except lifetime are assumed to be constant upto a dose of 10^{14} n/cm^2.

Keeping the above discussion in view, one can easily conclude that for explaining radiation-induced effects on magnetocurrent in the present work, only effect on lifetime (hence d/L ratio) has to be taken into account. Now taking this fact into consideration one can explain neutron irradiation effects on magnetocurrent as follows.

In germanium diodes the d/L ratio is large initially as seen from the high value of pre-irradiation magnetocurrent. On irradiation, this d/L ratio increases and crosses over the value of d/L for optimum magnetocurrent. Hence in germanium diodes, magnetocurrent is found to decrease with neutron irradiation. On the other hand, initial value of d/L ratio in silicon diodes is quite small as indicated from the small value of pre-irradiated magnetocurrent. Now on irradiation, with moderate doses, d/L ratio increases but still remains well below the d/L ratio required for optimum magnetocurrent.

The above study suggests that neutron irradiation can be used as an effective tool to control the sensitivity of mangnetodevices. A more detailed general study of this effect on various other type of diodes like power diodes, magneto-diodes, etc. is underway and will be reported later on.

The authors express their sincere thanks to Dr A K Nigam, Physics Department, Banaras Hindu University, India, and Prof. G K Mehta, Incharge, Van de Graff Accelerator Laboratory, IIT, Kanpur, for providing the Van de Graff Accelarator facilities for irradiation of diodes by fast neutrons. They are further thankful to the University Grants Commission, New Delhi, for the financial assistance in the form of a JRF to one of them (SLA).

References

1. Larin Frank, *Radiation effects in semiconductor devices*, (John Wiley, New York), 1968.
2. Gregory B L & Gwyn Charles, *Proc. IEEE*, 62 (1974), 1264.
3. Vavilov V S & Ukhin N A, *Radiation effects in semiconductors and semiconductor apparatuses*, (Plenum, New York), 1977.
4. Karakushan E I & Stafeev V I, *Soviet Phys. Solid St.*, 3 (1961), 493.
5. Karakushan E I & Stafeev V I, *Soviet Phys. Solid St.*, 3 (1962), 1476.
6. Karakushan E I, Kovarskii V Y, Komarovskikh K F, Gamolin E I & Stafeev V I, *Soviet Phys. Semicond.*, 3 (1970), 1453.
7. Buehler M G, *Proc. IEEE*, 56 (1968), 1741.
8. Cleland J W, Crawford (Jr) J H, Horovitz K Lark, Pigg J C & Young (Jr) F W, *Phys. Rev.*, 83 (1951), 312.
9. Cleland J W, Crawford (Jr) J H & Pigg J C, *Phys. Rev.*, 98 (1955), 1742.

Thermal Expansion of the Ceramic System Pb_{2-x} Ba_x $Li_{0.5}$ $Nb_{1.5}$ O_6

R RAJAN & R K KHARE*

Department of Physics, Indian Institute of Technology
Bombay 400 076

Received 30 *March* 1978; *revised received* 17 *March* 1980

The thermal expansions of the ceramic system Pb_{2-x} Ba_x $Li_{0.5}$ $Nb_{1.5}$ O_6 for different values of x are experimentally studied. From the data presented for two concentrations (x), it is observed that the ceramic system is predominantly ionic in bonding with brittle nature and melting at fairly low temperatures.

The general formula ABO_6X represents the pyrochlore group having the structure type of the mineral $CaNaNb_2O_6F$ studied first by Bystrom.[1] A and B are cations, X is O, OH or F. Cadmium niobate ($Cd_2Nb_2O_7$) and lead niobate ($Pb_2Nb_2O_7$) belong to this group. The X site may be vacant or partly vacant as in $Pb_{1.5}Nb_2O_{6.5}$ studied by Cook and Jaffe.[2] Recently, the electrical resistivity and the dielectric properties of the system $Pb_{2-x}Ba_x$ $Li_{0.5}Nb_{1.5}O_6$ have been reported[3,4] to show anomalous behaviour, with varying concentration x of barium ions and temperature. The thermal expansion values of these ceramics are reported here, as a part of characterization study. The thermal expansion of circular pellets of the ceramics, with $x = 0{\cdot}00$, $0{\cdot}05$, $0{\cdot}10$ and $0{\cdot}15$ have been studied in the temperature range 30-300°C.

The solid solutions were prepared[3] by the solid state reaction, in the form of thin circular pellets with diameter of about 11·5 mm and thickness 2·5 mm. The heterodyne beat method of thermal expansion measurement was tried with reproducible results.

The present measurements were made with the help of a high frequency capacitance meter, E12-1 Russian make, operating in the 700-300 kHz range.[4] The accuracy is 1 pF. The instrument incorporates two high frequency generators G_1, G_2 of the same design. A variable standard capacitor of 1000 pF, has been connected in the oscillation circuit of one generator G_1. Both the generators are tuned to zero beat, indicated by high resistance head phones. The experimental parallel plates containing the sample, are connected to the generator G_2 in parallel. Relative frequency detuning which occurs, is compensated by the reading variable capacitor of generator G_1. When the circuit inductances are equal, the capacitance being measured will be equal to the reading capacitance in G_1. The accuracy in the range of capacitance measured in the present case has been quoted to be ± 5%.

The experimental set of electrodes forming a two-terminal arrangement is surrounded by a furnace system going up to 400°C, the sintered circular pellet firmly gripped between the electrode plates by screw thread arrangement, so that the circular face of the sample was coplanar with the electrode faces. The distance between the electrodes is nearly the same as the thickness of the sample. The temperature in the range 30-300°C was measured by a copper-constantan thermocouple.

The temperature coefficient of capacitance is obtained by making the capacitance measurements of the set-up and sample for various temperatures keeping all other conditions unchanged. The temperature coefficient of capacitance is $\Delta C/C\Delta T$, where ΔC is the change in capacitance for a temperature difference of ΔT. The capacitance for a parallel plate capacitor is $C = A/4\pi d$. If it is assumed that d is kept unaltered, the thermal expansion for the ceramic sample occurs in the radial direction. The bulk volume changea lters the capacitance proportionally, so that $\Delta C/C\Delta T = \Delta V/V\Delta T = \beta$, the volume or cubical expansion coefficient, (where ΔV is change in volume; V initial volume, ΔT, temperature difference. The mean linear coefficient of thermal expansion $\bar{\alpha} = \beta/3$).

The experimental results are shown in Table 1, for mean $\Delta C/C\Delta T$ values, for the range indicated. The variations of mean β and α values for the range 30-300°C are shown in Table 2, for two samples with $x = 0{\cdot}05$ and $x = 0{\cdot}15$. Some comparative values are also included.

The mean coefficient of linear expansion $\bar{\alpha}$ for a material depends on the temperature and is highly variable if the material undergoes some sort of a phase transition.[5] The ceramic system $Pb_{2-x}Ba_x$ $Li_{0.5}Nb_{1.5}O_6$ has been reported to be showing anomalous dielectric behaviour[3,4] with concentration x of barium ions and temperature T. The present

Table 1—Experimental Values of $\Delta C/C\Delta T$ at Different Concentrations and Temperature Ranges

Concentration of barium ion	Temperature range °C	Mean $\frac{\Delta C}{C\Delta T} \times 10^5$/°C measured
0·00	40-75	122
0·05	30-85	273
0·10	35-115	71
0·15	30-130	150

*Present address : Fertilizer Corporation of India, Sindri.

Table 2—Values of β and $\bar{\alpha}$ at Different Temperatures for 2 Ceramic Samples

Temp., °C	$x=0{\cdot}5$		$x=0{\cdot}15$	
	$\beta\times10^5$/°C	$\bar{\alpha}\times10^5$/°C	$\beta\times10^5$/°C	$\bar{\alpha}\times10^5$/°C
130	90	30	150	50
155	76	25	117	39
190	39	13	73	24
230	23	8	34	11
240	19	6	28	9
265	9	3	12	4
285	5	2	3	1
300	3	1	9	3

work shows that the mean coefficient of cubical expansion β has high values in the range 30-130°C, where the maximum dielectric constant occurs (T_c). Beyond 130°C and in the range up to 300°C, the mean values of β are comparable to values given[5-8] for a normal insulator.

The values of the order of 10^{-5}/°C for these ceramics are large by a factor of 10 compared to highly covalent materials like diamond. It is surmised that these ceramics, are therefore, predominantly ionic in bonding, with brittle nature and melting or dissociating at fairly low temperatures.

References

1. Bystrom A, *Ark. Kemi Min. Geol.*, **18A** (No. 21) (1944).
2. Cook W R & Jaffe H, *Phys. Rev.*, 89 (1953), 1297.
3. Khare R K & Rajan R, *Indian J. pure appl. Phys.*, 15 (1977), 597.
4. Khare R K & Rajan R, *Indian J. pure appl. Phys.*, 16 (1978), 492.
5. Krishnan R S, *Progress in crystal physics*, 1 (1958), 10.
6. Touloukian Y S, *Thermophysical properties of matter* Vols. 12, 13 (Iliffe/Plenum, New York), 1975.
7. *American Institute of Physics Handbook*, (McGraw-Hill, New York), 1972, 4-119.
8. Kirchner H P, *Progress in solid state chemistry*, Vol. 1, edited by H Reiss (Pergamon Press, New York), 1964, 1.

Calculation of Ionic Radii of Alkali Halide Crystals through Screened Coulomb Potential

USHA PURI

Department of Physics, S M College, Bhagalpur

Received 11 *June* 1979

Screened Coulomb potential form for the repulsive interaction potential has been used to calculate ionic radii of twenty alkali halide crystals. The results present a consistently good agreement with the experimental values.

The atomic or ionic radii are usually estimated from the measured values of internuclear distance between the nuclei of bonded atoms or ions in a substance. Interest has been shown by workers[1-2] in the calculations of ionic radius as they play an important role in predicting the crystal structure, nature of crystalline interactions and chemical bonds, etc. Further, to produce various solid solutions of technological importance, the knowledge of appropriate ionic radii[2,3] is basically required. Many workers[4-10] have calculated the ionic radii using different methods.

In this note, ionic radii of alkali halide crystals have been presented using screened Coulomb potential which has been discussed and used for various properties of alkali halide crystals with encouraging results by Puri[11] and Puri and Srivastava.[12]

Expressing the repulsive energy as $\frac{b}{r}\exp[(r_+ + r_- - r)\lambda]$ where r_+ and r_- are the ionic radii of alkali and halogen ions respectively, the lattice energy per molecule is given by

$$W_L(r) = -\frac{Ae^2 z_1 z_2}{r} - \frac{C}{r^6} - \frac{D}{r^8} - + M\beta_{+-} \frac{b}{r}\exp[(r_+ + r_- - r)\lambda] + \frac{1}{2}\frac{M'}{r'} b \left[\beta_{++}\exp[(2r_+ - r)\lambda] + \beta_{--}\exp[(2r - r)\lambda]\right] \quad ...(1)$$

where C and D are van der Waals constants whose values are taken from Mayer.[13] Z_1, Z_2 are the valencies which for alkali halide crystals have a value 1; λ and b are the potential parameters; β_{++}, β_{--} and β_{+-} are factors introduced to allow for the dependence of the repulsion between the ions on their charges as suggested by Pauling,[6] M and M' are numbers of nearest unlike and like neighbours respectively; r' is the distance of second neighbour, A is the Madelung constant. $B_{pp'}$, the Pauling coefficients, are given[6] by

$$\beta_{pp'} = 1 + \frac{Z_p}{n_p} + \frac{Z_{p'}}{n_{p'}} \quad ...(2)$$

Z_p and n_p are respectively the valence and number of outer electrons of the Pth ion. The repulsive parameters can be determined through either Hilderband equation[14] or Mie-Gruneisen equations [Eqs. (1·4) and (1·5) of Ref. 2 for negligible pressure]. It leads to the following relations using Hilderband's condition :

$$r = r_+ + r_- + \frac{1}{\lambda}\ln\left[\frac{M\beta_{+-}}{\tau}\frac{b}{r}(\lambda r + 1)\left\{1 + \frac{M'}{2M}\frac{r}{r'}\frac{(\lambda r' + 1)}{(\lambda r + 1)}\right\}\right.$$

$$\times \left(\frac{\beta_{++}}{\beta_{+-}} \exp\left[(r_+ - r_-)\lambda\right] + \frac{\beta_{--}}{\beta_{+-}} \exp\left[(r_- - r_+)\lambda\right] \right)$$

$$\exp\left[(r-r')\lambda\right] \Big] \qquad \ldots(3)$$

$$\frac{\left(\frac{\tau}{\sigma}\lambda r - 1\right) + \frac{\tau}{\sigma}\left(2 + \frac{2}{\lambda r} - \frac{\sigma}{\tau \lambda r}\right)}{\left(\frac{\tau}{\sigma}\lambda r' - 1\right) + \frac{\tau}{\sigma}\left(2 + \frac{2}{\lambda r'} - \frac{\sigma}{\tau \lambda r}\right)}$$

$$= -\frac{M'}{2M}\left\{\frac{\beta_{++}}{\beta_{+-}} \exp\left[(r_+ - r_-)\lambda\right] + \frac{\beta_{--}}{\beta_{+-}} \exp\left[(r_- - r_+)\right]\right\} \exp\left[(r-r')\lambda\right] \qquad \ldots(4)$$

where $\tau = \frac{Ae^2}{r} + \frac{6C}{r^6} + \frac{8D}{r^8} - \frac{3VT\beta}{K}$ ...(5)

r is the internuclear distance in equilibrium.

$$\sigma = \frac{9v}{K} F(T, P) + \frac{2A\,C^2}{r} + \frac{42e}{r^6} + \frac{72\,D}{r^8} \qquad \ldots(6)$$

and

$$F(T, P) = 1 + T\left[\frac{1}{K}\left(\frac{\partial K}{\sigma T}\right)_P + \frac{\beta}{K^2}\left(\frac{\partial K}{\sigma P}\right)_T + \frac{2}{3}\beta\right] \qquad \ldots(7)$$

K and β are the compressibility and coefficient of thermal expansion respectively. Eq. (4) differs from a similar expression obtained by using Born-Mayer's form (Eq. 6·19 of Ref. 2) in respect of the left hand side of the equation. Assuming a certain value of $(r_+ - r_-)$, λ can be determined from Eq. (4).

It is to be noted that any attempt to determine λ uniquely without the use of $(r_+ - r_-)$ by eliminating the bracket on the right hand side of Eq. (4), through Eqs. (1) and (3) leads to a quadratic equation for λ, giving imaginary values. This happens in case of Born-Mayer's form also and is because of the uncertainties in the values of crystal parameters of Table 7 of Ref. 2. In the evaluation of λ, we have therefore, taken $(r_+ - r_-)$ from the work of Gourary.[15] The evaluated values of λ are given in Table 1 along with the van der Waals constants from Mayer.[13] Parameters used in calculation have been prescribed in Table 2.

The calculation of b and $(r_+ + r_-)$ is generally tedious. Tosi and Fumi[7] have prescribed a method which can be used for the purpose but on account of its complexities in the computation, the method has not been favoured much by workers. We have preferred to evaluate b through Eq. (3) taking values of r_+ and r_- of Nacl from Gourary[15] for which $r - (r_+ + r_-) = 0$ and assuming the same b for all crystals. Although the approach is not unique and can be criticized, we have observed the procedure to present good results. The value of b, r_+ and r_- obtained in this way are presented in Table 1.

Table 1—van der Waals Constants and Calculated Value of Potential Parameters and Ionic Radii

Crystal	vander Waals constant (Ref. 11)		$\lambda \times 10^{-8}$ (cm^{-1})	r_+(Å)	r_-(Å)
	C (10^{-60} ergs cm^6)	D (10^{-76} ergs cm^8)			
LiF	18	11	2·8169	0·945	1·165
LiCl	113	104	3·0303	0·940	1·640
LiBr	183	190	3·1250	0·953	1·813
LiI	363	470	2·9851	0·914	2·024
NaF	46	31	2·8818	1·193	1·183
NaCl	180	180	3·1056	1·175	1·645
NaBr	271	300	2·924	1·176	1·806
NaI	482	630	2·7624	1·163	2·042
KF	167	150	2·9326	1·519	1·156
KCl	452	560	2·7624	1·518	1·668
KBr	605	800	2·7933	1·506	1·816
KI	924	1420	2·7027	1·490	2·050
RbF	278	290	3·1153	1·690	1·179
RbCl	691	960	2·9070	1·655	1·664
RbBr	898	1340	2·7778	1·654	1·823
RbI	1330	2240	2·7778	1·632	2·051
CsF	495	600	2·7313	1·833	1·130
CsCl	1530	2600	3·0864	1·826	1·606
CsBr	2070	3600	2·8736	1·837	1·777
CsI	2970	5800	1·8169	1·827	2·017

$b = 0{\cdot}6953 \times 10^{-20}$ ergs cm.

Table 2—Values of Parameters used in Calculations

	LiX•	NaX, KX, RbX Csf	CsCl, CsBr, CsI
A	1·7476	1·7476	1·7627
β_{++}	2·20	1·25	1·25
β_{--}	0·75	0·75	0·75
M	6	6	8
M'	12	12	6
r'/r	1·414	1·414	1·155

•X is the halide ion

The mean values of radii obtained in the present study are given in Table 3 and compared with the experimental[15-18] values. Also those calculated by Agrawal and Jaishanker[9] (A-J), Tosi and Fumi[7] (T, F) Bansigir[8] (B), Pauling[1] (P) and Bansigir and

Table 3—Values of Mean Radii in Å

Ion	Exptl		Present study	Theoretical				
	Witte *et al.* (Ref. 16-18)	Electron density map (Ref. 15)		(A-J) (Ref. 9)	(T-F) (Ref. 7)	(B) (Ref. 8)	(P) (Ref. 1)	(B-J) (Ref. 10)
Li^+	0·9	0·94	1·938		0·902	0·86	0·60	0·98
Na^+	1·17 (Ref. 16) 1·18 (Ref. 18)	1·17	1·177	1·17	1·205	1·16	0·95	1·11
K^+		1·49	1·508	1·55	1·512	1·52	1·33	1·53
Rb^+		1·63	1·648	1·67	1·65	1·67	1·48	1·68
Cs^+		1·86	1·831	1·85	1·80	1·85	1·69	1·87
F^-	1·1	1·16	1·160	1·16	1·194	1·15	1·36	1·20
Cl^-	1·65 (Ref. 16) 1·64 (Ref. 18)	1·64	1·646	1·67	1·646	1·62	1·81	1·61
Br^-		1·80	1·807	1·84	1·796	1·78	1·95	1·77
I^-		2·05	2 037	2·03	2·008	1·98	2·16	1·96

Jaishanker[10] (B-J) are included therein for comparison. Table 3 shows that our values present a consistently good agreement with the experimental values.

The author is thankful to Dr P L Srivastava for helpful discussion and suggestions.

References

1. Pauling L, *The nature of chemical bond* (Cornell University Press, Ithaca), 1963, 518.
2. Tosi M P, *Solid state physics*, Vol. XVI, edited by F Seitz & Turnbull (Academic Press, New York), 1964, 1.
3. Shanon R D & Prewitt C T, *J. inorg. nucl. chem.*, 32 (1970), 1427.
4. Goldsmidt V M, cited by Tosi M P in *Solid state physics*, Vol. XVI (Academic Press, New York), 1964, 1.
5. Zachariasen W H, cited by Kittel C in *Introduction of solid state physics*, (Wiley, New York), 1956, Table 3·5.
6. Pauling L, *Proc. R. Soc.*, **A114** (1927), 181; *J. Am. chem. Soc.*, **49** (1927); 765; *Z. Krist.*, 67 (1928), 377.
7. Tosi M P & Fumi F G, *J. Phys. Chem. Solids*, 25 (1964), 45.
8. Bansigir K G, *Indian J. pure appl. Phys.*, 7 (1969), 293.
9. Agrawal L D & Jaishanker, *Indian J. pure appl. Phys.*, **12** (1974), 85.
10. Bisarya S D & Jaishanker, *Indian J. pure appl. Phys.*, **10** (1975), 214.
11. Puri U, *Indian J. pure appl. Phys.*, 15 (1977), 387.
12. Puri U & Srivastava P L, *J. chim. Phys.*, 74 (1977), 1034.
13. Mayer J E, *J. chem. Phys.*, **1** (1933), 270.
14. Hilderband J H, *Z. Phys.*, 67 (1931), 127.
15. Gourary B S, *Solid st. Phys.*, **10** (1960), 143.
16. Schonecht G, *Z. Naturf.*, **12a** (1957), 983.
17. Krug J, Witte H & Wolfel E, *Z. phys. Chem.*, 4 (1955), 36.
18. Witte H & Wolfel E, *Z. phys. Chem.*, 3 (1955), 296.

Evaluation of Critical Currents & Voltages in the Single Injection Current in an Insulator

Y K Sharma

Department of Physics, R B S College, Agra 282 003

Received 15 *March* 1978; *accepted* 26 *February* 1980

The regional approximation method is used to evaluate the critical currents and critical voltages in the single injection current in an insulator with a single set of traps lying below the Fermi level operating under carrier density dependent mobility regime. It is shown that there is a very large change in current for a very restricted change in voltage.

The injection of electrons or holes in an insulator can be explained on the energy band theory.[1] This injection phenomenon is extended under high field conditions by several workers,[1-4] and the author has worked[5,6] on the carrier density-dependent mobility with the well known regional approximation method (RAM). In this injection field, the RAM has proved to be a powerful tool in investigating the current-

voltage characteristics under different regimes and configurations.

In a low mobility insulator, the average mobility (μ) is varied with the carrier concentration (n) as[7,8]

$$\mu = h\, n\,(x) \qquad \ldots(1)$$

where h is the constant of proportionality.

Consider an insulator containing a single set of traps lying below the Fermi level and provided with an injecting contact (cathode) at $x=0$, and an electron collecting contact (anode) at $x = L$. At low currents, there will be the space charge region on the cathode side and ohmic region to the anode side. The equations characterizing the current flow and Poisson's law are

$$J = e\,\mu\, n\, E \qquad \ldots(2)$$

$$\frac{\epsilon}{e}\frac{dE}{dx} = [n\,(x) - n_0] + [p_{t,0} - p_t\,(x)] \qquad \ldots(3)$$

where,

$$p_t\,(x) = \frac{N_t N}{g\, n(x)}\,,\quad p_{t,0} = \frac{N_t N}{g\, n_0},$$

$$N = N_c \exp\left(\frac{E_t - E_c}{kT}\right) \qquad \ldots(4)$$

where the symbols have the usual meanings and Eqs. (2)-(4) are subject to the boundary condition:

$$E\,(0) = 0 \qquad \ldots(5)$$

The problem is solved with the help of the regional approximation based on obvious physical considerations.[1-3] The insulator is divided into three regions as shown in Fig. 1. The injected carrier concentration (n_i) is a decreasing function of x. At not too high currents, there will be a plane x_2 (J) at which n_i is equal to the thermally generated free carriers (n_0). The situation of the transition planes depends upon the current. To the right of the plane x_2, where $n_0 > n_i$, we neglect n_i; to the left of the plane x_2, where $n_i > n_0$, we neglect n_0. Thus the transition plane x_2 (J) separates the insulator into two regions. One of them is space charge limited and the other is ohmic

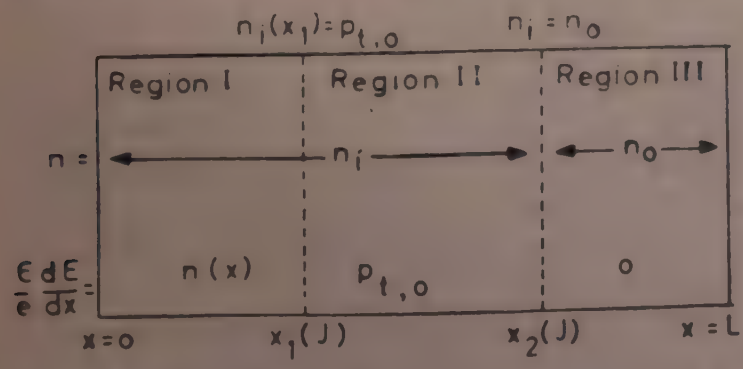

Fig. 1—Schematic regional approximator diagram for the single injection in an insulator with traps lying below the Fermi level

(towards anode). Due to the presence of an additional term $(p_{t,0} - p_t)$ in Eq. (3), the space charge region can be separated into two regions, i.e. the regions I and II. Thus, there will be a transition plane x_1 (J), where $n_i\,(x_1) = n\,(x_1) = p_{t,0}$. To the left of the plane x_1, $n > p_{t,0}$ and $p_{t,0}$ is neglected; to the right of the plane x_1, upto plane x_2, where $(p_{t,0} - p_t) > (n - n_0)$, $(n - n_0)$ as well as p_t can be neglected. The equations characterizing the different regions of the insulator are as follows :

Region I $(0 \leqslant x \leqslant x_1)$

$$J = e\,\mu\, n\, E;\ \frac{\epsilon}{e}\frac{dE}{dx} = n\,(x);\ \mu = h\, n\,(x) \qquad \ldots(6)$$

Region II $(x_1 \leqslant x \leqslant x_2)$

$$J = e\,\mu\, n\, E;\ \frac{\epsilon}{e}\frac{dE}{dx} = p_{t,0};\ \mu = h\, n\,(x) \qquad \ldots(7)$$

Region III $(x_2 \leqslant x \leqslant L)$

$$J = e\,\mu\, n_0\, E;\ \frac{\epsilon}{e}\frac{dE}{dx} = 0;\ \mu = h\, n_0 \qquad \ldots(8)$$

Hence the insulator is divided into three regions by the two transition planes x_1 and x_2, where regions I and II are space charge limited and the region III is ohmic. The continuity relations for the electric field strength at the transition planes x_1 and x_2 are given by

$$E(x_1^-) = E\,(x_1^+) \text{ and } E(x_2^-) = E\,(x_2^+)$$

where the transition planes x_1 and x_2 are defined by

$$n\,(x_1) = p_{t,0},\ n\,(x_2) = n_0$$

Dimensionless C-V characteristic—It is convenient to employ the following dimensionless variables

$$u = \frac{n_0}{n\,(x)} = \frac{n_0\, e\,\mu\, E}{J} = n_0\sqrt{\frac{he\,E}{J}};$$

$$w = \frac{e^2\, n_0^2\,\mu\, x}{\epsilon\, J} = \frac{e\, n_0^2\, x}{\epsilon}\sqrt{\frac{h\, e}{JE}};$$

$$v = \frac{e^3\, n_0^3\,\mu^2\, V\,(x)}{\epsilon\, J^2} = \frac{e^2\, n_0^3\, h\, V\,(x)}{\epsilon\, J\, E} \qquad \ldots(9)$$

where the mobility follows from Eqs. (1) and (2), and is given by

$$\mu = \sqrt{\frac{J\,h}{e\,E}} \qquad \ldots(10)$$

The *C-V* characteristic in the dimensionless notations can be obtained from Eqs. (9)

$$\frac{1}{w_a} = \frac{\epsilon\, J}{e^2\, n_0^2\,\mu_a\, L} \text{ and } \frac{v_a}{w_a^2} = \frac{\epsilon\, V}{e\, n_0\, L^2} \qquad \ldots(11)$$

where, $x = L$, $V = V(L)$ and the subscript a on any quantity denotes the value of that quantity at anode. In Eq. (11), μ_a is the mobility of the carriers at anode and corresponds to $E(x) = E_a$,

$$\mu_a = h\, n_a = \sqrt{\frac{J\, h}{e\, E_a}}$$

The dimensionless characteristic $1/w_a$ versus v_a/w_a^2 is really the C-V characteristic (J/L) versus (V/L^2). Eq. (11) gives the exact characteristic directly from the dimensionless variables.

Critical currents—The critical currents are the hall mark to the different current-voltage regimes. Consider he C-V regime for which the current is less than first critical current $(J_{cr,1})$, then all the three regions are present together. The three regions can be described in terms of the dimension variables

Region I $\quad 2\, u^2\, d\, u = d\,(u\, w),\ u^2 = \dfrac{3\, w}{2}$

Region II $\quad u\, d\, u = \dfrac{A}{2}\, d\,(u\, w),$

$$u^2 - u_1^2 = A\ (u\, w - u_1\ w_1) \rightarrow w = \frac{u}{A} - \frac{1}{3\, A^3\, u}$$

where $A = p_{t,0}/n_0$ ...(12)

Region III $\dfrac{d\, u}{d\, w} = 0,\ u = u_2 = \text{constant} \rightarrow u = 1$

From Eqs. (9) and (12) we have for the transition planes x_1 and x_2 (connecting the regions I and II, and II and III)

$$x = x_1,\ u_1 = \frac{1}{A},\ w_1 = \frac{1}{3\, A^2},$$

$$x_1 = \frac{2\, \epsilon\, J}{3\, A^3\, h\, e^2\, n_0^3}$$

and

$$x = x_2,\ u_2 = 1,\ w_2 = \frac{1}{A} - \frac{1}{3\, A^3} \simeq \frac{1}{A},$$

$$x_2 = \frac{\epsilon\, J}{A\, h\, e^2\, n_0^3}$$

and also corresponding to each of these transition planes x_2 and x_1, there are two critical currents $J_{cr,1}$ and $J_{cr,2}$ (currents at which the region III and the region II respectively leave the insulator) respectively

$$x_2\,(J_{cr,1}) = L,\ x_1\,(J_{cr,2}) = L$$

For the current $J < J_{cr,1}$, all the regions are present in the insulator and the region III gives the main contribution to the C-V characteristic. This corresponds to the ohm's law regime. In the case $J_{cr,1} < J < J_{cr,2}$, there are only two regions I and II in the insulator and the C-V characteristic corresponds to trap-filled limited regime. As current increases further, $J > J_{cr,2}$, then only regions I entirely fills the insulator. This is the perfect trap-free regime of the insulator. Thus, these regimes are separated by the critical currents

$$J_{cr,2} = \frac{3\, A^3\, h\, e^2\, n_0^3\, L}{2\, \epsilon},\ J_{cr,1} = \frac{A\, h\, e^2\, n_0^3\, L}{\epsilon} \qquad ...(13)$$

Critical voltages—The critical voltages $V_{cr,1}$ and $V_{cr,2}$ correspond to the critical currents $J_{cr,1}$ and $J_{cr,2}$ respectively, and can be easily evaluated from Eq. (9). In general, the three dimensionless variables give

$$\frac{V(x)}{E(x)} = \frac{\int_0^x E(x)\, d\, x}{E(x)} \rightarrow v = \frac{1}{u^2} \iint u^2\, d\,(u\, w) \qquad ...(14)$$

From Eqs. (12)-(14), the variable v for the regions I and II becomes

Region I $\quad v = 2\ (u^3/5) \rightarrow v_1 = \dfrac{2}{5\, A^3}$ ...(15)

Region II $\quad v = v_1 + \dfrac{1}{u^2} \displaystyle\int_{w_1}^{w} \int_{u_1}^{u} u^2\, d\,(u\, w) \rightarrow v$

$$v = v_1 + \frac{u^2}{2\, A} - \frac{1}{2\, A^5\, u^2} \rightarrow v_2$$

$$v_2 = \frac{1}{2\, A} + \frac{2}{5\, A^3} - \frac{1}{2\, A^5}$$

Eq. (15) gives the critical values of the dimensionless variables v at anode, i.e, $v_{a,cr,1} \simeq 1/2\, A$ and $v_{a,cr,2} = 2/5\, A^3$ corresponding to $J = J_{cr,1}$ and $J = J_{cr,2}$ respectively. The critical values $v_{a,cr,1}$, $v_{a,cr,2}$ and Eq. (9) give the critical voltages as

$$V_{cr,1} = \frac{A\, e\, n_0 L^2}{2\, \epsilon},\ V_{cr,2} = \frac{9\, A\, e\, n_0\, L^2}{1\,0\, \epsilon} \qquad ..(16)$$

In this note, the RAM is used to evaluate the critical currents and the critical voltages similar to the case when mobility is constant.[1,9] The ratios of the critical currents and critical voltages can be obtained from Eq. (13) and (16),

$$\frac{J_{cr,2}}{J_{cr,1}} = \frac{3\, A^2}{2},\ \frac{V_{cr,2}}{V_{cr,1}} = \frac{9}{5} \qquad (17)$$

Eq. (17) shows that there is a very large change in current occurring over a very restricted change in voltage, even more than that in the case for the constant mobility. However, the different expressions of the same problem for the constant mobility and the carrier density dependent mobility are similar in nature.

From the expressions of the critical currents, it can be easily pointed out that there is a rapid increase in the current as current increases from ohm's law regime to the trap free square law regime,

which is due to the fact that in the transition (TFL) regime all the traps are filled with electrons and the insulator behaves just like a trap free insulator, i.e. all the injected carriers contribute the current and the traps no longer can affect the current flow. It is assumed that a single set of traps is present inside the insulator. If several sets (of traps) are present together, then each set has a separate *C-V* characteristics.

References

1. Lampert M A & Mark P, *Current Injection in solids* (Academic Press, New York), 1970.
2. Sharma Y K, *Phys. Rev.*, B10 (1974), 3273.
3. Sharma Y K, *Indian J. pure appl. Phys.*, 14 (1976), 391, 927; 15 (1977), 574.
4. Sharma Y K & Srivastava B B, *Solid St.-Electron.*, 17 (1974), 1214.
5. Sharma Y K, *Vij. Par. Anu. Pat.*, 18 (1975), 203.
6. Sharma Y K, Balwant Vid, *J. Agri. Sci.*, XVIII (1976), 54.
7. Sharma Y K, Srivastava B B & Sharma V K, *Can. J. Phys.*, 52 (1974), 1844.
8. Wintle H J, *J. appl. Phys.*, 43 (1972), 2927.
9. Lampert M A & Schilling R B, *Current injection in solids: the regional approximation method, In Semiconductor and semimetals*, Vol 6, edited by Willardson R K & Beer A (Academic Press, New York), 1970.

Thermal Conductivities of Binary Gas Mixtures

J D PANDEY

Department of Chemistry, University of Allahabad
Allahabad
&
S R PRAJAPATI

Department of Chemistry, K N Government Postgraduate College, Gyanpur (Varanasi)

Received 7 *February* 1979; *revised received* 24 *December* 1979

Thermal conductivities of some binary gas mixtures were calculated at 50 and 100°C from Wassiljewa Coefficients not containing viscosity coefficients as proposed by the authors. These calculated values are in good agreement with the experimental values of Gray *et al.* [*Trans. Faraday Soc.*, 65 (1969), 1032; 66 (1970), 127].

Without the knowledge of the viscosity terms,[1-3] the calculation of Wassiljewa coefficients (A_{ij}) for the thermal conductivities of binary gas mixtures is not possible. Therefore, alternative procedures have been suggested to estimate Wassiljewa coefficients using Hirschfelder-Eucken approximation[4] and Lindsay-Bromley or Mason-Saxena method so that the derived expressions do not contain viscosity terms.

Wassiljewa equation[2] describes successfully thermal conductivities of binary gas mixture, as

$$\lambda = \frac{\lambda_i}{1+A_{ij}\,x_j/x_i} + \frac{\lambda_j}{1+A_{ji}\,x_i/x_j} \qquad ...(1)$$

where, λ and λ_i are the thermal conductivities of the mixture and pure component i respectively; x_i the mole fraction of component i and A_{ij} one of the Wassiljewa coefficients.

It has been noticed that with suitable approximations[4] the order of $[\lambda_i]_3/[\lambda_j]_3$ or $[\lambda_i]_1/[\lambda_j]_1$ is the same as that of λ_i/λ_j for the binary gas mixtures and similar is the case with $[\eta_i]_3/[\eta_j]_1$ and η_i/η_j. Therefore, the following approximation may be considered

$$\frac{[\lambda_i]_3}{[\lambda_j]_3} \approx \frac{[\lambda_i]_1}{[\lambda_j]_1} \approx \frac{\lambda_i}{\lambda_j} \text{ and } \frac{[\eta_i]_1}{[\eta_j]_1} \approx \frac{\eta_i}{\eta_j} \qquad ...(2)$$

Using Hirschfelder-Eucken first approximation and higher third approximation to the coefficient of thermal conductivity of pure polyatomic gas and remembering the fact that the approximation factors[4] $f^{8}_{\lambda_i}$ and $f^{3}_{\lambda_j}$ are very close to unity, the improved forms of Lindsay-Bromely and Mason-Saxena[2] equations may be written with the help of Eq. (2), as

$$A_{ij} = \frac{1}{4}\left[\, 1 + \left\{ \frac{\lambda_i}{\lambda_j}\left(\frac{M_i}{M_j}\right)^{1/4} \frac{\frac{4}{15}C_{V_j} + \frac{3}{5}R}{\frac{4}{15}C_{V_i} + \frac{3}{5}R} \right.\right.$$

$$\left.\left. \frac{T+S_i}{T+S_j} \right\}^{1/2} \right]^2 \frac{T+S_{ij}}{T+S_i} \qquad ...(3)$$

and

$$A_{ij} = 0{\cdot}3765\left(1+\frac{M_i}{M_j}\right)^{-1/2}\left[1+\left(\frac{\lambda_i}{\lambda_j}\right)^{1/2}\left(\frac{M_i}{M_j}\right)^{1/4}\right.$$

$$\left.\left\{ \frac{\frac{4}{15}C_{V_j} + \frac{3}{5}R}{\frac{4}{15}C_{V_i} + \frac{3}{5}R} \right\}^{1/2}\right]^2 \qquad ...(4)$$

where, η_i, M_i and C_{V_i} are respectively the viscosity, the molecular weight and the molar heat capacity at constant volume of the component i; S is Sutherland's constant and $S_{ij} = (S_iS_j)^{1/2}$ if one or both the gases are nonpolar and $S_{ij} = 0{\cdot}73\,(S_iS_j)^{1/2}$ if one or both the gases are polar. Using Eqs. (1) and (3), and (1) and (4) the values of λ of binary gas mixtures, viz. H_2+N_2O, O_2+N_2O, CH_4+NH_3 and NH_3+Ar are calculated and presented in Table 1 and found to be in good agreement with the experimental values.[5,6] Therefore, it appears that the

above approximations taken in Eq. (2) are valid. The Wassiljewa coefficients calculated from Eqs. (3) and (4) along with these percentage mean absolute deviation are given in Table 2.

Table 1—Values of Thermal Conductivity (λ) (cal km^{-1} sec^{-1} K^{-1}) of Binary Gas Mixtures

System $i+j$	Temp., °C	Mole fraction x_i	λ Exptl.	λ From Eqs. (1) & (3)	% dev.	λ From Eqs. (1) & (4)	% dev.
H_2+N_2O	50	0·1416	7·12	6·92	−2·8	7·14	+0·3
		0·4921	16·16	15·47	−4·3	16·31	+0·9
		0·9062	37·22	36·67	−1·5	37·52	+0·8
	100	0·1416	8·40	8·18	−2·6	8·40	0·0
		0·4921	18·53	17·76	−4·2	18·61	+0·4
		0·9062	41·69	41·13	−1·3	42·01	+0·8
O_2+N_2O	50	0·1014	4·72	4·72	0·0	4·64	−1·7
		0·5031	5·54	5·54	0·0	5·29	−4·5
		0·9054	6·54	0·53	−0·2	6·41	−2·0
	100	0·1014	5·67	5·71	+0·7	5·59	−1·4
		0·5031	6·50	6·63	+2·0	6·21	−4·4
		0·9054	7·46	7·51	+0·7	7·32	−1·9
CH_4+NH_3	50	0·102	6·86	6·93	+1·0	6·78	−1·2
		0·5025	8·15	8·28	+1·6	7·83	−3·9
		0·905	8·815	8·92	+1·2	8·74	−0·9
	100	0·102	8·46	8·54	+0·9	8·38	−0·9
		0·5025	9·935	10·09	+1·6	9·59	−3·5
		0·905	10·705	10·80	+0·9	10·61	−0·9
NH_3+Ar	50	0·1015	4·78	4·91	+2·7	4·67	−2·3
		0·5000	5·735	6·03	+5·1	5·41	−5·7
		0·9035	6·365	6·47	+1·6	6·27	−1·5
	100	0·1015	5·45	5·59	+2·6	5·31	−2·6
		0·5000	6·775	7·14	+5·4	6·44	−4·9
		0·9035	7·795	7·94	+1·9	7·72	−1·0

Table 2—Wassiljewa Coefficients for the Four Binary Gas Mixtures Studied

System $i+j$	Temp. °C	From Eq. (3) A_{ij}	From Eq. (3) A_{ji}	dev. %	From Eq. (4) A_{ij}	From Eq. (4) A_{ji}	dev. %
H_2+N_2O	50	2·617	0·438	2·87	2·550	0·205	0·67
	100	2·553	0·450	2·70	2·529	0·206	0·40
O_2+N_2O	50	1·311	0·747	0·07	1·481	0·779	2·73
	100	1·281	0·685	1·13	1·443	0·795	2·57
CH_4+NH_3	50	0·980	0·736	1·27	1·018	0·914	2·00
	100	0·966	0·754	1·13	0·990	0·936	1·77
NH_3+Ar	50	0·738	0·960	3·13	1·008	1·059	3·17
	100	0·768	0·945	3·30	1·034	1·026	2·83

One of authors (SRP) is grateful to Dr S C Gupta, Joint Director (HE) U P, Allahabad for inspiration and Dr S S Khanna for providing the research facilities.

References

1. Lindsay A L & Bromley L A, *Indian Engng. Chem.*, 42 (1950), 1508.
2. Mason E A & Saxena S C, *Phys. Fluids*, 1 (1968), 361.
3. Wassiljewa A, *Phys. Z.*, 5 (1904), 737.
4. Hirschfelder J O, Curtiss E & Bird R B, *Molecular theory of gases and liquids* (Wiley, New York), 1964.
5. Gray P, Holland S & Maczek A O S, *Trans. Faraday Soc.*, 65 (1969), 1032.
6. Maczek A S O & Gray P, *Trans. Faraday Soc.*, 66 (1970), 127.

Estimation of Thermal Diffusion Factor of N_2-CO_2 Gas Mixture from Thermal Diffusion Column Data

S K Datta & S Acharyya

Department of Physics, University College
West Dinajpur 733 134

Received 27 *August* 1979; *revised received* 31 *December* 1979

The experimental thermal diffusion factor α_T of N_2-CO_2 gas mixture of different compositions have been estimated at $\bar{T} = 460$ K (Maxwellian-Sliekerian cases) and $T_e = 300$ K (Lennard-Jones case) from previously determined column data [*Z. Naturf.*, **20** (1965), 655] only to show that the inelastic collision effect, dealt by Monchik *et al.*[6] [*J. chem. Phys.*, **49** (1968), 1178] does not influence this mixture thus confirming predictions of A E Humphreys & P Grey [*Proc. R. Soc.*, **A320** (1970), 397; **A322**; (1971), 89] based on experimental observations.

In the last few years, thermal diffusion phenomenon in isotopic and polyatomic gas mixtures was regarded as a sensitive tool for investigating interactions between molecules. Here, one usually measures the variation of α_T either with temperature at a fixed composition or with composition at a fixed temperature.[1] The former is sensitive to the nature of the potential between molecules rather than to details of the collision process,[2] while the latter contains some quantities which are believed to be sensitive to the history of collision.

A large number of workers[3,4] studied the inelastic collision effect on thermal diffusion in polyatomic binary gas mixtures, but their experimental results are hardly improved by the existing theories[5] of inelastic collisions. Chottopadhyaya and Acharyya[6] showed that the theory of inelastic collision effect on thermal diffusion was not widely applicable. Recently, Humphrey and Gray,[7] measured α_T of N_2-CO_2 gas mixture by using a two-bulb apparatus and found a reasonable agreement with the theoretical ones based on elastic collision.

In order to verify this conclusion, we were tempted to analyze the thermal diffusion column data of Youssef *et al.*[8] and to get α_T of N_2-CO_2 mixture at $\bar{T} = 460$ K by Maxwellian and Sliekerien methods and at $\bar{T}_c = 300$ K by L-J method respectively.

According to Furry-Hones and Onsager column theory,[9] for a closed column of length L the logarithm of the equilibrium separation factor q_e of a binary gas mixture at any mean temperature $\bar{T}$, [given by $\bar{T} = (T_h + T_c)/2$, T_h and T_c being the hot and cold wall column temperatures in K] is given by

$$\ln q_e = \frac{H L}{K_c + K_d} \qquad ...(1)$$

Here, H, K_c and K_d are functions of the transport coefficients of gas mixtures and pressure in atmosphere. Eq. (1) can thus be expressed as

$$\ln q_e = \frac{a p^2}{1 + b p^4}, \qquad ...(2)$$

where $a = \frac{H L}{K_c} p^2$ and $b = \frac{K_d}{K_c} p^4$.

Again, due to the asymmetry in the column geometry, parasitic remixing occurs. This has been taken into account by Furry-Jones[10] by simply adding a term K_p, proportional to P^4 in the denominator of Eq. (1). As a result, Eq. (1) can now be written as

$$p^2/\ln q_e = \frac{1}{a'} p^4 + \frac{b'}{a'} \qquad ...(3)$$

which is a straight line having certain slope and intercept from which both a and b could be evaluated by $a = a'(1 + K_p/K_c)$ and $b = b'(1 + K_p/K_c)$. Experimentally the ratio K_p/K_c is found to be nearly composition independent. Hence to obtain b', the ratio of intercept and slope of $p^2/\ln q_e$ against p^4 curve and the variation of q_e with pressure at least at one composition of the mixture must be measured. Thus

$$\alpha_T = \frac{K_d}{H' L}\left(1 + \frac{1}{b'}\right) \ln q_e \qquad ...(4)$$

where

$H = H' \alpha_T$, is used to obtain α_T at different composition of the mixture. In practice H and K_d can be given by three methods due to Maxwell, Slieker and Lennard-Jones respectively for the nearly plane case.

(i) *Maxwellian* ($n = 1$, α_T *assumed temperature independent*)

$$H = \frac{2\pi}{6!}\left\{\frac{\alpha_T \rho^2 g}{\eta}\right\}\frac{1}{2}(r_1 + r_2)(r_1 - r_2)^3 (2u)^2 h' \qquad ...(5)$$

$$K_d = 2\pi\{\rho D\}\, 1/2\,(r_1 + r_2)\, r_1 - r_2) K_d' \qquad ...(6)$$

(ii) *Sliekerian* (*Interaction model independent*)

$$H = C_1 = (\text{S.F})_1 r^4 \left\{\frac{\rho^2 g \alpha_T}{\eta}\right\}\left(\frac{\Delta T}{\bar{T}}\right)^2 \qquad ...(7)$$

where $u = \frac{T_h - T_c}{T_h + T_c}$ $a = \frac{r_2}{r_1}$

$$K_d = C_2 = \pi\{\rho D\} r_1^2 (1 - a^2) \qquad ...(8)$$

and $\bar{T} = \frac{T_h + T_c}{2}$;

(iii) *Lennard-Jones* (*Involved with interaction model*)

$$H = \frac{2\pi}{6!}\left\{\frac{\alpha_T \rho^2 g}{\eta}\right\}_1 r_1^4 h \qquad ...(9)$$

$$K_d = 2\pi\{\rho D\}_1 r_1^2 K_d' \qquad ...(10)$$

where h', K_d'; $(\text{S.F})_1$; h and K_d, etc. are the dimensionless shape factors due to Maxwell,[10] Slieker[11] and L-J [12] respectively. The quantities, ρ the mass density and D the diffusion coefficient were calculated from the perfect gas equation and from Ref. 8, while η the coefficient of viscosity of the mixture was calculated theoretically, since experimental viscosity for the mixture was not available; r_1 and r_2 are the radii of the cold and hot walls of the column respectively.

In this work we obtained best fitted straight lines of $p^2/\ln q_e$ against P^4 at eight compositions of the mixture from which b' was accurately obtained. Then with $(1 + 1/b')$ and Eq. (4), α_T at different compositions for the three prescribed cases, i.e. Maxwell, Slieker and L-J were evaluated and shown graphically by curves 3 and 4 at $\bar{T} = 460$ K and by 7 at $T_c = 300$ K in Fig. 1 with the theoretical α_T

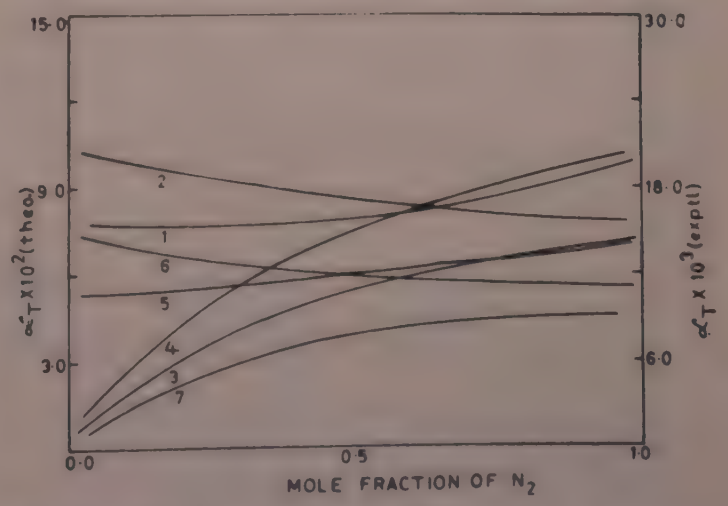

Fig. 1—Thermal diffusion factor of N_2-CO_2 gas mixture against mole fraction of nitrogen [1, Theoretical α_T (elastic) at $\bar{T} = 460$ K; 2, theoretical α_T with exptl. λ_1 λ_2 and λ_{12} at $\bar{T} = 460$ K; 3, exptl. α_T (Maxwell) at $\bar{T} = 460$ K; 4, expt. α_T (Slieker) at $\bar{T} = 460$ K; 5, theoretical α_T (elastic) at $T_c = 300$ K; 6, theoretical α_T with exptl. λ_1, λ_2 and λ_{12} at $T_c = 300$ K; 7, expt. α_T (L-J) at $T_c = 300$ K]

curves 1 and 5 at $\bar{T} = 460$ K and $T_c = 300$ K respectively based on elastic collisions, where $\alpha_{T\,theo}$ is given by

$$\alpha_{T_{theo}} = A\,(6\,C^*_{12} - 5) \qquad ...(11)$$

A is a complicated function, of compositions, mass and theoretical thermal conductivity λ of components and their mixtures. The factor $(6\,C^*_{12} - 5)$ depends solely on temperature. The ratio of collision integrals C^*_{12} is a function of $T^* = T/(\epsilon/k)$; T being the temperature and (ϵ/k) the depth of the L-J (12-6) potential well.

It is found from Fig. 1 that the experimental α_T obtained in three cases agree with the theoretical elastic values so far as the trend of α_T with composition is concerned particularly in the range 40% of N_2 onwards. Though much reliance cannot be stressed on the magnitude of α_T obtained by T.D. column method, the column-data yield the actual trend of α_T with composition. In order to locate the inelastic collisions, if any, we used the experimental conductivities of the components[14] and the experimental thermal conductivity values of the mixture, interpolated from Ref. 15 in Eq. (2) to obtain α_T. The data thus obtained are shown by the curves 2 and 6 in Fig. 1 graphically. There is wide divergence between theoretical and experimental variations. Thus we may conclude that in this mixture of diatomic and polyatomic components both being nonpolar, the elastic theory is enough to explain the trend of variation of α_T with composition as observed by other workers.

References

1. Datta S K, Saha I L & Acharyya S, *J. Phys. B.*, (communicated).
2. Mason E A & Monchik L, *J. chem. Phys.*, 36 (1962), 1622.
3. Acharyya S & Barua A K, *J. Phys.*, B3 (1970), 1052.
4. Watson W W & Mathur B P, *J. chem. Phys.*, 49 (1968), 5537.
5. Monchik L, Sandler S I & Mason E A, *J. chem. Phys.*, 49 (1968), 1178.
6. Chhottopadhyay T K & Acharyya S, *J. Phys.*, B7 (1974), 2277.
7. Humphreys A E & Gray P, *Proc. R. Soc.*, A320 (1970), 397; A322 (1971), 89.
8. Youssef A Hanna M M & Migahed M D, *Z. Naturf.*, 20 (1965), 655.
9. Furry W H, Jones R C & Onsager L, *Phys. Rev.*, 55 (1939), 1083.
10. Furry W H & Jonnes R C, *Phys. Rev.*, 69 (1946), 459.
11. Slieker C J G, *Z. Naturf.*, 20 (1965), 521.
12. Vonhalle E & Hoglund R L, *T D column shape factors based on L-J (12:6) model*, Rept no. K 1679, (1966).
13. Hirschfelder J O, Curtiss C F & Bird RBMTGL (N Y) John Wiley (1964)
14. Westenberg A A, & de Hass N, *Phys. Fluids*, 5 (1962), 266.
15. Barua A K, Manna A, Mukhopadhyaya P & Das Gupta A, *J. Phys.*, B3 (1970), 619.

RKRV Potential Energy Curve & Dissociation Energy of CaO

N Sreedhara Murthy & U D Prahllad
Department of Physics, University of Mysore
Mysore 570 006
and
T V Ramakrishna Rao & G Thimma Naidu
Sri Venkateswara University Postgraduate Centre
Anantapur 515 003

Received 6 April 1979; revised received 5 November 1979

Experimental potential energy curve for the $X^1\Sigma^+$ state of CaO has been calculated using the method of Rydberg-Klein-Rees as modified by Vanderslice(RKRV). The dissociation energy of the ground state of CaO has been estimated to be 4·4 eV by the method of curve fitting using Hulbert-Hirschfelder potential energy function with the RKRV curve.

The diatomic molecule CaO has astrophysical significance, as some of its lines might conceivably appear as interstellar lines.[1] The curves of the potential energy and internuclear distance form a convenient way of displaying the energy levels of diatomic molecules and are of considerable importance for understanding of kinetic mechanics, spectral phenomena, stellar structures and many associated problems. Also, they permit ready application of the Franck-Condon principle to radiative transitions, dissociation and predissociation.

The dissociation energy of CaO determined by a number of workers has yielded different values as shown in Table 1. Gaydon[8] has recommended a value of $4{\cdot}3 \pm 0{\cdot}7$ eV. As the 5-parameter Hulburt-Hirschfelder (H-H) potential function is seen to be superior to other functions, the energy values obtained by H-H function have been compared with the experimental energy values to estimate the dissociation energy for the ground state of CaO by the method of curve fitting.

Potential energy curves—The turning points are calculated using the RKR method as extended by Vanderslice *et al.*[9,10] (RKRV) using the relation

$$r_{max,min} = (f/g + f^2)^{-1/2} \pm f \qquad ...(1)$$

Table 1—Experimental Values of the Dissociation Energy (D_e) of the X State of CaO

Workers	Method	D_e, eV
Colin *et al.*[2]	mass spectroscopic	3·70
Drowart *et al.*[3]	mass spectroscopic	4·04
Drummond and Barrow[4]	thermochemical	5·02
Lagerqvist and Huldt[5]	flame photometry	4·72
Veitz and Gurvich[6]	flame photometry	5·02
Engelke *et al.*[7]	chemiluminescence	4·80

Further simplified expressions for f and g, as given by Singh and Jain[11] and Murthy and Murthy,[18] have been used.

In their notation

$$f = \left(\frac{8\pi^2\mu_c}{h}\right)^{-1/2} Z_i$$

and

$$g = \left(\frac{2\pi^2\mu_c}{h}\right)\sum_{i=1}^{n}\left[2\alpha_i\,(\omega x)_i^{-1}\left(U_i^{1/2}-U_{i-1}^{1/2}\right) + \left\{2B_i-\alpha_i\omega_i\,(\omega x_i)^{-1}\right\}(Z_i-Z_{i-1})\right]$$

where

$$Z_i = (\omega x)_i^{-1/2}\ln\left[\frac{\omega_i-2\,(\omega x)_i\,(v+\frac{1}{2})}{\omega_i-2\,(\omega x)_i^{1/2}\,U_i^{1/2}}\right]$$

For obtaining the values of ω_i and $(\omega x)_i$, four vibrational levels U_i at a time and least squared $G(v)/(v+\frac{1}{2})$ as a function of $(v+\frac{1}{2})$ are taken. The constants thus obtained are used only over the middle two levels. Similarly by a series of sets of overlapping levels, molecular constants are determined for each set. The molecular constants needed for these calculations are taken from Rosen.[13] The turning points thus obtained are listed in Table 2 along with r_{max} and r_{min} values according to the Morse formula for comparison including the extrapolated highest bound level ($v = 68$) for both the potentials.

Estimation of dissociation energy—The procedure used for the estimation of dissociation energy of the ground state of CaO is the same as that of Murthy and Prahllad[14] and Murthy and Bagare[15,16] in the case of BeO, MgO and AlO. It involves the comparison of the energy values obtained by using RKRV turning points with the Lippincott potential function with the experimental energy values $G(v)$ for different values of dissociation energy. The value of D_e for which there is the best agreement between the $G(v)$ value and the values calculated by the potential function for all the observed vibrational levels is taken to be the dissociation energy of the molecule. In the case of CaO, however, 5-parameter H-H potential energy function has been used for curve fitting, as its average performance is distinctly superior to the Lippincott[17] function.

The H-H potential function[18] used in the present context is

$$U(r) = D_e\,[(1-e^{-x})^2 + cx^3e^{-2x}\,(1+bx)]$$

Table 2—Turning Points of the Vibrational Motion

	$G(v)$	RKRV Potential		Morse	
v	cm^{-1}	r_{max}, Å	r_{min} Å	r_{max}, Å	r_{min} Å
0	364·87	1·889	1·762	1·889	1·762
1	1087·39	1·943	1·722	1·944	1.722
2	1800·29	1·983	1·695	1·984	1·697
3	2503·57	2·018	1·675	2·019	1·677
4	3197·23	2·049	1·658	2·051	1·660
5	3881·27	2·078	1·643	2·081	1·646
6	4555·68	2·105	1·630	2·109	1·634
7	5220·48	2·132	1·619	2·136	1·623
8	5875·66	2·158	1·608	2·163	1·613
9	6521·22	2·183	1·598	2·188	1·603
10	7157·16	2·207	1·589	2·214	1·595
11	7783·48	2·231	1·580	2·239	1 587
12	8400·18	2·255	1·572	2·263	1·580
13	9007·26	2·279	1·564	2·288	1·573
14	9604·72	2·302	1·556	2·312	1·566
68	25467·58	6·192	0·922	6·726	1·456

where

$$r = \frac{\omega_e}{2(B_e\,D_e)^{1/2}}\left(\frac{r-r_e}{r_e}\right) \qquad ...(2)$$

$$c = 1+a_1\left(\frac{D_e}{a_0}\right)^{1/2} \qquad ...(3)$$

$$b = 2-\left(\frac{7}{12}-\frac{D_e\,a_2}{a_0}\right)\Big/c \qquad ...(4)$$

and a_0, a_1 and a_2 are Dunham coefficients.[19]

The results of calculation obtained in the case of the X state of CaO by the curve fitting procedure explained above are collected in Table 3 along with the percentage deviation. The average percentage deviation is also given.

Results and discussion—This procedure was tried with the Lippincott potential function[17] for the X state of CaO which gave a low value of dissociation energy as the percentage deviation in this case is more and showed a poor fitting. Eqs. (2), (3) and (4) are functions of dissociation energy. Hence assuming the dissociation energy for each vibrational state, we have calculated the constants c, b and x. These values have been used to calculate the energy values $U(r)$, using the H-H function. The calculations have been carried out for the curve fitting for the values of D_e ranging from 3·5 to 5·5 eV at intervals of 0·1 eV. Only relevant results are given in Table 3. The best fit of $U(r)$ with the experimental values of energy is obtained for $D_e = 4·4$ eV (35500 cm^{-1}) as the percentage deviation is minimum in this case.

Table 3—Comparison of Observed and Calculated Energy Values

r, Å	$G(v)$, cm^{-1}	$D_e = 4{\cdot}3$ eV		$D_e = 4{\cdot}4$ eV		$D_e = 4{\cdot}5$ eV	
		$U(r)$, cm^{-1}	% deviation	$U(r)$ cm^{-1}	% deviation	$U(r)$ cm^{-1}	% deviation
1·889	364·87	366·43	0·43	366·43	0·43	366·43	0·43
1·943	1087·39	1089·62	0·21	1089·63	0·21	1089·64	0·21
1·983	1800·29	1802·39	0·12	1802·44	0·12	1802·48	0·12
2·018	2503·57	2505·04	0·06	2505·16	0·06	2505·25	0·07
2·049	3197·23	3197·65	0·01	3197·88	0·02	3198·07	0·03
2·078	3881·27	3880·27	0·03	3880·68	0·02	3881·02	0·01
2·105	4555·68	4553·30	0·05	4553·95	0·04	4554·50	0·03
2·132	5220·48	5217·36	0·06	5218·34	0·04	5219·16	0·03
2·158	5875·66	5871·40	0·07	5872·80	0·05	5873·99	0·03
2·183	6521·22	6516·03	0·08	6517·96	0·05	6519·61	0·02
2·207	7157·16	7151·67	0 08	7154·23	0·04	7156·44	0·02
2·231	7783·48	7779·72	0·05	7783·07	0·01	7785·96	0·03
2·255	8400·18	8398·05	0·03	8402·32	0·03	8406·01	0·07
2·279	9007·26	9005·77	0·62	9011·12	0·04	9015·75	0·09
2·302	9604·72	9607·21	0·03	9613·80	0·09	9619·54	0·15
1·762	364·87	363·07	0·49	363·07	0·49	363·07	0·49
1·722	1087·39	1084·72	0·25	1084·71	0·25	1084·71	0·25
1·695	1800·29	1798·32	0·11	1798·31	0·11	1798·29	0·11
1·675	2503·57	2504·11	0·02	2504·07	0·02	2504·05	0·02
1·658	3197·23	3202·64	0·17	3207·57	0·17	3202·51	0·17
1·643	3881·27	3894·28	0·34	3894·16	0·33	3894·08	0·33
1·630	4555·68	4579·24	0·52	4579·08	0·51	4578·97	0·51
1·619	5220·48	5257·27	0·70	5257·05	0·70	5256·88	0·70
1·608	5875·66	5930·44	0·93	5930·12	0·93	5929·95	0·92
1·598	6521·22	6598·02	1·18	6597·66	1·17	6597·42	1·17
1·589	7157·16	7260·91	1·45	7260·48	1·44	7260·18	1·44
1·580	7783·48	7920·39	1·76	7919·86	1·75	7919·51	1·75
1·572	8400·18	8574·93	2·08	8574·30	2·07	8573·89	2·07
1·564	9007·26	9225·57	2·42	9224·83	2·42	9224·36	2·41
1·556	9604·72	9873·22	2·80	9872·33	2·79	9871·81	2·78
Average % deviation			0·551		0·547		0·548

As it is pointed out by Steele and Lippincott[20] that the average error in the dissociation energy in H-H function is about 2%, the error in our estimation does not exceed 0·1 eV. The present value of dissociation energy for the X state of CaO is in the range suggested by Gaydon[8] and also near the experimental values obtained by mass spectroscopic and chemiluminescence methods, though Herzberg[21] prefers the higher value in this range. Further, this value of D_e is significant as it is obtained by using true potential energy curve based on experimental data.

Two of the authors (NSM, UDP) are grateful to Prof. B Sanjeevaiah for encouragement. One of them (UDP) thankfully acknowledges the University Grants Commission for the grant of junior research fellowship at the University of Mysore..

References

1. Herzberg G, *Memories Soc. R. Sci. Liege*, 15 (1955), 291.
2. Colin R, Goldfinger P & Teunehome M, *Trans. Faraday Soc.*, 60 (1964), 306.
3. Drowart J, Exsteen G & Verhaegen G, *Trans. Faraday Soc.*, 60 (1964), 1920-33.

4. Drummond G & Barrow R F, *Trans. Faraday Soc.*, 47 (1951), 1275-7.
5. Largerqvist A & Huldt L, *Z. Naturf.*, 89 (1953), 493-9.
6. Veitz I V & Gurvich L V, *Optics Spectrosc.*, 2 (1957), 274.
7. Engelke F, Sander R K & Zare R N, *J. chem. Phys.*, 65 (1976), 1146-55.
8. Gaydon A G, *Dissociation energies* (Chapman and Hall) London, 3rd Edn, 1968.
9. Vanderslice J T, Mason E A, Maisch W G & Lippincott E R, *J. molec. Spectrosc.*, 3 (1959), 17-29.
10. Vanderslice J T, Mason E A, Maisch W G & Lippincott E R, *J. molec. Spectrosc.*, 33 (1960), 614-5.
11. Singh N L & Jain D C, *Proc. phys. Soc.*, 79 (1962), 274-8.
12. Murthy N S & Murthy B N, *J. Phys.*, B3 (1970), L15.
13. Rosen B, *Spectroscopic data relative to diatomic molecules*, 1970.
14. Murthy N S & Prahllad U D, *J. Phys.*, B11 (1978), 825-9.
15. Murthy N S, Bagare S P, *J. Phys.*, B11 (1978), 623-6.
16. Murthy N S, Bagare S P & Murthy B N, *JQSRT*, 19 (1978), 455-9.
17. Lippincott E R, Steele D & Caldwell P, *J. chem. Phys.*, 35 (1961), 123-41.
18. Hulburt H M & Hirschfelder J O, *J. chem. Phys.*, 9 (1941), 61-9.
19. Dunham J L, *Phys. Rev.*, 41 (1932), 721-31.
20. Steele D & Lippincott E R, *Rev. mod. Phys.*, 34 (1962), 239-51.
21. Huber K P & Herzberg G, *Molecular spectra and molecular Structure : IV-Constants of diatomic molecules* (Van Nostrand, Amsterdam), 1979.

Energy Calculation of Anharmonic Oscillator by Dalgarno Sum Rule

ADARSH GHOSH & P G KHUBCHANDANI

Jai Hind College, Bombay 20

Received 14 *June* 1979

The sum rule given by A Dalgarno and J T Lewis [*Proc. R. Soc.*: *A*, 233 (1955), 70] has been applied with success to the anharmonic oscillator. The second order energy correction due to the x^3 term is compared with first order correction due to x^4 term.

In the elementary perturbation theory the second order perturbation energy is given by

$$E_n^{(2)} = \sum_{m \neq n} \frac{\langle n \mid V \mid m \rangle \langle m \mid V \mid n \rangle}{E_n - E_m} \qquad \ldots(1)$$

where the notation is self-explanatory. Usually the intermediate states are not known and, therefore, the summation is not possible.

Dalgarno[1] has shown that if for a state Ψ_n it is possible to solve for a function f such that

$$2 \nabla f . \nabla \Psi_n + \Psi_n \nabla^2 f = V \Psi_n \qquad \ldots(2)$$

then

$$\sum_{m \neq n} \frac{\langle n \mid V \mid m \rangle \langle m \mid V \mid n \rangle}{E_n - E_m} = \langle n \mid f V \mid n \rangle - \langle n \mid f \mid n \rangle \langle n \mid V \mid n \rangle \qquad \ldots(3)$$

Dalgarno has used this method to calculate the long range forces between a proton and a hydrogen atom.

In the present note, we have used the Dalgarno method to calculate the energy of an anharmonic oscillator. We have calculated the second order correction to the ground state energy E_0 due to x^3 term and compared it with the first order correction due to x^4 term. The important point to note is that it is possible to solve the pertinent differential equation in this case.

For an anharmonic oscillator the Hamiltonian is written as

$$H = H_0 + V_3 + V_4 = \left(- \frac{\hbar^2}{2\mu} \frac{d^2}{dx^2} + \frac{1}{2} k_1 x^2 \right) + \frac{1}{6} k_2 x^3 + \frac{1}{24} k_3 x^4 \qquad \ldots(4)$$

where we have not written the higher terms. The unperturbed wavefunction for a simple harmonic oscillator is given by

$$\Psi_0 = \left(\frac{\alpha}{\pi} \right)^{1/4} \exp \left\{ - \frac{1}{2} \alpha x^2 \right\} \qquad \ldots(5)$$

where

$$\alpha = \frac{\mu \omega}{\hbar}$$

To calculate the second order correction due to V_3, we substitute for Ψ_0 from Eq. (5) and V_3 from Eq. (4) in Eq. (2) to obtain

$$\frac{d^2 f}{dx^2} - 2\alpha x \frac{df}{dx} = \frac{1}{6} k_2 x^3 \qquad \ldots(6)$$

A solution of Eq. (6) is

$$f(x) = - \frac{k_2}{12\alpha^2} \left(\frac{\alpha x^3}{3} + x \right) \qquad \ldots(7)$$

On substituting this in Eq. (3) we obtain

$$E_0^{(2)} (V_3) = \int_{-\infty}^{\infty} \Psi_0^* \, f \, V_3 \, \Psi_0 \, dx \qquad \ldots(8)$$

The additional term is obviously zero because V_3 is odd.

A simple calculation gives

$$E_0^{(2)} (V_3) = - \frac{11}{576} \cdot \frac{k_3^2}{\alpha^4} .$$

The first order correction due to the V_4 term is simply

$$E_0^{(1)}(V_4) = \int_{-\infty}^{\infty} \Psi_0^* \; V_3 \; \Psi_0 \, dx$$

which yields

$$E_0^{(1)}(V_4) = \frac{k_3}{32\,\alpha^2}.$$

giving $$\frac{E_0^{(2)}(V_3)}{E_0^{(1)}(V_4)} = -\frac{0{\cdot}62\,k_3^2}{k_3\,\alpha^2}$$

This result agrees with the one already obtained as mentioned by Flugge.[2] As could be seen $E_0^{(2)}(V_3)$ and $E_0^{(1)}(V_4)$ are comparable.

References

1. Dalgarno A & Lewis J T, *Proc. R. Soc.*: *A*, **233** (1955), 70.
2. Flugge S, *Practical quantum mechanics*, (Springer Verlag, Berlin), 1971.

Letters to the Editor

Errors in Line Width Analysis due to Unresolved Hyperfine Structures

The line widths in the ESR spectra of a paramagnetic molecule tumbling in liquid solutions can be often fitted to the equation:

$$\Delta H_M = A_0 + BM + CM^2 + DM^3 \qquad \ldots(1)$$

where ΔH_M is the peak-to-peak derivative width of the hyperfine transition with which the nuclear magnetic quantum number M is associated.[1] In the case of copper (II) complexes studied by several workers, the term DM^3 is quite small and can be neglected compared to other terms. In many cases, even when the lines are broadened due to unresolved ligand hyperfine structures, one can use Eq. (1) to fit the line widths. However, the parameters obtained by ignoring the unresolved hyperfine structures could be significantly different from the 'true' values of A_0, B, C, D associated with ESR transitions. This can be seen from the following example. Sastry *et al.*[2] have studied catena-μ-isothiocyanato-(N′-pyridylmethylene-N″-salicyloylhydrazinato-NN′O) copper (II), [Cu(sip)SCN] in dimethylformamide (DMF). Fig. 1(a) is the computer simulated spectrum using the parameters given by Sastry *et al.* for this complex, and using an equation similar to Eq. (7) of Ref. 2, by extending the summation to cover the natural abundance of ^{63}Cu and ^{65}Cu isotopes. These parameters A_0, B, C (Table 1) have been obtained by neglecting the possible unresolved ligand hyperfine structures. Yet the simulated spectrum fits the observed spectrum reasonably.

However, the anisotropic ESR parameters of Cu(sip)SCN obtained from the frozen solution spectra are consistent with a model, in which the unpaired electron is in the $d_{x^2-y^2}$ orbital (with lobes pointing towards near neighbours). The value of α^2 (which is a measure of the covalent σ-bonding) estimated was $\sim 0{\cdot}7$, suggesting a significant transfer of spin to near neighbours. The near neighbours in this case are one oxygen and three nitrogens.[3] In similar situations, nitrogen hyperfine splittings A_N ranging from 11-16 gauss have been observed.[4-6] Thus there is a good probability that the ESR spectrum reported by Sastry *et al.*[2] has unresolved ligand hyperfine structures. Fig. 1(b) has been obtained using A_N = 14 gauss for the three nitrogens and chosing A_0, B, C (Table 1), such that the simulated spectrum matches well with Fig. 1(a), [such a simulation makes use of an equation similar to Eq. (7) of Ref. 2, but includes all the ligand hyperfine split transitions in the summation]. Table 1 shows that A_0 estimated in the approximation $A_N = 0$ could be substantially higher than the 'true' A_0, when the ligand hyperfine splittings of this order are present.

Table 1—Line Width Parameters (in gauss) for Cu(sip)SCN in DMF at Room Temperature

Isotropic part of metal hyperfine splitting used = 62·25 gauss for ^{63}Cu

Type of determination	A_0	B	C
From Ref. 2 and using $A_N = 0$ [Fig. 1(a)]	59·7	−13·9	1·98
Simulation using A_N = 14 gauss [Fig. 1(b)]	36·0	−23·0	1·98
Using Kivelson's expressions and anisotropic ESR parameters from Ref. 2 with $\omega\,\tau_R = 7{\cdot}0$	23·8	−14·1	2·1

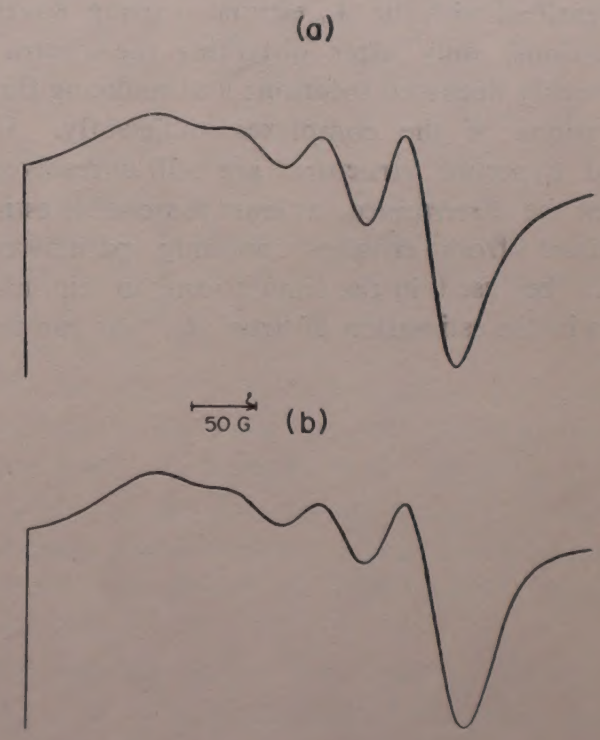

Fig. 1—Computer simulated ESR spectra for Cu(sip)SCN in DMF using the parameters given in Table 1, [(a) with $A_N = 0$; (b) with A_N = 14 gauss]

Further, concentration dependent mechanisms contribute significantly to broaden the line, thus increasing A_0, for concentrations $> 1 \times 10^{-3}$ M in typical Cu(II) complexes. Presence of dissolved oxygen (which will be present if the solutions are not thoroughly degassed) increases the line widths significantly as can be seen in Fig. 7 of Ref. 7. Fast equilibria involving solvent coordinated species could also make small contributions to line widths.

Sastry *et al.* [2,8,9] have reported values of A_0 larger than that expected using Kivelson's expressions.[10,11] The line width parameters determined for Cu(sip)SCN using the anisotropic ESR parameters[10,11] and a value of $\omega \tau_R = 7{\cdot}0$ (τ_R is the reorientational correlation time) are also given in Table 1. A_0 includes spin rotation interaction contribution. Sastry *et al.* attributed this singificant difference between the observed A_0 and calculated A_0 to other mechanisms.[9]

Before building theoretical models to explain such deviations, the experimental data reported in these papers[2,8,9] have to be carefully reexamined in the light of above mentioned points since one can expect ligand hyperfine structures in all these complexes. It is possible to minimize the errors in the estimation of 'true' A_0 from experiments (which can be identified with the A_0 estimated using Kivelson's expressions) only after obtaining the spectra from thoroughly degassed solutions and reducing the concentrations of the complexes sufficiently. If the ligand hyperfine structures are still unresolved and cannot be determined, at least reasonable estimates (obtained from covalent bonding parameter α^2) should be used in the simulations, to minimize the errors in the estimation of 'true' A_0. As can be seen from Table 1, substantial error could be present i the A_0, estimated neglecting ligand hyperfin structure.

B S Prabhanand
Chemical Physics Grou
Tata Institute of Fundamenta
Research, Bombay, 400 00

Received 24 *July* 198

References

1. Kivelson D, *Electron spin relaxation in liquids*, edited by L T Muus & P W Atkins (Plenum Press, New York), 1972, 213.
2. Sastry B A, Asadullah S Md, Chary E S, Deb A & Pelizzi C, *Indian J. pure appl Phys.*, 17 (1979), 590
3. Domiano P, Musatti A, Naradalli M, Pelizzi C & Predierl G, *J. chem. Soc. Dalton Trans.*, 11 (1975), 2357.
4. McGarvey B R, *Transition metal chemistry*, Vol. 3 edited by R L Carlin (Marcel Dekker, New York) 1966, 89,
5. Kivelson D & Neimen R, *J. chem. Phys.*, 35 (1961), 149.
6. Prabhananda B S, *Indian J. Chem.*, 18A (1979), 290
7. Prabhananda B S, Shah S J & Venkataraman B, *Proc. Indian Acad. Sci.*, 6A (1972), 231.
8. Sastry B A, Asadullah S Md, Ponticelli G & Massacesi M, *Spectrochim. Acta*, 35A (1979), 817.
9. Sastry B A, Chary M N, Asadullah S Md, Ponticelli G & Pinna R, *J. inorg. nucl. Chem.*, 41 (1979), 1381.
10. Wilson R & Kivelson D, *J. chem. Phys.*, 44 (1966), 154.
11. Atkins P W & Kivelson D, *J. chem. Phys.*, 44 (1966), 169.

INSTRUCTIONS TO CONTRIBUTORS

Manuscripts should be typewritten in double space and on *only one side* of good quality paper; the original and *one carbon copy are to be submitted.*

Papers must be written in clear and concise English. Good attention to spelling and grammar should be given. Long introductions should be avoided. Standard international nomenclature should be followed in giving names of chemical compounds. Standard abbreviations for units of measurement should be used in the text, tables and illustrations. The abbreviations should be used without fullstops.

Title—The title should be neither too brief/general nor unnecessarily long. It should reflect the content of the paper so as to derive the maximum advantage in indexing and information retrieval. A short title for use as running title should also be supplied. If a paper forms part of a series, a subtitle indicating the aspects of the work covered in the paper should be provided.

Abstract—The abstract should indicate the scope of the work and the principal findings of the paper. It should not exceed 3% of the length of the paper and, barring exceptional cases, it should not exceed 200 words. The abstract should be prepared in such a form that abstracting periodicals can use it without modification.

Data—Only such primary data as are essential for understanding the discussion and the main conclusions emerging from the study should be included. All such secondary data as are of interest to a specific category of readership may, if necessary, be deposited in the editorial office (or retained by the authors) for supply on demand. A footnote to this effect may be inserted at a suitable place in the paper.

Mathematical portions—Special attention should be given to the mathematical portions of the paper. Equations must be well separated from the text and written clearly with good separation between the successive lines. The usual norms of breaking long mathematical expressions may be adhered to. Equations should be numbered consecutively in Arabic numerals with the number in parentheses near the right hand margin. Superscripts and subscripts should be clearly indicated in pencil by ∨ and ∧ sign respectively. Capital and small letters, particularly of the same letter when both occur, as well as letters or symbols likely to be confused one for the other, should be clearly distinguished. Special characters (e.g. Greek, script, vector, tensor, matrix, etc.) required must be indicated by marginal notes. Letters and symbols which should appear in bold face must be clearly indicated. To simplify typesetting: (i) long and complicated mathematical expressions which are frequently repeated should be replaced with single letter/symbol, without clashing with the others used in the paper; (ii) the "exp" form of complex exponential functions should be used: and (iii) to simplify fractions, the solidus (/) is to be used and fractional exponents are to be used instead of root signs, e.g.

write $\left(4\omega_{pl} K_{s\lambda}^2 \Big/ \tilde{\omega} K_D^2\right)^{1/2}$ and *not* $\sqrt{4 \frac{\omega_{pl} K_{s\lambda}^2}{\tilde{\omega} K_D^2}}$

write $\exp\{-i\omega_0 (t_1 - t_2)/2\}$ and *not* $e^{-i\omega_0 (t_1 - t_2)/2}$

Tables—Tables should be typed *on separate sheets* of paper without any text matter on the page. They should be numbered consecutively in Arabic numerals and should bear brief titles. *Column headings should be brief.* Units of measurements should be abbreviated and placed below the headings. Nil results should be indicated and distinguished clearly from absence of data. Graphs as well as tables, both representing the same set of data, must be strictly avoided. Inclusion of structural formulae inside the tables should be avoided as far as possible. Tables should be referred to in the text by numbers and not by terms like 'above', 'below', 'preçeding' or 'following'.

Illustrations—All illustrations should be numbered consecutively in Arabic numerals. Captions and legends to the figures should be self-explanatory and should be typed on a separate sheet of paper and attached at the end of the manuscript. Line drawings should be made with Indian ink on white drawing paper (perferably Bristol board), cellophane sheet or tracing cloth. In addition to the originals, a set of blue-prints or photostat copies should be sent. For satisfactory reproduction, the graphs and line drawings should be drawn to approximately twice the printed size.

The lettering should be uniform, perferably in stencil, so as to be *not less than 2 mm after reduction* widthwise to 3" or 6" as required. The size of geometrical shapes (used to distinguish different graphs), dot, lines, etc. should be sufficiently large to permit the necessary reduction without loss of detail. In the case of *photographs*, prints *must be on glossy paper and contrasty*. If an illustration is taken from another publication, reference to the source should be given and prior permission secured. Illustrations should be protected by thick cardboard packing against creases, folds and broken corners during transit. Illustrations should be referred to in the text by numbers and not by terms like 'above', 'below', 'preceding' or 'following'.

Infrared, ultraviolet, NMR and other spectra, DTA curves, etc. should be included only if they pertain to new compounds and/or are essential to the discussion; otherwise only significant numerical data should be included in the text.

References—The list of references should be prepared strictly in accordance with the style followed

in the Journal. In the text, references to literatures should be numbered consecutively, in the order of their first occurence, and should be indicated by superscripts at the relevant places; as far as possible the placement of references on numerals of other symbols should be avoided; in such cases the reference may be given in parentheses in running text, e.g. "this yielded for n a value of 2·3 (Ref. 5)". Full bibliographic details for all the references mentioned in the text should be listed in serial order at the end of the paper.

In citing references to research papers, names and initials of authors should be followed, in order, by the title of the periodical in the abbreviated form (underlined), the volume number (two lines underneath), the year within circular brackets and the page reference [e.g. Venkatesh, H G & Guha Sarkar, G, *Indian J. pure appl. Phys.*, **12** (1974), 502]. For names of periodicals, the standard abbreviations listed in the *World list of scientific periodicals* edited by P Brown & G B Stratton (Butterworths & Co. Ltd, London), 4th Edition, 1963-65, should be used. If the reference is to an article published without any authorship in a periodical, the title of the article takes the place of the author in the citation [e.g. The content, influence and value of scientific conference papers and proceedings. *Unesco Bull. Libr.*, **16** (1952), 113-26.]. If a paper has been accepted for publication, the names of the authors and the journals should be given followed by the words "in press" within circular brackets [e.g. Sastry, B. A. & Sastry, G. S., *Physica*, (in press).].

In the list of references, unpublished work, accepted papers in press and personal communications should be clearly distinguished.

Even if a reference contains more than two authors, the names of all the authors with their respective initials should be given. The abbreviations *et al.*, *idem* and *ibid* should be avoided.

Reference to a book should include details in the following order: names and initials of authors, the title of the book (underlined), name of publisher and place of publication within circular brackets and year [e.g. Herzberg, G, *Spectra of diatomic molecules* (D Van Nostand & Co. Inc., New Jersey), 2nd Edn, 1950, 31.]. If the reference is to the work of an author published in a book by a different author or edited by a different person, the fact that it is cited from the source book should be clearly indicated [e.g. Garlick, G F J, cited in *Encyclopedia of Physics*, Vol. 26—*Light and matter* II, edited by S Flugge (Springer Verlag, Berlin), 1958, 1.].

Proceedings of conferences and symposia should be treated in the same manner as books. Reference to a paper presented at a conference, the proceedings of which are not published, should include, in the following order, names and initials of authors, title of the paper (underlined), name of the conference, place where the conference was held and date (Deekshitulu, B L, *Design and fabrication of drum scanner for picture processing*, paper presented in the Symposuim on Applied Optics, Indian Institute of Science, Bangalore, 28-30 Nov. 1974).

Reference to a thesis should include the name of the author, title of the thesis (underlined), university or institution to which it was submitted and year of submission (e.g. Chandrasekaran, K S., *Studies on crystal structure and absolute configuration of crystals*, Ph. D. thesis, Madras University, 1956).

Reference to a patent should include names of patentees, country of origin (underlined) and patent number, the organization to which the patent has been assigned within circular brackets, data of acceptance of the patent and reference to an abstracting periodical where available [Trepagnier, J H, *US Pat.* 2,463,219 (to E I du Pont de Nemours & Co.), 1 March 1949, *Chem. Abstr.*, **43** (1949). 7258.].

Abbreviations and symbols—Abbreviations used should conform to the style of the journals. The following prefixes to units of measurements may be used for expressing submultiples and multiples.

Submultiples	*Abbreviation*	*Multiples*	*Abbreviation*
Deci- ($=10^{-1}$)	deci	deca- ($=10^{1}$)	deca-
centi- ($=10^{-2}$)	c	hecto- (10^{2})	hecto
milli- (10^{-3})	m	kilo- ($=10^{3}$)	k
micro- ($=10^{-6}$)	μ	mega- ($=10^{6}$)	M
nano- ($=10^{-9}$)	n	giga- ($=10^{9}$)	G
pico- ($=10^{-12}$)	p	tera- ($=10^{12}$)	T
femto- ($=10^{-15}$)	f		
atto- ($=10^{-18}$)	at		

Frequently repeating combinations of words, e.g. electric field gradient (EFG), junction field effect transistor (JFET), stimulated Raman emission (SRE), should be abbreviated subsequently, indicating the abbreviated form in parentheses, as shown, at the place of their first occurrence,

Nomenclature—Where too many symbols are used in the text, a section entitled "Nomenclature", explaining the significance of the various symbols, may be given and placed just above the Acknowledgement section.

Acknowledgement--Acknowledgements should not be exuberant and must be made only to real assistance rendered in connection with the work reported in the paper.

Appendixes—Appendixes, typed on separate sheets, should be numbered consecutively, in Arabic numerals, in the order of their occurence in the text, and should be placed at the very end of the paper.

Printed and Published by Shri D S Sastry, Publications & Information Directorate, Council of Scientific & Industrial Research, New Delhi, at the Leipzig Press, D-52 South Extension Part I, New Delhi 110 049, India

Regd. D-(C)-540